# SKIN FRICTION, HEAT TRANSFER, AND PRESSURE MEASUREMENTS ON HYPERSONIC INLET COMPRESSION SURFACES IN THE MACH NUMBER RANGE 7.5 TO 16

M. O. Ryder, Jr.

# FOREWORD

The experimental research effort reported herein was conducted by the Applied Hypersonic Research Department of Cornell Aeronautical Laboratory of Cornell University, Buffalo, New York for the Flight Dynamics Laboratory, Research and Technology Division, Air Force Systems Command, United States Air Force, on Contract AF 33(615)-1845, under Task No. 136605 of Project 1366. The contractor's report number is AA-1948-Y-3.

The work reported herein covers both phases of a two-phase program which began in May 1964 and was conducted under the technical cognizance of Mr. G. Keith Richey, with the assistance of Mr. D. Sedlock, of the Flight Dynamics Laboratory's Internal Aerodynamics Group. The program was financed by the Air Force Flight Dynamics Laboratory Director's Fund. The final report was submitted in September 1965.

This technical report has been reviewed and is approved.

Philip P. Antonatos

Philip P. Antonatos
Chief, Flight Mechanics Division
Air Force Flight Dynamics Laboratory

## ABSTRACT

An experimental study of boundary layer flow, under the influence of adverse pressure gradients typical of hypersonic inlets, was conducted in the Cornell Aeronautical Laboratory 48-inch Hypersonic Shock Tunnel on two two-dimensional and three axisymmetric compression surface models instrumented with skin friction, heat transfer and pressure gages. Tests were conducted over a Mach and Reynolds number range of 7.5 to 16 and $3.2 \times 10^4$ per ft. to $4.7 \times 10^6$ per ft., respectively. The boundary layers on the two-dimensional models were laminar and attached for all conditions tested. Local laminar separation occurred for some conditions of the axisymmetric tests. Boundary layer transition occurred for the high Reynolds number runs at a Mach number of 8 on the axisymmetric models but the adverse pressure gradients were not large enough to cause the turbulent boundary layers to separate.

A data correlation based on local flow conditions at the edge of the boundary layer and zero pressure gradient is presented which correlates the heat transfer data quite well. The skin friction data are shown to correlate in a similar manner when the adverse pressure gradient is small but the correlation fails at large pressure gradients and for separated flow.

An important conclusion resulting from this program was that the skin friction gages gave a more accurate indication of localized boundary layer separation than either the heat transfer or static pressure distributions on the models tested.

TABLE OF CONTENTS

# LIST OF TABLES

# LIST OF ILLUSTRATIONS

LIST OF ILLUSTRATIONS (Cont.)

LIST OF ILLUSTRATIONS (Cont.)

## LIST OF ILLUSTRATIONS (Concluded)

# NOMENCLATURE AND SYMBOLS

| Symbol | IBM Printout | |
|---|---|---|
| $c$ | | Specific heat, ft-lbs/slug-°R |
| $c_H$ | | Heat transfer coefficient $\sim \frac{\dot{q}_M}{\rho_\infty U_\infty (H_0 - H_M)}$ |
| $c_p$ | | Specific heat at constant pressure |
| H | H( ) | Enthalpy, ft-lbs/slug |
| M | M | Mach number |
| p | P( ) | Pressure, psia |
| q | Q | Dynamic pressure, psia |
| $\dot{q}$ | Q(AV) | Average heat transfer rate, BTu/ft$^2$-sec |
| Re/ft | RE/FT | Reynolds number, $\frac{\rho_\infty U_\infty}{\mu_\infty}$ |
| T | T( ) | Temperature, °R |
| t | | Time, seconds |
| U | U | Velocity, ft/sec |
| x | | Station distance from model nose |
| $\sqrt{C^*}$ | SQRT. $C^*$ | Square root of the constant of proportionality in the linear viscosity law based on reference temperature, square root of Chapman-Rubesin constant |
| $\tau$ | TAU(M) | Skin Friction on model, psi |
| $\alpha$ | ATTACK | Angle of attack, degrees |
| $\gamma$ | | Specific heat ratio |
| $\mu$ | MU | Absolute viscosity coefficient, slugs/ft-sec |
| $\rho$ | RHO | Density, slugs/cu. ft. |
| $\phi$ | ROLL | Angle of roll, degrees |
| $\psi$ | YAW | Angle of yaw, degrees |

NOMENCLATURE AND SYMBOLS (Cont.)

| Subscripts | IBM Printout | |
|---|---|---|
| 1 | | Initial conditions in driven tube |
| 4 | | Conditions behind reflected shock |
| $\infty$ | | Free Stream conditions |
| i | (I) | Incident shock in driven gas |
| L | | Local flow conditions at the edge of the boundary layer |
| M | (M) | Model surface, initial conditions at model surface |
| o | (O) | Nozzle supply stagnation conditions |
| o' | PITOT | Stagnation conditions behind a normal shock |
| ts | (TS) | Initial test section pressure, psia |
| x | | Station distance from model nose |

| Superscript | |
|---|---|
| * | Eckert reference temperature |

# SECTION I

# INTRODUCTION

In the design of hypersonic inlets it is necessary to consider fully the boundary layer flow in that the presence of such a layer alters the effective shape of the inlet components and consequently the aerodynamic behavior of the inlet. Displacement of leading edge shocks by boundary layer growth can cause spillage of freestream flow which is within the inlet's geometric capture area, resulting in a reduced inlet mass flow; excessive boundary layer growth can cause choking, resulting in subsonic flow throughout the inlet and increased mass flow spillage; boundary layer transition may cause undesirable effects due to increased aerodynamic heating as well as the increased boundary layer thickness; and boundary layer separation will cause nonisentropic disturbances to propagate into the flow with resultant losses in total pressure.

The task reported herein is directed towards experimental investigation of the boundary layer on inlet compression surfaces at hypersonic Mach numbers under the influence of adverse pressure gradients. Direct local skin friction measurements were made to determine inlet skin friction distributions on compression surfaces and to provide data which can be used to evaluate the applicability of existing laminar boundary layer theories. The data obtained can be used to substantiate or improve theories concerning hypersonic boundary layer separation under the influence of adverse pressure gradients in laminar flow.

# SECTION II

# TEST EQUIPMENT

## 1. CAL 48-INCH LEG OF THE HYPERSONIC SHOCK TUNNEL

The basic components of the 48-Inch Leg of the Hypersonic Shock Tunnel are shown in Figure 1. The tunnel employs a constant-area shock tube with an 8-inch inner diameter. The driver tube is 20 feet long and is externally heated with a resistance heater up to temperatures of 1500°R. The driven tube length can be 50, 60, or 70 feet long by adding or removing tube sections. For this test program the 50 feet tube length was used. The driver gas was generally a mixture of helium and air with a maximum helium purity of 98.5% while the driven gas was air. Steady flow testing times of the order of 6 to 7 milliseconds, which allowed ample time to measure skin friction, pressure, and heat transfer rates on the models, were achieved using the tailored-interface technique to be described later.

Two axisymmetric contoured nozzles, providing parallel flow with no pressure gradients in the streamwise direction for several feet, were used for the expansion. This is very important since the presence of a streamwise pressure gradient can have a significant effect on model test results. One nozzle is designed for a Mach number of 8 and the other for 16. Both nozzles were used over a Mach number range by employing removable throat inserts of various diameters. Both nozzles have been calibrated, using pitot pressure survey rakes, over the range of operating conditions used in the subject program.

The test air expands through the nozzles into a 48-inch diameter test section in which the models are supported on an angle of attack sector as shown in Figures 2 and 3. Test air passes downstream of the test section into a receiver tank large enough to maintain the desired flow duration. Tunnel accelerations are isolated from the model by mounting the model support system on the laboratory floor and using a flexible bellows to provide a vacuum seal between the sector and the tunnel. The 16-inch diameter schlieren windows shown in the figures were used to obtain a single spark schlieren for most runs of the test program.

## 2. SHOCK TUNNEL OPERATING PRINCIPLES

The shock tube is separated into regions of high and low pressure by a diaphragm (Figure 4). The wave phenomena begin with the rupture of the diaphragm, permitting expansion of the high-pressure driver gas into the lower pressure section and the generation of a shock wave which propagates through the low-pressure air. Between the shock wave and the gas interface (the contact surface separating the driver gas and the driven air) there exists a steady state region which is at a high temperature and pressure.

The downstream end of the shock tube is terminated by a convergent-divergent nozzle. The ratio of the nozzle throat area to the shock tube cross-sectional area is small, however, so that the primary shock wave is nearly completely reflected upstream from the throat, leaving a region of almost stagnant, compressed, and heated air at the end of the low-pressure section of the shock tube. This processed air is expanded through the nozzle to the desired test condition.

By proper control of the initial conditions in the driver and driven sections, the gas interface becomes transparent to the shock wave reflected upstream from the throat, i.e., no gasdynamic waves result from this interface-shock interaction that can subsequently disturb the steady test-air-supply conditions. Since the states of the gases on both sides of the interface must be carefully matched, this method is called the "tailored-interface" technique (Ref. 1). The limiting wave which then determines the maximum available testing times for the tailored-interface technique are approximately eight times those achieved with the same length tube operating as a conventional nonreflected shock tunnel.

The temperature of the air behind the reflected shock in the driven section of the tube (corresponding to the "reservoir" or "supply" temperature in conventional wind tunnel terminology) is a function of the strength or velocity of the shock wave through the driven tube. If the stagnation temperature is to be duplicated at a given flight Mach number, the shock velocity or shock Mach number is then uniquely determined. The shock Mach number is, in turn, a function of the pressure ratio across the diaphragm for given driver gas mixtures and initial temperatures of the driver and driven gas. In order to tailor at various shock strengths, provision is made to vary the velocity of sound of the driver gas by mixing the driver gas with other gases and by heating.

## 3. MODELS

The models are of two general classes, two-dimensional (Phase I tests) and axisymmetric (Phase II tests) and are typical of the types of compression surfaces which might be used in hypersonic inlets. High shock losses at hypersonic speeds dictate that initial angles of inlet surfaces be small. Consequently the two-dimensional models begin at the leading edges as a 3° wedge and the axisymmetric begin as a 5° half-angle cone. Aft portions of the models are isentropic continuous compression surfaces which produce the adverse pressure gradient region of interest in this test program.

### a. Two-Dimensional Models

Model 2D1 turned from an initial wedge angle of 3° to a terminal angle of 7°. Model 2D2 turned from an initial wedge angle of 3° to a terminal angle of 10°. A downstream shift in the maximum pressure region on

the models, caused by the boundary layer growth, made it necessary to install extension wedges on the aft portions of the two-dimensional models to prevent base effects from feeding forward through the boundary layer to the adverse pressure gradient region of interest. Model 2D2 has a "depression" in the contour from X = 9.25 to 12.00 which resulted from an error in the original coordinates as given on the model drawing. The maximum depression below the proper contour is about 0.008 inches. It will be shown in the discussion of results section that the contour error had no discernible effects on the data. Photographs and drawings of the two-dimensional models comprise Figures 5, 6, 7 and 8, respectively. Locations of model instrumentation are given in Figures 9 and 10.

The desired leading edge condition for the two-dimensional models was sharp. The leading edge radii for both models was 0.005 inch or less. Maximum leading edge waviness for model 2D1 was ±0.002 inch as seen in a front view and ±0.001 as seen in the plan view. Corresponding numbers for model 2D2 were ±0.003 and ±0.01 inches, respectively.

The two-dimensional models were designed and fabricated by the General Electric Company on Air Force Contract Number AF 33(657)-9437. Models 2D1 and 2D2 are Model 1 and Model 17 ramp, respectively, in Reference 2. Model 2D1 was tested by General Electric in their own shock tunnels at Mach numbers of 16 and 20. Pressure and heat transfer data were obtained. Model 2D2 (G.E. Model 17 without cowl) was not tested previously, however, Model 17 was tested by General Electric at a Mach number of 12 and surface static pressures were obtained on the ramp.

b. Axisymmetric Models

The axisymmetric models consisted of a sharp 5° half-angle cone with three interchangeable after-bodies each giving a different amount of flow turning. Model numerical designations refer to the inviscid compression ratios of the models at Mach number 20, i.e., the ratio of the maximum model pressure to the cone pressure on the forward portion. Photographs and drawings of the axisymmetric models comprise Figures 11 and 12, respectively. Instrumentation locations are given on Figure 13.

The axisymmetric models A/10, A/20, and A/50 were designed and fabricated by Republic Aviation Corporation on Air Force Contract Number AF 33(657)-9697. These models have been tested previously by Republic (Ref. 3) at a Mach number of 22 and a unit Reynolds number per ft. of approximately 850,000. Data obtained were surface pressures, boundary layer pitot pressure distributions, and schlieren photographs.

All the models for the program were provided by the Air Force Flight Dynamics Laboratory.

## 4. INSTRUMENTATION

### a. Skin Friction

Two different types of skin friction gages were used for Phase I and Phase II testing. Both types are piezoelectric devices which function in principle in the same manner as the pressure transducer. Differences from the pressure transducer and from one another are primarily in details of arrangement of crystals and diaphragms. Both types are acceleration compensated and use lead zirconium titanate crystals.

Figure 14 shows a bisected view and a top view (diaphragm removed) of the 1/2-inch diameter skin friction gage used in Phase I tests (Ref. 4). Response is to a force applied tangent to the diaphragm to the right or left in either view. In the side view, the active diaphragm which is cemented to a pair of pins on a flexure which carries the force to the crystal can be seen. Rubber diaphragm support pads are cemented to the diaphragm backup plate but not to the diaphragm. These pads support the diaphragm during loading normal to the gage. Although the rubber support pads around the diaphragm pins makes the diaphragm support structure somewhat redundant, the combination of elasticity of the rubber and very high stiffness of the crystal results in essentially all of the load in the direction of the sensitive axis being taken by the crystal. Application of pressure forces to the crystal is minimized by providing bleed holes across the diaphragm to equalize the diaphragm pressure force. Further isolation of the crystal from pressure forces is accomplished by the flexure which is very weak in bending and hence allows the rubber support pads to absorb most of the normal force. In addition, what little normal force does get to the crystal is in a direction in which the crystal has zero theoretical and little actual sensitivity.

Figure 15 shows the 1/4-inch diameter skin friction transducer used in the Phase II tests. This gage is identical in operating principles to the larger gage used in Phase I except now the crystal is a cantilevered beam; clamped at one end and placed in bending by the skin friction force at the other end. This mode of crystal bending gives higher gage sensitivities than the simply supported beam type crystal mount. Flexuring is accomplished by notching the crystal near the diaphragm end. This flexure is primarily designed to prevent rotation of the diaphragm from stressing the crystal. As in the 1/2-inch diameter transducer, the diaphragm is supported on rubber pads. For this smaller transducer the edge gap around the diaphragm is sufficient to equalize the pressure across the diaphragm without any additional holes being added. The 1/4-inch diameter skin friction gage diaphragms were contoured to the local cone radius of the models. This program was the first time that the 1/4-inch gages were used.

For both the 1/2-inch and 1/4-inch diameter skin friction gages the acceleration components are located in the bottom of the case. These parts are identical to the active skin friction parts and provide electric signals due to acceleration which (essentially) equal the acceleration signals

from the skin friction components and are wired in opposition to provide acceleration compensation.

The crystals are bimorph configurations which consists of two layers of lead zirconium titanate that have been polarized in opposite directions in order that the combination will be sensitive to bending in one plane but relatively insensitive to all other strains. They will, therefore, have little response to temperature change. It will be noted in Figures 14 and 15 that the crystals are notched near the ends. This notching, in addition to serving as a flexure as mentioned above for 1/4-inch diameter gages, provides greater sensitivity by elimination of tension and compression near the ends of the crystals which would otherwise cancel some of the signal. The notches also minimize effects of any minute sliding of the crystal in its mount.

Calibration of both sizes of skin friction gages consists of using known weights to apply loads to the gage diaphragms in the skin friction direction. Gages have been calibrated in both positive and negative shear giving equally satisfactory operation in either direction. The combined operating range over which the gages have been routinely calibrated is .001 psi to .12 psi. Gage outputs have been experimentally demonstrated to be linear over this range of shear. The upper limit of linearity has not been precisely determined. It is assumed that the gages are linear through zero output. Additional information on the skin friction gages can be found in Section VII.

b. Heat Transfer

Heat transfer rates were determined by a technique that relies on sensing the transient surface temperature of the model. The sensing element is a thin platinum strip painted on a Pyrex substrate which conforms to the local model contour. The gage is then fired at controlled conditions, resulting in a thin film of metal, typically 0.1 micron thick by 5 mm by 0.5 mm, and fused to the Pyrex insert. Since the heat capacity of the gage is negligible, the film temperature is equal to the instantaneous surface temperature and is related to the heat transfer rate to the model by the theory outlined in Section V of this report and discussed in detail in Reference 5. Temperature histories from the platinum strips were fed into a passive analog network which produced a step output that was proportional to the heat transfer rate to the model. An IBM 7044 computer program then uses the analog network output voltages to compute heat transfer rates. The computer automatically makes small corrections for the variation with temperature of the heat transfer gage substrate (Pyrex) properties and the nonlinear resistance-temperature characteristics of the platinum strip.

c. Pressure

The model pressures were measured with miniature ceramic piezoelectric crystal transducers. Their small size permits installation

inside the model close to the orifice in the model surface, thus minimizing pneumatic lag. These transducers are available in several sizes and pressure ranges so that the type best suited for the estimated pressure range at a given model position can be used. Proper shielding on the sensing element precludes temperature effects during the short test time. In the transducer used to measure the very low pressures of certain portions of the current program, a dual-element transducer was used to reduce acceleration effects to an indicated pressure of 0.0001 psi/g. Gage pressures on the order of 0.001 psi were measured with this transducer. The pressure transducer indicates the pressure rise over the initial pre-run test section pressure -- usually of the order of 5 microns as determined by a Pirani gage which is periodically checked against a McLeod gage as a standard. The voltage output of each gage is calibrated against applied pressure through the model surface orifice after the gage has been installed in the model. Transducers are selected such that the voltage output is linear with pressure over the range of pressures encountered. Pressure transducers are normally calibrated before and after a series of runs. The details of the design, fabrication, and calibration of the pressure transducers used in the present test series are described in Reference 6.

d. Schlieren

Schlieren photographs for the Phase I (two-dimensional models) tests were taken using a double-pass parallel light system. A single-pass parallel light system was used for the nominal Mach number 7.5 tests in Phase II (axisymmetric models) and a double-pass conical light system was used for the higher Mach number testing in this Phase. All schlieren systems for both test phases used a horizontal knife edge. Schlieren system selection was dictated by sensitivity requirements and model width. Low density high Mach number flows required double-pass systems and the two-dimensional models required parallel light systems to avoid double images.

## 5. DATA ACQUISITION

The electric signals from the heat transfer, skin friction and pressure transducers were recorded on 48 channels at 50-microsecond intervals on the magnetic storage drum of a Navigation Computer Corporation MCL 100 data acquisition system. The information was then transferred to magnetic tape for use as the input to the data reduction program. The data were also reproduced on a pen-type recorder for immediate examination and preliminary calculation.

Since the number of data points to be monitored on each run was less than the 48 recorder channels available, some data points were monitored on two different channels with a different gain on each. This decreased the possibility of losing data because of improper gain estimates.

# SECTION III

# TEST PROCEDURE

## 1. TEST PROGRAM

The two-dimensional and axisymmetric model test program and test conditions are presented in Tables I and V, respectively. The test program was specified by the Air Force Flight Dynamics Laboratory. Runs 2 and 37 were void runs and have been excluded from Tables I and V. Run 2 was a self-burst run ; i.e., the shock tube diaphragms broke prematurely. Run 37 was void because the tunnel stagnation pressure measurements were recorded at amplifier gain settings which were too large.

## 2. CALIBRATION

### a. Skin Friction

The skin friction gages were calibrated using known weights to apply shear forces to the gage diaphragm Gage outputs were displayed on oscilloscopes and photographed using Polaroid cameras. Dividing the weights by the area of the diaphragm gave the equivalent shear stresses corresponding to the respective gage outputs. The gages were checked for electrical leakage after installation in the models.

### b. Heat Transfer

The heat transfer gages were calibrated prior to the tests to determine the changes in resistance of the elements with temperature. At the temperatures encountered in test tests, these changes are linear and the resistance at only two temperatures need be determined. This calibration is then used to set the gain of the recording equipment for the expected temperature increase.

### c. Pressure

The pressure gages were calibrated (i.e., voltage output versus applied pressure) and checked for air and electrical leakage after installation in the model. The voltage-pressure relation is linear over the range of pressure normally encountered during testing.

These calibrations, in conjunction with estimated values of model pressures provide the basis for adjusting amplifier gains to achieve maximum "readability" of the data recording system.

The detailed calibration data are kept on file at CAL.

## SECTION IV

## TEST CONDITIONS

The test conditions of pressure, temperature and Reynolds number are computed by assuming isentropic expansion of the test gas from the conditions behind the reflected shock in the tube to the test section Mach number which has been previously determined from tunnel airflow calibrations. The flow is expanded sufficiently so that the air in the test section is cool enough to obey the perfect gas laws.

The stagnation enthalpy and temperature of the air behind the reflected shock is determined from

$$H_o = H_1 \, (H_4/H_1) \tag{1}$$

and $T_o = T_1 \, (T_4/T_1)$, respectively (2)

where $H_4/H_1$ and $T_4/T_1$ are functions of $U_i$, the incident shock velocity (Ref. 7-9). $U_i$ is obtained by measuring the time taken by the shock wave to pass between two stations in the shock tube. $H_1$ is taken from Reference 10. Free-stream static temperature is obtained from

$$T_\infty = \frac{H_o}{C_p} \left(1 + \frac{\gamma - 1}{2} M_\infty^2\right)^{-1} \tag{3}$$

Free-stream pressure is calculated using

$$p_\infty = \frac{P}{P_p} \; p_o \left(1 + \frac{\gamma - 1}{2} M_\infty^2\right)^{-\frac{\gamma}{\gamma - 1}} \tag{4}$$

where

$$\frac{P}{P_p} = \frac{(p/p_o)_{real}}{(p/p_o)_{perf.}}$$

is the real gas correction to the ideal static to total pressure ratio as described in Reference 11 and $p_o$ is the measured pressure behind the reflected shock. The source data used in this technique are References 10 and 12.

Free-stream dynamic pressure is calculated from

$$q_\infty = \frac{\gamma}{2} p_\infty M_\infty^2 \qquad (5)$$

Values for absolute viscosity ($\mu$) used to compute Reynolds numbers were obtained from Reference 13 for temperatures below 500°R and from Reference 14 for temperatures above 500°R.

Stagnation conditions behind a normal shock in the test section are based on the data of Reference 12. The balance of the primary test section properties are based on perfect gas theory.

# SECTION V

# DATA REDUCTION

## 1. SKIN FRICTION

The skin friction gage output is a direct function of the average shear stress over the gage diaphragm and the sensitivity of the gage, which was determined during gage calibration. Dividing gage output by gage sensitivity gives average shear stress directly.

## 2. HEAT TRANSFER

The "thin-film" heat transfer gage is a resistance thermometer which reacts to the local surface temperature of the model. The theory of heat conduction in a nonhomogeneous body is used to relate the surface temperature to the rate of heat transfer. Since the resistance element has negligible effect on the Pyrex substrate surface temperature, the substrate can be characterized as being semi-infinite, homogeneous and isotropic. The general heat conduction equation is

$$\rho c(T) \frac{\partial T}{\partial t} = \frac{\partial}{\partial x}\left[K(T) \frac{\partial T}{\partial x}\right] \tag{6}$$

where $\rho$, c, and K are substrate density, specific heat and thermal conductivity, respectively, and x is the substrate depth.

If the substrate properties are independent of temperature; i.e., if the temperature change is less than 100°R, a closed-form solution is obtained for the heat transfer rate,

$$\dot{q}(t) = \frac{1}{2}\left(\frac{\pi \rho c K}{t}\right)^{1/2}\left[T(t) + \frac{1}{\pi}\int_0^t \frac{\lambda^{1/2} T(t) - t^{1/2} T(\lambda)}{(t-\lambda)^{3/2}}\, d\lambda\right] \tag{7}$$

For evaluating the integral numerically, the equation is recast in the following form:

$$\dot{q}(n) = \frac{1}{2\sqrt{\pi \Delta t}}\left[(\rho c K)_n^{1/2} T_n \left(\frac{\pi + \sum_{p=0}^{p=n-1} \frac{p^{1/2}}{(n-p)^{3/2}}}{n^{1/2}}\right) - \sum_{p=0}^{p=n-1} \frac{T_p (\rho c K)_p^{1/2}}{(n-p)^{3/2}}\right] \tag{8}$$

where t = time interval between tabulated data points (typically, 50 microseconds)

n = time index of the point

p = running time index

subscript n = value of parameters at $n^{th}$ time increment

subscript p = value of parameters at $p^{th}$ time increment

The temperature dependence of $(\rho cK)^{\frac{1}{2}}$ and the variation of the electrical properties of the resistance element with temperature are accounted for in the computer program.

In cases where the surface temperature change is less than 100°F, as is in these tests, Equation (7) may be solved directly by use of q-meters, which are passive electrical analog networks, in conjunction with the heat transfer gage. The analog is based on the fact that the equation for heat conduction in a semi-infinite solid is identical to that for a semi-infinite electrical transmission line with distributed series resistance and shunt capacitance. In practice, it has been found feasible to construct the analog of a finite number of circuit elements consisting of parallel resistor-capacitor elements in a series arrangement. For temperatures greater than 100°F a time and heat transfer rate dependent correction must be applied to the q-meter output.

## 3. PRESSURE

The pressure transducers measure the difference between the internal case pressure and the model pressure. The case pressure is equal to the initial test section pressure (or the order of 3 microns) and is added to the measured pressure to obtain the absolute pressure.

# SECTION VI

# DISCUSSION OF RESULTS

The results of this test program demonstrate the importance of the boundary layer effects on the flow over slender compression bodies typical of the components of hypersonic inlets. On slender models at hypersonic Mach numbers the boundary layer can significantly alter the effective shape of the body with the attendant result that the aerodynamics of the local flow field are vastly different from the inviscid flow case. Data gathered in this test program show that as the flow Reynolds number is reduced and the boundary layer becomes thicker, the effective model shape produced by boundary layer displacement of the inviscid flow field reduces the adverse pressure gradient and allows the boundary layer to remain attached. Although the objective of the test program was to gather skin friction data in laminar flow, natural transition occurred on the axisymmetric models for the higher Reynolds number runs at Mach 7.5 and provided data for turbulent flow.

## 1. TWO-DIMENSIONAL MODEL TESTS

These models were tested at nominal Mach numbers of 12, 14, and 16 and a range of Reynolds numbers at each Mach number. Details of the test conditions and run schedule are given in Table I. Data obtained were skin friction, heat transfer rates, pressure, and schlieren photographs. Tabulated skin friction, heat transfer and pressure data are given in Tables II, III, and IV, respectively. Skin friction, heat transfer and pressure plots are given in Figures 16, 17, and 18 respectively. The fairing of the data distributions was done to emphasize the distribution indicated by the data. Figures 19 and 20 are correlations which were generated according to the method of Reference 15 and supplied by the AFFDL for the skin friction and heat transfer data. The correlations will be discussed further in the last part of this section. Schlieren photographs for the two-dimensional model tests comprise Figure 21.

All the runs made on the two-dimensional models were laminar and the data gave no indications of separation. The tendency of the boundary layers to "fill-in" the models and reduce the effective turning reduced the pressure rise substantially from the inviscid values for the lower Reynolds number runs. In fact, for model $2D_1$ the boundary layer displacement effect made the effective surface more like a wedge than a continuous adverse gradient. Most of the plotted data give fairly smooth distributions as expected. The small irregularities in the distributions could be caused by surface imperfections on the models or scatter in the instrumentation performance. Examination of the data for runs 33, 34 and 39 (Figures 16, 17, and 18), indicate that at the high Reynolds number condition (Run 33) the data distributions are actually smoother than for the lower Reynolds number runs. If the scatter in the distributions was caused by model contour irregularities the highest scatter should be exhibited by those runs having the thinner boundary layers(higher Reynolds number). Hence, as mentioned in Section II,

it is concluded that any flow perturbations caused by the contour error for Model 2D2 are within the accuracy of the instrumentation and therefore not discernible. The obvious irregularities in the skin friction distributions on Model 2D2 for runs 34-40 (Figures 16a-16c) can not be explained except to say that the data traces from skin friction positions 4 and 5 on these runs indicated that noise and/or base line drift may have been a factor.

The apparent double shock from the leading edge, which can be seen in some of the schlieren photographs in Figure 21, is believed to be caused by waviness of the leading edges. Note that as the Reynolds number decreases (increasing boundary layer thickness) the structure of the leading edge shock becomes thinner and appears to be a single shock. This behavior is expected since the amount of waviness of the leading edge is fixed and the increased boundary layer thickness tends to smooth out the effective leading edge. Reference 2 also contains schlieren photographs which indicate this apparently thick bow shock structure. For this program the leading edge imperfections indicated by the schlieren photographs are not considered to be important because all data were taken at 5 or more inches downstream of the leading edge.

The horizontal bar, seen in Figure 21 across the bottom quarter of the schlieren window, can be used as a scale for making measurements on the photographs. The height of this bar is one inch in all of the schlieren photographs of the two-dimensional model tests. Spots seen in the schlieren photographs are in the optical system and not in the flow field.

## 2. AXISYMMETRIC MODEL TESTS

These models were tested at nominal Mach numbers of 7.5, 12, 14, and 16 with a Reynolds number variation at each Mach number. Details of the test conditions and run schedule are given in Table V. Data obtained were skin friction, heat transfer rates, pressure, and schlieren photographs. Tabulated skin friction, heat transfer and pressure data are given in Tables VI, VII, and VIII, respectively. Skin friction, heat transfer, and pressure plots are given in Figures 22, 23 and 24, respectively. The fairing of the data distributions was done to emphasize the distribution indicated by the data. Figures 25 and 26 are correlations supplied by AFFDL for the skin friction and heat transfer data. The correlations will be discussed further in the last part of this section. All of the schlieren photographs for the axisymmetric model tests comprise Figure 27.

Localized separation or incipient separation occurred for both models A/20 and A/50 for several conditions of the test. Incipient separation, as used in this report, refers to the condition in which the wall shear is positive but appreciably less than the value indicated by other skin friction gages in the same vicinity on the model. Separated skin friction data has been included in the report tables but of course the negative skin friction data could not be shown on the log plots used. Localized separation occurred for those test conditions and models which produced the larger adverse pressure

gradients. For model A/20 incipient separation occurred at the maximum Reynolds number condition at Mach 12 and 14.3 and for A/50 at all test conditions except for the high Reynolds number run at Mach number 8 which produced a turbulent boundary layer on the model. Locally detached flows occurred for A/50 at the lower Mach numbers but for A/20 at Mach number 8, where separation was anticipated, the skin friction gage in position seven, the position at which separation first appears, malfunctioned for some unknown reason and no data were obtained.

The data from this test program reflect the effects of the interaction of the model boundary layer and the inviscid flow field. Boundary layer displacement of the local inviscid flow field on an adverse pressure gradient model typical of hypersonic inlet compression surfaces can change the skin friction, heat transfer and pressure distributions on the model surface significantly for flow conditions which produce appreciable boundary layer thicknesses. The gross effect of the boundary layer on an adverse pressure gradient model is to decrease the adverse gradient below the gradient expected for the inviscid model contour. The boundary layer thickness decreases upon entering the compression region of the model due to the increase in local pressure. This decrease in boundary layer thickness in the flow direction along the model reduces the amount of turning experienced by the flow passing over the model and hence decreases the pressure rise which implies that the local flow Mach number is higher than for the inviscid flow case. A stable condition is established when the local static pressure, determined by the inviscid model contour and the boundary layer displacement thickness, equals the static pressure corresponding to the local flow Mach number. The thicker the boundary layer is on the forward portion of the model the greater is the "thinning" which takes place in the compression region and the larger is the reduction of the model adverse pressure gradient. In fact, the test results for models A/20 and A/50, at sufficiently high Mach number to Reynolds number ratios (thick boundary layers), indicated that the adverse pressure gradients were reduced sufficiently to allow the boundary layer to remain attached whereas for the low Mach number to Reynolds number ratio runs (thin boundary layers) the model pressure distributions approached the inviscid results, giving a larger adverse pressure gradient and separation occurred. The skin friction and heat transfer distributions on the models correspond to the model pressure resulting from the viscous inviscid flow's interaction and not to the inviscid pressure distributions. Consequently for thick boundary layers model heat transfer and skin friction distributions calculated from the inviscid pressure distributions can be grossly in error.

Most of the test runs were made at conditions which gave a laminar boundary layer over the entire length of the models, however runs 27, 28, 30 and 32 did produce natural transition at Mach 7.5 on the model as can be seen by examining the model data, Figures 22 (j, k, l), 23 (j, k, l) and 24 (j, k. l), or the schlieren photographs, Figures 27u, 27v, and 27w. In fact, most of the skin friction and heat transfer data were lost on run 27 (see Figures 22j and 23j) because laminar flow was expected and transition occurred. An examination of the data for runs 31 and 32 shows the difference in behavior of a laminar and turbulent boundary layer with regards to separ-

ation. Examination of the pressure data (Figure 24) shows that in the turbulent run (run 32) the adverse pressure gradient was as large or larger than the laminar run (31) but the skin friction (Fig. 22) and heat transfer (Fig. 23) data indicate that the turbulent boundary layer remained attached and the laminar one separated as would be expected from theoretical predictions (Ref. 16).

Figure 28 shows typical skin friction and heat transfer raw data for separated and attached flow. The data traces were taken from runs at Mach number 12. The attached data are from run 20 and the separated data are from run 23. Both the separated skin friction and heat transfer traces indicate that it took approximately 2 milliseconds or less to establish stabilized separated flow at the test conditions of the run. The minimum of 5 milliseconds of steady flow test time available was sufficient to establish and make measurements in the separated region for most test runs made. Skin friction data from run 21 position 8, run 25 position 6 and run 31 positions 8 and 9 indicates that the separated regions were not fully stabilized during the test times. Although instrumentation in the fully detached flow areas indicated steady values for these runs, the gages specified above which were adjacent to the separated regions gave positive shears which were steadily decreasing with time. For these unsteady measurements, the value of skin friction listed in the data tables is the value measured at the time the skin friction in the fully detached region stabilized.

The superiority of the skin friction gages in detecting separation compared to heat transfer, pressure or schlieren instrumentation can be seen in Figures 22, 23, 24 and 28. Heat transfer gages, used in conjunction with skin friction gages, will provide additional confirmation that separation has occurred but used alone it would be necessary to have very good theoretical predictions of the attached boundary layer heat transfer rates in order to discern separation. Pressure instrumentation on the model was spaced at the same axial stations as the skin friction gages in the adverse pressure gradient regions but the very localized region of separation covered such a small area (sometimes only one skin friction gage was affected) that the pressure plateau characteristic of separation was very small or not observable at all. Pressure data for runs 21, 23 and 31 (Figures 24h and 24l) do indeed show a slight plateau where separation was indicated by skin friction gages 6 and 7 (Figures 22h and 22l). However, on run 22 skin friction position 7 (Figure 22h) indicated separation but the pressure data do not show this as can be seen in Figure 24h. For small regions of separation, such as those encountered in these tests, the deviation from the attached boundary layer pressure distribution is sufficiently small that its detection by pressure measurements alone is quite uncertain. On the other hand, one skin friction gage measuring wall shear which is a vector quantity, gives a distinctive indication of separation.

The schlieren photographs, i.e., Figure 27s or 27x reveal little or perhaps nothing about the separated flow. Knowing from the skin friction data that separation did occur, it may be possible to detect a shock wave ahead of the region, but this is highly debatable because of the small scale of

the separation region. The support sting on the rear of the axisymmetric models is 2.04 inches in diameter and can be used as a reference for making measurements on the schlieren photographs. Examination of the no-flow schlieren photograph of Figure 27y indicates that the spots in the schlieren photographs are in the optical system and not in the flow field. Waviness in the model shock wave is felt to be indicative of freestream flow steadiness and is typical of shock tunnel schlieren photographs.

Note that skin friction position 2 on the axisymmetric models appears to be reading high compared to the other skin friction data. A post-test inspection of the skin friction gage alignment indicated that this gage diaphragm was protruding from the model surface as much as 0.003 of an inch. Qualitatively the effect of a protruding gage gives the observed result and the data were faired below position 2 data for all skin friction plots. Data from position 2 was not dropped, however, because the amount it is in error is not known. Additional discussion on the accuracy of skin friction gage in position 2 is presented in Section VII. Skin friction position 3 on the axisymmetric models was not used for any of the test runs. The gage for this position failed just prior to testing and a spare was not available.

## 3. CORRELATION OF SKIN FRICTION AND HEAT TRANSFER DATA*

The correlation of heat transfer data in the adverse pressure gradient region of the axisymmetric and two-dimensional models was accomplished by using parameters similar in form to those described in Reference 17 which had been successful in correlating favorable pressure gradient flows. Reference 17 used a correlation of the form

$$M_\infty^3 C_H = \frac{M_\infty^3 \dot{q}_M}{\rho_\infty U_\infty (H_o - H_M)} \text{ versus } \bar{\chi} = \frac{M_\infty^3 \sqrt{C}}{\sqrt{Re_{\infty, x}}} \qquad (9)$$

where C is the Chapman-Rubesin constant. This correlation was successful for heat transfer measurements in the leading edge interaction region for sharp edge two-dimensional models. Applying this equation to the data did not result in a valid correlation. However, if local flow conditions are used in the equation, then the data in the viscid-inviscid flow interaction on the compression surface does correlate which can be seen in Figures 20 and 26.

$$M_L^3 C_H = \frac{M_L^3 \dot{q}_M}{\rho_L U_L (H_o - H_M)} \text{ versus } \bar{\chi} = \frac{M_L^3 \sqrt{C}}{\sqrt{Re_{L, x}}} \qquad (10)$$

---

* Correlation work was performed by the AFFDL; for additional details see Reference 15.

In this equation, the local flow conditions at the edge of the boundary layer were determined by combining the measured tunnel conditions and experimental surface static pressure distributions with calculations of the total pressure recovery across the shock, taking into account the viscous effects on the shock pressure recovery (see Reference 15). The normal static pressure gradient through the boundary layer was assumed to be zero and hence, the flow conditions at the edge of the boundary layer were determined.

A similar correlation for the skin friction was employed of the form

$$M_L^3 \, C_{f_L} = \frac{M_L^3 \, \tau_M}{\frac{1}{2} \rho_L U_L^2} \quad \text{versus} \quad \bar{\chi} = \frac{M_L^3 \sqrt{C}}{\sqrt{Re_{L,x}}} \qquad (11)$$

The results can be found in Figures 19 and 25. This correlation does not account for pressure gradient effects and consequently there is an increasing divergence from the correlation for the strong adverse gradients when $\bar{\chi}$ decreases. This is particularly evident for the high compression A/20 and A/50 model data as shown in Figure 25. Skin friction data which is near separation will not correlate on this basis, although the heat transfer measurements in the separated region should correlate, but with increased scatter. For the two-dimensional models, the skin friction data correlates well on the basis of Equation (3). As shown in Figure 19, the 2D1 data correlates better than the 2D2 model data as a result of milder adverse pressure gradients.

# SECTION VII

# PRECISION OF DATA

## 1. TEST CONDITIONS

### a. Supply Conditions

The data reduction program computes free-stream static pressure from the following equation:

$$P_\infty = \left(\frac{P}{P_p}\right)\left(1 + 0.2 M_\infty^2\right)^{-3.5} P_0$$

where $(P/P_p)$ is the real gas correction for static to total pressure ratio and is not subject to error in an individual program.

Next consider the effect of $M_\infty$ on static pressure. Each nozzle-throat combination employed is calibrated previous to its use on a program by measuring the ratio of stagnation to reservoir pressure. The computed values of free-stream Mach number from a large number of runs at a given condition is used to calculate a standard deviation in nominal Mach number at that condition and these deviations are as follows:

| Nozzle | Nominal Mach Number | Standard Deviation | |
|---|---|---|---|
| | | $P_0 \leq 1000$ psi | $P_0 > 1000$ psi |
| A | 7.5 | ±0.0289 | ±0.0321 |
| D | 12 | not available | ±0.0583 |
| D | 14 | ±0.036 | ±0.148 |
| D | 16 | ±0.321 | ±0.172 |

Assuming a normal error distribution in the calibration, then the RMS Mach number value may be assumed to determine the actual value of $M_\infty$. The validity of this conclusion may be seen by an analysis of stagnation and reservoir pressure errors as they effect $M_\infty$. The ratio of stagnation to reservoir pressure can be expressed as:

$$\frac{P_0'}{P_0} = \left(\frac{6 M_\infty^2}{M^2+5}\right)^{7/2}\left(\frac{6}{7M_\infty^2-1}\right)^{5/2}$$

but since we are concerned with $M_\infty \geq 7.5$, a reasonable assumption is

$$M_\infty^2 + 5 \approx M_\infty^2, \quad \text{and} \quad 7M_\infty^2 - 1 \approx 7M_\infty^2$$

$$\therefore \frac{P_0'}{P_0} = \left(\frac{6M_\infty^2}{M_\infty^2+5}\right)^{7/2}\left(\frac{6}{7M^2}\right)^{5/2} = \frac{C}{M_\infty^5}$$

consider a change in pitot pressure $dP_o'$

$$\frac{1}{P_o} dP_o' = -\frac{5C\,dM_\infty}{M_\infty^6}$$

or

$$\frac{dP_o'}{P_o'} \quad \frac{P_o'}{P_o} = -\frac{5C\,dM_\infty}{M_\infty^6}$$

but $P_o' / P_o = C/M_\infty^5$

$$\therefore \frac{dP_o'}{P_o'} = -\frac{5C\,dM_\infty}{M_\infty^6} \quad \frac{M_\infty^5}{C} = -\frac{5\,dM_\infty}{M_\infty}$$

Similarly

$$\frac{dP_o}{P_o} = 5\,\frac{dM_\infty}{M_\infty}$$

Therefore, a 1% error in $M_\infty$ can be caused by a 5% error in pitot pressure.

Using the "most probable error" analysis (Ref. 18) we arrive at

$$\frac{dM_\infty}{M_\infty} = \sqrt{\frac{1}{25}\left(\frac{dP_o}{P_o}\right)^2 + \frac{1}{25}\left(\frac{dP_o'}{P_o'}\right)^2}$$

Based on the agreement of pressure transducers, the nozzle supply pressure measurements are considered accurate to ±7.5% for the runs with $P_o \leq 1000$ psi and ±2.45% for the runs having $P_o > 1000$ psi. Pitot measurements are accurate to within ±5%. It can be seen that the most probable error for $M_\infty$ is ±1.8% and ±1.11% for the low and high pressure conditions, respectively. The errors in $M_\infty$ due to pressure measurement errors are equal to or greater than the actual standard deviations in Mach number, hence negligible error are introduced into the free-stream static pressure calculation by way of the initial tunnel calibration.

However, since a large number of runs are not made at one condition during a test program, the effect of a single measurement of $p_o$ and $M_i$ on $M_\infty$ as taken from the calibration data must be considered. Fortuitously, a small percentage difference in $p_o$ or $M_i$ yields a neglibible percentage difference in $M_\infty$.

$$\frac{d\,(\Delta M_\infty / M_\infty)}{d\,(\Delta p_o / p_o)} << 1, \qquad \frac{d\,(\Delta M_\infty / M_\infty)}{d\,(\Delta M_i / M_i)} << 1$$

Therefore, errors in $M_\infty$ due to 7.5% and 1% possible errors in $p_o$ and $M_i$, respectively, can be neglected. The precision with which $P_\infty$ is measured, therefore, becomes approximately equivalent to the precision of measuring $p_o$ (i.e., ±7.5 for low pressure runs and ±2.45% for high pressure runs).

## 2. SKIN FRICTION

The errors involved in calibrating the skin friction gages are the following:

| | |
|---|---|
| Calibrating weight errors | ±0.4% |
| Metric diaphragm diameter | ±0.22% |
| Reduction of calibration data | ±2% |

Taking the square root of the sum of the squares of these errors gives an overall error for the calibrations of ±2.4%. The skin friction gage pre- and post-test calibrations actually agreed to within ±3% for all models. Linearity of all skin friction gages is within ±2% as determined from the calibrations.

To assess the accuracy of the test data it is necessary to consider calibration accuracy, the Navcor recording equipment resolution, and trace reading accuracy. The calibrations are known to within ±3%. Navcor error is about ±0.05 volts which produces an error of ±1% assuming a five volt data output. Maximum error in the data reduction trace reading is ±2%. Combining these gives a "most probable error" (Ref. 18) of ±3.8%.

Some other sources of error which are pertinent to individual skin friction gages and/or run conditions are pressure sensitivity, acceleration sensitivity, gage alignment with the model surface, and small outputs which increase the error due to Navcor resolution. Pressure and acceleration sensitivity is minimized by design of the skin friction gage. Gage alignment in the model is checked under a microscope and is initially to within ±0.0005 inch of the model surface. Recording equipment gains are in general, set to avoid small run outputs as much as possible. Instances where the above sources of error were greater than the majority of the data are summarized in the following table. The next two paragraphs will briefly discuss the remarks given in the table concerning pressure sensitivity and negative shear measurements.

| Position | Model | Est. Max. Error % | Remarks |
|---|---|---|---|
| 2 | A/10, A/20, A/50 | +10 | Gage protruding from model surface |
| 7 | A/20 | +10 | At high pressure, low skin friction conditions - run 30 |
| 10 | A/20 | -10 | At high pressure, low skin friction conditions - run 30 |
| 6 | A/50 | ±25 | For negative skin friction measurements only |
| 7 | A/50 | ±15 | For negative skin friction measurements only |
| 9 | A/50 | -8% | At high pressure, low skin friction conditions - run 31 |

Pressure sensitivity, i.e., output in response to pressure, of the skin friction gages is nominally 0.0007 of the shear sensitivity or less. The error in measured skin friction caused by pressure sensitivity is a function of the gage relative sensitivity to pressure and the ratio of skin friction to pressure to which the gage is exposed. Skin friction position 7 and 10 on A/20 and position 9 on A/50 had pressure sensitivities of 0.002, 0.0018 and 0.0012 respectively and were subjected to a pressure and skin friction environment which could produce a pressure sensitivity error of the magnitude given in the above table. The specific runs for which this worst condition of pressure error occurred are noted in the "Remarks" section of the above table.

Low amplifier gain settings were used for the skin friction gages which were expected to measure negative shears because of uncertainties in the estimated outputs. Consequently the resulting outputs to be recorded by the Navcor System were typically less than 1.0 volt and a consideration of the ±.05 volts resolution capability of the system gives the errors quoted in the above table. If higher amplifier gains had been used the negative skin friction data would have been as accurate as the shear data taken in the attached flow.

Except for the data points listed in the above table, the skin friction data have a maximum error due to pressure sensitivity of ±4 percent which when added to the "most probable error" of ±3.8% computed above gives an overall maximum error of ±7.8 percent. It should be noted that the ±4 percent pressure sensitivity error is computed for those gages, gage locations and test conditions giving the maximum error. The majority of the skin friction data have a smaller pressure sensitivity error because the test conditions and gage locations were such as to give a larger ratio of measured skin friction to measured pressure. The resulting accuracy for most of the skin friction data then becomes about ±5 percent.

## 3. HEAT TRANSFER

The characteristics of the heat transfer gages depend upon the thermal product ($\sqrt{\rho c K}$) and the change of resistance with temperature. The RMS deviation in the value of $\sqrt{\rho c K}$ for these gages is ±1.6%. The instantaneous surface temperature and the resistance are determined to within 1%. A series of shock tunnel tests designed to determine repeatability of the heat transfer data has shown that the RMS deviation of the repeatability is ±3%. Combining these results indicates that the relative RMS deviation of the heat transfer data is about ±3.7%.

## 4. PRESSURE

The pressure transducers are accurate to ±1% of their maximum calibration pressure. On the basis of consistency and repeatability of the pressure data, it is estimated that these data are accurate to within ±4%.

# SECTION VIII

# CONCLUSIONS

Hypersonic shock tunnel tests were conducted on two two-dimensional and three axisymmetric compression bodies typical of hypersonic inlet compression surfaces to obtain wall skin friction data in adverse pressure gradients. The models were instrumented in the continuous compression (adverse pressure gradient) regions with skin friction, heat transfer and pressure instrumentation. The two-dimensional models were tested at Mach numbers of 12, 14 and 16 and the axisymmetric models at 8, 12, 14 and 16 with a Reynolds number variation at each Mach number for each model. Wall measurements were obtained in the adverse pressure gradient regions for both attached and separated boundary layers. For most of the test runs made, the tailored-interface shock tunnel test time was sufficient to establish steady separated boundary layer flow. Comparisons of skin friction, heat transfer, pressure and schlieren data show the superiority of skin friction measurements in detecting localized separation. Whereas pressure and heat transfer instrumentation measure scalar quantity, skin friction instrumentation measures a vector quantity, i.e., magnitude and direction. It should also be noted that although good quality schlieren photographs were obtained for most runs of the test program, boundary layer separation was not readily discernible due to the small scale of the separated flow region.

For slender bodies typical of compression surfaces used in hypersonic inlets the interaction of the local inviscid flow and the model viscous boundary layer produces a pressure distribution (and a corresponding skin friction and heat transfer distribution) on the model which can be appreciably different from the pressure distribution obtained considering only the model inviscid contour. The phenomenological explanation of this interaction is that the aerodynamically effective shape of a body is determined by the body's geometrical contour plus the boundary layer displacement thickness and the effective shape determines a model pressure distribution which in turn implies a local inviscid flow Mach number distribution which in turn affects the boundary layer growth, etc. This interaction reaches a stable condition when the pressure at the edge of the boundary layer (which is the same as the model pressure in classical boundary layer theory) is the same as the local inviscid static pressure distribution. Obviously the interaction effect is more significant for slender bodies, where small changes in the effective contour of the model can produce appreciable percentage changes in the pressure distribution, than for blunt bodies and also is more important for high Mach number low Reynolds number flows where boundary layer thickness is appreciable when compared to local body thickness. The data obtained in this test program show the effects of this inviscid-viscid flow interaction quite clearly and is most easily recognized by examining the results for models A/20 and A/50 which had the highest compression ratios of all the models tested. The size of the separated flow regions became smaller, and in some cases vanished completely, as the ratio of Mach number to

Reynolds number became larger (thicker boundary layers). Measured pressure distributions confirm that the pressure gradient is becoming smaller as the boundary layer thickness increases. The two-dimensional models did not produce a large enough adverse pressure gradients to separate the boundary layers at any of the test conditions but the interaction of the boundary layer and the inviscid flow was still readily apparent. The pressure distribution on model 2D1 is very much like a wedge distribution even though the actual contour of the model was a continuous compression surface. The boundary layer "filled-in" the model contour giving it an effective wedge shape.

Although the test program was designed to obtain data for laminar boundary layers only, boundary layer transition occurred on the axisymmetric models at Mach number 8 and provided some information on the effects of adverse pressure gradients on turbulent boundary layers. The data indicate that a turbulent boundary layer can negotiate a greater adverse pressure gradient than a laminar boundary layer without separating, which is in agreement with theory and other experiments. A turbulent boundary layer inherently has more momentum than a laminar boundary layer because the velocity in a turbulent layer increases to approximately the inviscid flow velocity within a short distance of the wall whereas in a laminar layer a larger portion of the flow is at a low velocity. Consequently, the greater momentum of the turbulent layer requires a larger adverse pressure gradient to slow the flow and force the skin friction at the wall to zero.

A reasonable correlation of the model heat transfer and skin friction data can be accomplished using local flows properties in flat plate type correlation parameters which do not account for a pressure gradient over the models. Hence the quality of the correlations decreases as the adverse pressure gradient increases.

# SECTION IX

# REFERENCES


1. Hertzberg, A., Wittliff, C.E., and Wilson, M.R.: "The Tailored-Interface Hypersonic Shock Tunnel," Journal of the Aerospace Sciences, Vol. 26, No. 4, April 1959, pp. 219-228.

2. Harshman, D.L. et al: "Analytical and Experimental Evaluation of Inlet Compression Systems in the Mach Range 10 to 25," ASD-TDR 63-629, September 1963.

3. Sanator, R.J. et al: "Experimental and Theoretical Investigation of Inlets for Supersonic Combustion Ramjets", FDL-TDR 64-119, October 1964.

4. MacArthur, R.C.: "Transducer for Direct Measurement of Skin Friction in the Hypersonic Shock Tunnel," Cornell Aeronautical Laboratory, Inc., Report No. 129, August 1963.

5. Vidal, R.J.: "Transient Surface Temperature Measurements," Cornell Aeronautical Laboratory, Inc., Report No. 114, March 1962.

6. Martin, J.F., Duryea, G.R., and Stevenson, L.M.: "Instrumentation for Force and Pressure Measurements in a Hypersonic Shock Tunnel," CAL Report No. 113, January 1962.

7. Reece, J.W.: "Shock Tube Theory for Real Air with Applications to Wind Tunnel Testing and to Flight Simulation," CAL Experimental Facilities Division, WTH-003, October 1958 (Revised August 1959).

8. Wittliff, C.: Unpublished Normal Shock Calculations using Duff's Computing Procedure, Aerodynamics Research Department, CAL about 1963.

9. Lewis, Clark H. and Burgess, E.G.: "Charts of Normal Shock Wave Properties in Inperfect Air," AEDC-TDR-64-43, March 1964.

10. Hilsenrath, J., Beckett, C.W., et al: "Tables of Thermal Properties of Gases," National Bureau of Standards Circular 564, November 1955.

11. Reece, J.W.: "Test Section Conditions Generated in the Supersonic Expansion of Real Air," Reader's Forum, Journal of Aerospace Science, Vol. 29, No. 5, May 1962, pp. 617-618.

12. Neel, C.A. and Lewis, Clark H.: "Interpolations of Imperfect Air Thermodynamic Data, II, at Constant Pressure," AEDC-TDR-64-184, September 1964.

13. Hirschfelder, J.O., Curtis, C.F., and Bird, R.G.: Molecular Theory of Gases and Liquids, J. Wiley and Sons, 1954.

14. Hansen, C F.: "Approximations for Thermodynamic and Transport Properties of High-Temperature Air," NACA TN-4150, March 1958 (Revised NASA TR-50, 1959).

15. Richey, G. K." "An Analysis of the Laminar Boundary Layer-Inviscid Flow Interaction at Hypersonic Speeds," AIAA Paper No. 65-659, June 1965.

16. Schlichting, H.: Boundary Layer Theory, McGraw-Hill Book Co., 1960.

17. Cheng, H.K. et al: "Boundary Layer Displacement and Leading Edge Bluntness Effects in High Temperature Hypersonic Flow," J. Aero. Science, Vol. 28, No. 5, May 1961.

18. Topping, J: "Errors of Observation and their Treatment," Unwin Brothers Ltd., Woking and Londen, 1955.

Table I

RUN SCHEDULE AND TEST CONDITIONS FOR THE TWO-DIMENSIONAL MODEL TESTS

| RUN NO. | 33 | 34 | 35 | 36 | 38 | 39 |
|---|---|---|---|---|---|---|
| ATTACK | 0. | 0. | 0. | 0. | 0. | 0. |
| YAW | 0. | 0. | 0. | 0. | 0. | 0. |
| ROLL | 0. | 0. | 0. | 0. | 0. | 0. |
| M(I) | 4.600E 00 | 4.705E 00 | 4.230E 00 | 4.260E 00 | 4.494E 00 | 4.680E 00 |
| P(0) | 3.788E 03 | 1.445E 03 | 4.184E 03 | 2.069E 03 | 4.156E 03 | 5.891E 02 |
| H(0) | 3.192E 07 | 3.335E 07 | 2.754E 07 | 2.814E 07 | 3.124E 07 | 3.365E 07 |
| T(0) | 4.523E 03 | 4.683E 03 | 3.992E 03 | 4.062E 03 | 4.451E 03 | 4.715E 03 |
| M | 1.225E 01 | 1.182E 01 | 1.438E 01 | 1.399E 01 | 1.687E 01 | 1.163E 01 |
| U | 7.859E 03 | 8.024E 03 | 7.333E 03 | 7.407E 03 | 7.835E 03 | 8.055E 03 |
| T | 1.714E 02 | 1.919E 02 | 1.082E 02 | 1.167E 02 | 8.984E 01 | 1.998E 02 |
| P | 1.588E-02 | 7.271E-03 | 6.467E-03 | 3.723E-03 | 1.994E-03 | 3.251E-03 |
| Q | 1.668E 00 | 7.109E-01 | 9.363E-01 | 5.100E-01 | 3.970E-01 | 3.077E-01 |
| RHO | 7.778E-06 | 3.179E-06 | 5.014E-06 | 2.677E-06 | 1.862E-06 | 1.365E-06 |
| MU | 1.432E-07 | 1.597E-07 | 9.104E-08 | 9.816E-08 | 7.558E-08 | 1.660E-07 |
| RE/FT. | 4.268E 05 | 1.597E 05 | 4.039E 05 | 2.020E 05 | 1.931E 05 | 6.625E 04 |
| PITOT | 3.125E 00 | 1.333E 00 | 1.748E 00 | 9.526E-01 | 7.433E-01 | 5.769E-01 |
| T* | 1.019E 03 | 1.046E 03 | 9.305E 02 | 9.421E 02 | 1.007E 03 | 1.051E 03 |
| MU* | 6.064E-07 | 6.169E-07 | 5.706E-07 | 5.754E-07 | 6.017E-07 | 6.189E-07 |
| SQRT.C* | 8.439E-01 | 8.419E-01 | 8.539E-01 | 8.523E-01 | 8.428E-01 | 8.419E-01 |
| H(M) | 3.183E 06 | 3.183E 06 | 3.183E 06 | 3.183E 06 | 3.183E 06 | 3.183E 06 |
| T(M) | 5.300E 02 | 5.300E 02 | 5.300E 02 | 5.300E 02 | 5.300E 02 | 5.300E 02 |
| P(TS) | 1.934E-05 | 1.934E-05 | 1.934E-05 | 1.934E-05 | 1.934E-05 | 1.934E-05 |
| MODEL | $2D_2$ | $2D_2$ | $2D_2$ | $2D_2$ | $2D_2$ | $2D_2$ |

Table I (Cont'd.)

| RUN NO. | 40 | 41 | 42 | 43 | 44 | 45 |
|---|---|---|---|---|---|---|
| ATTACK | 0. | 0. | 0. | 0. | 0. | 0. |
| YAW | 0. | 0. | 0. | 0. | 0. | 0. |
| ROLL | 0. | 0. | 0. | 0. | 0. | 0. |
| M(I) | 4.153E 00 | 4.759E 00 | 4.702E 00 | 4.677E 00 | 4.342E 00 | 4.262E 00 |
| P(0) | 5.309E 02 | 4.000E 03 | 1.512E 03 | 5.558E 02 | 4.190E 03 | 2.072E 03 |
| H(0) | 2.707E 07 | 3.408E 07 | 3.354E 07 | 3.314E 07 | 2.899E 07 | 2.821E 07 |
| T(0) | 3.930E 03 | 4.778E 03 | 4.708E 03 | 4.651E 03 | 4.171E 03 | 4.071E 03 |
| M | 1.342E 01 | 1.215E 01 | 1.183E 01 | 1.162E 01 | 1.429E 01 | 1.399E 01 |
| U | 7.257E 03 | 8.119E 03 | 8.048E 03 | 7.994E 03 | 7.522E 03 | 7.417E 03 |
| T | 1.217E 02 | 1.86CE 02 | 1.925E 02 | 1.971E 02 | 1.154E 02 | 1.171E 02 |
| P | 1.260E-03 | 1.701E-02 | 7.517E-03 | 3.111E-03 | 6.565E-03 | 3.724E-03 |
| Q | 1.589E-01 | 1.756E 00 | 7.370E-01 | 2.940E-01 | 9.384E-01 | 5.100E-01 |
| RHO | 8.690E-07 | 7.673E-06 | 3.277E-06 | 1.325E-06 | 4.776E-06 | 2.670E-06 |
| MU | 1.023E-07 | 1.55CE-07 | 1.602E-07 | 1.638E-07 | 9.701E-08 | 9.843E-08 |
| RE/FT. | 6.164E 04 | 4.019E 05 | 1.646E 05 | 6.463E 04 | 3.703E 05 | 2.012E 05 |
| PITOT | 2.966E-01 | 3.295E 00 | 1.382E 00 | 5.511E-01 | 1.754E 00 | 9.528E-01 |
| T* | 9.203E 02 | 1.062E 03 | 1.050E 03 | 1.040E 03 | 9.603E 02 | 9.437E 02 |
| MU* | 5.664E-07 | 6.230E-07 | 6.185E-07 | 6.148E-07 | 5.829E-07 | 5.761E-07 |
| SQRT.C* | 8.557E-01 | 8.392E-01 | 8.414E-01 | 8.431E-01 | 8.496E-01 | 8.521E-01 |
| H(M) | 3.183E 06 | 3.183E 06 | 3.183E 06 | 3.183E 06 | 3.183E 06 | 3.183E 06 |
| T(M) | 5.300E 02 | 5.300E 02 | 5.300E 02 | 5.300E 02 | 5.300E 02 | 5.300E 02 |
| P(TS) | 1.934E-05 | 1.934E-05 | 1.934E-05 | 1.934E-05 | 1.934E-05 | 1.934E-05 |
| MODEL | $2D_2$ | $2D_1$ | $2D_1$ | $2D_1$ | $2D_1$ | $2D_1$ |

Table I (Concluded)

| RUN NO. | 46 | 47 | 48 | 49 |
|---|---|---|---|---|
| ATTACK | 0. | 0. | 0. | 0. |
| YAW | 0. | 0. | 0. | 0. |
| ROLL | 0. | 0. | 0. | 0. |
| M(I) | 4.200E 00 | 4.414E 00 | 4.500E 00 | 4.337E 00 |
| P(0) | 5.327E 02 | 3.844E 03 | 3.063E 03 | 5.212E 02 |
| H(0) | 2.753E 07 | 3.010E 07 | 3.135E 07 | 2.938E 07 |
| T(0) | 3.986E 03 | 4.312E 03 | 4.462E 03 | 4.215E 03 |
| M | 1.338E 01 | 1.694E 01 | 1.677E 01 | 1.567E 01 |
| U | 7.318E 03 | 7.691E 03 | 7.848E 03 | 7.588E 03 |
| T | 1.245E 02 | 8.579E 01 | 9.121E 01 | 9.759E 01 |
| P | 1.278E-03 | 1.825E-03 | 1.512E-03 | 4.097E-04 |
| Q | 1.602E-01 | 3.667E-01 | 2.975E-01 | 7.044E-02 |
| RHO | 8.616E-07 | 1.785E-06 | 1.391E-06 | 3.523E-07 |
| MU | 1.046E-07 | 7.216E-08 | 7.674E-08 | 8.211E-08 |
| RE/FT. | 6.027E 04 | 1.902E 05 | 1.422E 05 | 3.256E 04 |
| PITOT | 2.991E-01 | 6.859E-01 | 5.570E-01 | 1.317E-01 |
| T* | 9.296E 02 | 9.839E 02 | 1.009E 03 | 9.676E 02 |
| MU* | 5.703E-07 | 5.924E-07 | 6.024E-07 | 5.859E-07 |
| SQRT.C* | 8.543E-01 | 8.461E-01 | 8.425E-01 | 8.483E-01 |
| H(M) | 3.183E 06 | 3.183E 06 | 3.183E 06 | 3.183E 06 |
| T(M) | 5.300E 02 | 5.300E 02 | 5.300E 02 | 5.300E 02 |
| P(TS) | 1.934E-05 | 1.934E-05 | 1.934E-05 | 1.934E-05 |
| MODEL | $2D_1$ | $2D_1$ | $2D_1$ | $2D_1$ |

Table II

TWO-DIMENSIONAL MODEL SKIN FRICTION DATA

| RUN | GAGE | M | TAU(M) |
|---|---|---|---|
| 33 | 1 | 1.225E 01 | 2.801E-03 |
| 33 | 2 | 1.225E 01 | 1.681E-03 |
| 33 | 4 | 1.225E 01 | 1.679E-03 |
| 33 | 5 | 1.225E 01 | 1.652E-03 |
| 33 | 7 | 1.225E 01 | 1.450E-03 |
| 33 | 8 | 1.225E 01 | 1.617E-03 |
| 33 | 9 | 1.225E 01 | 1.856E-03 |
| 33 | 10 | 1.225E 01 | 3.695E-03 |
| 34 | 1 | 1.182E 01 | 1.938E-03 |
| 34 | 2 | 1.182E 01 | 1.076E-03 |
| 34 | 3 | 1.182E 01 | 1.037E-03 |
| 34 | 4 | 1.182E 01 | 1.171E-03 |
| 34 | 5 | 1.182E 01 | 1.122E-03 |
| 34 | 6 | 1.182E 01 | 1.139E-03 |
| 34 | 7 | 1.182E 01 | 1.116E-03 |
| 34 | 8 | 1.182E 01 | 1.165E-03 |
| 34 | 9 | 1.182E 01 | 1.310E-03 |
| 34 | 10 | 1.182E 01 | 2.271E-03 |
| 35 | 1 | 1.438E 01 | 1.982E-03 |
| 35 | 2 | 1.438E 01 | 1.105E-03 |
| 35 | 3 | 1.438E 01 | 1.047E-03 |
| 35 | 4 | 1.438E 01 | 1.105E-03 |
| 35 | 5 | 1.438E 01 | 1.081E-03 |
| 35 | 6 | 1.438E 01 | 8.990E-04 |
| 35 | 7 | 1.438E 01 | 9.882E-04 |
| 35 | 8 | 1.438E 01 | 9.814E-04 |
| 35 | 9 | 1.438E 01 | 9.489E-04 |
| 35 | 10 | 1.438E 01 | 2.163E-03 |
| 36 | 1 | 1.399E 01 | 1.483E-03 |
| 36 | 2 | 1.399E 01 | 7.459E-04 |
| 36 | 3 | 1.399E 01 | 7.632E-04 |
| 36 | 4 | 1.399E 01 | 8.563E-04 |
| 36 | 5 | 1.399E 01 | 8.218E-04 |
| 36 | 6 | 1.399E 01 | 7.020E-04 |
| 36 | 7 | 1.399E 01 | 7.460E-04 |
| 36 | 8 | 1.399E 01 | 7.768E-04 |
| 36 | 9 | 1.399E 01 | 8.159E-04 |
| 36 | 10 | 1.399E 01 | 1.500E-03 |

Table II (Cont'd.)

| RUN | GAGE | M | TAU(M) |
|---|---|---|---|
| 38 | 1 | 1.687E 01 | 1.454E-03 |
| 38 | 2 | 1.687E 01 | 7.698E-04 |
| 38 | 3 | 1.687E 01 | 7.744E-04 |
| 38 | 4 | 1.687E 01 | 8.124E-04 |
| 38 | 5 | 1.687E 01 | 8.349E-04 |
| 38 | 6 | 1.687E 01 | 7.020E-04 |
| 38 | 7 | 1.687E 01 | 7.460E-04 |
| 38 | 8 | 1.687E 01 | 8.312E-04 |
| 38 | 9 | 1.687E 01 | 9.404E-04 |
| 38 | 10 | 1.687E 01 | 1.644E-03 |
| 39 | 1 | 1.163E 01 | 1.318E-03 |
| 39 | 2 | 1.163E 01 | 6.575E-04 |
| 39 | 3 | 1.163E 01 | 6.712E-04 |
| 39 | 4 | 1.163E 01 | 7.365E-04 |
| 39 | 5 | 1.163E 01 | 6.979E-04 |
| 39 | 6 | 1.163E 01 | 6.162E-04 |
| 39 | 7 | 1.163E 01 | 6.849E-04 |
| 39 | 8 | 1.163E 01 | 7.103E-04 |
| 39 | 9 | 1.163E 01 | 7.653E-04 |
| 39 | 10 | 1.163E 01 | 1.228E-03 |
| 40 | 1 | 1.342E 01 | 8.610E-04 |
| 40 | 2 | 1.342E 01 | 4.328E-04 |
| 40 | 3 | 1.342E 01 | 4.130E-04 |
| 40 | 4 | 1.342E 01 | 4.830E-04 |
| 40 | 5 | 1.342E 01 | 4.597E-04 |
| 40 | 6 | 1.342E 01 | 3.757E-04 |
| 40 | 7 | 1.342E 01 | 4.341E-04 |
| 40 | 8 | 1.342E 01 | 4.292E-04 |
| 40 | 9 | 1.342E 01 | 4.585E-04 |
| 40 | 10 | 1.342E 01 | 7.171E-04 |
| 41 | 1 | 1.215E 01 | 2.963E-03 |
| 41 | 2 | 1.215E 01 | 1.889E-03 |
| 41 | 3 | 1.215E 01 | 1.706E-03 |
| 41 | 4 | 1.215E 01 | 1.740E-03 |
| 41 | 5 | 1.215E 01 | 1.655E-03 |
| 41 | 6 | 1.215E 01 | 1.585E-03 |
| 41 | 7 | 1.215E 01 | 1.611E-03 |
| 41 | 8 | 1.215E 01 | 1.670E-03 |
| 41 | 9 | 1.215E 01 | 1.704E-03 |
| 41 | 10 | 1.215E 01 | 2.057E-03 |

Table II (Cont'd.)

| RUN | GAGE | M | TAU(M) |
|---|---|---|---|
| 42 | 1 | 1.183E 01 | 1.961E-03 |
| 42 | 2 | 1.183E 01 | 1.219E-03 |
| 42 | 3 | 1.183E 01 | 1.072E-03 |
| 42 | 4 | 1.183E 01 | 1.046E-03 |
| 42 | 5 | 1.183E 01 | 1.032E-03 |
| 42 | 6 | 1.183E 01 | 1.043E-03 |
| 42 | 7 | 1.183E 01 | 1.058E-03 |
| 42 | 8 | 1.183E 01 | 1.090E-03 |
| 42 | 9 | 1.183E 01 | 1.093E-03 |
| 42 | 10 | 1.183E 01 | 1.247E-03 |
| 43 | 1 | 1.162E 01 | 1.320E-03 |
| 43 | 2 | 1.162E 01 | 7.943E-04 |
| 43 | 3 | 1.162E 01 | 7.248E-04 |
| 43 | 4 | 1.162E 01 | 6.873E-04 |
| 43 | 5 | 1.162E 01 | 6.707E-04 |
| 43 | 6 | 1.162E 01 | 6.709E-04 |
| 43 | 8 | 1.162E 01 | 6.702E-04 |
| 43 | 9 | 1.162E 01 | 6.735E-04 |
| 43 | 10 | 1.162E 01 | 7.346E-04 |
| 44 | 1 | 1.429E 01 | 2.023E-03 |
| 44 | 2 | 1.429E 01 | 1.154E-03 |
| 44 | 3 | 1.429E 01 | 1.012E-03 |
| 44 | 4 | 1.429E 01 | 1.033E-03 |
| 44 | 5 | 1.429E 01 | 1.056E-03 |
| 44 | 6 | 1.429E 01 | 1.075E-03 |
| 44 | 7 | 1.429E 01 | 1.039E-03 |
| 44 | 8 | 1.429E 01 | 1.090E-03 |
| 44 | 9 | 1.429E 01 | 1.136E-03 |
| 44 | 10 | 1.429E 01 | 1.265E-03 |
| 45 | 1 | 1.399E 01 | 1.515E-03 |
| 45 | 2 | 1.399E 01 | 8.956E-04 |
| 45 | 3 | 1.399E 01 | 7.942E-04 |
| 45 | 4 | 1.399E 01 | 7.947E-04 |
| 45 | 5 | 1.399E 01 | 7.596E-04 |
| 45 | 6 | 1.399E 01 | 7.769E-04 |
| 45 | 7 | 1.399E 01 | 7.663E-04 |
| 45 | 8 | 1.399E 01 | 7.668E-04 |
| 45 | 9 | 1.399E 01 | 7.503E-04 |
| 45 | 10 | 1.399E 01 | 8.689E-04 |

Table II (Concluded)

| RUN | GAGE | M | TAU(M) |
|---|---|---|---|
| 46 | 1 | 1.338E 01 | 8.880E-04 |
| 46 | 2 | 1.338E 01 | 5.232E-04 |
| 46 | 3 | 1.338E 01 | 4.770E-04 |
| 46 | 4 | 1.338E 01 | 3.900E-04 |
| 46 | 5 | 1.338E 01 | 4.382E-04 |
| 46 | 6 | 1.338E 01 | 4.148E-04 |
| 46 | 7 | 1.338E 01 | 4.362E-04 |
| 46 | 8 | 1.338E 01 | 4.219E-04 |
| 46 | 9 | 1.338E 01 | 4.364E-04 |
| 46 | 10 | 1.338E 01 | 4.628E-04 |
| 47 | 1 | 1.694E 01 | 1.394E-03 |
| 47 | 2 | 1.694E 01 | 8.481E-04 |
| 47 | 3 | 1.694E 01 | 7.114E-04 |
| 47 | 4 | 1.694E 01 | 6.402E-04 |
| 47 | 5 | 1.694E 01 | 7.171E-04 |
| 47 | 6 | 1.694E 01 | 7.354E-04 |
| 47 | 7 | 1.694E 01 | 6.839E-04 |
| 47 | 8 | 1.694E 01 | 7.633E-04 |
| 47 | 9 | 1.694E 01 | 7.869E-04 |
| 47 | 10 | 1.694E 01 | 8.786E-04 |
| 48 | 1 | 1.677E 01 | 1.340E-03 |
| 48 | 2 | 1.677E 01 | 7.975E-04 |
| 48 | 3 | 1.677E 01 | 6.969E-04 |
| 48 | 4 | 1.677E 01 | 7.108E-04 |
| 48 | 5 | 1.677E 01 | 6.430E-04 |
| 48 | 6 | 1.677E 01 | 6.573E-04 |
| 48 | 7 | 1.677E 01 | 6.531E-04 |
| 48 | 8 | 1.677E 01 | 6.773E-04 |
| 48 | 9 | 1.677E 01 | 7.022E-04 |
| 48 | 10 | 1.677E 01 | 7.718E-04 |
| 49 | 3 | 1.567E 01 | 3.909E-04 |
| 49 | 4 | 1.567E 01 | 3.664E-04 |
| 49 | 5 | 1.567E 01 | 4.048E-04 |
| 49 | 6 | 1.567E 01 | 3.944E-04 |
| 49 | 7 | 1.567E 01 | 4.081E-04 |
| 49 | 8 | 1.567E 01 | 3.951E-04 |
| 49 | 9 | 1.567E 01 | 3.471E-04 |
| 49 | 10 | 1.567E 01 | 4.175E-04 |

Table III

TWO-DIMENSIONAL MODEL HEAT TRANSFER DATA

| RUN | GAGE | Q(AV) |
|---|---|---|
| 33 | 1 | 2.447E 00 |
| 33 | 2 | 1.519E 00 |
| 33 | 3 | 1.961E 00 |
| 34 | 1 | 1.613E 00 |
| 34 | 2 | 9.661E-01 |
| 34 | 3 | 1.163E 00 |
| 34 | 4 | 1.598E 00 |
| 34 | 5 | 1.968E 00 |
| 34 | 6 | 2.186E 00 |
| 35 | 1 | 1.506E 00 |
| 35 | 2 | 9.061E-01 |
| 35 | 3 | 1.019E 00 |
| 35 | 5 | 1.710E 00 |
| 35 | 6 | 1.907E 00 |
| 36 | 1 | 1.062E 00 |
| 36 | 2 | 6.330E-01 |
| 36 | 3 | 7.399E-01 |
| 36 | 5 | 1.108E 00 |
| 36 | 6 | 1.364E 00 |
| 38 | 1 | 1.077E 00 |
| 38 | 2 | 6.126E-01 |
| 38 | 3 | 7.586E-01 |
| 38 | 4 | 9.392E-01 |
| 38 | 5 | 1.226E 00 |
| 38 | 6 | 1.521E 00 |
| 39 | 1 | 9.825E-01 |
| 39 | 2 | 5.612E-01 |
| 39 | 3 | 6.500E-01 |
| 39 | 4 | 7.798E-01 |
| 39 | 5 | 9.543E-01 |
| 39 | 6 | 1.135E 00 |
| 40 | 1 | 5.610E-01 |
| 40 | 2 | 3.020E-01 |
| 40 | 3 | 3.257E-01 |
| 40 | 4 | 3.857E-01 |
| 40 | 5 | 4.734E-01 |
| 40 | 6 | 5.582E-01 |
| 41 | 1 | 2.478E 00 |
| 41 | 2 | 1.433E 00 |
| 41 | 3 | 1.423E 00 |
| 41 | 4 | 1.711E 00 |
| 41 | 5 | 2.111E 00 |
| 41 | 6 | 2.458E 00 |
| 42 | 2 | 8.323E-01 |
| 42 | 3 | 9.054E-01 |
| 42 | 4 | 8.898E-01 |
| 42 | 5 | 1.042E 00 |
| 42 | 6 | 1.142E 00 |
| 43 | 1 | 9.374E-01 |
| 43 | 2 | 5.139E-01 |
| 43 | 3 | 5.201E-01 |
| 43 | 4 | 5.272E-01 |
| 43 | 5 | 5.957E-01 |
| 43 | 6 | 6.401E-01 |
| 44 | 1 | 1.482E 00 |
| 44 | 2 | 7.499E-01 |
| 44 | 3 | 7.950E-01 |
| 44 | 4 | 8.603E-01 |
| 44 | 5 | 1.011E 00 |
| 44 | 6 | 1.169E 00 |
| 45 | 1 | 1.044E 00 |
| 45 | 2 | 5.420E-01 |
| 45 | 3 | 5.561E-01 |
| 45 | 4 | 5.512E-01 |
| 45 | 5 | 6.346E-01 |
| 45 | 6 | 7.328E-01 |
| 46 | 1 | 5.549E-01 |
| 46 | 2 | 3.013E-01 |
| 46 | 3 | 2.895E-01 |
| 46 | 4 | 2.809E-01 |
| 46 | 5 | 3.104E-01 |
| 46 | 6 | 3.485E-01 |
| 47 | 1 | 9.422E-01 |
| 47 | 2 | 5.304E-01 |
| 47 | 3 | 5.143E-01 |
| 47 | 4 | 5.309E-01 |
| 47 | 5 | 6.139E-01 |
| 47 | 6 | 6.998E-01 |
| 48 | 1 | 9.297E-01 |
| 48 | 2 | 5.178E-01 |
| 48 | 3 | 5.182E-01 |
| 48 | 4 | 5.346E-01 |
| 48 | 5 | 5.809E-01 |
| 48 | 6 | 6.607E-01 |
| 49 | 1 | 4.651E-01 |
| 49 | 2 | 2.466E-01 |
| 49 | 3 | 2.453E-01 |
| 49 | 4 | 2.475E-01 |
| 49 | 5 | 2.601E-01 |
| 49 | 6 | 2.824E-01 |

Table IV

TWO-DIMENSIONAL MODEL PRESSURE DATA

| RUN | GAGE | M | P(M) | P(M)/P | P(M)/PITOT |
|---|---|---|---|---|---|
| 33 | 1 | 1.225E 01 | 4.580E-02 | 2.883E 00 | 1.466E-02 |
| 33 | 2 | 1.225E 01 | 5.340E-02 | 3.362E 00 | 1.709E-02 |
| 33 | 3 | 1.225E 01 | 6.433E-02 | 4.050E 00 | 2.059E-02 |
| 33 | 4 | 1.225E 01 | 7.097E-02 | 4.468E 00 | 2.271E-02 |
| 33 | 5 | 1.225E 01 | 9.929E-02 | 6.251E 00 | 3.177E-02 |
| 33 | 6 | 1.225E 01 | 1.432E-01 | 9.013E 00 | 4.581E-02 |
| 33 | 7 | 1.225E 01 | 1.701E-01 | 1.071E 01 | 5.443E-02 |
| 33 | 8 | 1.225E 01 | 1.977E-01 | 1.244E 01 | 6.325E-02 |
| 34 | 2 | 1.182E 01 | 2.237E-02 | 3.077E 00 | 1.678E-02 |
| 34 | 3 | 1.182E 01 | 2.666E-02 | 3.666E 00 | 2.000E-02 |
| 34 | 4 | 1.182E 01 | 3.081E-02 | 4.238E 00 | 2.312E-02 |
| 34 | 5 | 1.182E 01 | 3.889E-02 | 5.349E 00 | 2.918E-02 |
| 34 | 6 | 1.182E 01 | 5.252E-02 | 7.223E 00 | 3.941E-02 |
| 34 | 7 | 1.182E 01 | 6.642E-02 | 9.134E 00 | 4.983E-02 |
| 34 | 8 | 1.182E 01 | 8.178E-02 | 1.125E 01 | 6.135E-02 |
| 35 | 1 | 1.438E 01 | 2.628E-02 | 4.063E 00 | 1.503E-02 |
| 35 | 2 | 1.438E 01 | 2.836E-02 | 4.386E 00 | 1.623E-02 |
| 35 | 3 | 1.438E 01 | 3.427E-02 | 5.299E 00 | 1.960E-02 |
| 35 | 4 | 1.438E 01 | 4.192E-02 | 6.483E 00 | 2.398E-02 |
| 35 | 5 | 1.438E 01 | 5.071E-02 | 7.842E 00 | 2.901E-02 |
| 35 | 6 | 1.438E 01 | 7.584E-02 | 1.173E 01 | 4.338E-02 |
| 35 | 7 | 1.438E 01 | 9.223E-02 | 1.426E 01 | 5.276E-02 |
| 35 | 8 | 1.438E 01 | 1.134E-01 | 1.754E 01 | 6.487E-02 |
| 36 | 1 | 1.399E 01 | 1.535E-02 | 4.122E 00 | 1.611E-02 |
| 36 | 2 | 1.399E 01 | 1.551E-02 | 4.166E 00 | 1.628E-02 |
| 36 | 3 | 1.399E 01 | 1.808E-02 | 4.857E 00 | 1.898E-02 |
| 36 | 4 | 1.399E 01 | 2.150E-02 | 5.774E 00 | 2.257E-02 |
| 36 | 5 | 1.399E 01 | 2.584E-02 | 6.940E 00 | 2.713E-02 |
| 36 | 6 | 1.399E 01 | 3.662E-02 | 9.836E 00 | 3.844E-02 |
| 36 | 7 | 1.399E 01 | 4.633E-02 | 1.244E 01 | 4.863E-02 |
| 36 | 8 | 1.399E 01 | 5.947E-02 | 1.597E 01 | 6.243E-02 |
| 38 | 1 | 1.687E 01 | 1.200E-02 | 6.020E 00 | 1.615E-02 |
| 38 | 2 | 1.687E 01 | 1.183E-02 | 5.932E 00 | 1.591E-02 |
| 38 | 3 | 1.687E 01 | 1.324E-02 | 6.640E 00 | 1.781E-02 |
| 38 | 4 | 1.687E 01 | 1.665E-02 | 8.353E 00 | 2.241E-02 |
| 38 | 5 | 1.687E 01 | 1.814E-02 | 9.101E 00 | 2.441E-02 |
| 38 | 6 | 1.687E 01 | 2.538E-02 | 1.273E 01 | 3.414E-02 |
| 38 | 7 | 1.687E 01 | 3.428E-02 | 1.720E 01 | 4.613E-02 |
| 38 | 8 | 1.687E 01 | 4.628E-02 | 2.321E 01 | 6.226E-02 |

Table IV (Cont'd.)

| RUN | GAGE | M | P(M) | P(M)/P | P(M)/PITOT |
|---|---|---|---|---|---|
| 39 | 1 | 1.163E 01 | 9.451E-03 | 2.907E 00 | 1.638E-02 |
| 39 | 2 | 1.163E 01 | 9.259E-03 | 2.848E 00 | 1.605E-02 |
| 39 | 3 | 1.163E 01 | 1.047E-02 | 3.222E 00 | 1.815E-02 |
| 39 | 4 | 1.163E 01 | 1.172E-02 | 3.605E 00 | 2.031E-02 |
| 39 | 5 | 1.163E 01 | 1.336E-02 | 4.110E 00 | 2.316E-02 |
| 39 | 6 | 1.163E 01 | 1.692E-02 | 5.204E 00 | 2.933E-02 |
| 39 | 7 | 1.163E 01 | 2.224E-02 | 6.841E 00 | 3.855E-02 |
| 39 | 8 | 1.163E 01 | 2.902E-02 | 8.927E 00 | 5.030E-02 |
| 40 | 1 | 1.342E 01 | 4.864E-03 | 3.859E 00 | 1.640E-02 |
| 40 | 2 | 1.342E 01 | 4.631E-03 | 3.674E 00 | 1.561E-02 |
| 40 | 3 | 1.342E 01 | 5.164E-03 | 4.098E 00 | 1.741E-02 |
| 40 | 4 | 1.342E 01 | 5.765E-03 | 4.575E 00 | 1.944E-02 |
| 40 | 5 | 1.342E 01 | 6.246E-03 | 4.956E 00 | 2.106E-02 |
| 40 | 6 | 1.342E 01 | 7.775E-03 | 6.169E 00 | 2.621E-02 |
| 40 | 7 | 1.342E 01 | 1.030E-02 | 8.172E 00 | 3.472E-02 |
| 40 | 8 | 1.342E 01 | 1.378E-02 | 1.093E 01 | 4.646E-02 |
| 41 | 1 | 1.215E 01 | 4.300E-02 | 2.528E 00 | 1.305E-02 |
| 41 | 2 | 1.215E 01 | 4.774E-02 | 2.807E 00 | 1.449E-02 |
| 41 | 3 | 1.215E 01 | 4.410E-02 | 2.593E 00 | 1.338E-02 |
| 41 | 4 | 1.215E 01 | 4.679E-02 | 2.751E 00 | 1.420E-02 |
| 41 | 6 | 1.215E 01 | 5.531E-02 | 3.253E 00 | 1.679E-02 |
| 41 | 7 | 1.215E 01 | 6.929E-02 | 4.075E 00 | 2.073E-02 |
| 41 | 8 | 1.215E 01 | 9.306E-02 | 5.472E 00 | 2.825E-02 |
| 42 | 1 | 1.183E 01 | 1.866E-02 | 2.482E 00 | 1.350E-02 |
| 42 | 2 | 1.183E 01 | 2.076E-02 | 2.761E 00 | 1.502E-02 |
| 42 | 3 | 1.183E 01 | 1.814E-02 | 2.413E 00 | 1.313E-02 |
| 42 | 4 | 1.183E 01 | 1.984E-02 | 2.639E 00 | 1.436E-02 |
| 42 | 6 | 1.183E 01 | 2.171E-02 | 2.888E 00 | 1.571E-02 |
| 42 | 7 | 1.183E 01 | 2.568E-02 | 3.417E 00 | 1.858E-02 |
| 42 | 8 | 1.183E 01 | 3.345E-02 | 4.450E 00 | 2.421E-02 |
| 43 | 1 | 1.162E 01 | 8.340E-03 | 2.681E 00 | 1.513E-02 |
| 43 | 2 | 1.162E 01 | 9.134E-03 | 2.936E 00 | 1.657E-02 |
| 43 | 3 | 1.162E 01 | 8.300E-03 | 2.668E 00 | 1.506E-02 |
| 43 | 4 | 1.162E 01 | 8.562E-03 | 2.752E 00 | 1.554E-02 |
| 43 | 6 | 1.162E 01 | 9.170E-03 | 2.948E 00 | 1.664E-02 |
| 43 | 7 | 1.162E 01 | 1.020E-02 | 3.279E 00 | 1.851E-02 |
| 43 | 8 | 1.162E 01 | 1.248E-02 | 4.012E 00 | 2.265E-02 |
| 44 | 1 | 1.429E 01 | 2.277E-02 | 3.469E 00 | 1.298E-02 |
| 44 | 2 | 1.429E 01 | 2.559E-02 | 3.897E 00 | 1.459E-02 |
| 44 | 3 | 1.429E 01 | 2.296E-02 | 3.498E 00 | 1.309E-02 |
| 44 | 4 | 1.429E 01 | 2.412E-02 | 3.674E 00 | 1.375E-02 |

Table IV (Concluded)

| RUN | GAGE | M | P(M) | P(M)/P | P(M)/PITOT |
|---|---|---|---|---|---|
| 44 | 6 | 1.429E 01 | 2.802E-02 | 4.269E 00 | 1.598E-02 |
| 44 | 7 | 1.429E 01 | 3.250E-02 | 4.951E 00 | 1.853E-02 |
| 44 | 8 | 1.429E 01 | 4.605E-02 | 7.014E 00 | 2.625E-02 |
| 45 | 1 | 1.399E 01 | 1.349E-02 | 3.621E 00 | 1.415E-02 |
| 45 | 2 | 1.399E 01 | 1.495E-02 | 4.014E 00 | 1.569E-02 |
| 45 | 3 | 1.399E 01 | 1.348E-02 | 3.618E 00 | 1.414E-02 |
| 45 | 4 | 1.399E 01 | 1.286E-02 | 3.452E 00 | 1.349E-02 |
| 45 | 6 | 1.399E 01 | 1.562E-02 | 4.194E 00 | 1.639E-02 |
| 45 | 7 | 1.399E 01 | 1.771E-02 | 4.756E 00 | 1.859E-02 |
| 45 | 8 | 1.399E 01 | 2.399E-02 | 6.442E 00 | 2.518E-02 |
| 46 | 1 | 1.338E 01 | 4.472E-03 | 3.499E 00 | 1.495E-02 |
| 46 | 2 | 1.338E 01 | 4.754E-03 | 3.720E 00 | 1.589E-02 |
| 46 | 3 | 1.338E 01 | 4.175E-03 | 3.267E 00 | 1.396E-02 |
| 46 | 4 | 1.338E 01 | 4.269E-03 | 3.340E 00 | 1.427E-02 |
| 46 | 6 | 1.338E 01 | 4.466E-03 | 3.495E 00 | 1.493E-02 |
| 46 | 7 | 1.338E 01 | 4.724E-03 | 3.697E 00 | 1.579E-02 |
| 46 | 8 | 1.338E 01 | 5.906E-03 | 4.622E 00 | 1.974E-02 |
| 47 | 1 | 1.694E 01 | 9.648E-03 | 5.288E 00 | 1.407E-02 |
| 47 | 2 | 1.694E 01 | 1.057E-02 | 5.793E 00 | 1.541E-02 |
| 47 | 3 | 1.694E 01 | 9.714E-03 | 5.324E 00 | 1.416E-02 |
| 47 | 4 | 1.694E 01 | 1.040E-02 | 5.698E 00 | 1.516E-02 |
| 47 | 6 | 1.694E 01 | 1.102E-02 | 6.038E 00 | 1.606E-02 |
| 47 | 7 | 1.694E 01 | 1.252E-02 | 6.863E 00 | 1.826E-02 |
| 47 | 8 | 1.694E 01 | 1.664E-02 | 9.118E 00 | 2.425E-02 |
| 48 | 1 | 1.677E 01 | 8.880E-03 | 5.874E 00 | 1.594E-02 |
| 48 | 2 | 1.677E 01 | 9.419E-03 | 6.231E 00 | 1.691E-02 |
| 48 | 3 | 1.677E 01 | 8.480E-03 | 5.609E 00 | 1.522E-02 |
| 48 | 4 | 1.677E 01 | 8.972E-03 | 5.935E 00 | 1.611E-02 |
| 48 | 6 | 1.677E 01 | 9.592E-03 | 6.345E 00 | 1.722E-02 |
| 48 | 7 | 1.677E 01 | 1.055E-02 | 6.976E 00 | 1.893E-02 |
| 48 | 8 | 1.677E 01 | 1.365E-02 | 9.032E 00 | 2.451E-02 |
| 49 | 1 | 1.567E 01 | 2.478E-03 | 6.047E 00 | 1.881E-02 |
| 49 | 2 | 1.567E 01 | 2.522E-03 | 6.154E 00 | 1.915E-02 |
| 49 | 3 | 1.567E 01 | 2.168E-03 | 5.292E 00 | 1.646E-02 |
| 49 | 4 | 1.567E 01 | 2.215E-03 | 5.406E 00 | 1.682E-02 |
| 49 | 6 | 1.567E 01 | 2.229E-03 | 5.440E 00 | 1.693E-02 |
| 49 | 7 | 1.567E 01 | 2.375E-03 | 5.797E 00 | 1.804E-02 |
| 49 | 8 | 1.567E 01 | 2.827E-03 | 6.899E 00 | 2.146E-02 |

Table V

RUN SCHEDULE AND TEST CONDITIONS FOR THE AXISYMMETRIC MODEL TESTS

| RUN NO. | 1 | 3 | 4 | 5 | 6 | 7 | 8 |
|---|---|---|---|---|---|---|---|
| ATTACK | 0. | 0. | 0. | 0. | 0. | 0. | 0. |
| YAW | 0. | 0. | 0. | 0. | 0. | 0. | 0. |
| ROLL | 0. | 0. | 0. | 0. | 0. | 0. | 0. |
| M(I) | 4.731E 00 | 4.253E 00 | 4.552E 00 | 4.229E 00 | 4.380E 00 | 4.497E 00 | 4.259E 00 |
| P(0) | 3.721E 03 | 3.809E 03 | 3.761E 03 | 3.767E 03 | 3.538E 03 | 2.884E 03 | 1.972E 03 |
| H(0) | 3.323E 07 | 2.734E 07 | 3.097E 07 | 2.705E 07 | 2.882E 07 | 3.031E 07 | 2.743E 07 |
| T(0) | 4.673E 03 | 3.962E 03 | 4.406E 03 | 3.927E 03 | 4.143E 03 | 4.326E 03 | 3.967E 03 |
| M | 1.214E 01 | 1.432E 01 | 1.228E 01 | 1.434E 01 | 1.696E 01 | 1.674E 01 | 1.396E 01 |
| U | 8.017E 03 | 7.305E 03 | 7.742E 03 | 7.267E 03 | 7.527E 03 | 7.717E 03 | 7.313E 03 |
| T | 1.816E 02 | 1.083E 02 | 1.654E 02 | 1.070E 02 | 8.200E 01 | 8.845E 01 | 1.143E 02 |
| P | 1.615E-02 | 6.066E-03 | 1.578E-02 | 5.988E-03 | 1.708E-03 | 1.466E-03 | 3.646E-03 |
| Q | 1.665E 00 | 8.708E-01 | 1.666E 00 | 8.614E-01 | 3.439E-01 | 2.876E-01 | 4.972E-01 |
| RHO | 7.460E-06 | 4.699E-06 | 8.005E-06 | 4.697E-06 | 1.748E-06 | 1.391E-06 | 2.677E-06 |
| MU | 1.515E-07 | 9.112E-08 | 1.383E-07 | 9.000E-08 | 6.897E-08 | 7.441E-08 | 9.611E-08 |
| RE/FT. | 3.948E 05 | 3.767E 05 | 4.480E 05 | 3.792E 05 | 1.908E 05 | 1.442E 05 | 2.037E 05 |
| PITOT | 3.121E 00 | 1.626E 00 | 3.119E 00 | 1.608E 00 | 6.428E-01 | 5.381E-01 | 9.282E-01 |
| T* | 1.044E 03 | 9.255E 02 | 9.995E 02 | 9.197E 02 | 9.556E 02 | 9.862E 02 | 9.264E 02 |
| MU* | 6.163E-07 | 5.686E-07 | 5.987E-07 | 5.661E-07 | 5.810E-07 | 5.934E-07 | 5.690E-07 |
| SQRT.C* | 8.412E-01 | 8.546E-01 | 8.462E-01 | 8.555E-01 | 8.502E-01 | 8.457E-01 | 8.546E-01 |
| H(M) | 3.183E 06 | 3.183E 06 | 3.183E 06 | 3.183E 06 | 3.183E 06 | 3.183E 06 | 3.183E 06 |
| T(M) | 5.300E 02 | 5.300E 02 | 5.300E 02 | 5.300E 02 | 5.300E 02 | 5.300E 02 | 5.300E 02 |
| P(TS) | 3.868E-05 | 1.934E-05 | 1.934E-05 | 1.934E-05 | 1.934E-05 | 3.868E-05 | 1.934E-05 |
| MODEL | A/10 | A/10 | A/10 | A/10 | A/10 | A/10 | A/10 |

Table V (Cont'd.)

| RUN NO. | 9 | 10 | 11 | 12 | 13 | 14 | 15 |
|---|---|---|---|---|---|---|---|
| ATTACK | 0. | 0. | 0. | 0. | 0. | 0. | 0. |
| YAW | 0. | 0. | 0. | 0. | 0. | 0. | 0. |
| ROLL | 0. | 0. | 0. | 0. | 0. | 0. | 0. |
| M(I) | 4.708E 00 | 4.743E 00 | 4.456E 00 | 4.415E 00 | 4.274E 00 | 4.347E 00 | 4.798E 00 |
| P(0) | 5.323E 02 | 5.372E 02 | 2.905E 03 | 3.676E 03 | 3.762E 03 | 2.057E 03 | 3.788E 03 |
| H(0) | 3.283E 07 | 3.327E 07 | 2.982E 07 | 2.929E 07 | 2.757E 07 | 2.846E 07 | 3.409E 07 |
| T(0) | 4.606E 03 | 4.656E 03 | 4.267E 03 | 4.204E 03 | 3.991E 03 | 4.093E 03 | 4.773E 03 |
| M | 1.159E 01 | 1.156E 01 | 1.680E 01 | 1.693E 01 | 1.430E 01 | 1.391E 01 | 1.209E 01 |
| U | 7.956E 03 | 8.009E 03 | 7.654E 03 | 7.587E 03 | 7.336E 03 | 7.448E 03 | 8.119E 03 |
| T | 1.963E 02 | 1.998E 02 | 8.646E 01 | 8.361E 01 | 1.096E 02 | 1.193E 02 | 1.877E 02 |
| P | 3.053E-03 | 3.101E-03 | 1.459E-03 | 1.782E-03 | 6.024E-03 | 3.814E-03 | 1.657E-02 |
| Q | 2.869E-01 | 2.901E-01 | 2.882E-01 | 3.576E-01 | 8.620E-01 | 5.168E-01 | 1.696E 00 |
| RHO | 1.305E-06 | 1.303E-06 | 1.416E-06 | 1.789E-06 | 4.612E-06 | 2.683E-06 | 7.408E-06 |
| MU | 1.632E-07 | 1.660E-07 | 7.273E-08 | 7.033E-08 | 9.219E-08 | 1.003E-07 | 1.564E-07 |
| RE/FT. | 6.362E 04 | 6.284E 04 | 1.491E 05 | 1.930E 05 | 3.670E 05 | 1.992E 05 | 3.847E 05 |
| PITOT | 5.377E-01 | 5.440E-01 | 5.390E-01 | 6.685E-01 | 1.609E 00 | 9.656E-01 | 3.181E 00 |
| T* | 1.033E 03 | 1.041E 03 | 9.763E 02 | 9.659E 02 | 9.303E 02 | 9.474E 02 | 1.061E 03 |
| MU* | 6.119E-07 | 6.151E-07 | 5.894E-07 | 5.852E-07 | 5.706E-07 | 5.776E-07 | 6.227E-07 |
| SQRT.C* | 8.441E-01 | 8.432E-01 | 8.471E-01 | 8.487E-01 | 8.539E-01 | 8.516E-01 | 8.395E-01 |
| H(M) | 3.183E 06 | 3.183E 06 | 3.183E 06 | 3.183E 06 | 3.183E 06 | 3.183E 06 | 3.183E 06 |
| T(M) | 5.300E 02 | 5.300E 02 | 5.300E 02 | 5.300E 02 | 5.300E 02 | 5.300E 02 | 5.300E 02 |
| P(TS) | 1.934E-05 | 1.934E-05 | 1.934E-05 | 1.934E-05 | 1.934E-05 | 1.934E-05 | 1.934E-05 |
| MODEL | A/10 | A/20 | A/20 | A/20 | A/20 | A/20 | A/20 |

Table V (Cont'd.)

| RUN NO. | 16 | 17 | 18 | 19 | 20 | 21 | 22 |
|---|---|---|---|---|---|---|---|
| ATTACK | 0. | 0. | 0. | 0. | 0. | 0. | 0. |
| YAW | 0. | 0. | 0. | 0. | 0. | 0. | 0. |
| ROLL | 0. | 0. | 0. | 0. | 0. | 0. | 0. |
| M(I) | 4.784E 00 | 4.419E 00 | 4.435E 00 | 4.474E 00 | 4.754E 00 | 4.772E 00 | 4.753E 00 |
| P(0) | 1.422E 03 | 3.775E 03 | 4.887E 02 | 2.929E 03 | 5.117E 02 | 3.701E 03 | 1.439E 03 |
| H(0) | 3.388E 07 | 2.934E 07 | 2.949E 07 | 3.004E 07 | 3.340E 07 | 3.376E 07 | 3.349E 07 |
| T(0) | 4.738E 03 | 4.211E 03 | 4.218E 03 | 4.293E 03 | 4.670E 03 | 4.734E 03 | 4.693E 03 |
| M | 1.175E 01 | 1.693E 01 | 1.549E 01 | 1.678E 01 | 1.154E 01 | 1.210E 01 | 1.178E 01 |
| U | 8.086E 03 | 7.593E 03 | 7.600E 03 | 7.682E 03 | 8.024E 03 | 8.079E 03 | 8.040E 03 |
| T | 1.971E 02 | 8.373E 01 | 1.003E 02 | 8.727E 01 | 2.011E 02 | 1.855E 02 | 1.940E 02 |
| P | 7.359E-03 | 1.828E-03 | 4.155E-04 | 1.476E-03 | 2.972E-03 | 1.619E-02 | 7.388E-03 |
| Q | 7.113E-01 | 3.669E-01 | 6.975E-02 | 2.908E-01 | 2.773E-01 | 1.660E 00 | 7.175E-01 |
| RHO | 3.133E-06 | 1.833E-06 | 3.477E-07 | 1.419E-06 | 1.240E-06 | 7.325E-06 | 3.197E-06 |
| MU | 1.639E-07 | 7.043E-08 | 8.437E-08 | 7.341E-08 | 1.670E-07 | 1.546E-07 | 1.614E-07 |
| RE/FT. | 1.545E 05 | 1.976E 05 | 3.132E 04 | 1.485E 05 | 5.957E 04 | 3.827E 05 | 1.593E 05 |
| PITOT | 1.334E 00 | 6.860E-01 | 1.304E-01 | 5.439E-01 | 5.199E-01 | 3.114E 00 | 1.345E 00 |
| T* | 1.055E 03 | 9.669E 02 | 9.682E 02 | 9.807E 02 | 1.044E 03 | 1.054E 03 | 1.047E 03 |
| MU* | 6.205E-07 | 5.856E-07 | 5.861E-07 | 5.912E-07 | 6.161E-07 | 6.202E-07 | 6.175E-07 |
| SQRT.C* | 8.411E-01 | 8.485E-01 | 8.483E-01 | 8.465E-01 | 8.430E-01 | 8.401E-01 | 8.418E-01 |
| H(M) | 3.183E 06 | 3.183E 06 | 3.183E 06 | 3.183E 06 | 3.183E 06 | 3.183E 06 | 3.183E 06 |
| T(M) | 5.300E 02 | 5.300E 02 | 5.300E 02 | 5.300E 02 | 5.300E 02 | 5.300E 02 | 5.300E 02 |
| P(TS) | 1.934E-05 | 1.934E-05 | 1.934E-05 | 1.934E-05 | 1.934E-05 | 1.934E-05 | 1.934E-05 |
| MODEL | A/20 | A/50 | A/50 | A/50 | A/50 | A/50 | A/50 |

Table V (Cont'd.)

| RUN NO. | 23 | 24 | 25 | 26 | 27 | 28 | 29 |
|---|---|---|---|---|---|---|---|
| ATTACK | 0. | 0. | 0. | 0. | C. | 0. | 0. |
| YAW | 0. | 0. | 0. | 0. | C. | 0. | 0. |
| ROLL | 0. | 0. | C. | 0. | C. | 0. | 0. |
| M(I) | 4.757E 00 | 4.274E 00 | 4.231E C0 | 3.966E 00 | 4.004E 00 | 4.005E 00 | 4.207E 00 |
| P(0) | 3.632E 03 | 3.742E 03 | 2.018E C3 | 4.234E 02 | 2.848E 03 | 1.386E 03 | 3.985E 02 |
| H(0) | 3.356E 07 | 2.757E 07 | 2.71CE C7 | 2.415E 07 | 2.454E 07 | 2.457E 07 | 2.684E 07 |
| T(0) | 4.711E 03 | 3.991E 03 | 3.927E C3 | 3.557E 03 | 3.612E 03 | 3.612E 03 | 3.893E 03 |
| M | 1.211E 01 | 1.430E 01 | 1.40CE C1 | 7.662E 00 | 7.888E 00 | 7.766E 00 | 7.545E 00 |
| U | 8.056E 03 | 7.336E 03 | 7.270E C3 | 6.671E 03 | 6.739E 03 | 6.736E 03 | 7.024E 03 |
| T | 1.843E 02 | 1.096E 02 | 1.123E C2 | 3.156E 02 | 3.038E 02 | 3.132E 02 | 3.608E 02 |
| P | 1.592E-02 | 5.998E-03 | 3.689E-C3 | 4.438E-02 | 2.562E-01 | 1.342E-01 | 4.381E-02 |
| Q | 1.633E 00 | 8.580E-01 | 5.059E-C1 | 1.824E 00 | 1.116E 01 | 5.666E 00 | 1.746E 00 |
| RHO | 7.246E-06 | 4.591E-06 | 2.756E-C6 | 1.180E-05 | 7.076E-05 | 3.596E-05 | 1.019E-05 |
| MU | 1.537E-07 | 9.222E-08 | 9.446E-C8 | 2.522E-07 | 2.440E-07 | 2.506E-07 | 2.825E-07 |
| RE/FT. | 3.798E 05 | 3.652E 05 | 2.121E C5 | 3.121E 05 | 1.954E 06 | 9.667E 05 | 2.533E 05 |
| PITOT | 3.062E 00 | 1.602E 00 | 9.442E-C1 | 3.396E 00 | 2.079E 01 | 1.055E 01 | 3.258E 00 |
| T* | 1.050E 03 | 9.303E 02 | 9.197E C2 | 8.581E 02 | 8.671E 02 | 8.671E 02 | 9.140E 02 |
| MU* | 6.187E-07 | 5.706E-07 | 5.661E-C7 | 5.400E-07 | 5.439E-07 | 5.439E-07 | 5.638E-07 |
| SQRT.C* | 8.406E-01 | 8.539E-01 | 8.555E-C1 | 8.873E-01 | 8.837E-01 | 8.854E-01 | 8.875E-01 |
| H(M) | 3.183E 06 | 3.183E 06 | 3.183E C6 | 3.183E 06 | 3.183E 06 | 3.183E 06 | 3.183E 06 |
| T(M) | 5.300E 02 | 5.300E 02 | 5.300E C2 | 5.300E 02 | 5.300E 02 | 5.300E 02 | 5.300E 02 |
| P(TS) | 1.934E-05 | 1.934E-05 | 1.934E-C5 | 1.934E-05 | 1.934E-05 | 1.934E-05 | 1.934E-05 |
| MODEL | A/50 | A/50 | A/50 | A/10 | A/10 | A/10 | A/20 |

Table V (Concluded)

| RUN NO. | 30 | 31 | 32 |
|---|---|---|---|
| ATTACK | 0. | 0. | 0. |
| YAW | 0. | 0. | 0. |
| ROLL | 0. | 0. | 0. |
| M(I) | 2.452E 00 | 3.984E 00 | 2.414E 00 |
| P(0) | 1.548E 03 | 4.022E 02 | 1.539E 03 |
| H(0) | 1.067E 07 | 2.434E 07 | 1.042E 07 |
| T(0) | 1.684E 03 | 3.582E 03 | 1.644E 03 |
| M | 7.844E 00 | 7.650E 00 | 7.850E 00 |
| U | 4.442E 03 | 6.697E 03 | 4.390E 03 |
| T | 1.335E 02 | 3.191E 02 | 1.302E 02 |
| P | 1.828E-01 | 4.244E-02 | 1.815E-01 |
| Q | 7.873E 00 | 1.738E 00 | 7.832E 00 |
| RHO | 1.149E-04 | 1.116E-05 | 1.170E-04 |
| MU | 1.121E-07 | 2.546E-07 | 1.094E-07 |
| RE/FT. | 4.553E 06 | 2.936E 05 | 4.697E 06 |
| PITOT | 1.449E 01 | 3.238E 00 | 1.441E 01 |
| T* | 5.458E 02 | 8.622E 02 | 5.390E 02 |
| MU* | 3.888E-07 | 5.417E-07 | 3.851E-07 |
| SQRT.C* | 9.210E-01 | 8.873E-01 | 9.222E-01 |
| H(M) | 3.183E 06 | 3.183E 06 | 3.183E 06 |
| T(M) | 5.300E 02 | 5.300E 02 | 5.300E 02 |
| P(TS) | 1.934E-05 | 1.934E-05 | 1.934E-05 |
| MODEL | A/20 | A/50 | A/50 |

Table VI

AXISYMMETRIC MODEL SKIN FRICTION DATA

| RUN | GAGE | M | TAU(M) |
|---|---|---|---|
| 1 | 1 | 1.214E 01 | 3.126E-03 |
| 1 | 2 | 1.214E 01 | 3.427E-03 |
| 1 | 4 | 1.214E 01 | 2.673E-03 |
| 1 | 5 | 1.214E 01 | 3.541E-03 |
| 1 | 6 | 1.214E 01 | 4.481E-03 |
| 1 | 7 | 1.214E 01 | 4.669E-03 |
| 1 | 8 | 1.214E 01 | 6.023E-03 |
| 1 | 9 | 1.214E 01 | 8.097E-03 |
| 1 | 10 | 1.214E 01 | 6.937E-03 |
| 3 | 1 | 1.432E 01 | 2.052E-03 |
| 3 | 2 | 1.432E 01 | 2.200E-03 |
| 3 | 4 | 1.432E 01 | 1.734E-03 |
| 3 | 5 | 1.432E 01 | 2.265E-03 |
| 3 | 6 | 1.432E 01 | 2.792E-03 |
| 3 | 7 | 1.432E 01 | 2.899E-03 |
| 3 | 8 | 1.432E 01 | 3.831E-03 |
| 3 | 9 | 1.432E 01 | 5.020E-03 |
| 3 | 10 | 1.432E 01 | 4.871E-03 |
| 4 | 1 | 1.228E 01 | 2.948E-03 |
| 4 | 2 | 1.228E 01 | 3.819E-03 |
| 4 | 4 | 1.228E 01 | 2.601E-03 |
| 4 | 5 | 1.228E 01 | 3.245E-03 |
| 4 | 6 | 1.228E 01 | 3.976E-03 |
| 4 | 7 | 1.228E 01 | 4.106E-03 |
| 4 | 8 | 1.228E 01 | 5.415E-03 |
| 4 | 9 | 1.228E 01 | 7.514E-03 |
| 4 | 10 | 1.228E 01 | 6.631E-03 |
| 5 | 1 | 1.434E 01 | 1.898E-03 |
| 5 | 2 | 1.434E 01 | 2.433E-03 |
| 5 | 4 | 1.434E 01 | 1.729E-03 |
| 5 | 5 | 1.434E 01 | 2.092E-03 |

Table VI (Cont'd.)

| RUN | GAGE | M | TAU(M) |
|---|---|---|---|
| 5 | 6 | 1.434E 01 | 2.465E-03 |
| 5 | 7 | 1.434E 01 | 2.519E-03 |
| 5 | 8 | 1.434E 01 | 3.413E-03 |
| 5 | 9 | 1.434E 01 | 4.607E-03 |
| 5 | 10 | 1.434E 01 | 4.419E-03 |
| 6 | 1 | 1.696E 01 | 1.365E-03 |
| 6 | 2 | 1.696E 01 | 1.650E-03 |
| 6 | 4 | 1.696E 01 | 1.149E-03 |
| 6 | 5 | 1.696E 01 | 1.370E-03 |
| 6 | 6 | 1.696E 01 | 1.593E-03 |
| 6 | 7 | 1.696E 01 | 1.665E-03 |
| 6 | 8 | 1.696E 01 | 1.990E-03 |
| 6 | 9 | 1.696E 01 | 2.623E-03 |
| 6 | 10 | 1.696E 01 | 2.643E-03 |
| 7 | 1 | 1.674E 01 | 1.293E-03 |
| 7 | 2 | 1.674E 01 | 1.543E-03 |
| 7 | 4 | 1.674E 01 | 1.079E-03 |
| 7 | 5 | 1.674E 01 | 1.301E-03 |
| 7 | 6 | 1.674E 01 | 1.498E-03 |
| 7 | 7 | 1.674E 01 | 1.552E-03 |
| 7 | 8 | 1.674E 01 | 1.851E-03 |
| 7 | 9 | 1.674E 01 | 2.279E-03 |
| 7 | 10 | 1.674E 01 | 2.365E-03 |
| 8 | 1 | 1.396E 01 | 1.549E-03 |
| 8 | 2 | 1.396E 01 | 1.890E-03 |
| 8 | 4 | 1.396E 01 | 1.349E-03 |
| 8 | 5 | 1.396E 01 | 1.647E-03 |
| 8 | 6 | 1.396E 01 | 1.920E-03 |
| 8 | 7 | 1.396E 01 | 1.868E-03 |
| 8 | 8 | 1.396E 01 | 2.444E-03 |
| 8 | 9 | 1.396E 01 | 3.023E-03 |
| 8 | 10 | 1.396E 01 | 3.255E-03 |

Table VI (Cont'd.)

| RUN | GAGE | M | TAU(M) |
|---|---|---|---|
| 9 | 1 | 1.159E 01 | 1.348E-03 |
| 9 | 2 | 1.159E 01 | 1.580E-03 |
| 9 | 4 | 1.159E 01 | 1.156E-03 |
| 9 | 5 | 1.159E 01 | 1.337E-03 |
| 9 | 6 | 1.159E 01 | 1.529E-03 |
| 9 | 7 | 1.159E 01 | 1.577E-03 |
| 9 | 8 | 1.159E 01 | 1.802E-03 |
| 9 | 9 | 1.159E 01 | 2.186E-03 |
| 9 | 10 | 1.159E 01 | 2.272E-03 |
| 10 | 1 | 1.156E 01 | 1.368E-03 |
| 10 | 2 | 1.156E 01 | 1.608E-03 |
| 10 | 4 | 1.156E 01 | 1.168E-03 |
| 10 | 5 | 1.156E 01 | 1.345E-03 |
| 10 | 6 | 1.156E 01 | 1.495E-03 |
| 10 | 7 | 1.156E 01 | 1.814E-03 |
| 10 | 8 | 1.156E 01 | 1.849E-03 |
| 10 | 9 | 1.156E 01 | 2.506E-03 |
| 10 | 10 | 1.156E 01 | 2.724E-03 |
| 11 | 1 | 1.680E 01 | 1.357E-03 |
| 11 | 2 | 1.680E 01 | 1.597E-03 |
| 11 | 4 | 1.680E 01 | 1.110E-03 |
| 11 | 5 | 1.680E 01 | 1.362E-03 |
| 11 | 6 | 1.680E 01 | 1.514E-03 |
| 11 | 7 | 1.680E 01 | 1.602E-03 |
| 11 | 8 | 1.680E 01 | 1.761E-03 |
| 11 | 9 | 1.680E 01 | 2.534E-03 |
| 11 | 10 | 1.680E 01 | 3.005E-03 |
| 12 | 1 | 1.693E 01 | 1.384E-03 |
| 12 | 2 | 1.693E 01 | 1.650E-03 |
| 12 | 4 | 1.693E 01 | 1.170E-03 |
| 12 | 5 | 1.693E 01 | 1.363E-03 |

Table VI (Cont'd.)

| RUN | GAGE | M | TAU(M) |
|---|---|---|---|
| 12 | 6 | 1.693E 01 | 1.514E-03 |
| 12 | 7 | 1.693E 01 | 1.559E-03 |
| 12 | 8 | 1.693E 01 | 1.859E-03 |
| 12 | 9 | 1.693E 01 | 2.631E-03 |
| 12 | 10 | 1.693E 01 | 3.299E-03 |
| 13 | 1 | 1.430E 01 | 1.901E-03 |
| 13 | 2 | 1.430E 01 | 2.353E-03 |
| 13 | 4 | 1.430E 01 | 1.712E-03 |
| 13 | 5 | 1.430E 01 | 1.964E-03 |
| 13 | 6 | 1.430E 01 | 2.210E-03 |
| 13 | 7 | 1.430E 01 | 1.197E-03 |
| 13 | 8 | 1.430E 01 | 3.010E-03 |
| 13 | 9 | 1.430E 01 | 4.529E-03 |
| 13 | 10 | 1.430E 01 | 5.305E-03 |
| 14 | 1 | 1.391E 01 | 1.597E-03 |
| 14 | 2 | 1.391E 01 | 1.935E-03 |
| 14 | 4 | 1.391E 01 | 1.385E-03 |
| 14 | 5 | 1.391E 01 | 1.622E-03 |
| 14 | 6 | 1.391E 01 | 1.865E-03 |
| 14 | 7 | 1.391E 01 | 1.872E-03 |
| 14 | 8 | 1.391E 01 | 2.380E-03 |
| 14 | 9 | 1.391E 01 | 3.210E-03 |
| 14 | 10 | 1.391E 01 | 4.138E-03 |
| 15 | 1 | 1.209E 01 | 3.160E-03 |
| 15 | 2 | 1.209E 01 | 4.068E-03 |
| 15 | 4 | 1.209E 01 | 2.601E-03 |
| 15 | 5 | 1.209E 01 | 3.385E-03 |
| 15 | 6 | 1.209E 01 | 4.203E-03 |
| 15 | 7 | 1.209E 01 | 3.143E-03 |
| 15 | 8 | 1.209E 01 | 6.246E-03 |
| 15 | 9 | 1.209E 01 | 8.952E-03 |
| 15 | 10 | 1.209E 01 | 8.190E-03 |

Table VI (Cont'd.)

| RUN | GAGE | M | TAU(M) |
|---|---|---|---|
| 16 | 1 | 1.175E 01 | 2.047E-03 |
| 16 | 2 | 1.175E 01 | 2.539E-03 |
| 16 | 4 | 1.175E 01 | 1.756E-03 |
| 16 | 5 | 1.175E 01 | 2.092E-03 |
| 16 | 6 | 1.175E 01 | 2.442E-03 |
| 16 | 7 | 1.175E 01 | 2.763E-03 |
| 16 | 8 | 1.175E 01 | 3.160E-03 |
| 16 | 9 | 1.175E 01 | 4.706E-03 |
| 16 | 10 | 1.175E 01 | 5.109E-03 |
| 17 | 1 | 1.693E 01 | 1.454E-03 |
| 17 | 2 | 1.693E 01 | 1.743E-03 |
| 17 | 4 | 1.693E 01 | 1.264E-03 |
| 17 | 5 | 1.693E 01 | 1.417E-03 |
| 17 | 6 | 1.693E 01 | 1.583E-03 |
| 17 | 7 | 1.693E 01 | 6.457E-04 |
| 17 | 8 | 1.693E 01 | 1.474E-03 |
| 17 | 9 | 1.693E 01 | 3.008E-03 |
| 17 | 10 | 1.693E 01 | 5.796E-03 |
| 18 | 1 | 1.549E 01 | 7.453E-04 |
| 18 | 2 | 1.549E 01 | 8.175E-04 |
| 18 | 4 | 1.549E 01 | 6.242E-04 |
| 18 | 5 | 1.549E 01 | 7.066E-04 |
| 18 | 6 | 1.549E 01 | 7.839E-04 |
| 18 | 7 | 1.549E 01 | 7.023E-04 |
| 18 | 8 | 1.549E 01 | 9.856E-04 |
| 18 | 9 | 1.549E 01 | 1.085E-03 |
| 18 | 10 | 1.549E 01 | 1.449E-03 |
| 19 | 1 | 1.678E 01 | 1.331E-03 |
| 19 | 2 | 1.678E 01 | 1.543E-03 |
| 19 | 4 | 1.678E 01 | 1.103E-03 |
| 19 | 5 | 1.678E 01 | 1.310E-03 |

Table VI (Cont'd.)

| RUN | GAGE | M | TAU(M) |
|---|---|---|---|
| 19 | 6 | 1.678E 01 | 1.435E-03 |
| 19 | 7 | 1.678E 01 | 6.655E-04 |
| 19 | 8 | 1.678E 01 | 1.222E-03 |
| 19 | 9 | 1.678E 01 | 2.791E-03 |
| 19 | 10 | 1.678E 01 | 5.585E-03 |
| 20 | 1 | 1.154E 01 | 1.312E-03 |
| 20 | 2 | 1.154E 01 | 1.551E-03 |
| 20 | 4 | 1.154E 01 | 1.160E-03 |
| 20 | 5 | 1.154E 01 | 1.318E-03 |
| 20 | 6 | 1.154E 01 | 1.448E-03 |
| 20 | 7 | 1.154E 01 | 9.303E-04 |
| 20 | 8 | 1.154E 01 | 1.581E-03 |
| 20 | 9 | 1.154E 01 | 2.388E-03 |
| 20 | 10 | 1.154E 01 | 4.292E-03 |
| 21 | 1 | 1.210E 01 | 2.956E-03 |
| 21 | 2 | 1.210E 01 | 3.766E-03 |
| 21 | 4 | 1.210E 01 | 2.615E-03 |
| 21 | 5 | 1.210E 01 | 3.138E-03 |
| 21 | 8 | 1.210E 01 | 3.044E-03 |
| 21 | 9 | 1.210E 01 | 1.018E-02 |
| 21 | 10 | 1.210E 01 | 1.529E-02 |
| 22 | 1 | 1.178E 01 | 2.077E-03 |
| 22 | 2 | 1.178E 01 | 2.611E-03 |
| 22 | 4 | 1.178E 01 | 1.766E-03 |
| 22 | 5 | 1.178E 01 | 2.174E-03 |
| 22 | 6 | 1.178E 01 | 1.931E-03 |
| 22 | 7 | 1.178E 01 | -3.398E-04 |
| 22 | 8 | 1.178E 01 | 2.682E-03 |
| 22 | 9 | 1.178E 01 | 6.191E-03 |
| 22 | 10 | 1.178E 01 | 1.019E-02 |
| 23 | 1 | 1.211E 01 | 2.964E-03 |

Table VI (Cont'd.)

| RUN | GAGE | M | TAU(M) |
|---|---|---|---|
| 23 | 2 | 1.211E 01 | 3.817E-03 |
| 23 | 4 | 1.211E 01 | 2.635E-03 |
| 23 | 5 | 1.211E 01 | 3.278E-03 |
| 23 | 6 | 1.211E 01 | -9.344E-04 |
| 23 | 7 | 1.211E 01 | -2.209E-03 |
| 23 | 8 | 1.211E 01 | 4.148E-03 |
| 23 | 9 | 1.211E 01 | 1.060E-02 |
| 23 | 10 | 1.211E 01 | 1.619E-02 |
| 24 | 1 | 1.430E 01 | 1.943E-03 |
| 24 | 2 | 1.430E 01 | 2.771E-03 |
| 24 | 4 | 1.430E 01 | 1.803E-03 |
| 24 | 5 | 1.430E 01 | 2.030E-03 |
| 24 | 6 | 1.430E 01 | -2.336E-04 |
| 24 | 7 | 1.430E 01 | -1.133E-03 |
| 24 | 8 | 1.430E 01 | 1.687E-03 |
| 24 | 9 | 1.430E 01 | 5.427E-03 |
| 24 | 10 | 1.430E 01 | 1.060E-02 |
| 25 | 1 | 1.400E 01 | 1.535E-03 |
| 25 | 2 | 1.400E 01 | 2.008E-03 |
| 25 | 4 | 1.400E 01 | 1.363E-03 |
| 25 | 5 | 1.400E 01 | 1.562E-03 |
| 25 | 6 | 1.400E 01 | 1.298E-03 |
| 25 | 7 | 1.400E 01 | -3.034E-04 |
| 25 | 8 | 1.400E 01 | 1.373E-03 |
| 25 | 9 | 1.400E 01 | 3.744E-03 |
| 25 | 10 | 1.400E 01 | 7.238E-03 |
| 26 | 1 | 7.662E 00 | 2.663E-03 |
| 26 | 2 | 7.662E 00 | 3.695E-03 |
| 26 | 4 | 7.662E 00 | 2.868E-03 |
| 26 | 5 | 7.662E 00 | 2.811E-03 |
| 26 | 6 | 7.662E 00 | 3.165E-03 |
| 26 | 7 | 7.662E 00 | 3.776E-03 |

Table VI (Cont'd.)

| RUN | GAGE | M | TAU(M) |
|---|---|---|---|
| 26 | 8 | 7.662E 00 | 3.768E-03 |
| 26 | 9 | 7.662E 00 | 6.362E-03 |
| 26 | 10 | 7.662E 00 | 5.053E-03 |
| 27 | 1 | 7.888E 00 | 8.726E-03 |
| 27 | 10 | 7.888E 00 | 3.706E-02 |
| 28 | 1 | 7.766E 00 | 4.899E-03 |
| 28 | 2 | 7.766E 00 | 8.063E-03 |
| 28 | 4 | 7.766E 00 | 6.162E-03 |
| 28 | 5 | 7.766E 00 | 8.236E-03 |
| 28 | 6 | 7.766E 00 | 1.598E-02 |
| 28 | 7 | 7.766E 00 | 2.158E-02 |
| 28 | 8 | 7.766E 00 | 2.214E-02 |
| 28 | 9 | 7.766E 00 | 2.845E-02 |
| 28 | 10 | 7.766E 00 | 1.782E-02 |
| 29 | 1 | 7.545E 00 | 2.881E-03 |
| 29 | 2 | 7.545E 00 | 4.037E-03 |
| 29 | 4 | 7.545E 00 | 2.890E-03 |
| 29 | 5 | 7.545E 00 | 3.138E-03 |
| 29 | 6 | 7.545E 00 | 3.433E-03 |
| 29 | 8 | 7.545E 00 | 5.067E-03 |
| 29 | 9 | 7.545E 00 | 7.723E-03 |
| 29 | 10 | 7.545E 00 | 6.296E-03 |
| 30 | 1 | 7.844E 00 | 1.214E-02 |
| 30 | 2 | 7.844E 00 | 2.186E-02 |
| 30 | 4 | 7.844E 00 | 1.470E-02 |
| 30 | 5 | 7.844E 00 | 1.779E-02 |
| 30 | 6 | 7.844E 00 | 2.474E-02 |
| 30 | 7 | 7.844E 00 | 4.721E-02 |
| 30 | 8 | 7.844E 00 | 3.855E-02 |
| 30 | 9 | 7.844E 00 | 4.778E-02 |
| 30 | 10 | 7.844E 00 | 1.698E-02 |

Table VI (Concluded)

| RUN | GAGE | M | TAU(M) |
|---|---|---|---|
| 31 | 1 | 7.650E 00 | 2.730E-03 |
| 31 | 2 | 7.650E 00 | 3.605E-03 |
| 31 | 4 | 7.650E 00 | 2.731E-03 |
| 31 | 5 | 7.650E 00 | 2.800E-03 |
| 31 | 6 | 7.650E 00 | -3.893E-04 |
| 31 | 8 | 7.650E 00 | 4.313E-03 |
| 31 | 9 | 7.650E 00 | 7.691E-03 |
| 31 | 10 | 7.650E 00 | 1.095E-02 |
| 32 | 1 | 7.850E 00 | 1.181E-02 |
| 32 | 2 | 7.850E 00 | 2.116E-02 |
| 32 | 4 | 7.850E 00 | 1.434E-02 |
| 32 | 5 | 7.850E 00 | 1.701E-02 |
| 32 | 6 | 7.850E 00 | 2.803E-02 |
| 32 | 7 | 7.850E 00 | 6.165E-02 |
| 32 | 8 | 7.850E 00 | 7.294E-02 |
| 32 | 9 | 7.850E 00 | 6.481E-02 |
| 32 | 10 | 7.850E 00 | 4.636E-02 |

Table VII

AXISYMMETRIC MODEL HEAT TRANSFER DATA

| RUN | GAGE | Q(AV) | RUN | GAGE | Q(AV) |
|---|---|---|---|---|---|
| 1 | 1 | 2.823E 00 | 7 | 1 | 9.783E-01 |
| 1 | 2 | 2.863E 00 | 7 | 2 | 1.024E 00 |
| 1 | 3 | 3.451E 00 | 7 | 3 | 1.170E 00 |
| 1 | 4 | 5.570E 00 | 7 | 4 | 1.624E 00 |
| 1 | 5 | 7.289E 00 | 7 | 5 | 2.101E 00 |
| 1 | 6 | 6.398E 00 | 7 | 6 | 2.254E 00 |
| 3 | 1 | 1.599E 00 | 8 | 1 | 1.112E 00 |
| 3 | 2 | 1.615E 00 | 8 | 2 | 1.227E 00 |
| 3 | 3 | 2.022E 00 | 8 | 3 | 1.421E 00 |
| 3 | 4 | 3.096E 00 | 8 | 4 | 2.115E 00 |
| 3 | 5 | 4.162E 00 | 8 | 5 | 2.753E 00 |
| 3 | 6 | 3.911E 00 | 8 | 6 | 2.821E 00 |
| 4 | 1 | 2.425E 00 | 9 | 1 | 1.003E 00 |
| 4 | 2 | 2.712E 00 | 9 | 2 | 1.119E 00 |
| 4 | 3 | 3.670E 00 | 9 | 3 | 1.285E 00 |
| 4 | 4 | 5.776E 00 | 9 | 4 | 1.820E 00 |
| 4 | 5 | 7.528E 00 | 9 | 5 | 2.244E 00 |
| 4 | 6 | 6.527E 00 | 9 | 6 | 2.337E 00 |
| 5 | 1 | 1.355E 00 | 10 | 1 | 1.109E 00 |
| 5 | 2 | 1.539E 00 | 10 | 2 | 1.163E 00 |
| 5 | 3 | 1.846E 00 | 10 | 3 | 1.300E 00 |
| 5 | 4 | 2.887E 00 | 10 | 4 | 1.726E 00 |
| 5 | 5 | 3.819E 00 | 10 | 5 | 2.550E 00 |
| 5 | 6 | 3.635E 00 | 10 | 6 | 2.956E 00 |
| 6 | 1 | 9.557E-01 | 11 | 1 | 9.820E-01 |
| 6 | 2 | 1.063E 00 | 11 | 2 | 1.035E 00 |
| 6 | 3 | 1.260E 00 | 11 | 3 | 1.146E 00 |
| 6 | 4 | 1.755E 00 | 11 | 4 | 1.619E 00 |
| 6 | 5 | 2.330E 00 | 11 | 5 | 2.602E 00 |
| 6 | 6 | 2.425E 00 | 11 | 6 | 3.211E 00 |

Table VII (Cont'd.)

| RUN | GAGE | Q(AV) | RUN | GAGE | Q(AV) |
|---|---|---|---|---|---|
| 12 | 1 | 9.689E-01 | 17 | 1 | 1.064E 00 |
| 12 | 2 | 1.086E 00 | 17 | 2 | 1.160E 00 |
| 12 | 3 | 1.239E 00 | 17 | 3 | 1.333E 00 |
| 12 | 4 | 1.828E 00 | 17 | 4 | 1.432E 00 |
| 12 | 5 | 2.871E 00 | 17 | 5 | 3.968E 00 |
| 12 | 6 | 3.560E 00 | 17 | 6 | 5.629E 00 |
| 13 | 1 | 1.324E 00 | 18 | 1 | 4.665E-01 |
| 13 | 2 | 1.581E 00 | 18 | 2 | 5.035E-01 |
| 13 | 3 | 1.992E 00 | 18 | 3 | 5.353E-01 |
| 13 | 4 | 2.824E 00 | 18 | 4 | 5.149E-01 |
| 13 | 5 | 5.288E 00 | 18 | 5 | 1.115E 00 |
| 13 | 6 | 5.194E 00 | 18 | 6 | 1.341E 00 |
| 14 | 1 | 1.136E 00 | 19 | 1 | 9.990E-01 |
| 14 | 2 | 1.283E 00 | 19 | 2 | 1.077E 00 |
| 14 | 3 | 1.516E 00 | 19 | 3 | 1.232E 00 |
| 14 | 4 | 2.223E 00 | 19 | 4 | 1.287E 00 |
| 14 | 5 | 3.643E 00 | 19 | 5 | 3.616E 00 |
| 14 | 6 | 4.230E 00 | 19 | 6 | 5.624E 00 |
| 15 | 1 | 2.478E 00 | 20 | 1 | 1.028E 00 |
| 15 | 2 | 3.026E 00 | 20 | 2 | 1.083E 00 |
| 15 | 3 | 3.638E 00 | 20 | 3 | 1.239E 00 |
| 15 | 4 | 5.600E 00 | 20 | 4 | 1.208E 00 |
| 15 | 5 | 1.062E 01 | 20 | 5 | 3.189E 00 |
| 15 | 6 | 9.426E 00 | 20 | 6 | 4.532E 00 |
| 16 | 1 | 1.652E 00 | 21 | 1 | 2.416E 00 |
| 16 | 2 | 1.801E 00 | 21 | 2 | 2.901E 00 |
| 16 | 3 | 2.142E 00 | 21 | 3 | 3.573E 00 |
| 16 | 4 | 3.099E 00 | 21 | 4 | 2.109E 00 |
| 16 | 5 | 5.348E 00 | 21 | 5 | 1.492E 01 |
| 16 | 6 | 5.782E 00 | 21 | 6 | 1.299E 01 |

Table VII (Concluded)

| RUN | GAGE | Q(AV) | RUN | GAGE | Q(AV) |
|---|---|---|---|---|---|
| 22 | 1 | 1.663E 00 | 28 | 1 | 3.899E 00 |
| 22 | 2 | 1.876E 00 | 28 | 2 | 5.208E 00 |
| 22 | 3 | 2.262E 00 | 28 | 3 | 8.256E 00 |
| 22 | 4 | 2.315E 00 | 28 | 4 | 1.844E 01 |
| 22 | 5 | 7.998E 00 | 28 | 5 | 2.727E 01 |
| 22 | 6 | 9.016E 00 | 28 | 6 | 1.533E 01 |
| 23 | 1 | 2.393E 00 | 29 | 1 | 2.322E 00 |
| 23 | 2 | 2.800E 00 | 29 | 2 | 2.580E 00 |
| 23 | 3 | 3.606E 00 | 29 | 3 | 2.973E 00 |
| 23 | 4 | 2.365E 00 | 29 | 4 | 4.268E 00 |
| 23 | 5 | 1.589E 01 | 29 | 5 | 7.258E 00 |
| 23 | 6 | 1.281E 01 | 29 | 6 | 6.191E 00 |
| 24 | 1 | 1.372E 00 | 30 | 1 | 5.270E 00 |
| 24 | 2 | 1.674E 00 | 30 | 2 | 5.662E 00 |
| 24 | 3 | 2.047E 00 | 30 | 3 | 7.143E 00 |
| 24 | 4 | 1.477E 00 | 30 | 4 | 1.046E 01 |
| 24 | 5 | 8.052E 00 | 30 | 5 | 1.677E 01 |
| 24 | 6 | 8.179E 00 | 30 | 6 | 1.201E 01 |
| 25 | 1 | 1.106E 00 | 31 | 1 | 1.984E 00 |
| 25 | 2 | 1.240E 00 | 31 | 2 | 2.114E 00 |
| 25 | 3 | 1.490E 00 | 31 | 3 | 2.381E 00 |
| 25 | 4 | 2.104E 00 | 31 | 4 | 1.498E 00 |
| 25 | 6 | 6.214E 00 | 31 | 5 | 6.893E 00 |
| | | | 31 | 6 | 7.105E 00 |
| 26 | 1 | 1.984E 00 | | | |
| 26 | 2 | 2.378E 00 | 32 | 1 | 5.138E 00 |
| 26 | 3 | 2.786E 00 | 32 | 2 | 5.596E 00 |
| 26 | 4 | 4.339E 00 | 32 | 3 | 6.993E 00 |
| 26 | 5 | 5.430E 00 | 32 | 4 | 1.038E 01 |
| 26 | 6 | 3.637E 00 | 32 | 5 | 2.438E 01 |
| | | | 32 | 6 | 1.553E 01 |
| 27 | 1 | 8.059E 00 | | | |

Table VIII

AXISYMMETRIC MODEL PRESSURE DATA

| RUN | GAGE | M | P(M) | P(M)/P | P(M)/PITOT |
|---|---|---|---|---|---|
| 1 | 1 | 1.214E 01 | 4.671E-02 | 2.893E 00 | 1.496E-02 |
| 1 | 2 | 1.214E 01 | 4.716E-02 | 2.921E 00 | 1.511E-02 |
| 1 | 3 | 1.214E 01 | 7.786E-02 | 4.822E 00 | 2.494E-02 |
| 1 | 4 | 1.214E 01 | 1.312E-01 | 8.126E 00 | 4.203E-02 |
| 1 | 5 | 1.214E 01 | 1.813E-01 | 1.123E 01 | 5.808E-02 |
| 1 | 6 | 1.214E 01 | 1.945E-01 | 1.204E 01 | 6.230E-02 |
| 1 | 7 | 1.214E 01 | 2.041E-01 | 1.264E 01 | 6.538E-02 |
| 1 | 8 | 1.214E 01 | 1.772E-01 | 1.098E 01 | 5.678E-02 |
| 3 | 2 | 1.432E 01 | 2.323E-02 | 3.829E 00 | 1.429E-02 |
| 3 | 3 | 1.432E 01 | 3.912E-02 | 6.448E 00 | 2.406E-02 |
| 3 | 4 | 1.432E 01 | 6.888E-02 | 1.135E 01 | 4.237E-02 |
| 3 | 5 | 1.432E 01 | 9.129E-02 | 1.505E 01 | 5.616E-02 |
| 3 | 6 | 1.432E 01 | 8.823E-02 | 1.454E 01 | 5.428E-02 |
| 3 | 7 | 1.432E 01 | 1.102E-01 | 1.817E 01 | 6.780E-02 |
| 3 | 8 | 1.432E 01 | 1.029E-01 | 1.696E 01 | 6.327E-02 |
| 4 | 1 | 1.228E 01 | 4.568E-02 | 2.896E 00 | 1.465E-02 |
| 4 | 2 | 1.228E 01 | 4.201E-02 | 2.663E 00 | 1.347E-02 |
| 4 | 3 | 1.228E 01 | 7.276E-02 | 4.612E 00 | 2.333E-02 |
| 4 | 4 | 1.228E 01 | 1.179E-01 | 7.472E 00 | 3.779E-02 |
| 4 | 5 | 1.228E 01 | 1.729E-01 | 1.096E 01 | 5.542E-02 |
| 4 | 6 | 1.228E 01 | 1.761E-01 | 1.116E 01 | 5.645E-02 |
| 4 | 7 | 1.228E 01 | 1.993E-01 | 1.263E 01 | 6.388E-02 |
| 4 | 8 | 1.228E 01 | 1.508E-01 | 9.561E 00 | 4.836E-02 |
| 5 | 1 | 1.434E 01 | 2.260E-02 | 3.774E 00 | 1.406E-02 |
| 5 | 2 | 1.434E 01 | 2.103E-02 | 3.511E 00 | 1.308E-02 |
| 5 | 3 | 1.434E 01 | 3.558E-02 | 5.942E 00 | 2.213E-02 |
| 5 | 4 | 1.434E 01 | 5.839E-02 | 9.750E 00 | 3.631E-02 |
| 5 | 5 | 1.434E 01 | 8.235E-02 | 1.375E 01 | 5.122E-02 |
| 5 | 6 | 1.434E 01 | 8.589E-02 | 1.434E 01 | 5.342E-02 |
| 5 | 7 | 1.434E 01 | 1.007E-01 | 1.682E 01 | 6.266E-02 |
| 6 | 1 | 1.696E 01 | 9.650E-03 | 5.649E 00 | 1.501E-02 |

Table VIII (Cont'd.)

| RUN | GAGE | M | P(M) | P(M)/P | P(M)/PITOT |
|---|---|---|---|---|---|
| 6 | 3 | 1.696E 01 | 1.421E-02 | 8.317E 00 | 2.210E-02 |
| 6 | 4 | 1.696E 01 | 2.263E-02 | 1.325E 01 | 3.521E-02 |
| 6 | 5 | 1.696E 01 | 2.819E-02 | 1.650E 01 | 4.385E-02 |
| 6 | 6 | 1.696E 01 | 3.116E-02 | 1.824E 01 | 4.848E-02 |
| 6 | 7 | 1.696E 01 | 3.609E-02 | 2.113E 01 | 5.615E-02 |
| 6 | 8 | 1.696E 01 | 3.189E-02 | 1.867E 01 | 4.961E-02 |
| 7 | 1 | 1.674E 01 | 8.148E-03 | 5.559E 00 | 1.514E-02 |
| 7 | 2 | 1.674E 01 | 7.733E-03 | 5.276E 00 | 1.437E-02 |
| 7 | 3 | 1.674E 01 | 1.186E-02 | 8.094E 00 | 2.205E-02 |
| 7 | 4 | 1.674E 01 | 1.738E-02 | 1.186E 01 | 3.231E-02 |
| 7 | 5 | 1.674E 01 | 2.334E-02 | 1.593E 01 | 4.338E-02 |
| 7 | 6 | 1.674E 01 | 2.474E-02 | 1.688E 01 | 4.597E-02 |
| 7 | 7 | 1.674E 01 | 3.010E-02 | 2.053E 01 | 5.594E-02 |
| 7 | 8 | 1.674E 01 | 2.680E-02 | 1.828E 01 | 4.981E-02 |
| 8 | 1 | 1.396E 01 | 1.337E-02 | 3.668E 00 | 1.441E-02 |
| 8 | 2 | 1.396E 01 | 1.268E-02 | 3.478E 00 | 1.366E-02 |
| 8 | 3 | 1.396E 01 | 1.976E-02 | 5.419E 00 | 2.128E-02 |
| 8 | 4 | 1.396E 01 | 3.025E-02 | 8.297E 00 | 3.259E-02 |
| 8 | 5 | 1.396E 01 | 4.385E-02 | 1.203E 01 | 4.723E-02 |
| 8 | 6 | 1.396E 01 | 4.322E-02 | 1.186E 01 | 4.657E-02 |
| 8 | 7 | 1.396E 01 | 5.529E-02 | 1.517E 01 | 5.956E-02 |
| 8 | 8 | 1.396E 01 | 4.370E-02 | 1.199E 01 | 4.708E-02 |
| 9 | 2 | 1.159E 01 | 7.311E-03 | 2.395E 00 | 1.360E-02 |
| 9 | 3 | 1.159E 01 | 1.134E-02 | 3.716E 00 | 2.109E-02 |
| 9 | 4 | 1.159E 01 | 1.621E-02 | 5.310E 00 | 3.014E-02 |
| 9 | 5 | 1.159E 01 | 2.340E-02 | 7.667E 00 | 4.353E-02 |
| 9 | 6 | 1.159E 01 | 2.096E-02 | 6.867E 00 | 3.898E-02 |
| 9 | 7 | 1.159E 01 | 2.776E-02 | 9.093E 00 | 5.162E-02 |
| 9 | 8 | 1.159E 01 | 2.220E-02 | 7.274E 00 | 4.130E-02 |
| 10 | 1 | 1.156E 01 | 8.527E-03 | 2.749E 00 | 1.568E-02 |
| 10 | 2 | 1.156E 01 | 7.053E-03 | 2.274E 00 | 1.297E-02 |

Table VIII (Cont'd.)

| RUN | GAGE | M | P(M) | P(M)/P | P(M)/PITOT |
|---|---|---|---|---|---|
| 10 | 3 | 1.156E 01 | 1.186E-02 | 3.824E 00 | 2.180E-02 |
| 10 | 4 | 1.156E 01 | 2.062E-02 | 6.649E 00 | 3.791E-02 |
| 10 | 5 | 1.156E 01 | 2.428E-02 | 7.829E 00 | 4.464E-02 |
| 10 | 6 | 1.156E 01 | 2.669E-02 | 8.604E 00 | 4.906E-02 |
| 10 | 7 | 1.156E 01 | 3.200E-02 | 1.032E 01 | 5.883E-02 |
| 10 | 8 | 1.156E 01 | 3.033E-02 | 9.780E 00 | 5.576E-02 |
| 11 | 1 | 1.680E 01 | 8.281E-03 | 5.675E 00 | 1.536E-02 |
| 11 | 2 | 1.680E 01 | 6.012E-03 | 4.120E 00 | 1.115E-02 |
| 11 | 3 | 1.680E 01 | 1.180E-02 | 8.084E 00 | 2.189E-02 |
| 11 | 4 | 1.680E 01 | 1.717E-02 | 1.176E 01 | 3.185E-02 |
| 11 | 5 | 1.680E 01 | 2.818E-02 | 1.931E 01 | 5.228E-02 |
| 11 | 6 | 1.680E 01 | 3.234E-02 | 2.216E 01 | 6.000E-02 |
| 11 | 8 | 1.680E 01 | 3.800E-02 | 2.604E 01 | 7.051E-02 |
| 12 | 1 | 1.693E 01 | 9.358E-03 | 5.250E 00 | 1.400E-02 |
| 12 | 2 | 1.693E 01 | 7.029E-03 | 3.944E 00 | 1.052E-02 |
| 12 | 3 | 1.693E 01 | 1.378E-02 | 7.730E 00 | 2.061E-02 |
| 12 | 4 | 1.693E 01 | 2.141E-02 | 1.201E 01 | 3.203E-02 |
| 12 | 5 | 1.693E 01 | 3.568E-02 | 2.002E 01 | 5.337E-02 |
| 12 | 6 | 1.693E 01 | 3.811E-02 | 2.138E 01 | 5.702E-02 |
| 12 | 8 | 1.693E 01 | 4.996E-02 | 2.803E 01 | 7.474E-02 |
| 13 | 1 | 1.430E 01 | 2.249E-02 | 3.734E 00 | 1.397E-02 |
| 13 | 2 | 1.430E 01 | 1.577E-02 | 2.619E 00 | 9.801E-03 |
| 13 | 3 | 1.430E 01 | 3.408E-02 | 5.657E 00 | 2.117E-02 |
| 13 | 4 | 1.430E 01 | 5.589E-02 | 9.278E 00 | 3.472E-02 |
| 13 | 5 | 1.430E 01 | 9.390E-02 | 1.559E 01 | 5.834E-02 |
| 13 | 6 | 1.430E 01 | 1.166E-01 | 1.936E 01 | 7.246E-02 |
| 13 | 7 | 1.430E 01 | 1.497E-01 | 2.485E 01 | 9.302E-02 |
| 13 | 8 | 1.430E 01 | 1.240E-01 | 2.058E 01 | 7.704E-02 |
| 14 | 2 | 1.391E 01 | 1.134E-02 | 2.974E 00 | 1.175E-02 |
| 14 | 3 | 1.391E 01 | 2.058E-02 | 5.397E 00 | 2.132E-02 |
| 14 | 4 | 1.391E 01 | 3.005E-02 | 7.879E 00 | 3.112E-02 |

Table VIII (Cont'd.)

| RUN | GAGE | M | P(M) | P(M)/P | P(M)/PITOT |
|---|---|---|---|---|---|
| 14 | 5 | 1.391E 01 | 6.555E-02 | 1.719E 01 | 6.789E-02 |
| 14 | 6 | 1.391E 01 | 6.189E-02 | 1.623E 01 | 6.410E-02 |
| 14 | 7 | 1.391E 01 | 8.310E-02 | 2.179E 01 | 8.606E-02 |
| 14 | 8 | 1.391E 01 | 6.966E-02 | 1.826E 01 | 7.214E-02 |
| 15 | 1 | 1.209E 01 | 4.568E-02 | 2.757E 00 | 1.436E-02 |
| 15 | 2 | 1.209E 01 | 3.357E-02 | 2.026E 00 | 1.055E-02 |
| 15 | 3 | 1.209E 01 | 7.096E-02 | 4.283E 00 | 2.231E-02 |
| 15 | 4 | 1.209E 01 | 1.127E-01 | 6.804E 00 | 3.544E-02 |
| 15 | 5 | 1.209E 01 | 1.931E-01 | 1.166E 01 | 6.071E-02 |
| 15 | 6 | 1.209E 01 | 2.716E-01 | 1.639E 01 | 8.537E-02 |
| 15 | 7 | 1.209E 01 | 2.870E-01 | 1.732E 01 | 9.022E-02 |
| 15 | 8 | 1.209E 01 | 2.345E-01 | 1.415E 01 | 7.372E-02 |
| 16 | 1 | 1.175E 01 | 2.053E-02 | 2.790E 00 | 1.539E-02 |
| 16 | 2 | 1.175E 01 | 1.788E-02 | 2.430E 00 | 1.341E-02 |
| 16 | 3 | 1.175E 01 | 1.532E-02 | 2.082E 00 | 1.148E-02 |
| 16 | 4 | 1.175E 01 | 4.656E-02 | 6.326E 00 | 3.490E-02 |
| 16 | 5 | 1.175E 01 | 7.422E-02 | 1.009E 01 | 5.563E-02 |
| 16 | 6 | 1.175E 01 | 9.840E-02 | 1.337E 01 | 7.375E-02 |
| 16 | 7 | 1.175E 01 | 1.218E-01 | 1.655E 01 | 9.131E-02 |
| 16 | 8 | 1.175E 01 | 1.049E-01 | 1.426E 01 | 7.866E-02 |
| 17 | 1 | 1.693E 01 | 9.896E-03 | 5.412E 00 | 1.443E-02 |
| 17 | 2 | 1.693E 01 | 8.506E-03 | 4.652E 00 | 1.240E-02 |
| 17 | 3 | 1.693E 01 | 6.206E-03 | 3.394E 00 | 9.047E-03 |
| 17 | 4 | 1.693E 01 | 2.251E-02 | 1.231E 01 | 3.281E-02 |
| 17 | 5 | 1.693E 01 | 3.578E-02 | 1.957E 01 | 5.215E-02 |
| 17 | 6 | 1.693E 01 | 6.006E-02 | 3.285E 01 | 8.755E-02 |
| 17 | 7 | 1.693E 01 | 9.949E-02 | 5.441E 01 | 1.450E-01 |
| 17 | 8 | 1.693E 01 | 7.791E-02 | 4.261E 01 | 1.136E-01 |
| 18 | 1 | 1.549E 01 | 2.004E-03 | 4.824E 00 | 1.537E-02 |
| 18 | 2 | 1.549E 01 | 1.595E-03 | 3.838E 00 | 1.223E-02 |
| 18 | 3 | 1.549E 01 | 1.215E-03 | 2.924E 00 | 9.314E-03 |

Table VIII (Cont'd.)

| RUN | GAGE | M | P(M) | P(M)/P | P(M)/PITOT |
|---|---|---|---|---|---|
| 18 | 4 | 1.549E 01 | 2.899E-03 | 6.977E 00 | 2.223E-02 |
| 18 | 5 | 1.549E 01 | 5.979E-03 | 1.439E 01 | 4.584E-02 |
| 18 | 6 | 1.549E 01 | 7.493E-03 | 1.803E 01 | 5.745E-02 |
| 18 | 8 | 1.549E 01 | 7.940E-03 | 1.911E 01 | 6.088E-02 |
| 19 | 1 | 1.678E 01 | 7.989E-03 | 5.414E 00 | 1.469E-02 |
| 19 | 2 | 1.678E 01 | 5.646E-03 | 3.826E 00 | 1.038E-02 |
| 19 | 3 | 1.678E 01 | 2.162E-03 | 1.465E 00 | 3.975E-03 |
| 19 | 4 | 1.678E 01 | 2.075E-02 | 1.406E 01 | 3.815E-02 |
| 19 | 5 | 1.678E 01 | 3.053E-02 | 2.069E 01 | 5.613E-02 |
| 19 | 6 | 1.678E 01 | 4.988E-02 | 3.381E 01 | 9.171E-02 |
| 19 | 7 | 1.678E 01 | 8.376E-02 | 5.677E 01 | 1.540E-01 |
| 19 | 8 | 1.678E 01 | 7.781E-02 | 5.274E 01 | 1.431E-01 |
| 20 | 1 | 1.154E 01 | 8.327E-03 | 2.802E 00 | 1.602E-02 |
| 20 | 2 | 1.154E 01 | 5.829E-03 | 1.961E 00 | 1.121E-02 |
| 20 | 4 | 1.154E 01 | 1.627E-02 | 5.475E 00 | 3.130E-02 |
| 20 | 5 | 1.154E 01 | 2.880E-02 | 9.691E 00 | 5.540E-02 |
| 20 | 6 | 1.154E 01 | 4.177E-02 | 1.405E 01 | 8.034E-02 |
| 20 | 7 | 1.154E 01 | 6.511E-02 | 2.191E 01 | 1.252E-01 |
| 21 | 1 | 1.210E 01 | 4.450E-02 | 2.748E 00 | 1.429E-02 |
| 21 | 2 | 1.210E 01 | 3.066E-02 | 1.894E 00 | 9.848E-03 |
| 21 | 3 | 1.210E 01 | 2.224E-02 | 1.373E 00 | 7.141E-03 |
| 21 | 4 | 1.210E 01 | 1.782E-01 | 1.100E 01 | 5.722E-02 |
| 21 | 5 | 1.210E 01 | 2.616E-01 | 1.616E 01 | 8.402E-02 |
| 21 | 6 | 1.210E 01 | 4.372E-01 | 2.700E 01 | 1.404E-01 |
| 21 | 7 | 1.210E 01 | 6.510E-01 | 4.020E 01 | 2.091E-01 |
| 21 | 8 | 1.210E 01 | 4.030E-01 | 2.489E 01 | 1.294E-01 |
| 22 | 1 | 1.178E 01 | 2.023E-02 | 2.738E 00 | 1.504E-02 |
| 22 | 2 | 1.178E 01 | 1.623E-02 | 2.197E 00 | 1.206E-02 |
| 22 | 4 | 1.178E 01 | 5.435E-02 | 7.356E 00 | 4.039E-02 |
| 22 | 5 | 1.178E 01 | 9.478E-02 | 1.283E 01 | 7.044E-02 |
| 22 | 6 | 1.178E 01 | 1.512E-01 | 2.047E 01 | 1.124E-01 |

Table VIII (Cont'd.)

| RUN | GAGE | M | P(M) | P(M)/P | P(M)/PITOT |
|---|---|---|---|---|---|
| 22 | 7 | 1.178E 01 | 2.285E-01 | 3.093E 01 | 1.698E-01 |
| 22 | 8 | 1.178E 01 | 1.753E-01 | 2.372E 01 | 1.303E-01 |
| 23 | 1 | 1.211E 01 | 4.453E-02 | 2.798E 00 | 1.454E-02 |
| 23 | 2 | 1.211E 01 | 3.294E-02 | 2.069E 00 | 1.076E-02 |
| 23 | 3 | 1.211E 01 | 3.459E-02 | 2.173E 00 | 1.129E-02 |
| 23 | 4 | 1.211E 01 | 1.709E-01 | 1.074E 01 | 5.580E-02 |
| 23 | 5 | 1.211E 01 | 2.461E-01 | 1.546E 01 | 8.038E-02 |
| 23 | 6 | 1.211E 01 | 4.133E-01 | 2.597E 01 | 1.350E-01 |
| 23 | 7 | 1.211E 01 | 6.341E-01 | 3.984E 01 | 2.071E-01 |
| 23 | 8 | 1.211E 01 | 3.842E-01 | 2.414E 01 | 1.255E-01 |
| 24 | 1 | 1.430E 01 | 2.238E-02 | 3.732E 00 | 1.397E-02 |
| 24 | 2 | 1.430E 01 | 1.567E-02 | 2.612E 00 | 9.781E-03 |
| 24 | 4 | 1.430E 01 | 8.218E-02 | 1.370E 01 | 5.130E-02 |
| 24 | 5 | 1.430E 01 | 1.270E-01 | 2.117E 01 | 7.925E-02 |
| 24 | 6 | 1.430E 01 | 1.876E-01 | 3.128E 01 | 1.171E-01 |
| 24 | 7 | 1.430E 01 | 3.190E-01 | 5.318E 01 | 1.991E-01 |
| 24 | 8 | 1.430E 01 | 2.169E-01 | 3.616E 01 | 1.354E-01 |
| 25 | 1 | 1.400E 01 | 1.391E-02 | 3.771E 00 | 1.473E-02 |
| 25 | 2 | 1.400E 01 | 1.083E-02 | 2.935E 00 | 1.147E-02 |
| 25 | 7 | 1.400E 01 | 1.577E-01 | 4.275E 01 | 1.670E-01 |
| 25 | 8 | 1.400E 01 | 1.238E-01 | 3.355E 01 | 1.311E-01 |
| 26 | 1 | 7.662E 00 | 8.323E-02 | 1.876E 00 | 2.451E-02 |
| 26 | 2 | 7.662E 00 | 8.710E-02 | 1.963E 00 | 2.565E-02 |
| 26 | 3 | 7.662E 00 | 1.214E-01 | 2.735E 00 | 3.574E-02 |
| 26 | 4 | 7.662E 00 | 1.965E-01 | 4.428E 00 | 5.786E-02 |
| 26 | 5 | 7.662E 00 | 2.841E-01 | 6.403E 00 | 8.367E-02 |
| 26 | 7 | 7.662E 00 | 2.520E-01 | 5.679E 00 | 7.421E-02 |
| 27 | 1 | 7.888E 00 | 4.762E-01 | 1.859E 00 | 2.291E-02 |
| 27 | 2 | 7.888E 00 | 5.123E-01 | 2.000E 00 | 2.465E-02 |
| 27 | 3 | 7.888E 00 | 7.484E-01 | 2.921E 00 | 3.600E-02 |

Table VIII (Cont'd.)

| RUN | GAGE | M | P(M) | P(M)/P | P(M)/PITOT |
|---|---|---|---|---|---|
| 27 | 4 | 7.888E 00 | 1.290E 00 | 5.036E 00 | 6.207E-02 |
| 27 | 5 | 7.888E 00 | 1.596E 00 | 6.228E 00 | 7.676E-02 |
| 27 | 6 | 7.888E 00 | 1.566E 00 | 6.113E 00 | 7.535E-02 |
| 27 | 7 | 7.888E 00 | 1.472E 00 | 5.746E 00 | 7.082E-02 |
| 27 | 8 | 7.888E 00 | 1.158E 00 | 4.518E 00 | 5.569E-02 |
| 28 | 1 | 7.766E 00 | 2.476E-01 | 1.845E 00 | 2.346E-02 |
| 28 | 2 | 7.766E 00 | 2.638E-01 | 1.966E 00 | 2.499E-02 |
| 28 | 3 | 7.766E 00 | 3.796E-01 | 2.829E 00 | 3.597E-02 |
| 28 | 4 | 7.766E 00 | 6.583E-01 | 4.905E 00 | 6.237E-02 |
| 28 | 5 | 7.766E 00 | 8.068E-01 | 6.012E 00 | 7.644E-02 |
| 28 | 6 | 7.766E 00 | 8.227E-01 | 6.130E 00 | 7.795E-02 |
| 28 | 7 | 7.766E 00 | 7.490E-01 | 5.581E 00 | 7.096E-02 |
| 28 | 8 | 7.766E 00 | 5.783E-01 | 4.309E 00 | 5.480E-02 |
| 29 | 1 | 7.545E 00 | 7.901E-02 | 1.804E 00 | 2.425E-02 |
| 29 | 2 | 7.545E 00 | 8.032E-02 | 1.833E 00 | 2.466E-02 |
| 29 | 3 | 7.545E 00 | 1.144E-01 | 2.612E 00 | 3.513E-02 |
| 29 | 5 | 7.545E 00 | 2.702E-01 | 6.167E 00 | 8.293E-02 |
| 29 | 6 | 7.545E 00 | 3.551E-01 | 8.106E 00 | 1.090E-01 |
| 29 | 7 | 7.545E 00 | 3.242E-01 | 7.401E 00 | 9.953E-02 |
| 29 | 8 | 7.545E 00 | 2.697E-01 | 6.156E 00 | 8.278E-02 |
| 30 | 1 | 7.844E 00 | 3.717E-01 | 2.033E 00 | 2.565E-02 |
| 30 | 2 | 7.844E 00 | 3.818E-01 | 2.089E 00 | 2.636E-02 |
| 30 | 3 | 7.844E 00 | 5.232E-01 | 2.863E 00 | 3.612E-02 |
| 30 | 4 | 7.844E 00 | 8.253E-01 | 4.516E 00 | 5.697E-02 |
| 30 | 5 | 7.844E 00 | 1.271E 00 | 6.952E 00 | 8.771E-02 |
| 30 | 6 | 7.844E 00 | 1.483E 00 | 8.115E 00 | 1.024E-01 |
| 30 | 7 | 7.844E 00 | 1.308E 00 | 7.155E 00 | 9.027E-02 |
| 30 | 8 | 7.844E 00 | 1.012E 00 | 5.538E 00 | 6.986E-02 |
| 31 | 1 | 7.650E 00 | 7.949E-02 | 1.873E 00 | 2.455E-02 |
| 31 | 2 | 7.650E 00 | 8.497E-02 | 2.002E 00 | 2.624E-02 |
| 31 | 3 | 7.650E 00 | 1.176E-01 | 2.772E 00 | 3.633E-02 |

Table VIII (Concluded)

| RUN | GAGE | M | P(M) | P(M)/P | P(M)/PITOT |
|---|---|---|---|---|---|
| 31 | 4 | 7.650E 00 | 2.585E-01 | 6.092E 00 | 7.986E-02 |
| 31 | 5 | 7.650E 00 | 3.031E-01 | 7.142E 00 | 9.362E-02 |
| 31 | 6 | 7.650E 00 | 5.441E-01 | 1.282E 01 | 1.681E-01 |
| 31 | 7 | 7.650E 00 | 5.533E-01 | 1.304E 01 | 1.709E-01 |
| 31 | 8 | 7.650E 00 | 3.713E-01 | 8.749E 00 | 1.147E-01 |
| 32 | 1 | 7.850E 00 | 3.641E-01 | 2.005E 00 | 2.527E-02 |
| 32 | 2 | 7.850E 00 | 3.802E-01 | 2.094E 00 | 2.639E-02 |
| 32 | 3 | 7.850E 00 | 5.209E-01 | 2.869E 00 | 3.615E-02 |
| 32 | 4 | 7.850E 00 | 8.383E-01 | 4.618E 00 | 5.818E-02 |
| 32 | 5 | 7.850E 00 | 1.770E 00 | 9.750E 00 | 1.228E-01 |
| 32 | 6 | 7.850E 00 | 2.578E 00 | 1.420E 01 | 1.790E-01 |
| 32 | 7 | 7.850E 00 | 2.600E 00 | 1.432E 01 | 1.805E-01 |
| 32 | 8 | 7.850E 00 | 1.594E 00 | 8.781E 00 | 1.106E-01 |

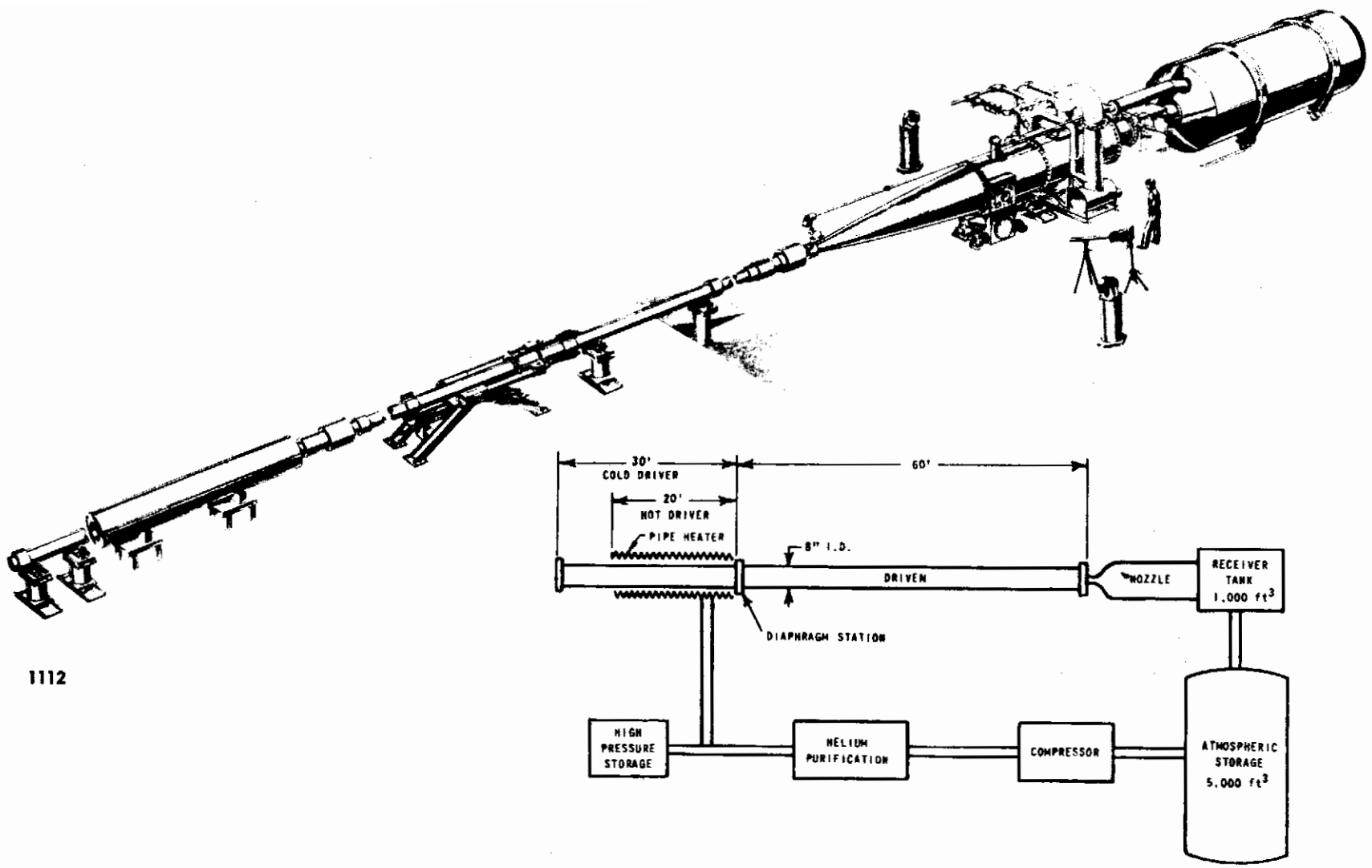


Figure 1 CAL 48-INCH LEG OF THE HYPERSONIC SHOCK TUNNEL

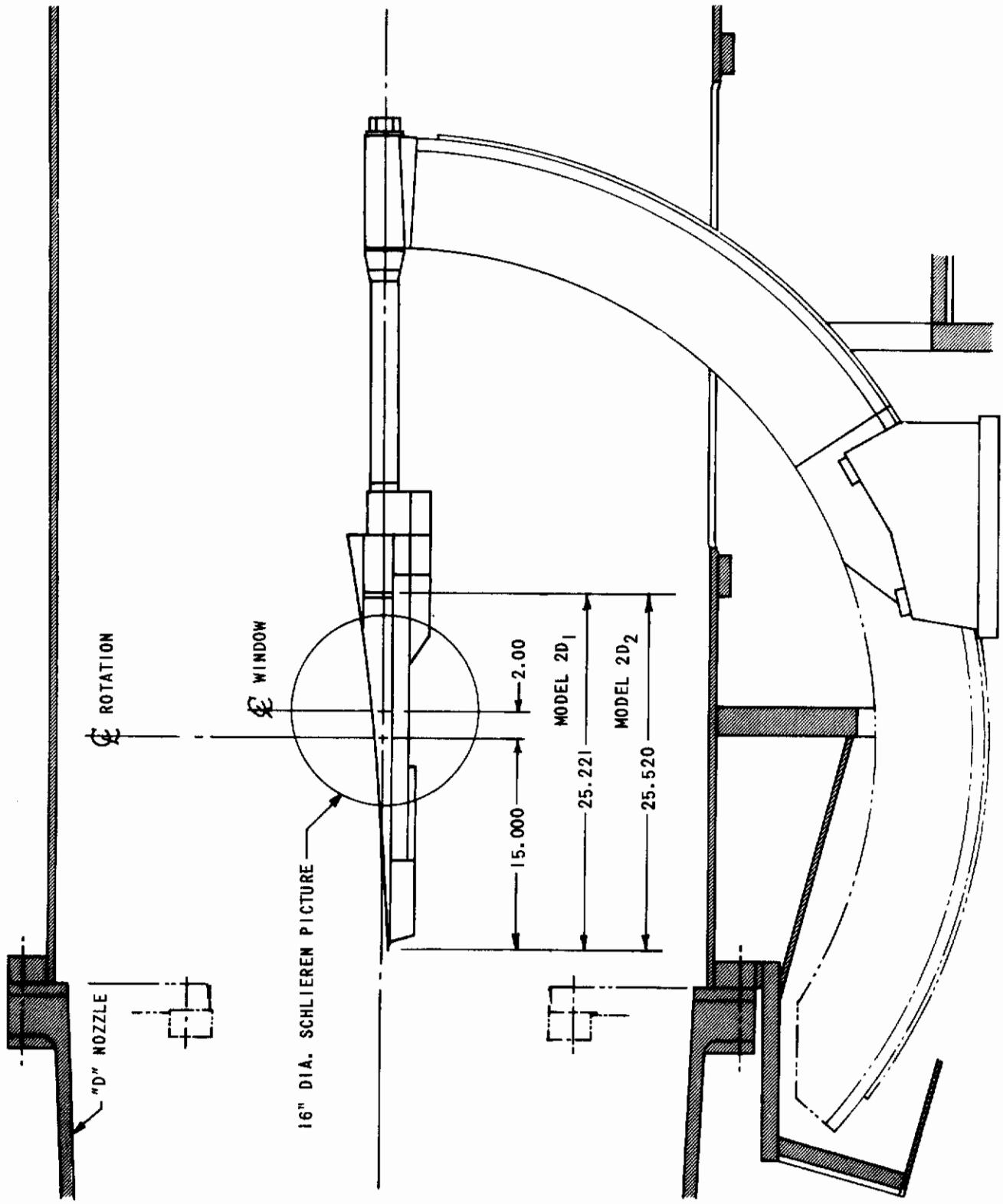


Figure 2 INSTALLATION OF THE TWO-DIMENSIONAL MODELS IN THE 48-INCH LEG

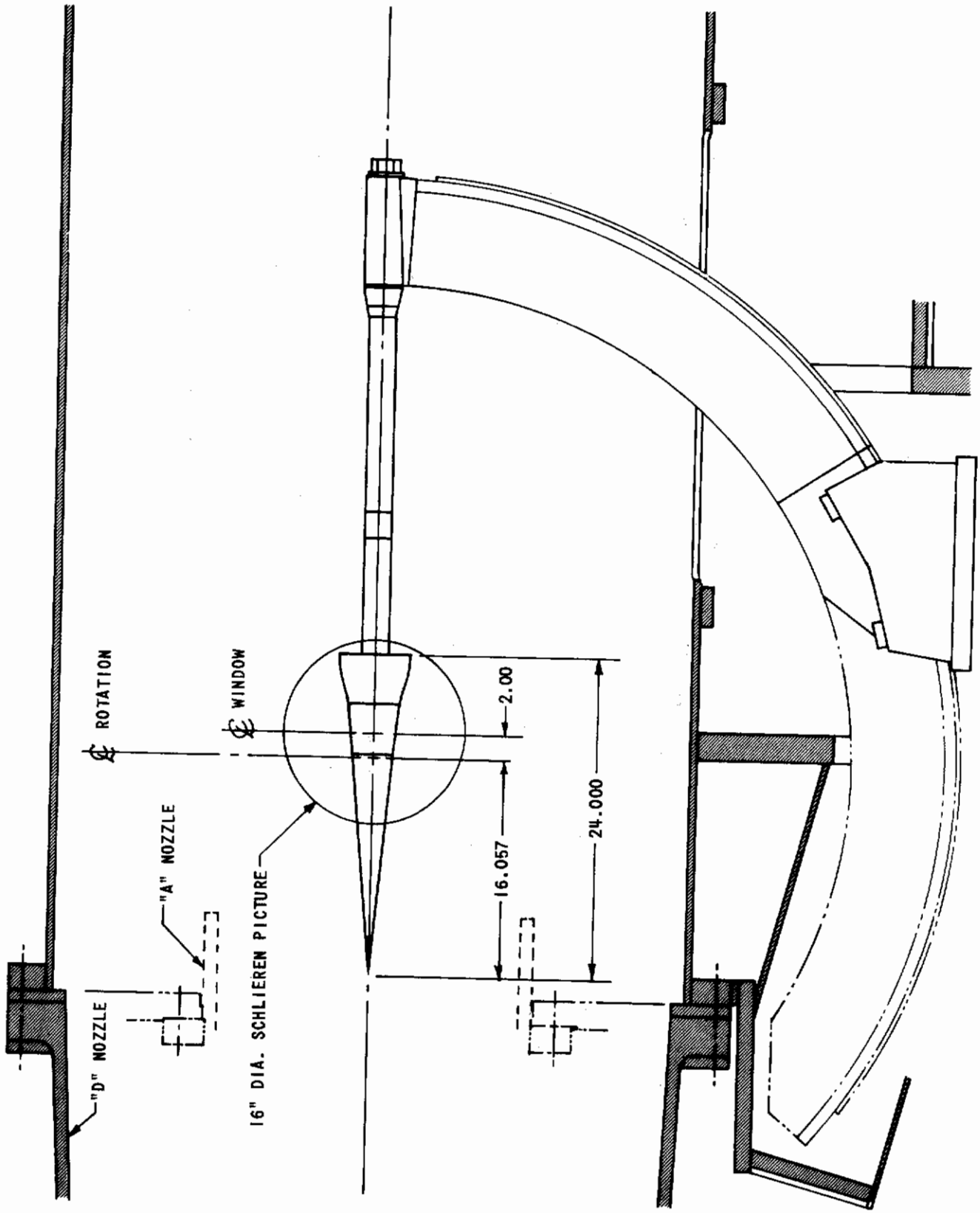


Figure 3 INSTALLATION OF THE AXISYMMETRIC MODELS IN THE 48-INCH LEG

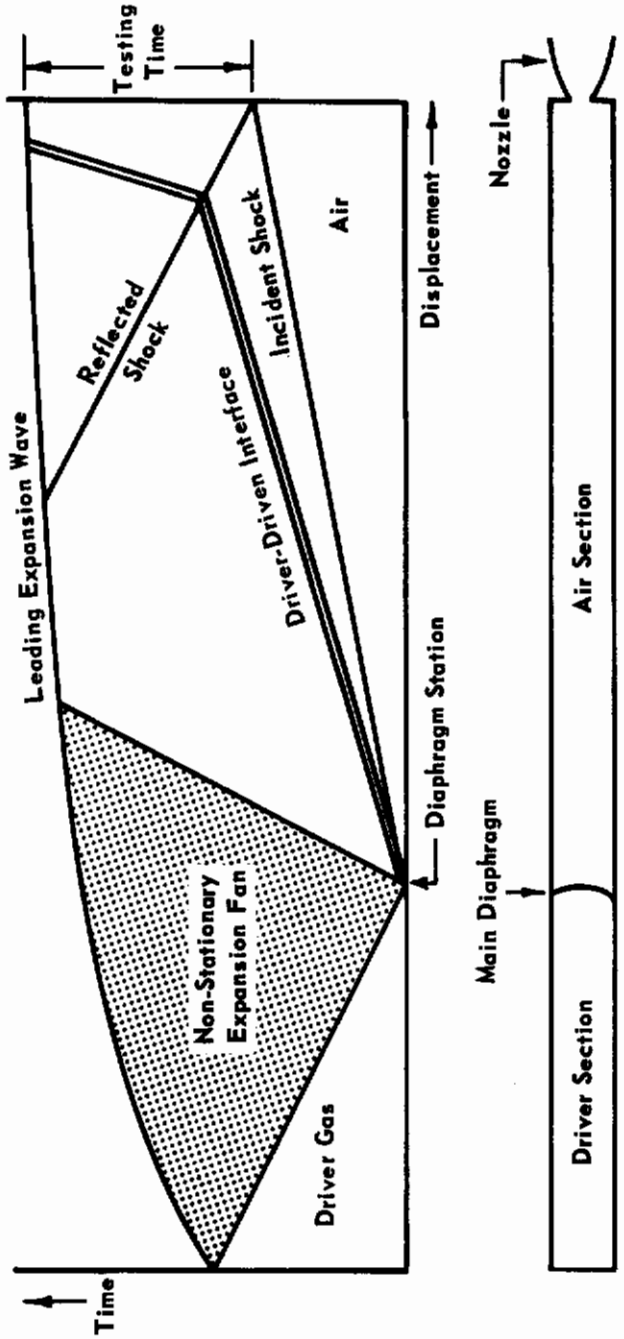


Figure 4 WAVE DIAGRAM FOR TAILORED-INTERFACE SCHOCK TUBE

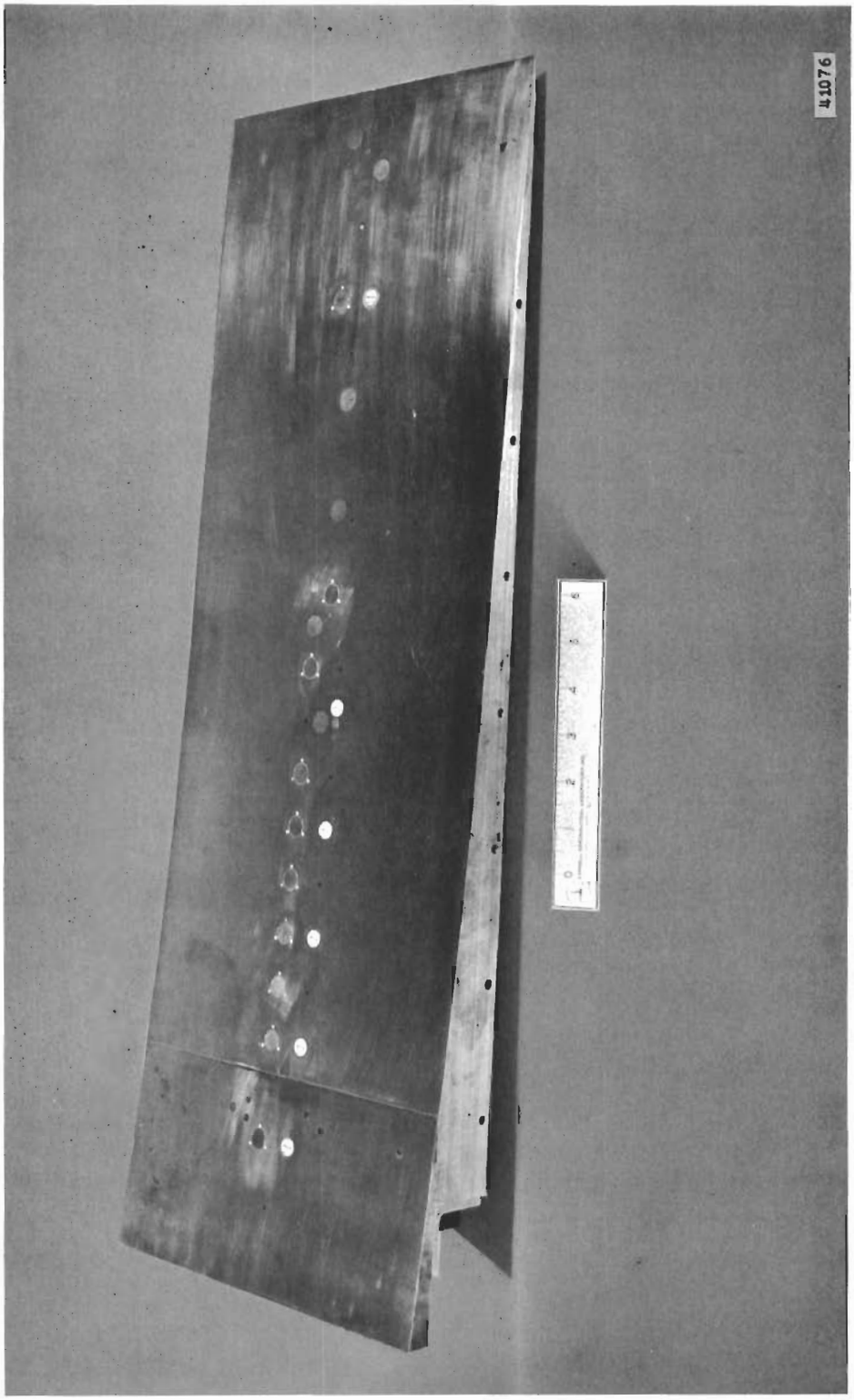


Figure 5 MODEL 2D1

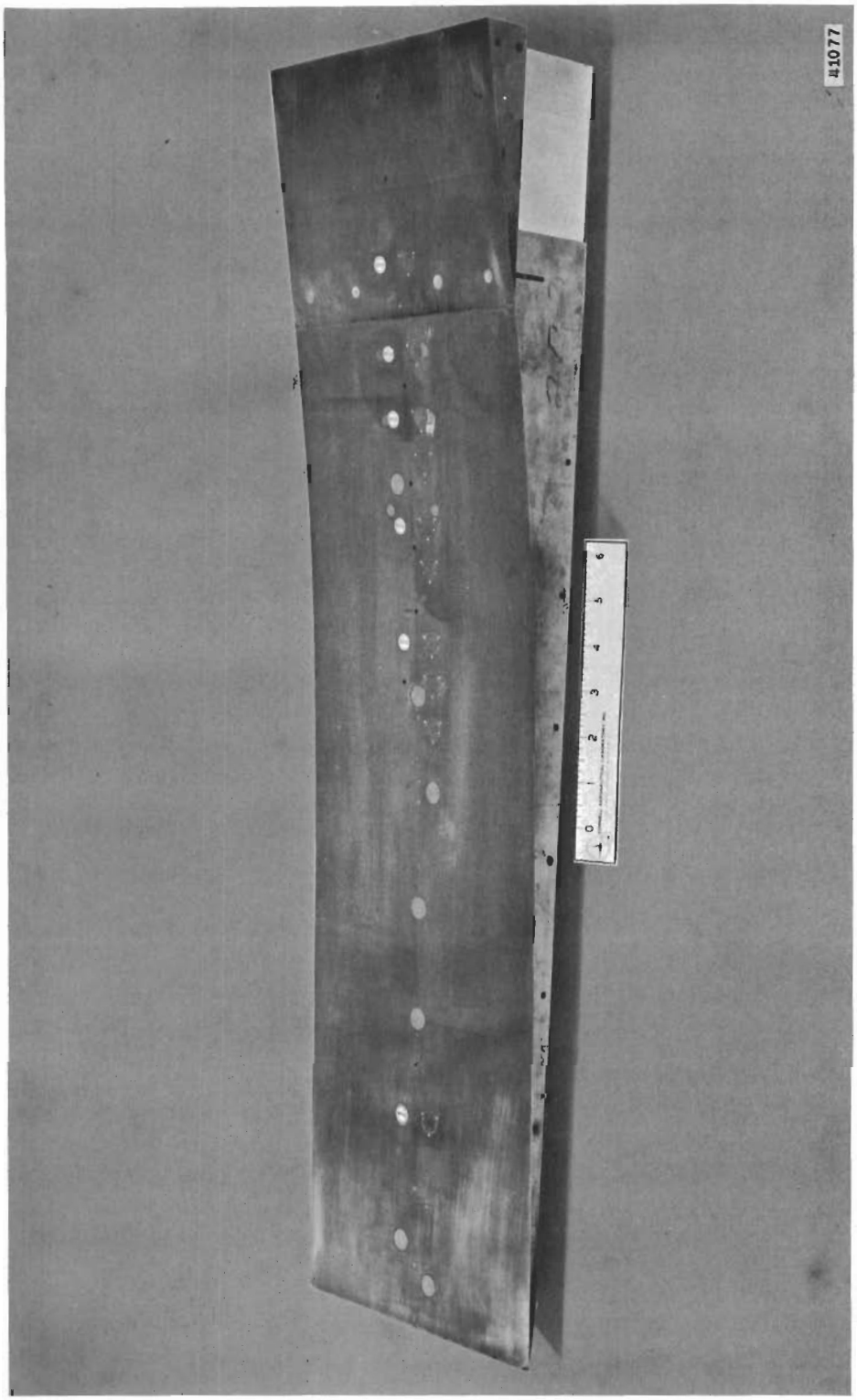


Figure 6 MODEL 2D2

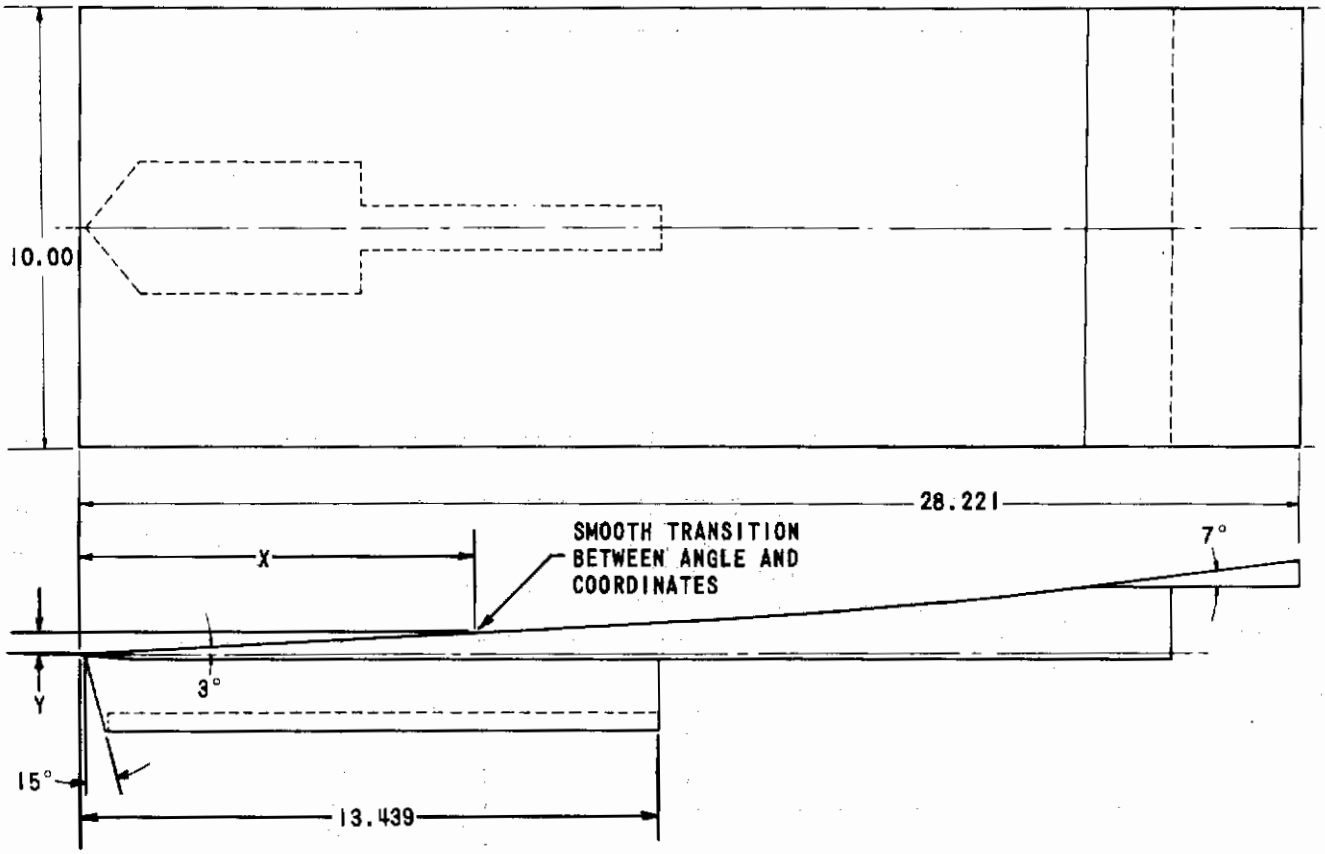


| COORDINATES | | | |
|---|---|---|---|
| X | Y | X | Y |
| 11.03 | .577 | 18.490 | 1.042 |
| 11.33 | .596 | 19.086 | 1.094 |
| 11.929 | .620 | 19.683 | 1.147 |
| 12.525 | .650 | 20.279 | 1.205 |
| 13.122 | .679 | 20.577 | 1.235 |
| 13.718 | .712 | 20.876 | 1.266 |
| 14.3147 | .749 | 21.174 | 1.298 |
| 14.911 | .787 | 21.770 | 1.363 |
| 15.508 | .824 | 22.068 | 1.397 |
| 16.104 | .864 | 22.367 | 1.431 |
| 16.700 | .907 | 22.665 | 1.465 |
| 17.297 | .951 | 22.963 | 1.501 |
| 17.893 | .996 | 23.221 | 1.536 |

Figure 7 MODEL 2D1

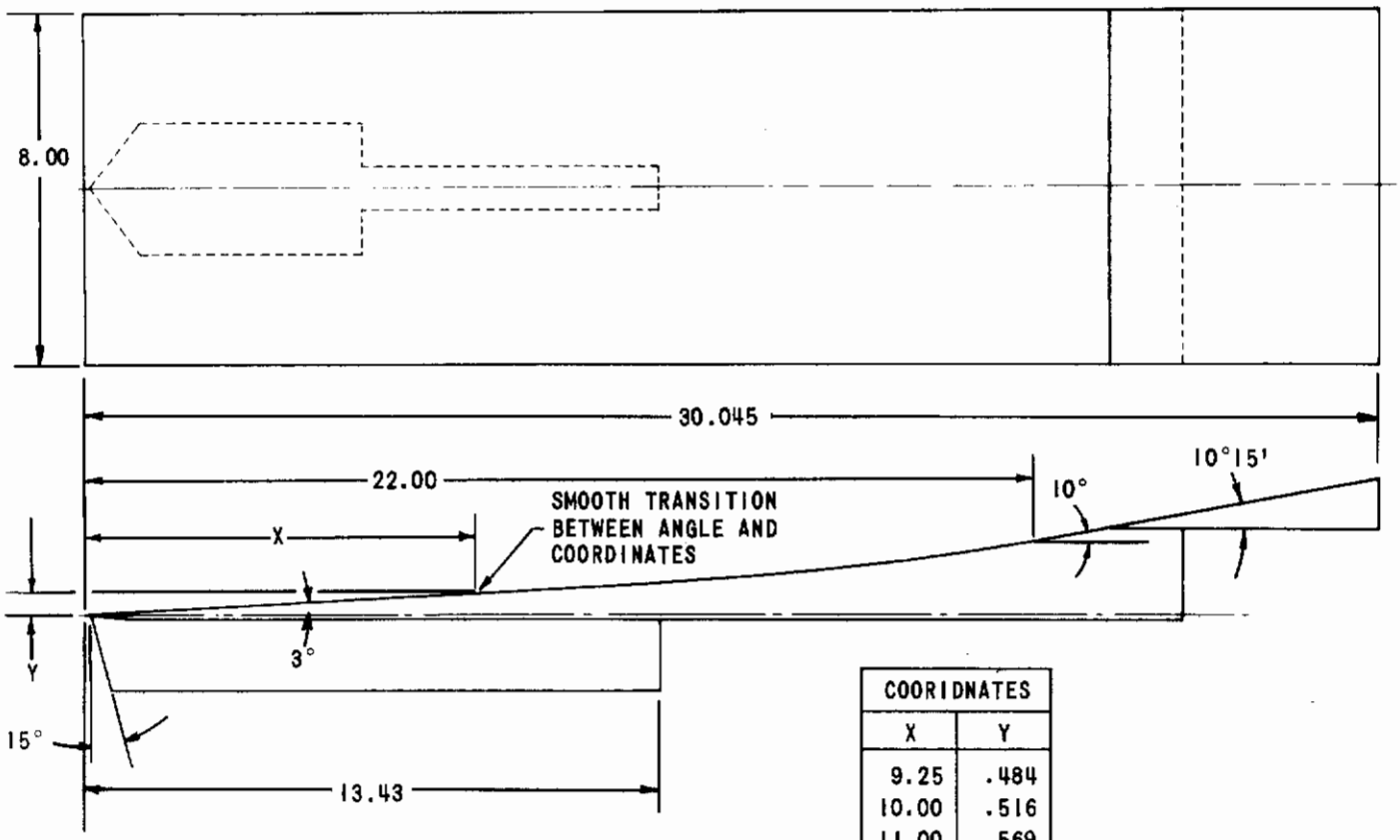


| COORIDNATES | |
|---|---|
| X | Y |
| 9.25 | .484 |
| 10.00 | .516 |
| 11.00 | .569 |
| 12.00 | .628 |
| 13.00 | .691 |
| 14.00 | .760 |
| 15.00 | .835 |
| 16.00 | .915 |
| 17.00 | 1.005 |
| 17.50 | 1.054 |
| 18.00 | 1.105 |
| 18.50 | 1.160 |
| 19.00 | 1.220 |
| 19.50 | 1.283 |
| 20.00 | 1.350 |
| 20.50 | 1.420 |
| 21.00 | 1.494 |
| 21.50 | 1.573 |
| 22.00 | 1.660 |

Figure 8 MODEL 2D2

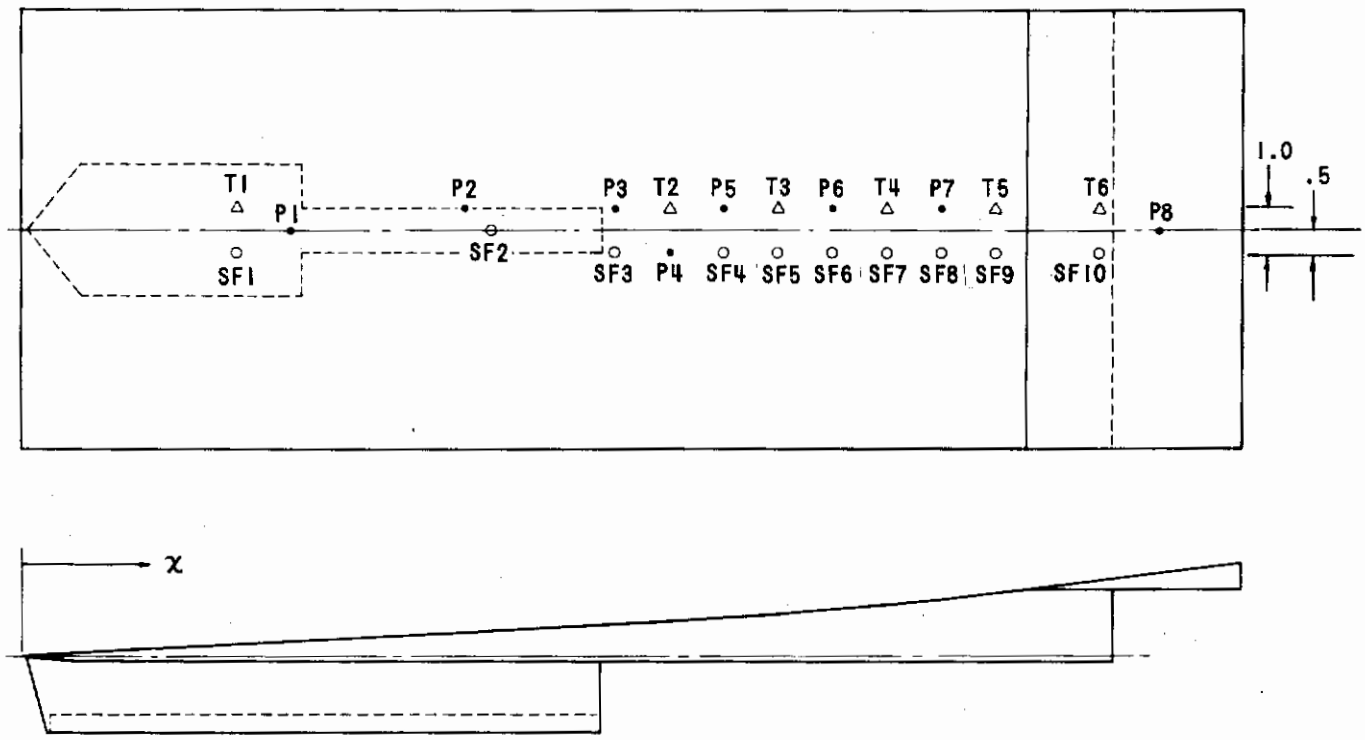


| GAGE | X | GAGE | X | GAGE | X |
|---|---|---|---|---|---|
| T1 | 5.00 | SF1 | 5.00 | P1 | 6.30 |
| T2 | 14.65 | SF2 | 12.00 | P2 | 10.25 |
| T3 | 17.50 | SF3 | 13.75 | P3 | 13.75 |
| T4 | 20.00 | SF4 | 16.25 | P4 | 15.00 |
| T5 | 22.50 | SF5 | 17.50 | P5 | 16.25 |
| T6 | 24.78 | SF6 | 18.75 | P6 | 18.75 |
| | | SF7 | 20.00 | P7 | 21.25 |
| | | SF8 | 21.25 | P8 | 26.25 |
| | | SF9 | 22.50 | | |
| | | SF10 | 24.78 | | |

Figure 9 MODEL 2D1 INSTRUMENTATION LOCATIONS

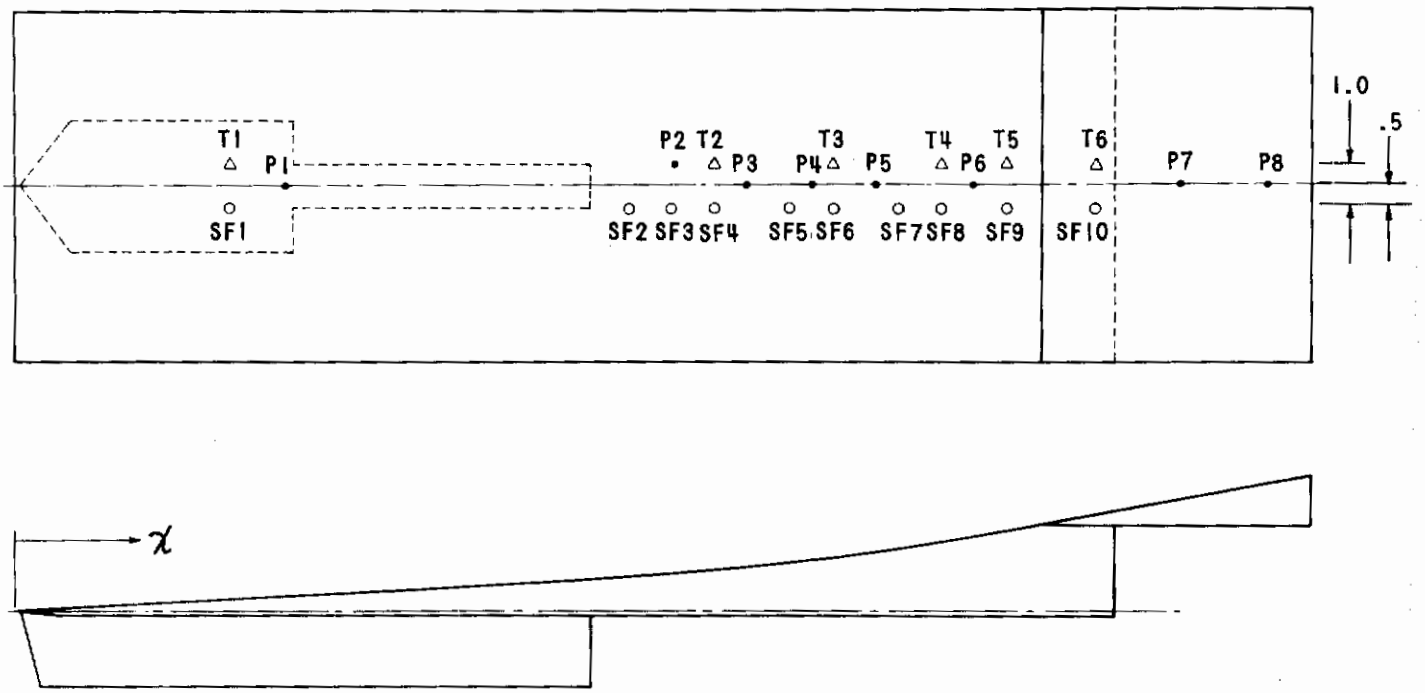


| GAGE | X | GAGE | X | GAGE | X |
|---|---|---|---|---|---|
| T1 | 5.00 | SF1 | 5.00 | P1 | 6.28 |
| T2 | 15.31 | SF2 | 14.25 | P2 | 15.31 |
| T3 | 19.00 | SF3 | 15.31 | P3 | 17.00 |
| T4 | 21.50 | SF4 | 16.25 | P4 | 18.00 |
| T5 | 23.00 | SF5 | 18.00 | P5 | 20.00 |
| T6 | 25.07 | SF6 | 19.00 | P6 | 22.25 |
| | | SF7 | 20.50 | P7 | 27.00 |
| | | SF8 | 21.50 | P8 | 28.84 |
| | | SF9 | 23.00 | | |
| | | SF10 | 25.07 | | |

Figure 10 MODEL 2D2 INSTRUMENTATION LOCATIONS

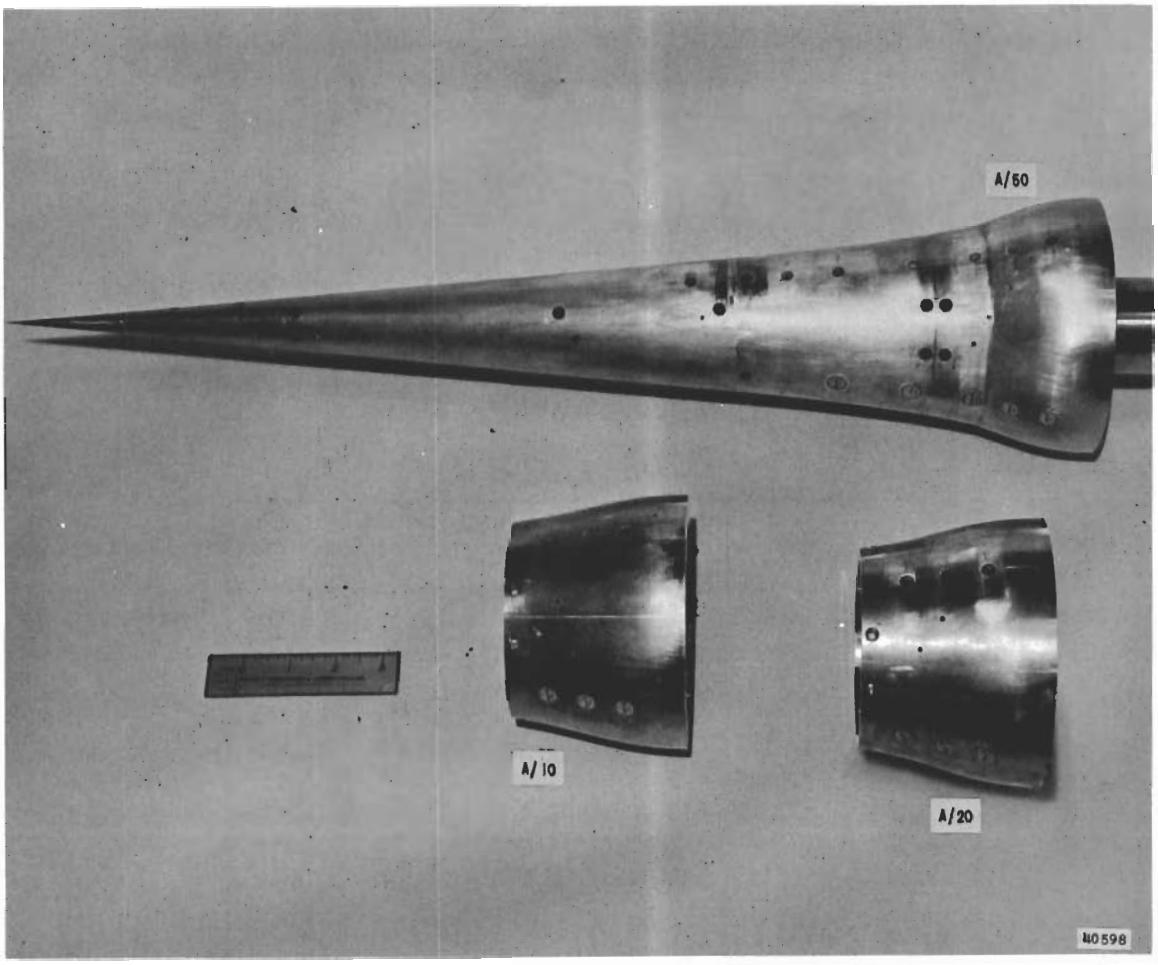


Figure 11 MODELS A/10, A/20 AND A/50

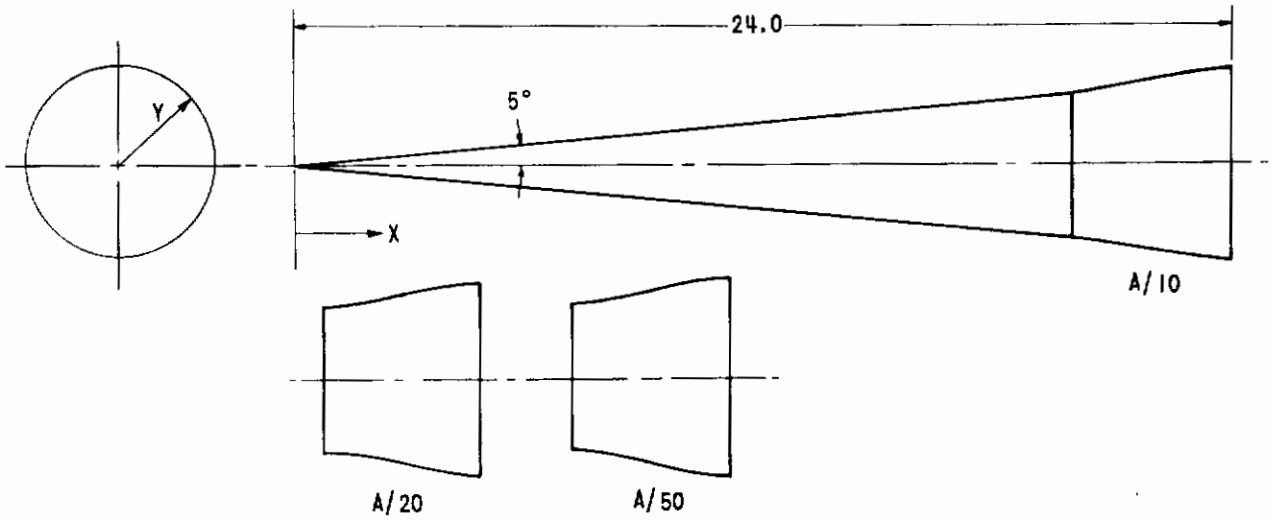


| COORDINATES - INCHES | | | | | |
|---|---|---|---|---|---|
| X | Y | X | Y | Y | Y |
| | | | A/10 | A/20 | A/50 |
| 16.37 | 1.432 | | | | |
| 16.796 | 1.471 | 21.8 | 2.184 | 2.197 | 2.216 |
| 17.189 | 1.509 | 22.0 | 2.229 | 2.252 | 2.289 |
| 17.551 | 1.545 | 22.375 | 2.313 | 2.357 | 2.424 |
| 18.190 | 1.614 | 22.6 | 2.360 | 2.415 | 2.499 |
| 18.720 | 1.675 | 23.0 | 2.426 | 2.495 | 2.603 |
| 19.185 | 1.733 | 23.4 | 2.470 | 2.549 | 2.671 |
| 19.584 | 1.787 | 23.8 | 2.492 | 2.576 | 2.705 |
| 19.926 | 1.836 | 24.0 | 2.494 | 2.579 | 2.709 |
| 20.222 | 1.880 | | | | |
| 20.488 | 1.924 | | | | |
| 20.699 | 1.958 | | | | |
| 20.892 | 1.990 | | | | |
| 21.059 | 2.018 | | | | |
| 21.206 | 2.042 | | | | |
| 21.396 | 2.092 | | | | |
| 21.505 | 2.114 | | | | |

Figure 12 MODELS A/10, A/20 AND A/50

| H.T. GAGE | X |
|---|---|
| T1 | 15.375 |
| T2 | 18.5 |
| T3 | 20.06 |
| T4 | 21.313 |
| T5 | 22.06 |
| T6 | 22.813 |

| S.F. GAGE | X |
|---|---|
| SF1 | 15.375 |
| SF2 | 17.438 |
| SF3 | 18.5 |
| SF4 | 19.03 |
| SF5 | 20.06 |
| SF6 | 21.313 |
| SF7 | 21.688 |
| SF8 | 22.06 |
| SF9 | 22.438 |
| SF10 | 22.813 |

| PRESS GAGE | X |
|---|---|
| P1 | 15.375 |
| P2 | 17.438 |
| P3 | 20.06 |
| P4 | 21.313 |
| P5 | 21.688 |
| P6 | 22.06 |
| P7 | 22.438 |
| P8 | 22.813 |

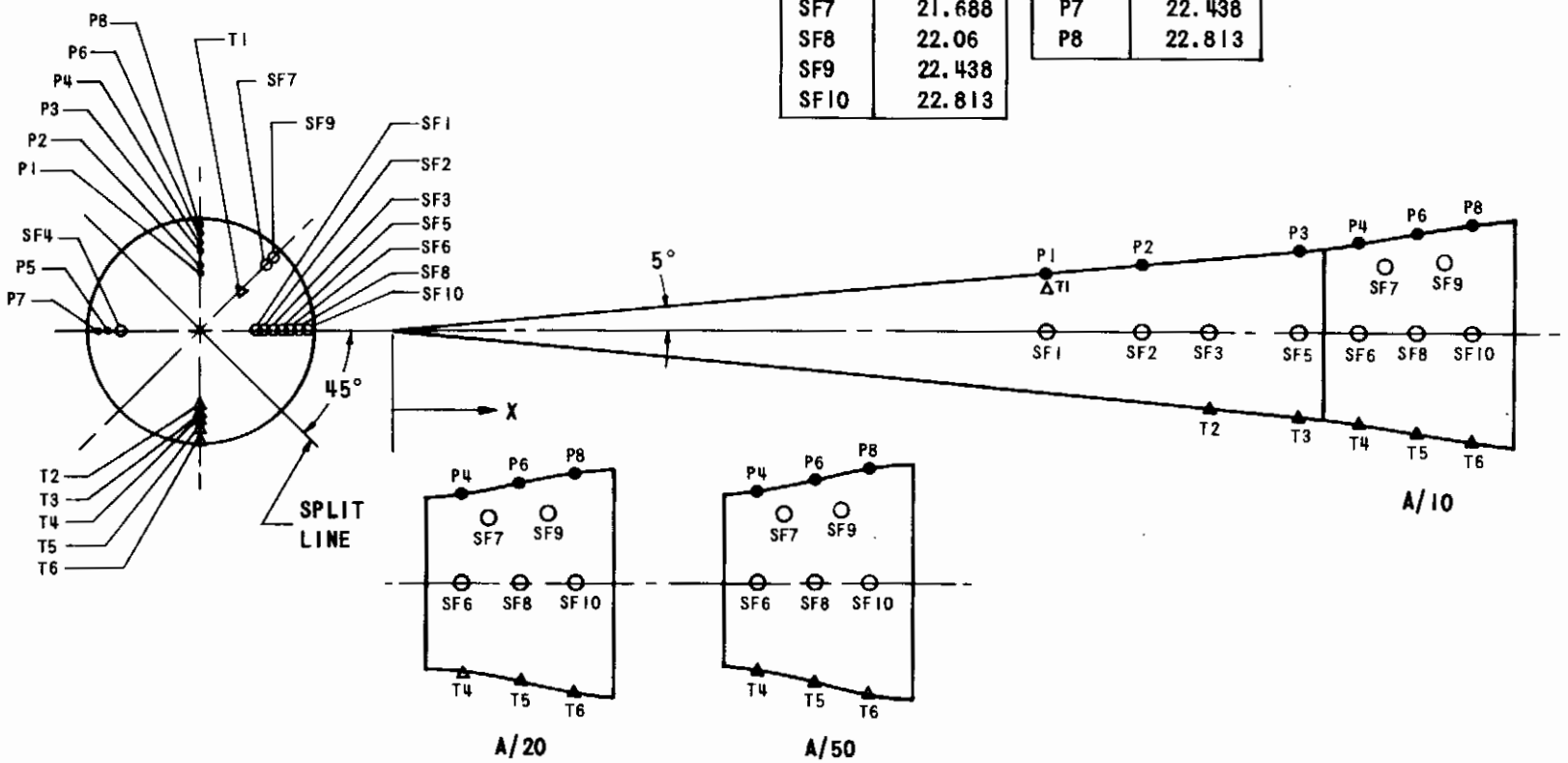


Figure 13 MODELS A/10, A/20 AND A/50 INSTRUMENTATION LOCATIONS

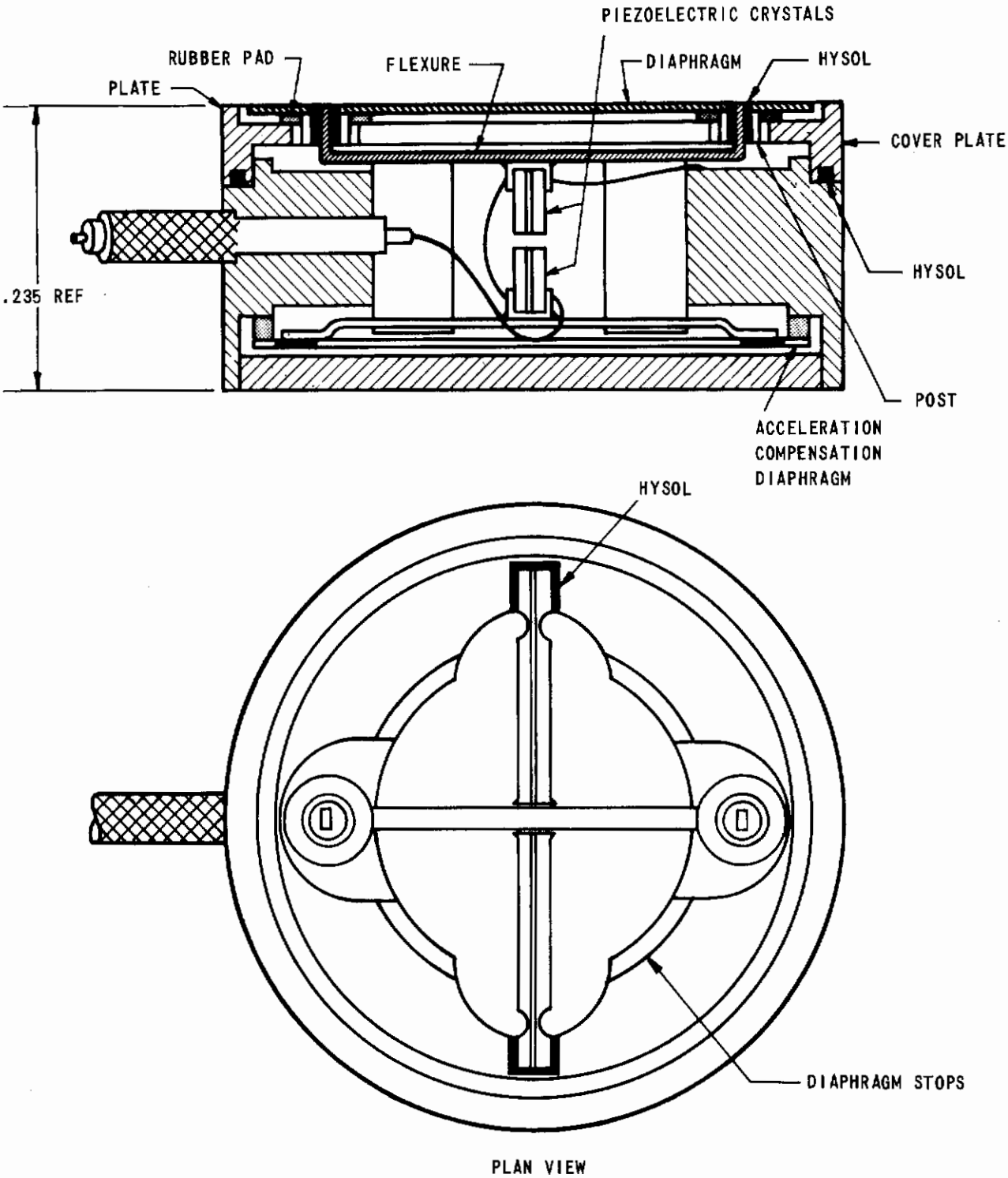


Figure 14 DRAWING OF SKIN FRICTION GAGE PZT50-22AC

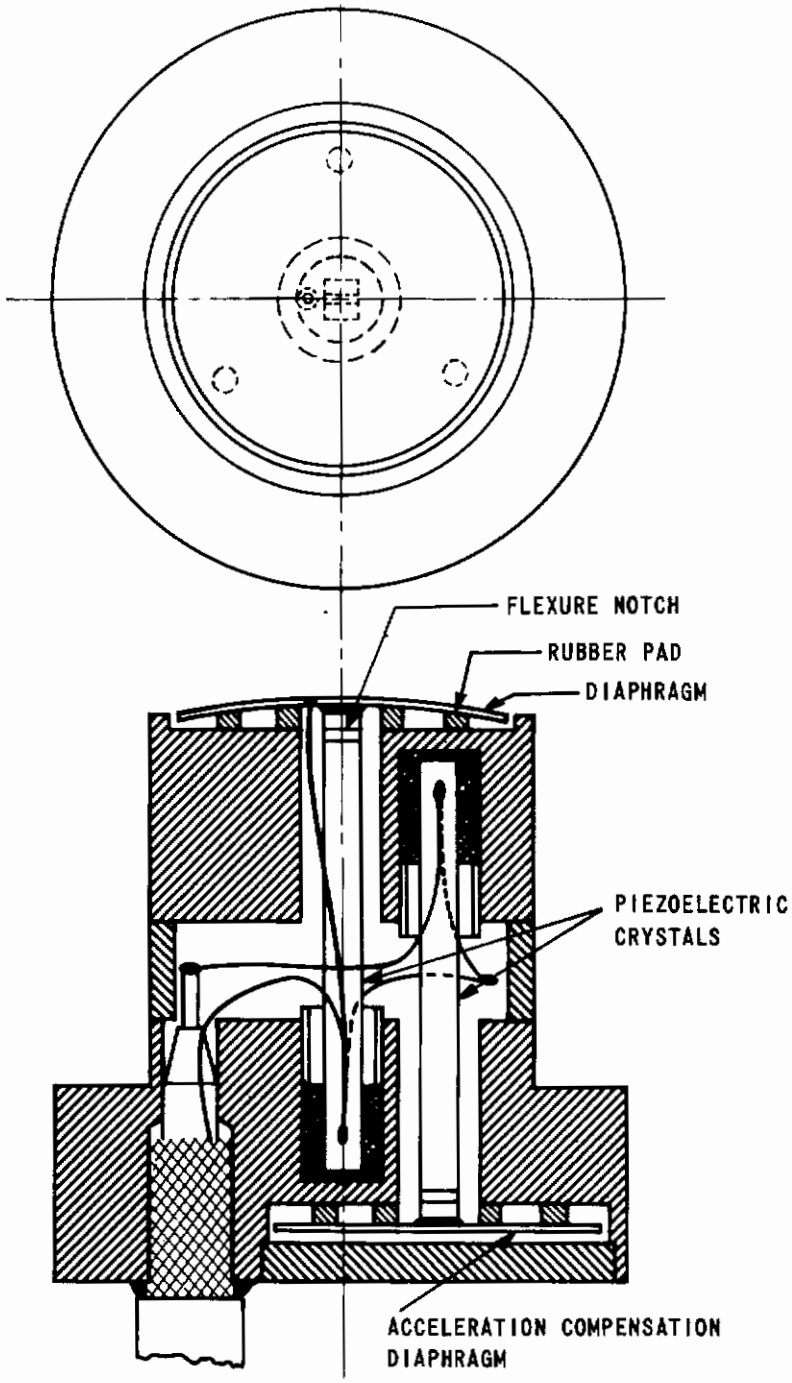


Figure 15 DRAWING OF SKIN FRICTION GAGE PZT25-37AC


Figure 16 SKIN FRICTION DISTRIBUTIONS ON THE TWO-DIMENSIONAL MODELS
(a) MODEL 2D2, MACH NUMBER 12

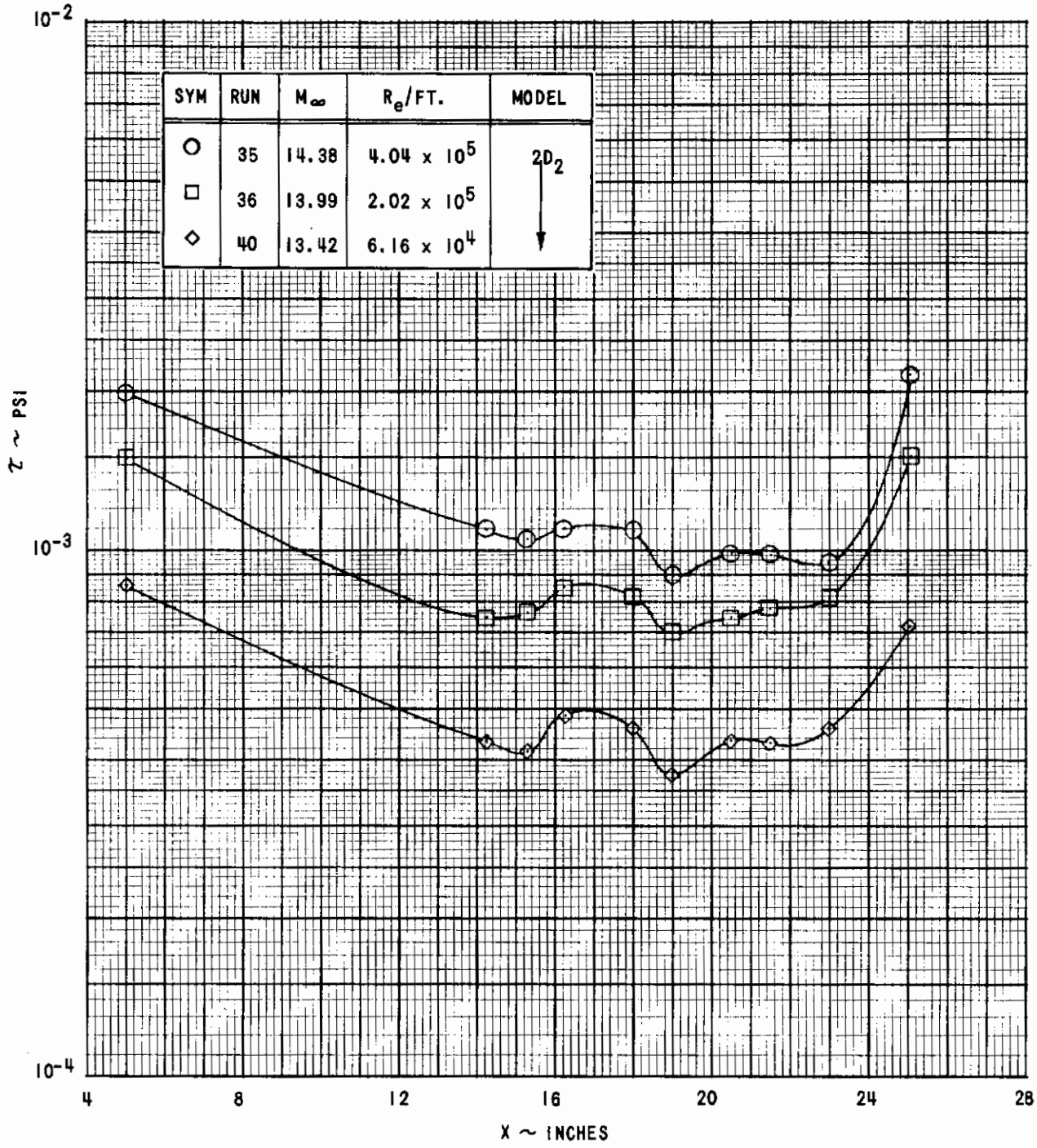


Figure 16 (Cont'd.) (b) MODEL 2D2, MACH NUMBER 14

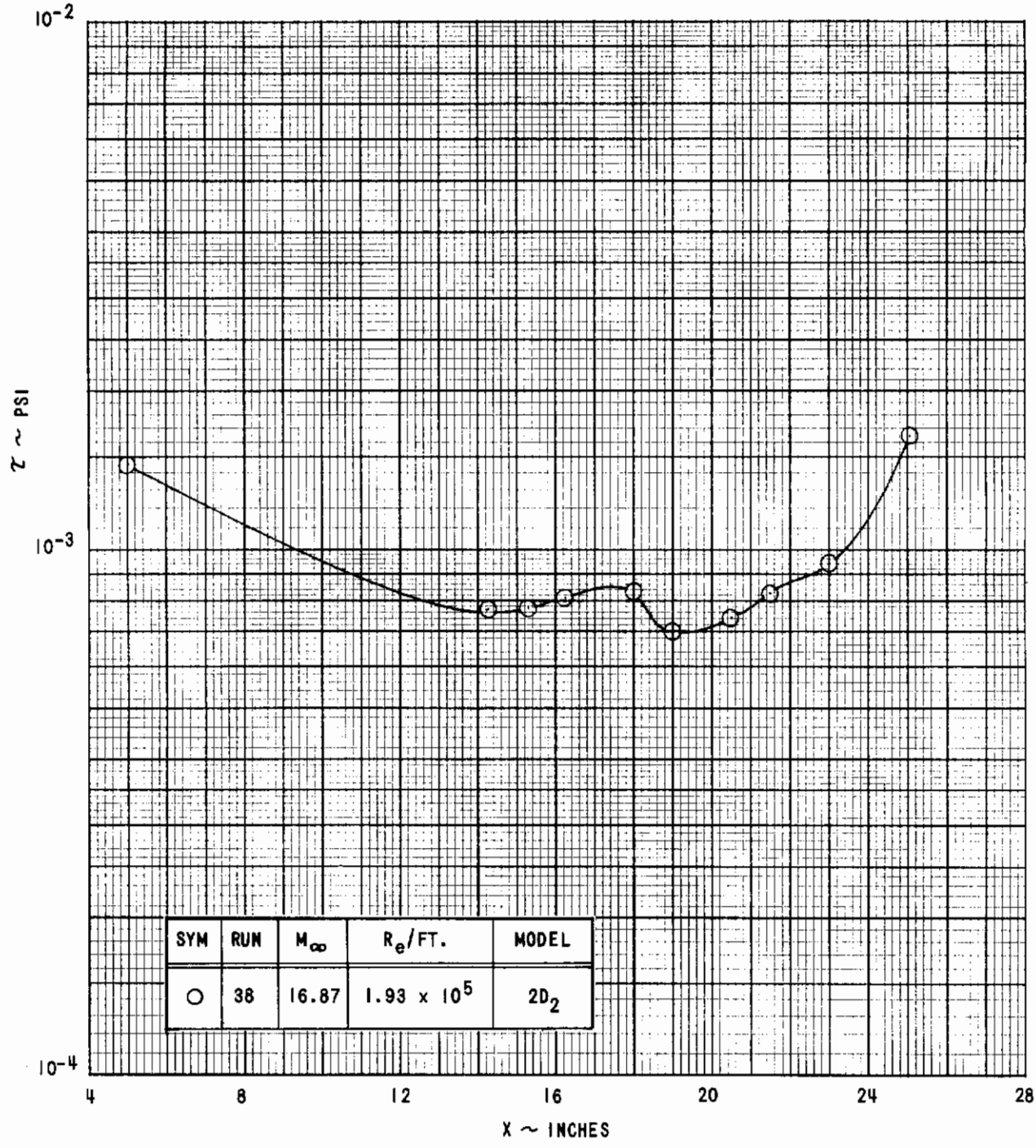


Figure 16 (Cont'd.) (c) MODEL 2D2, MACH NUMBER 16

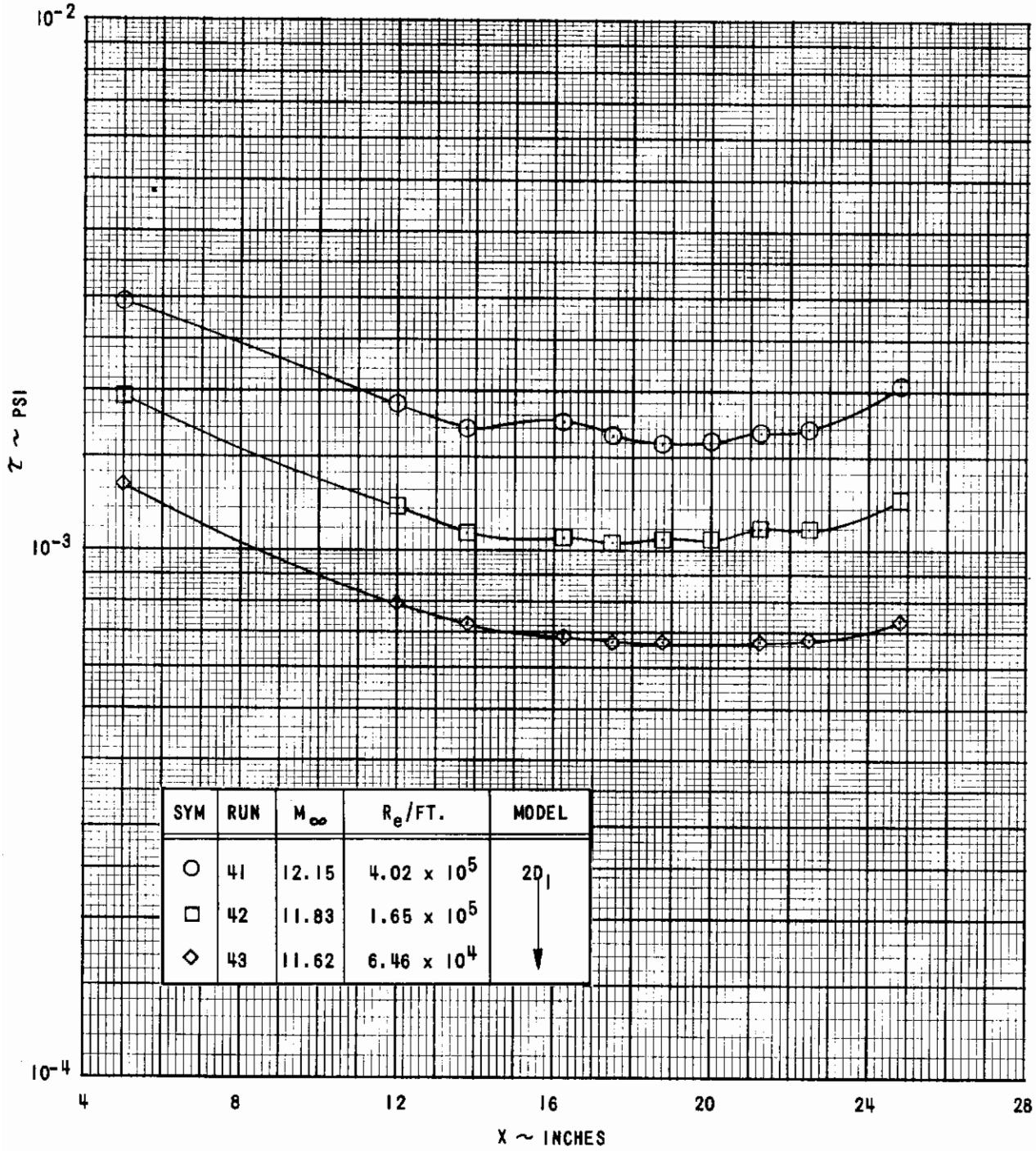


Figure 16 (Cont'd.) (d) MODEL 2D1, MACH NUMBER 12

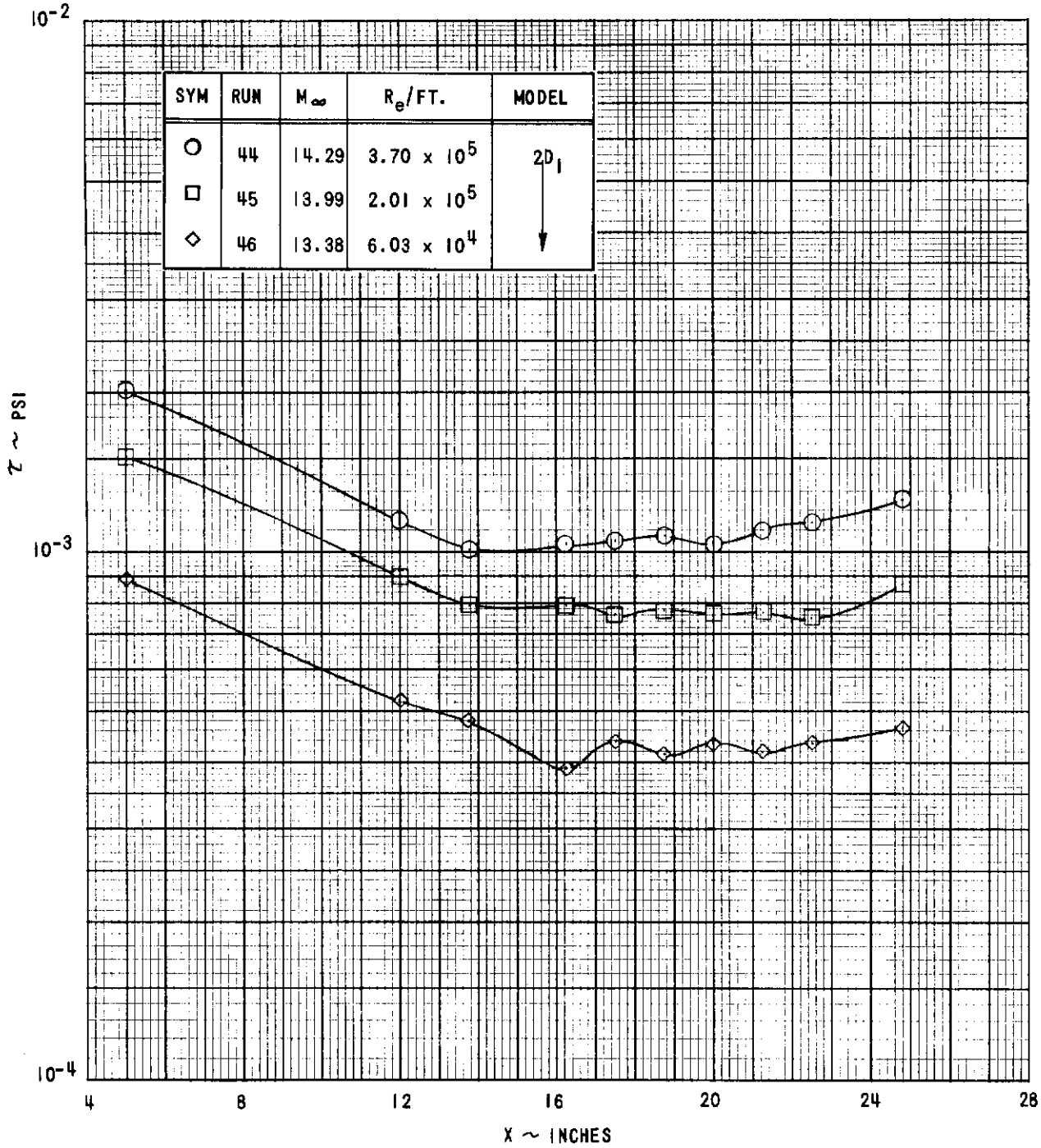


Figure 16 (Cont'd.) (e) MODEL 2D1, MACH NUMBER 14

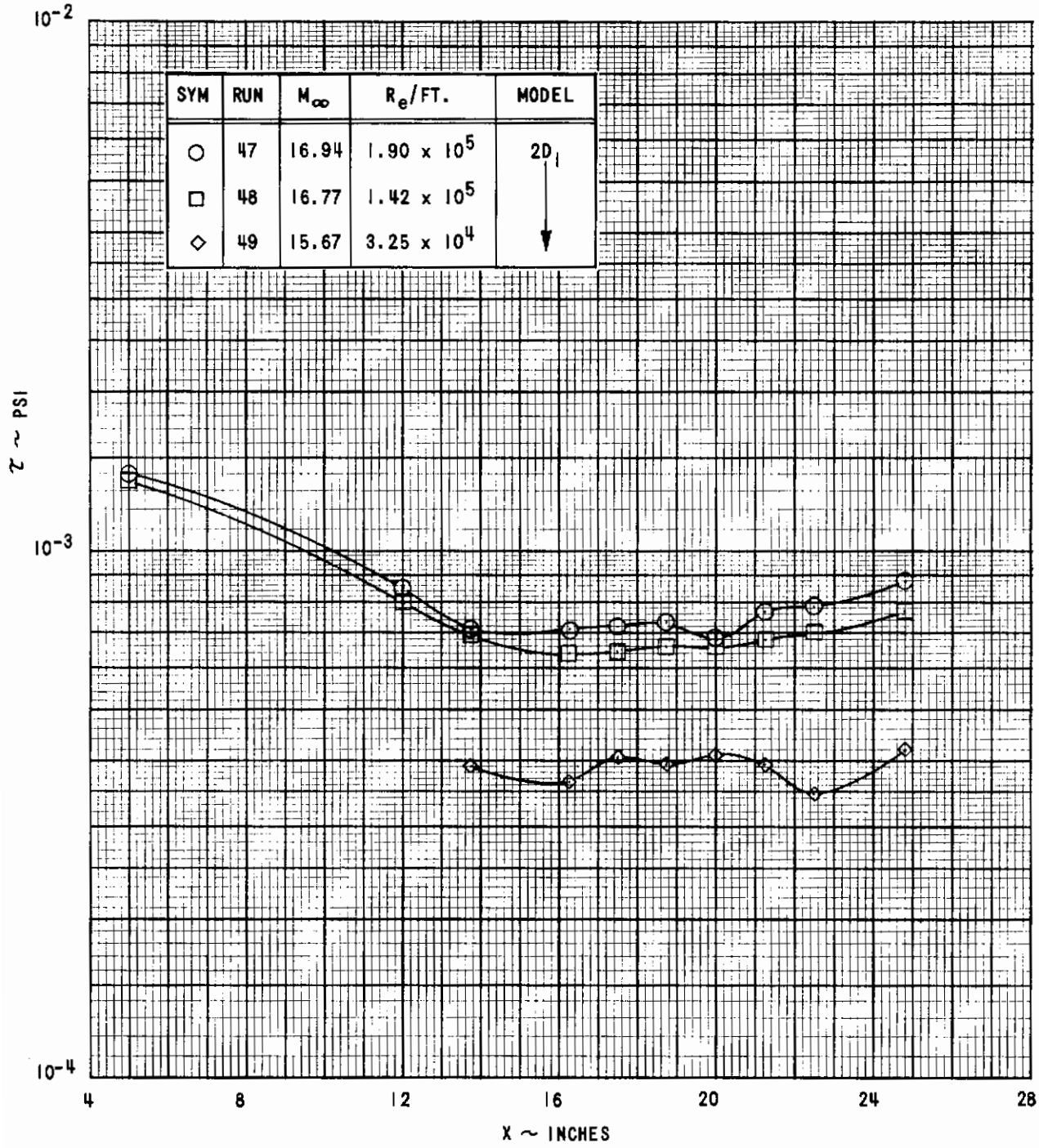


Figure 16 (Concluded) (f) MODEL 2D1, MACH NUMBER 16

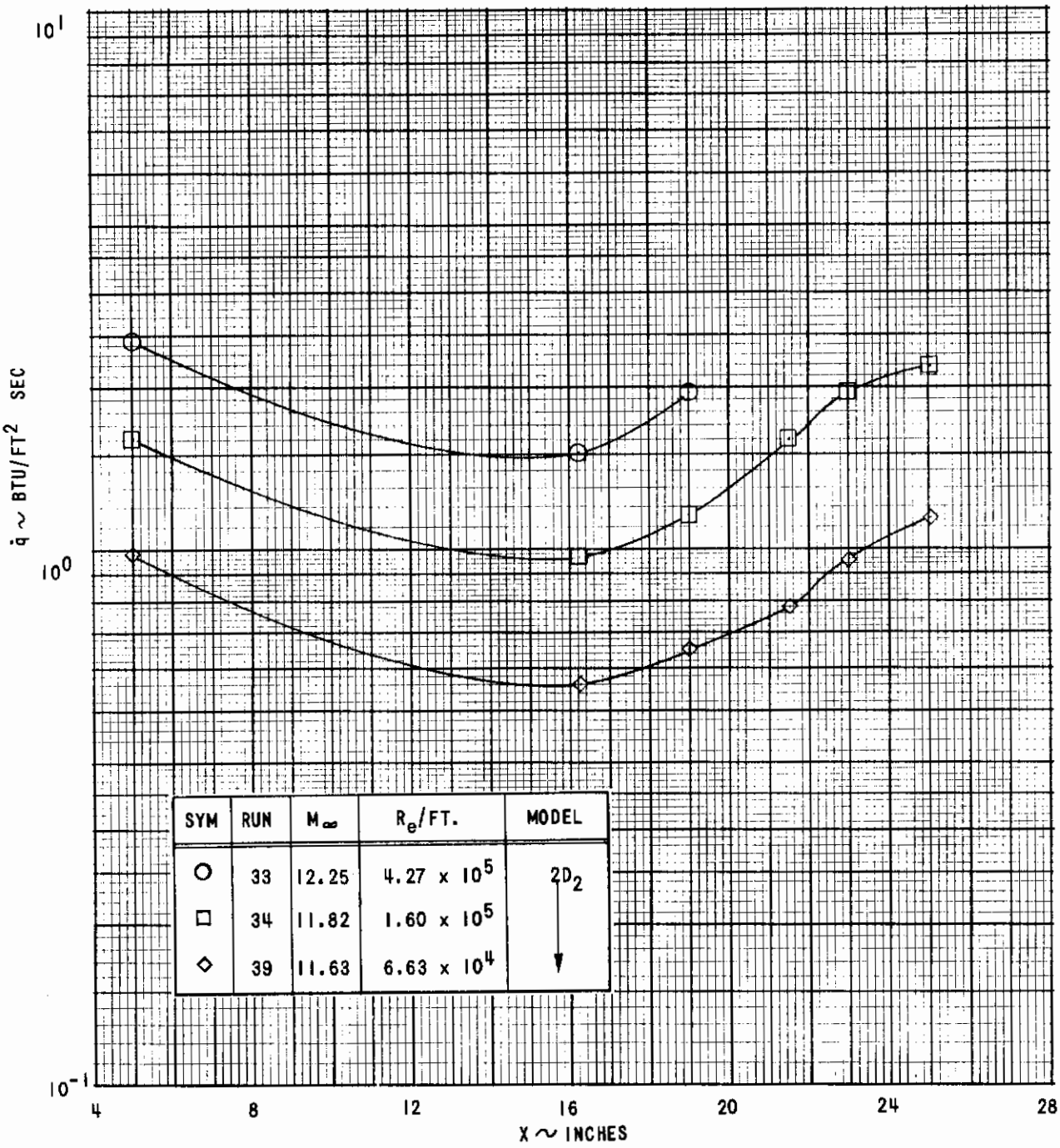


Figure 17 HEAT TRANSFER DISTRIBUTIONS ON THE TWO-DIMENSIONAL MODELS
(a) MODEL 2D2, MACH NUMBER 12

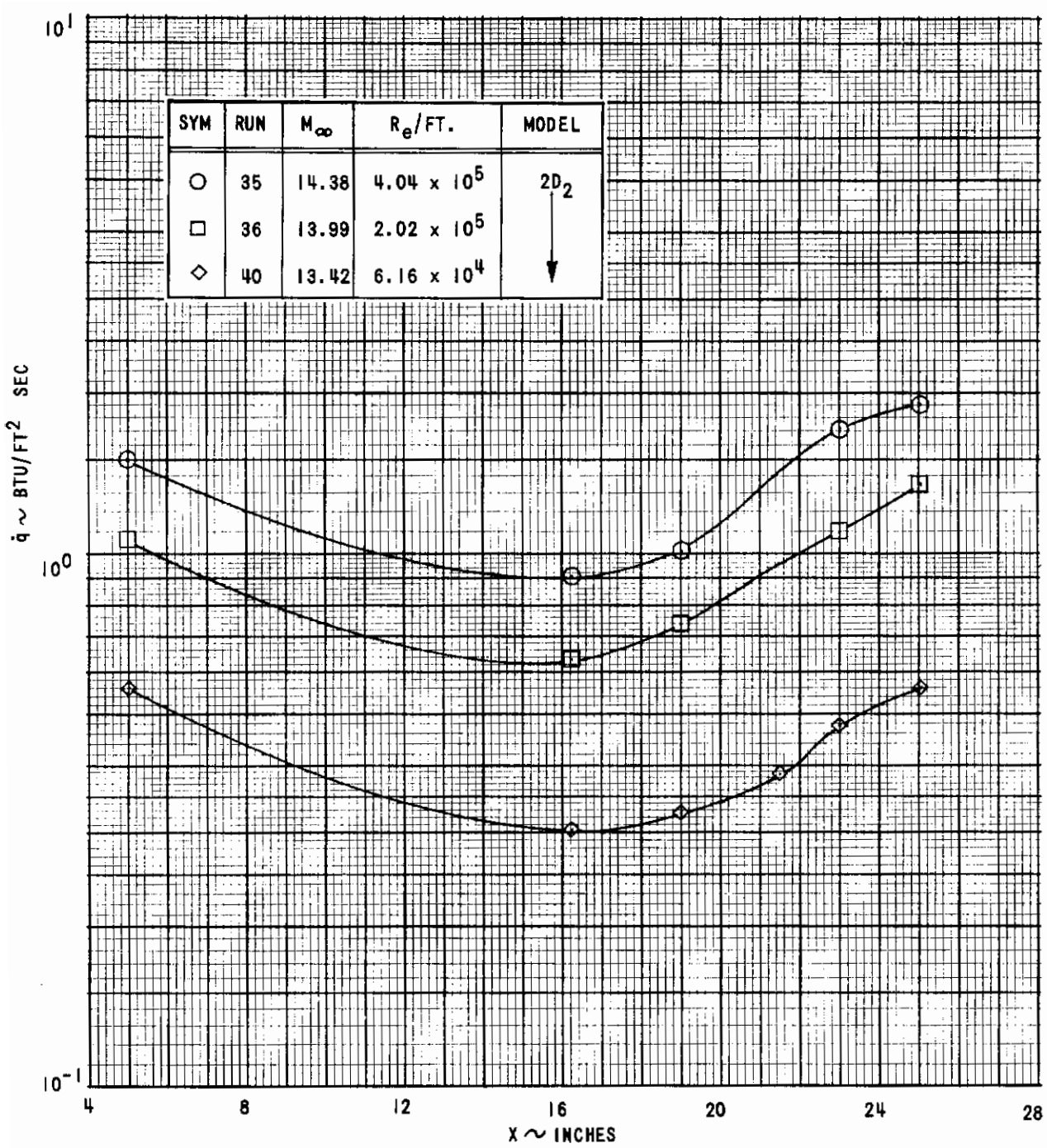


Figure 17 (Cont'd.) (b) MODEL 2D2, MACH NUMBER 14

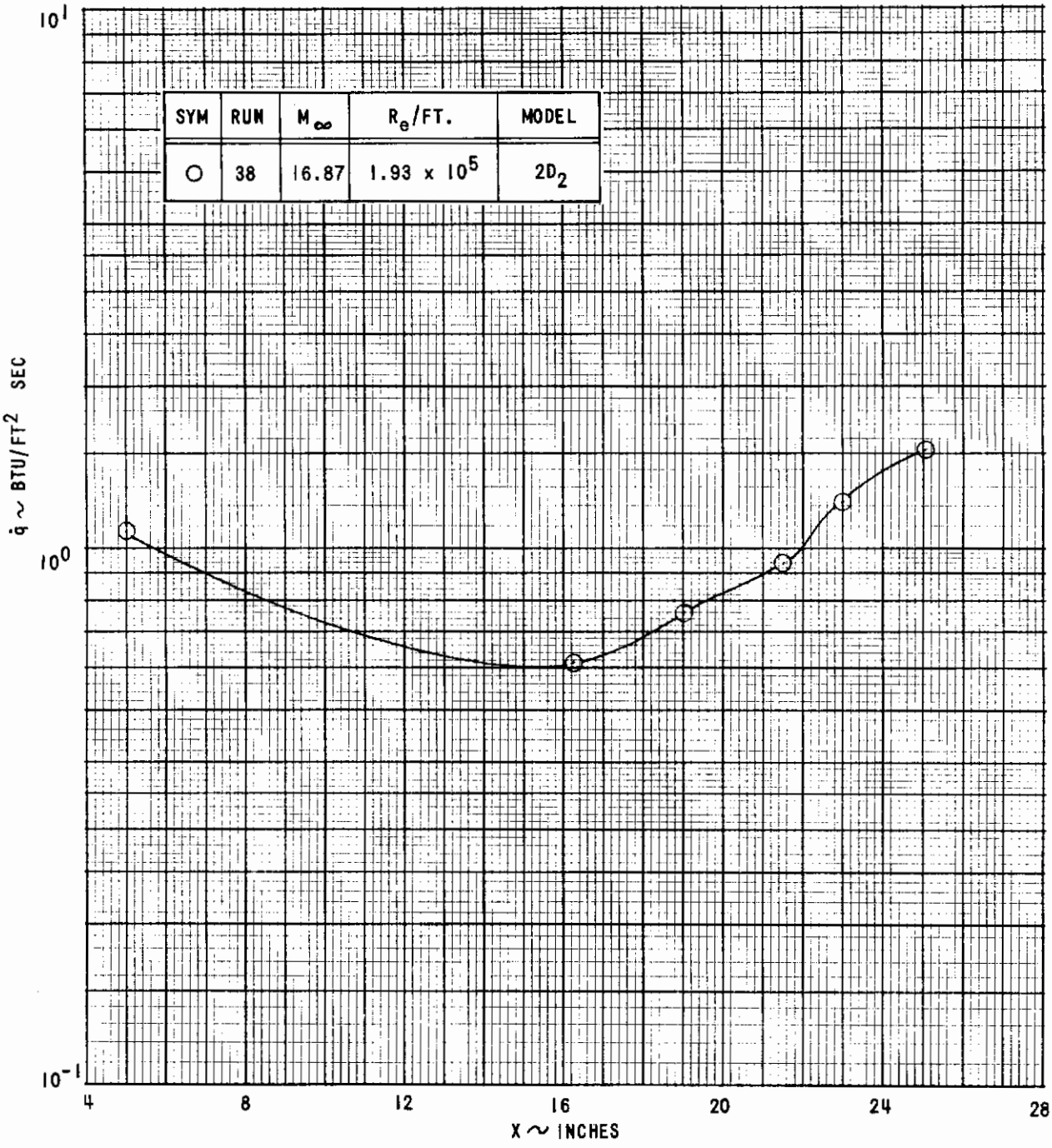


Figure 17 (Cont'd.) (c) MODEL 2D2, MACH NUMBER 16

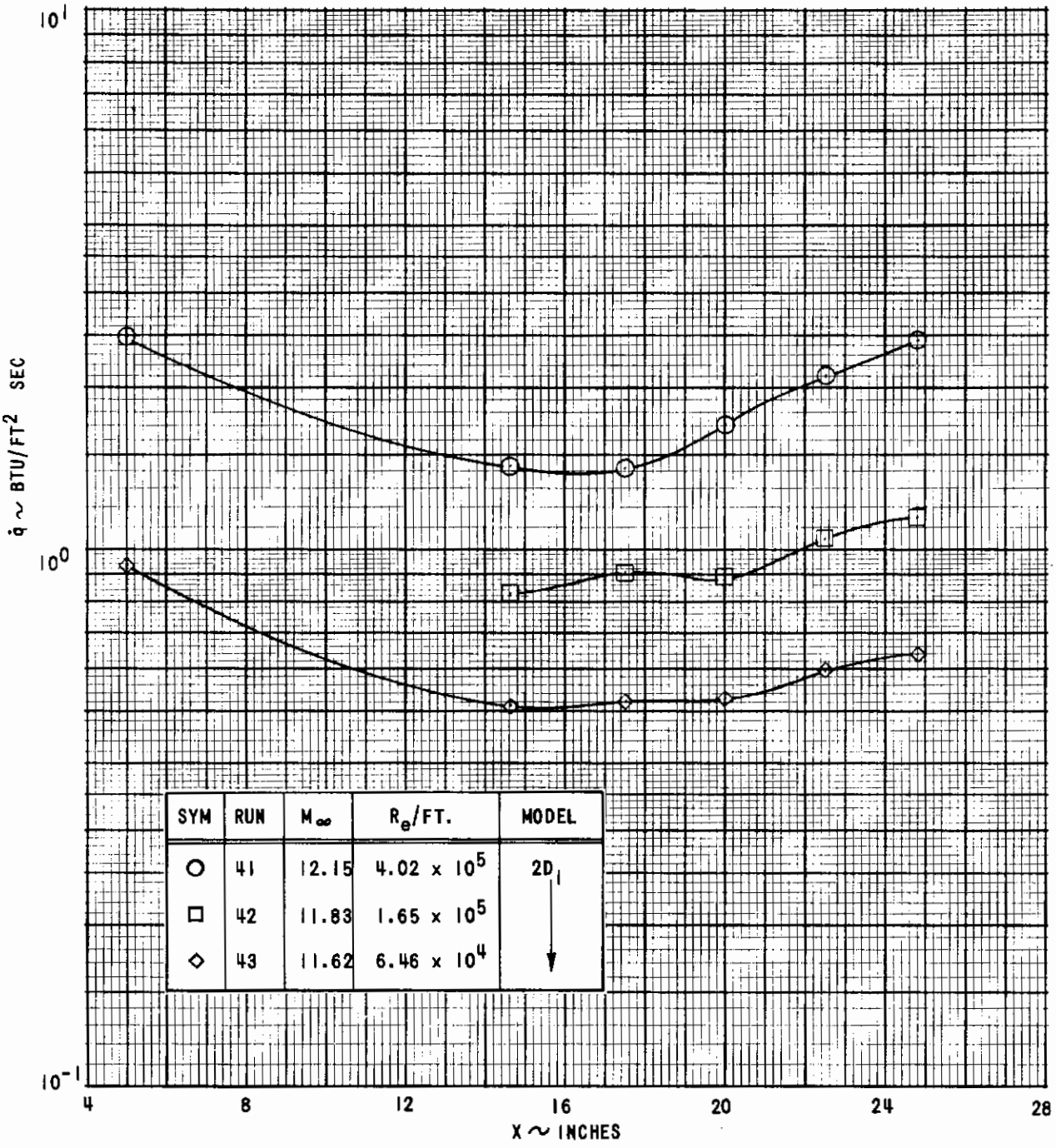


Figure 17 (Cont'd.) (d) MODEL 2D1, MACH NUMBER 12

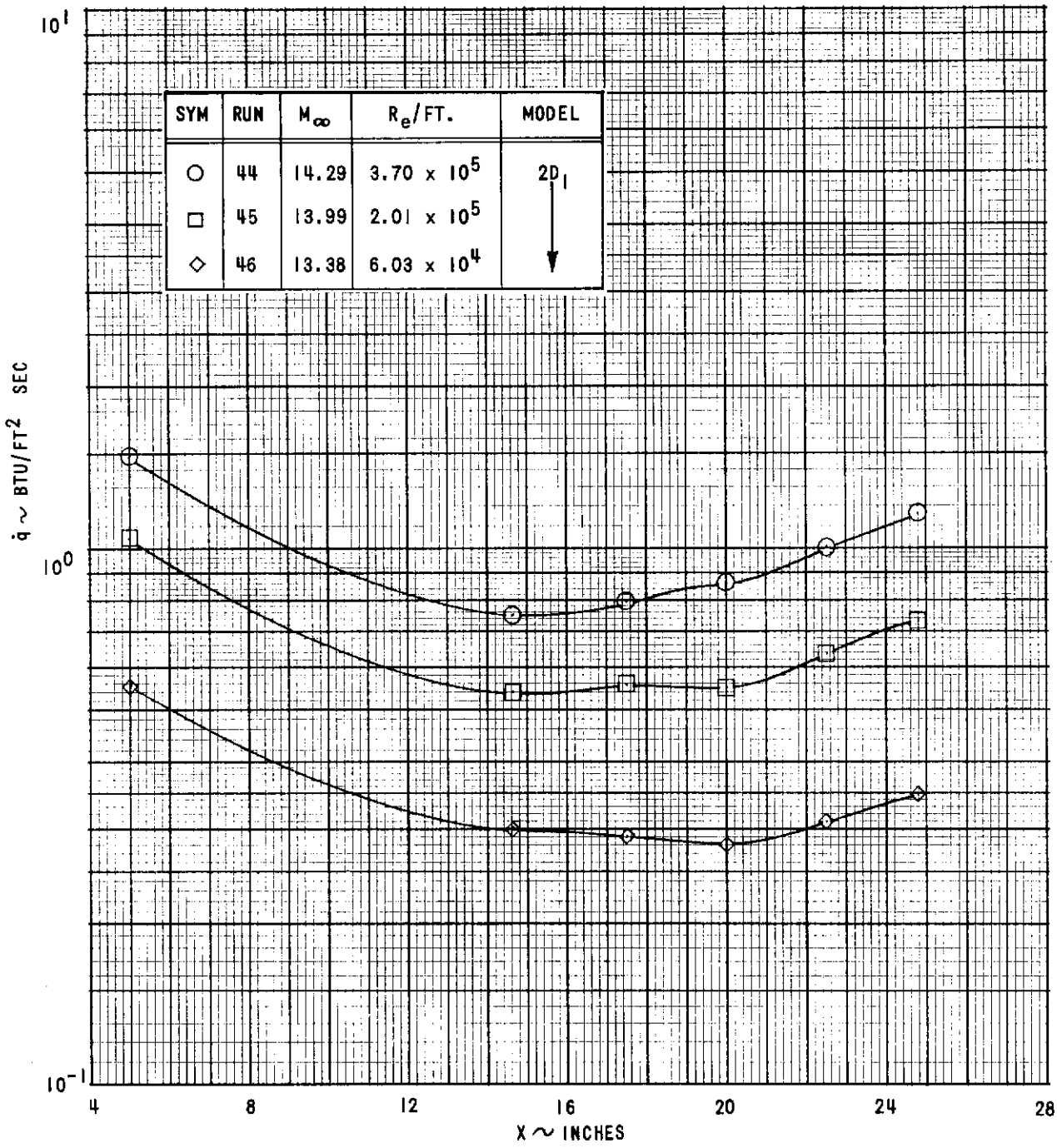


Figure 17 (Cont'd.) (e) MODEL 2D1, MACH NUMBER 14

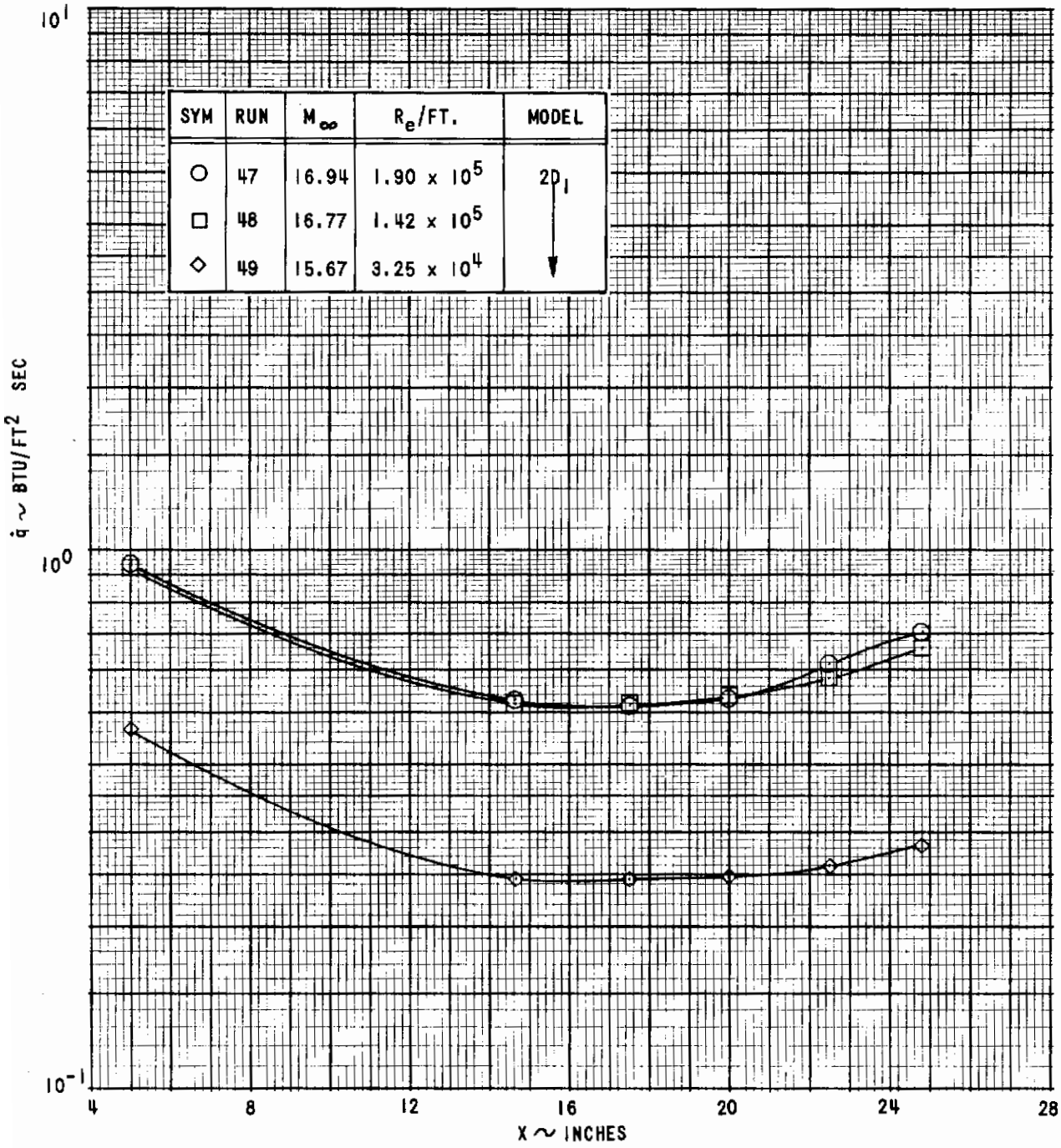


Figure 17 (Concluded) (f) MODEL 2D1, MACH NUMBER 16

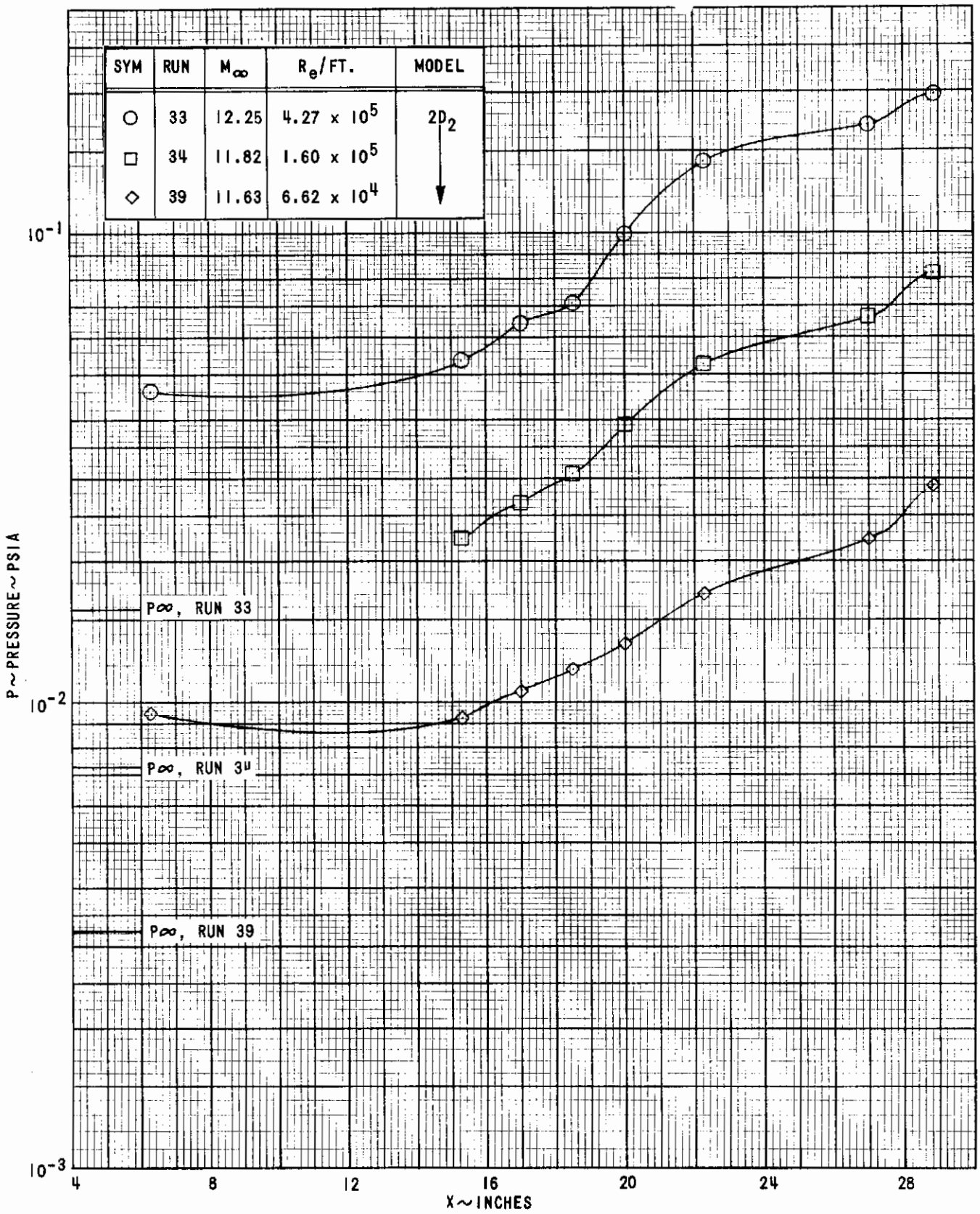


Figure 18 PRESSURE DISTRIBUTION ON THE TWO-DIMENSIONAL MODELS
(a) MODEL 2D2, MACH NUMBER 12

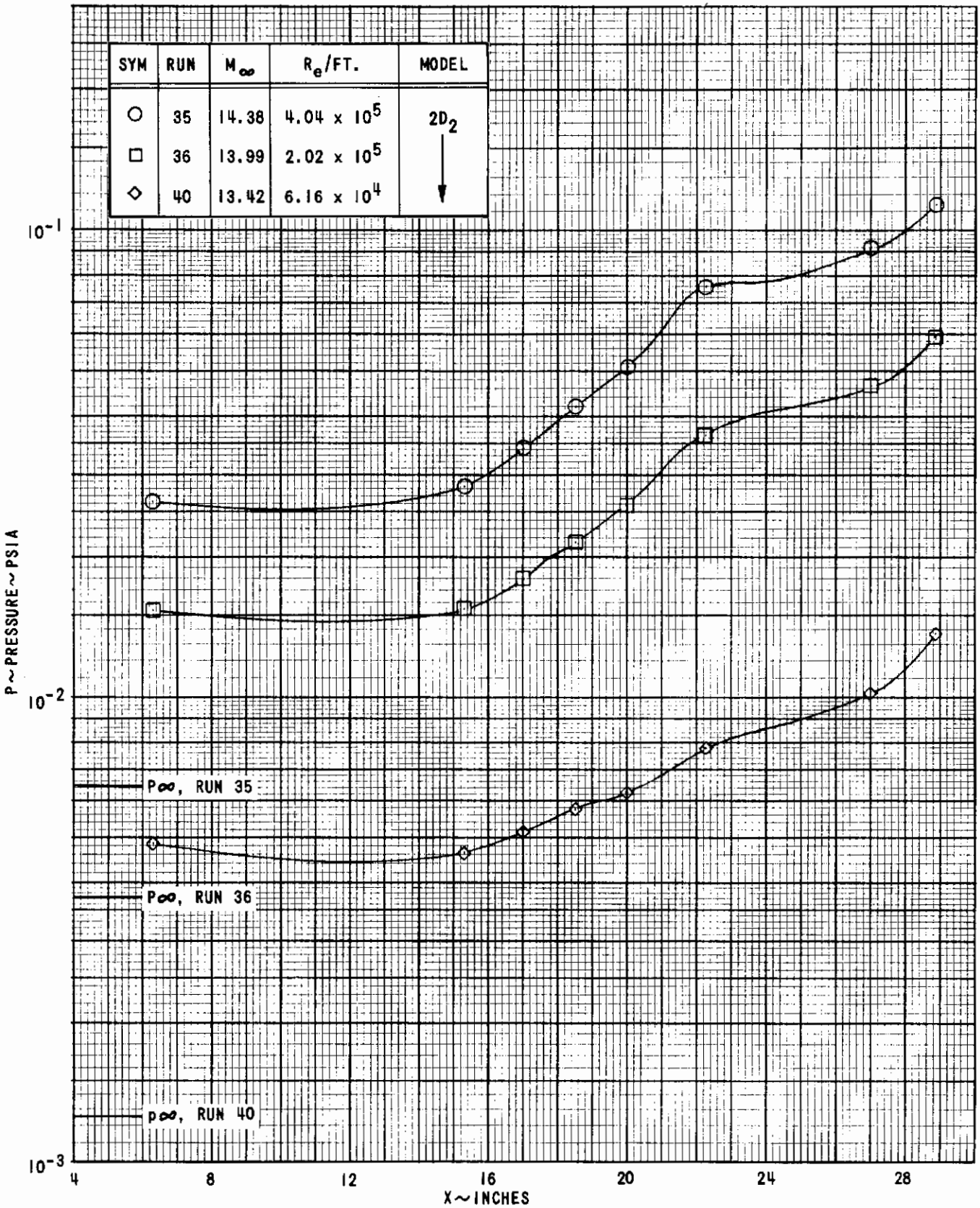


Figure 18 (Cont'd.) (b) MODEL 2D2, MACH NUMBER 14

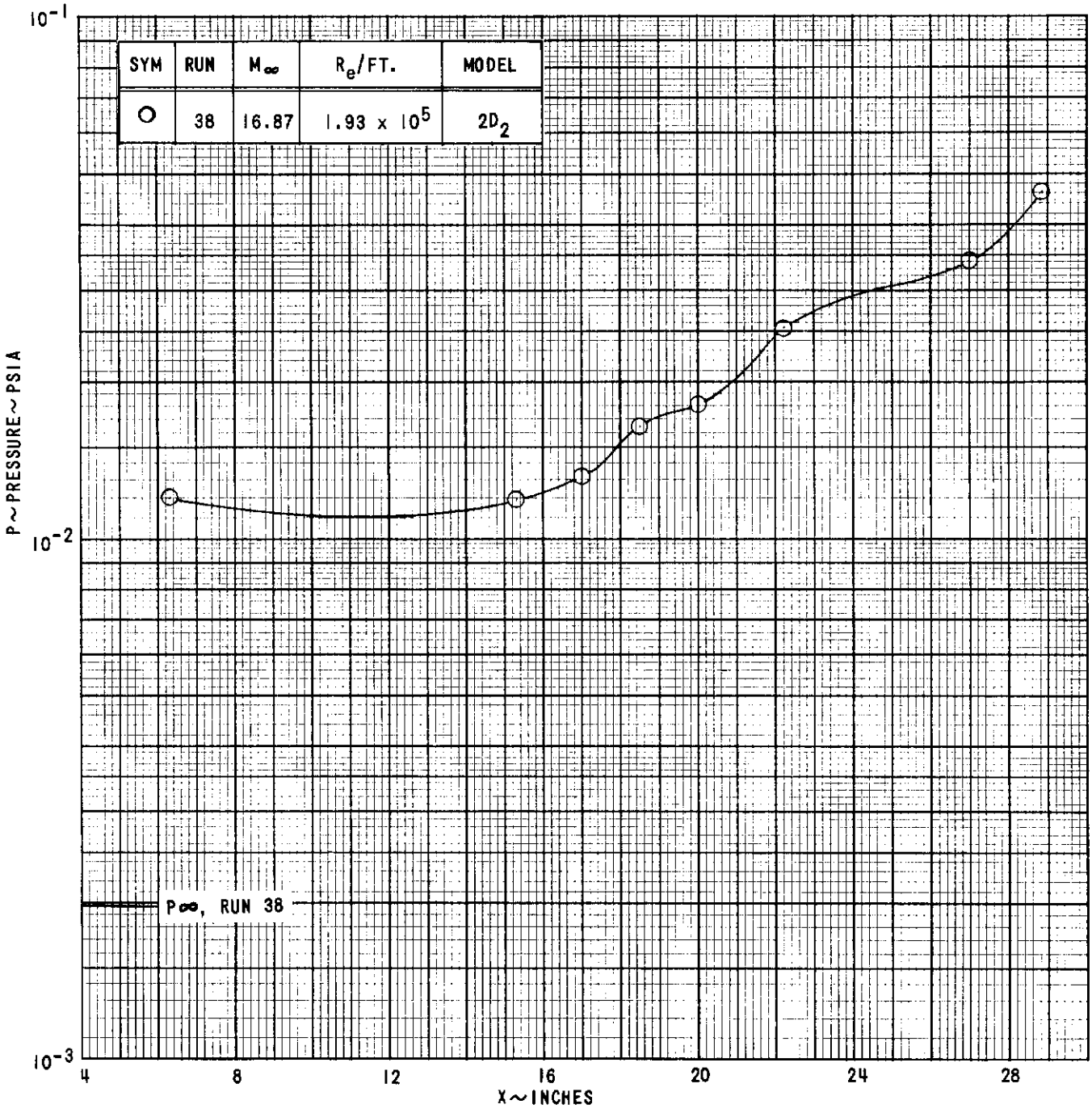


Figure 18 (Cont'd.) (c) MODEL 2D2, MACH NUMBER 16

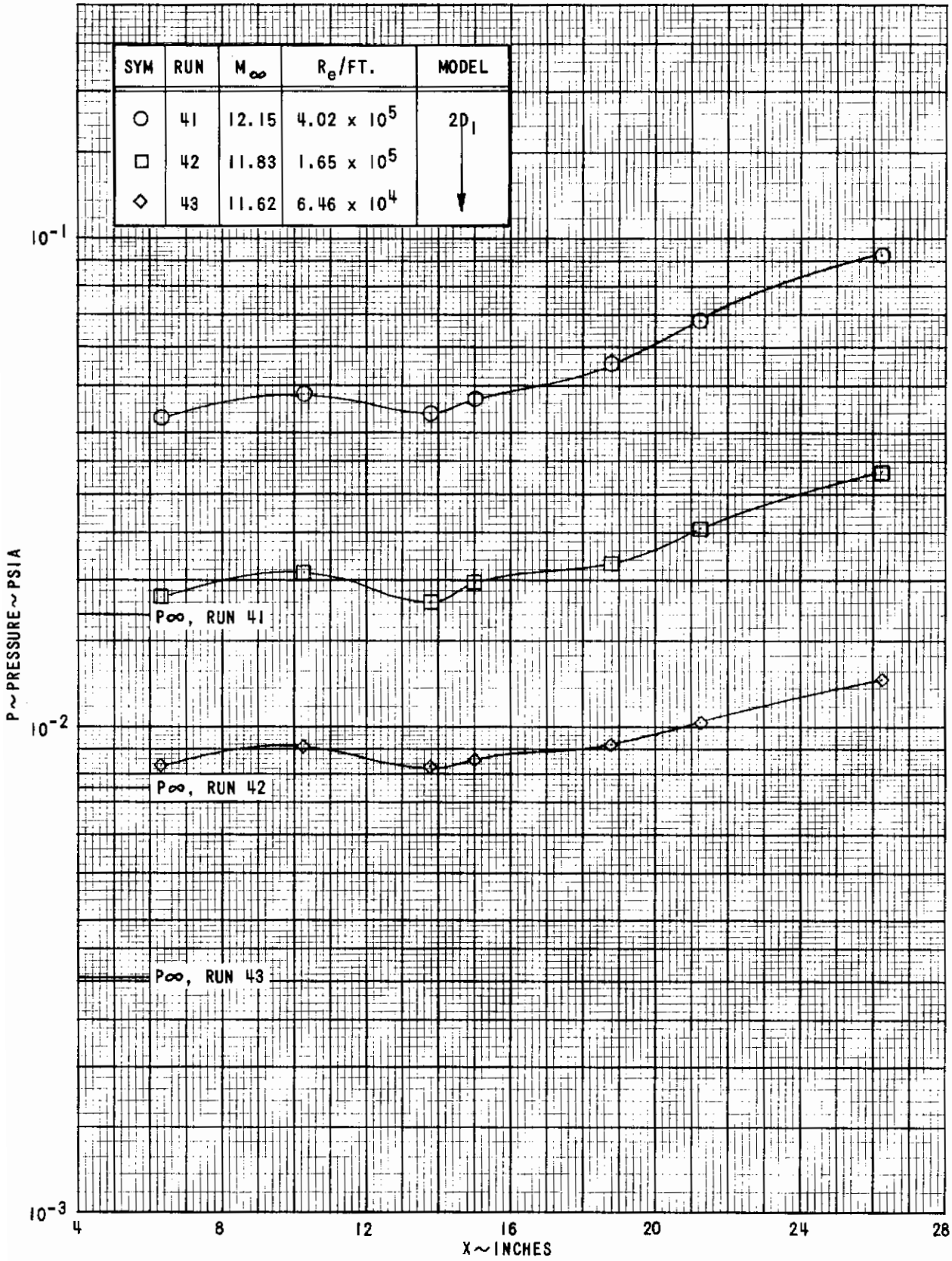


Figure 18 (Cont'd.) (d) MODEL 2D1, MACH NUMBER 12

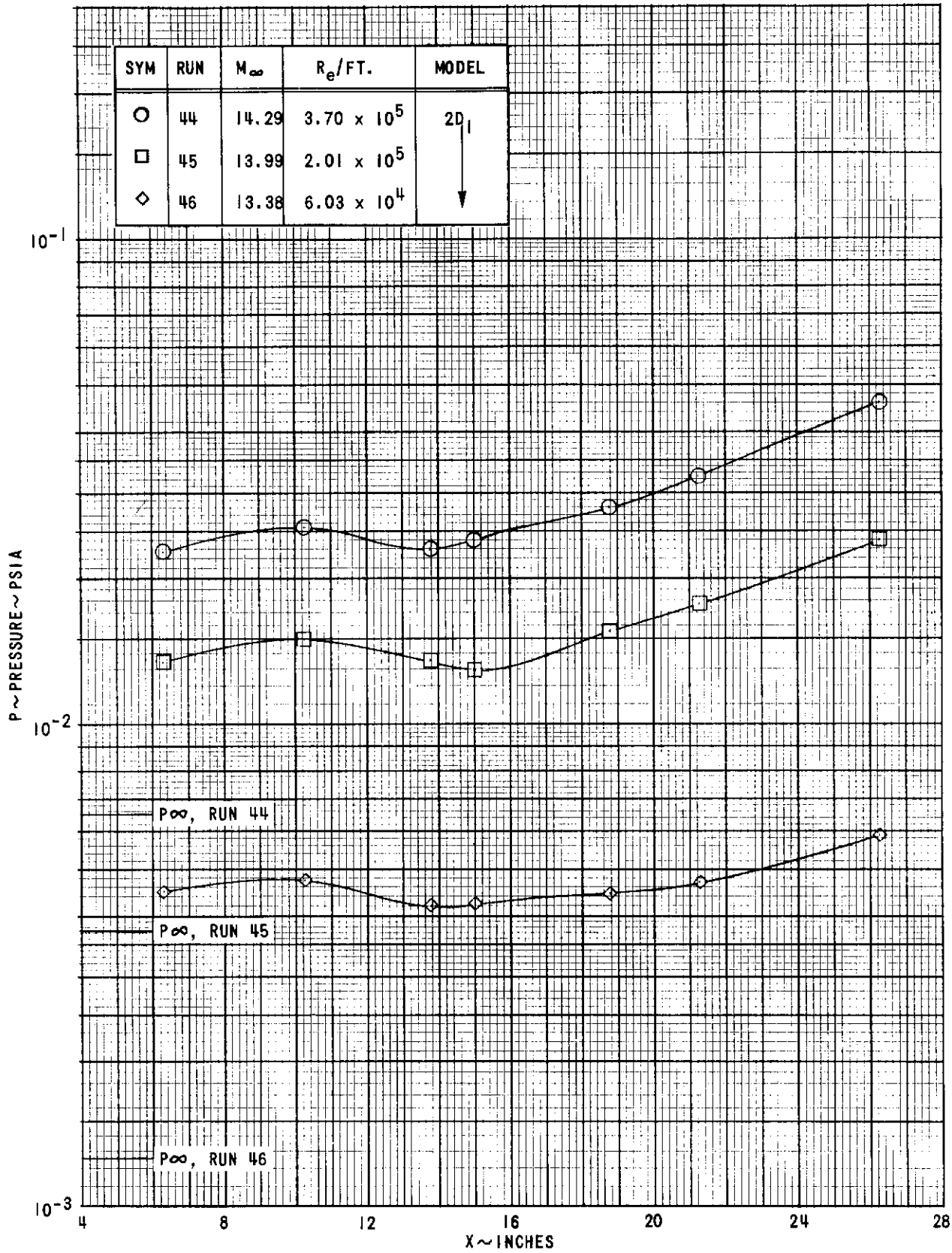


Figure 18 (Cont'd.) (e) MODEL 2D1, MACH NUMBER 14

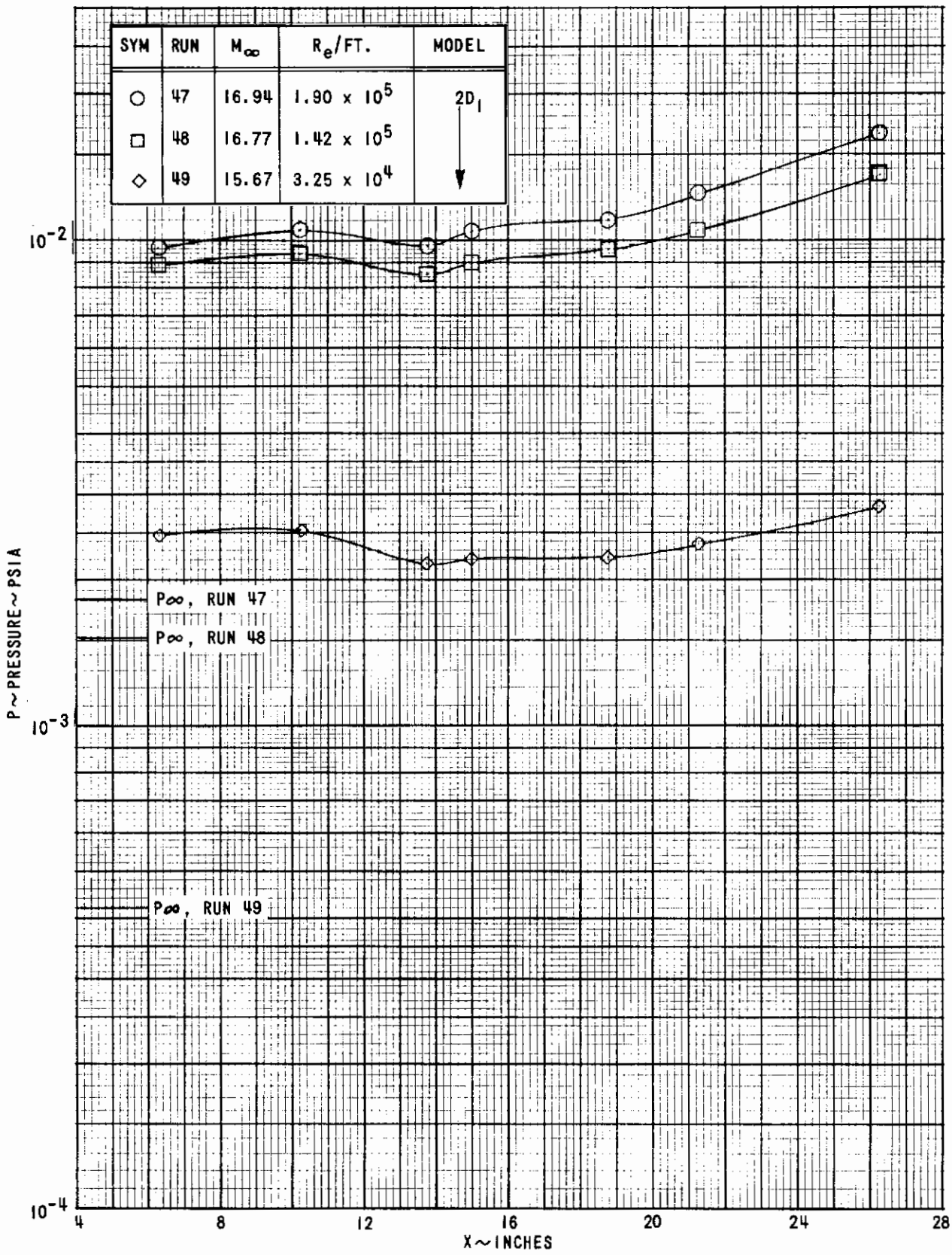


Figure 18 (Concluded) (f) MODEL 2DI, MACH NUMBER 16

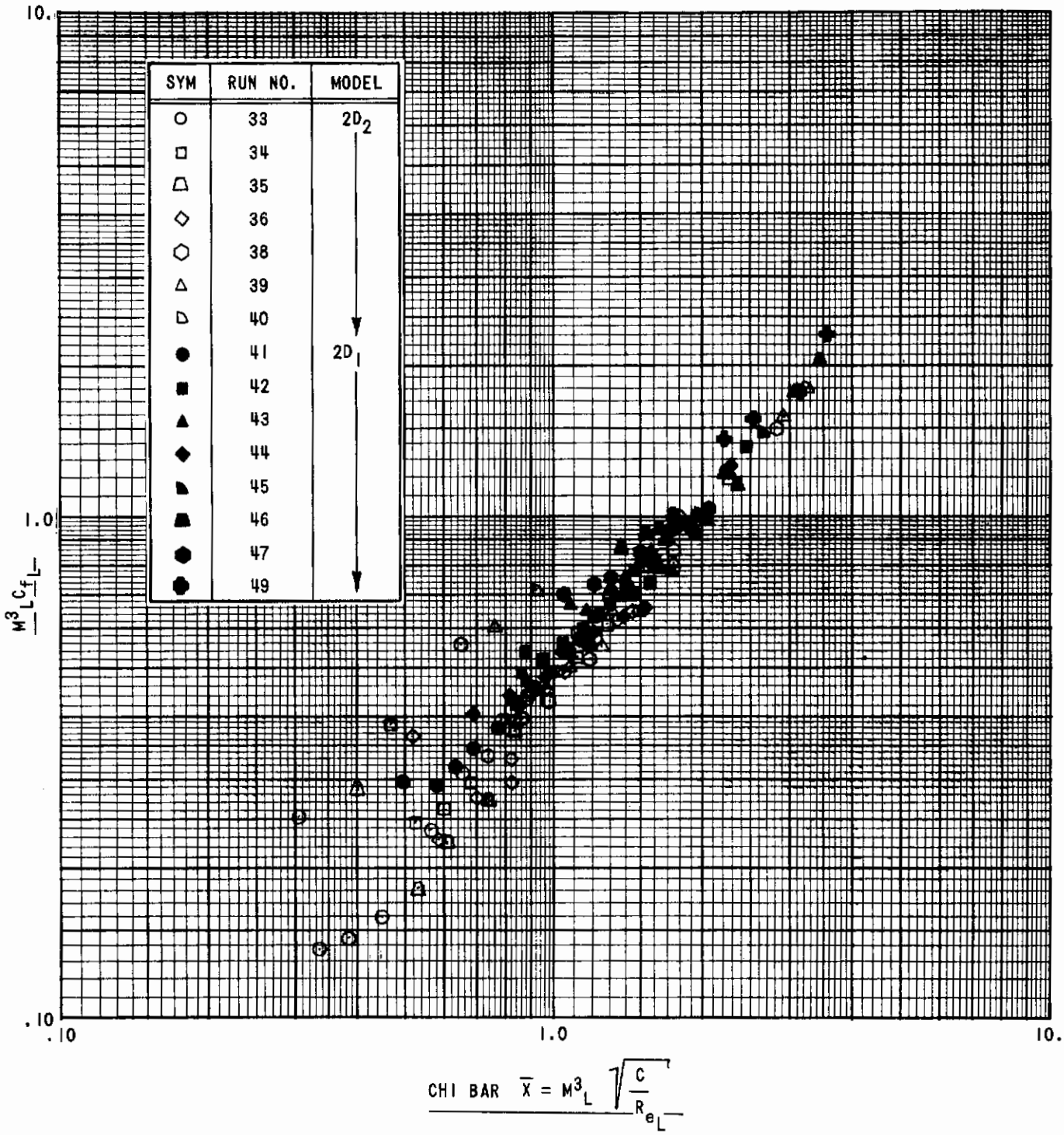


Figure 19 CORRELATED SKIN FRICTION DATA FROM THE TWO-DIMENSIONAL MODEL TESTS

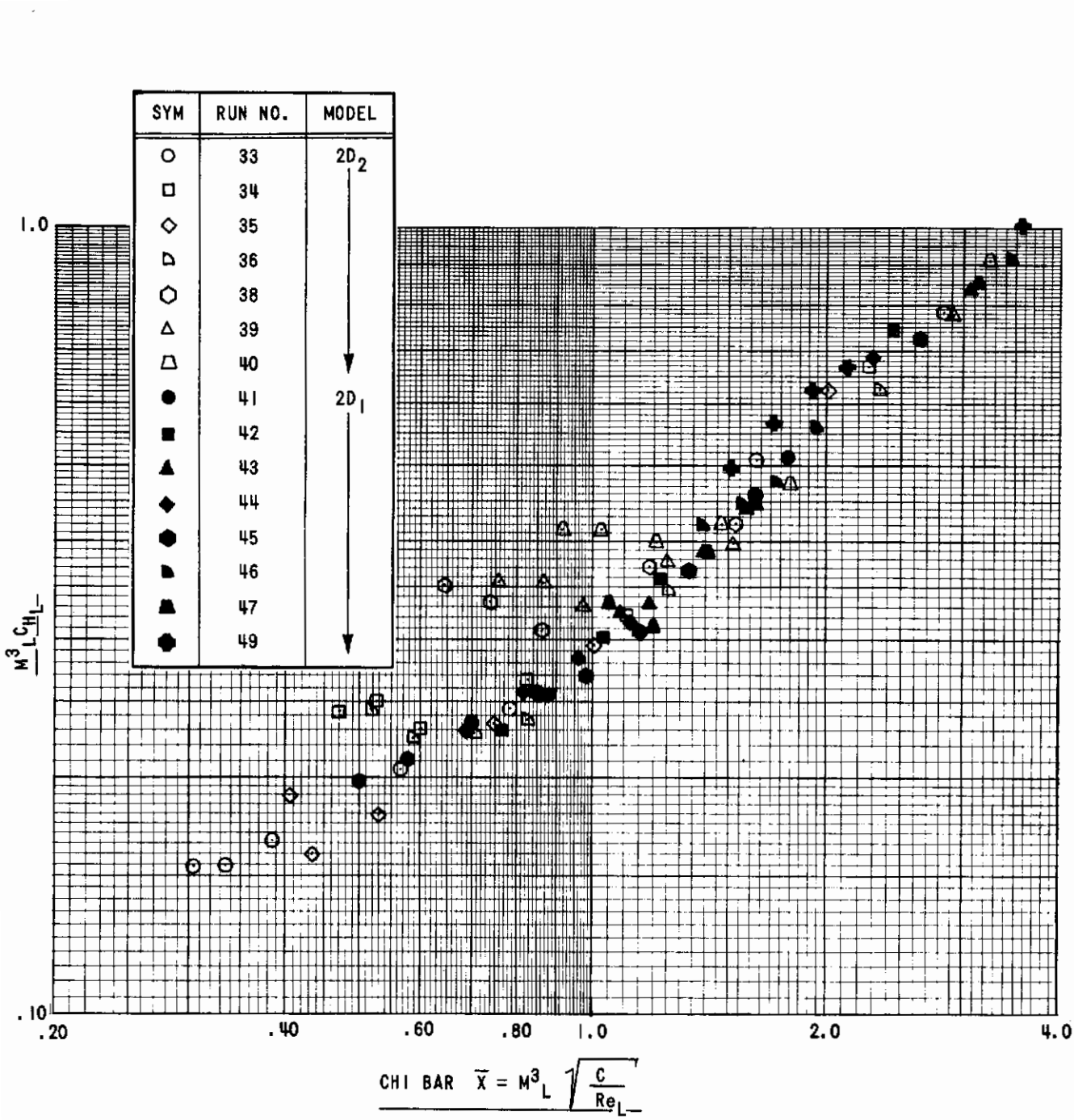


Figure 20 CORRELATED HEAT TRANSFER DATA FROM THE TWO-DIMENSIONAL MODEL TESTS

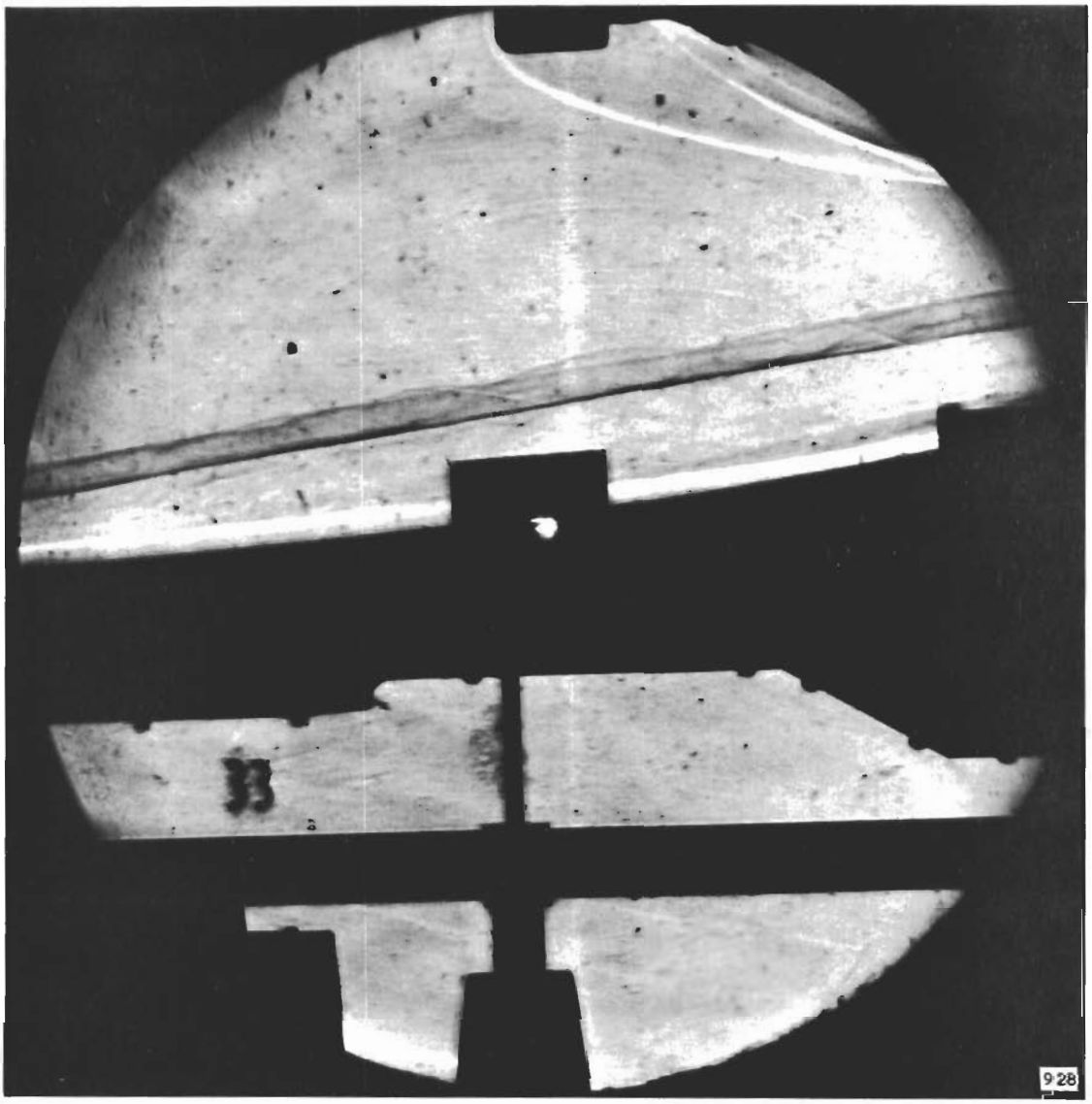


Figure 21 TWO-DIMENSIONAL MODEL SCHLIEREN PHOTOGRAPHS
(a) MODEL 2D2, RUN 33

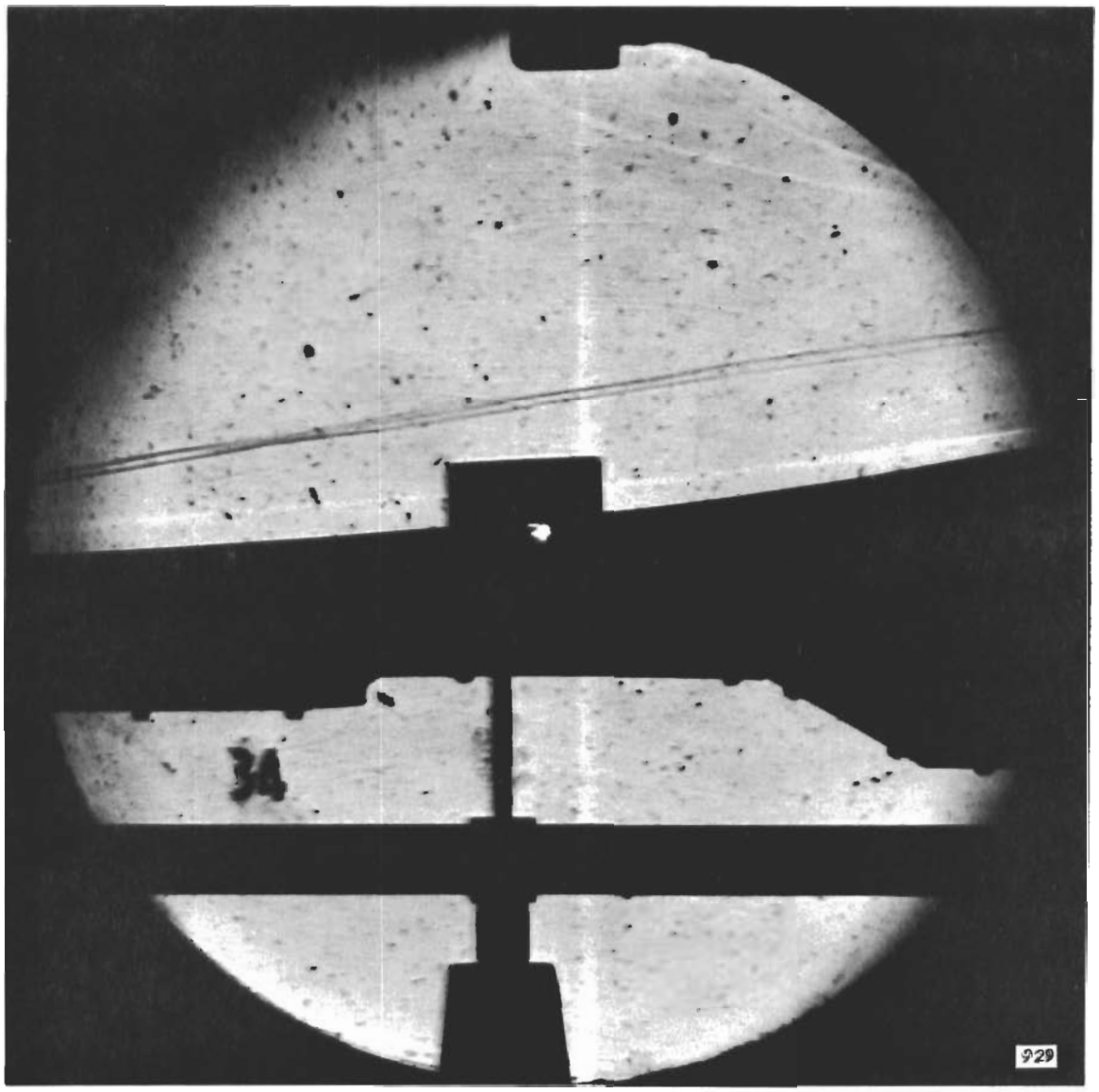


Figure 21 (Cont'd.) (b) MODEL 2D2, RUN 34

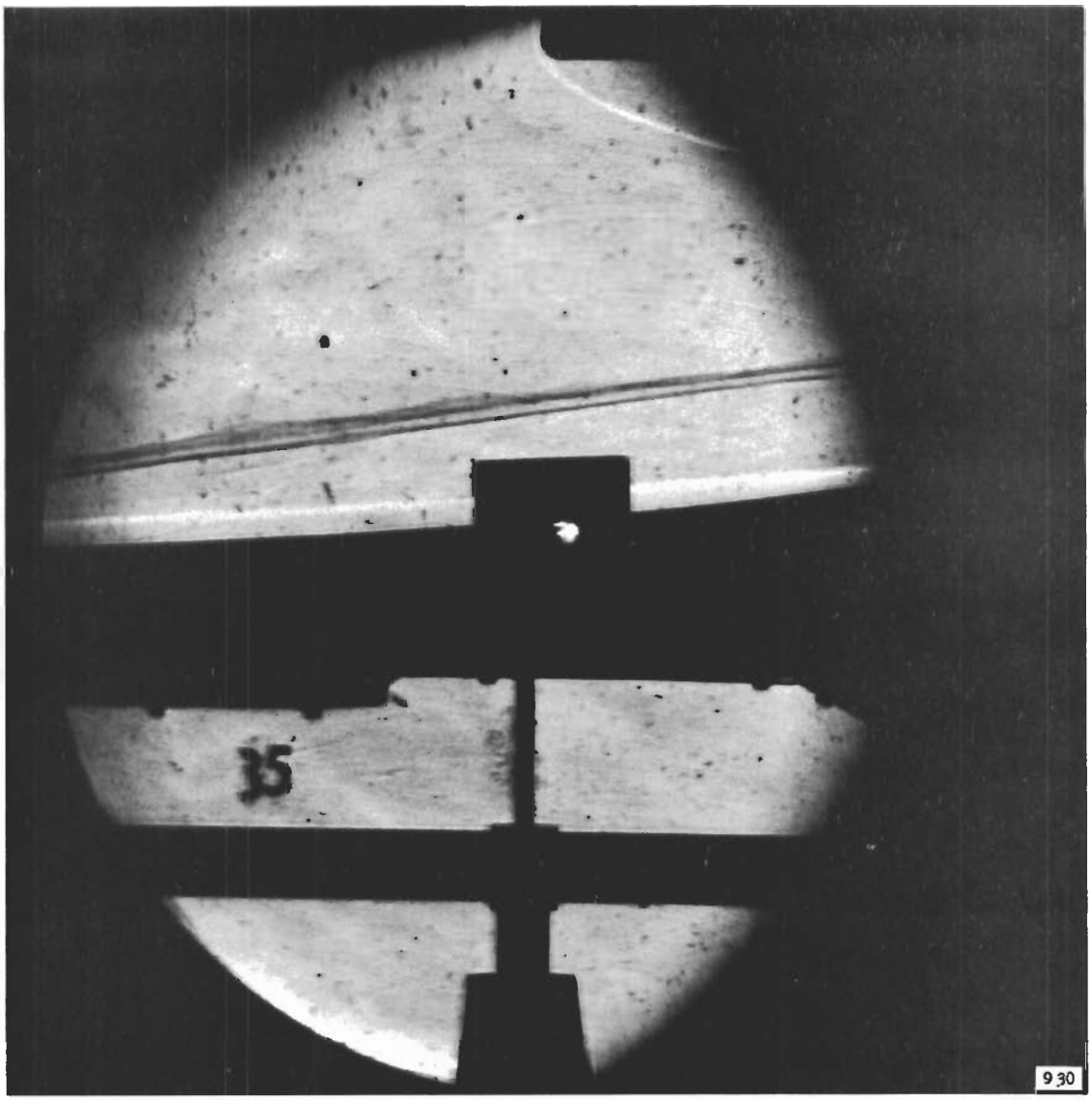


Figure 21 (Cont'd.) (c) MODEL 2D2, RUN 35

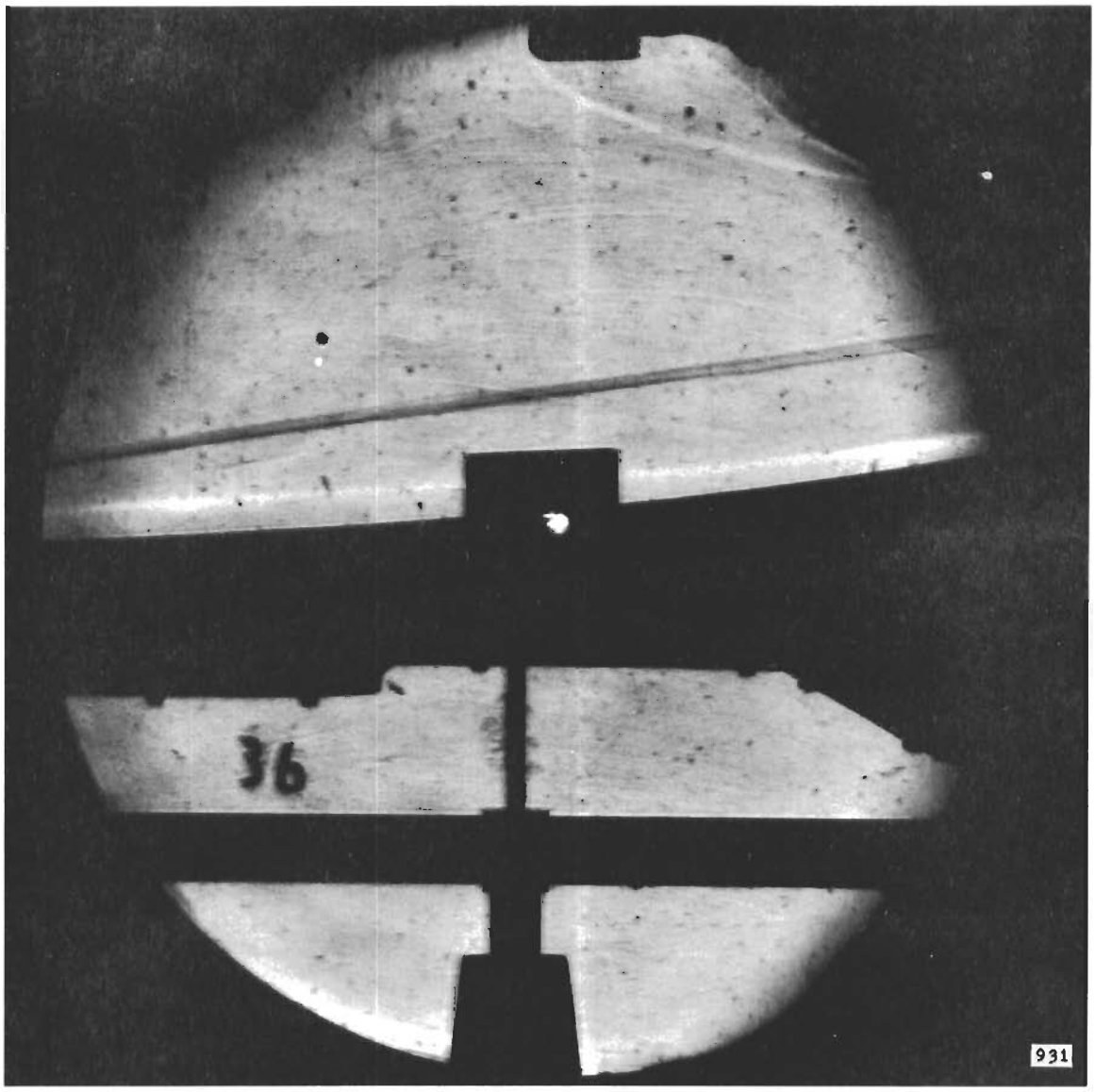


Figure 21 (Cont'd.) (d) MODEL 2D2, RUN 36

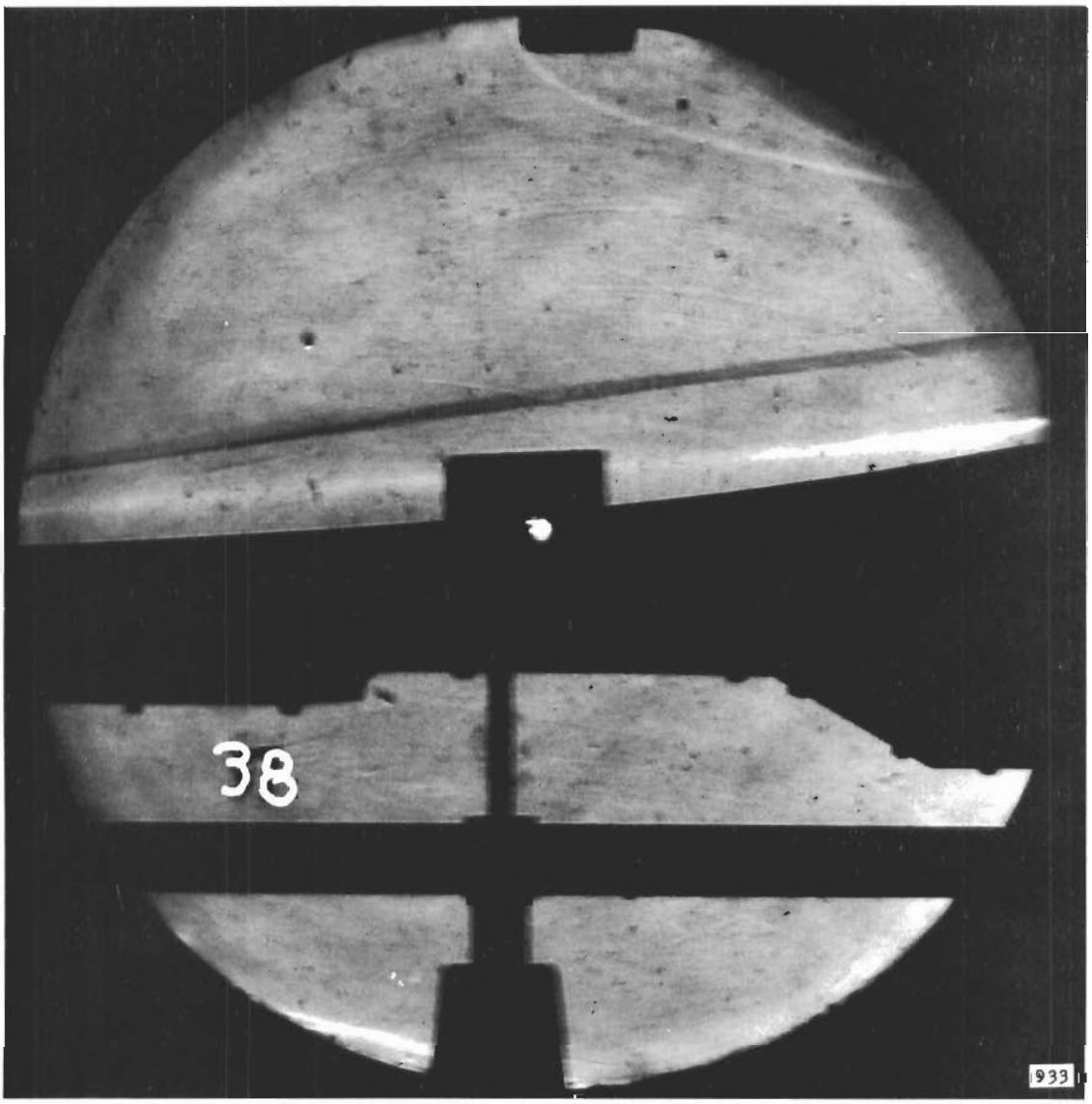


Figure 21 (Cont'd.) (e) MODEL 2D2, RUN 38

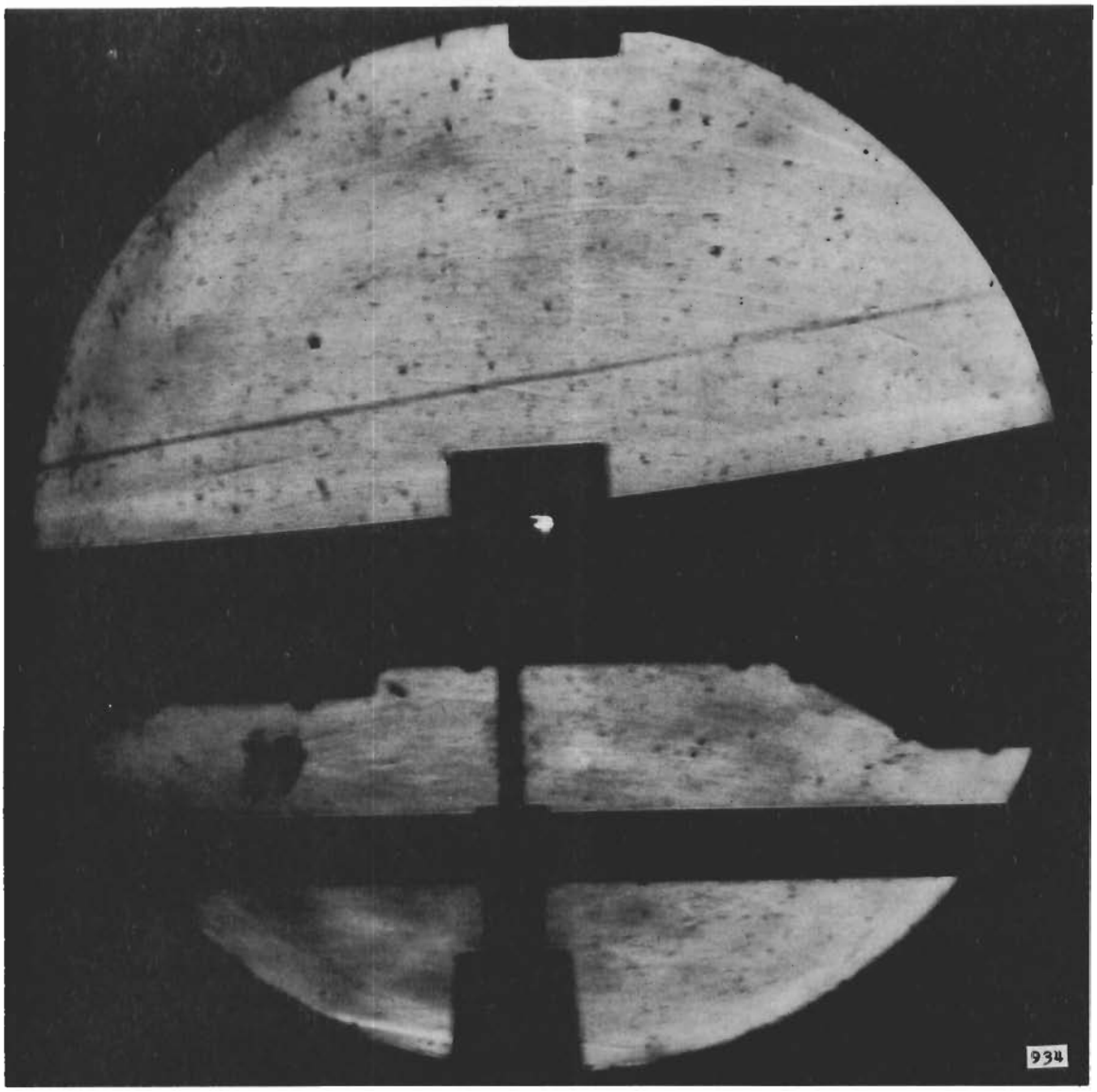


Figure 21 (Cont'd.) (f) MODEL 2D2, RUN 39

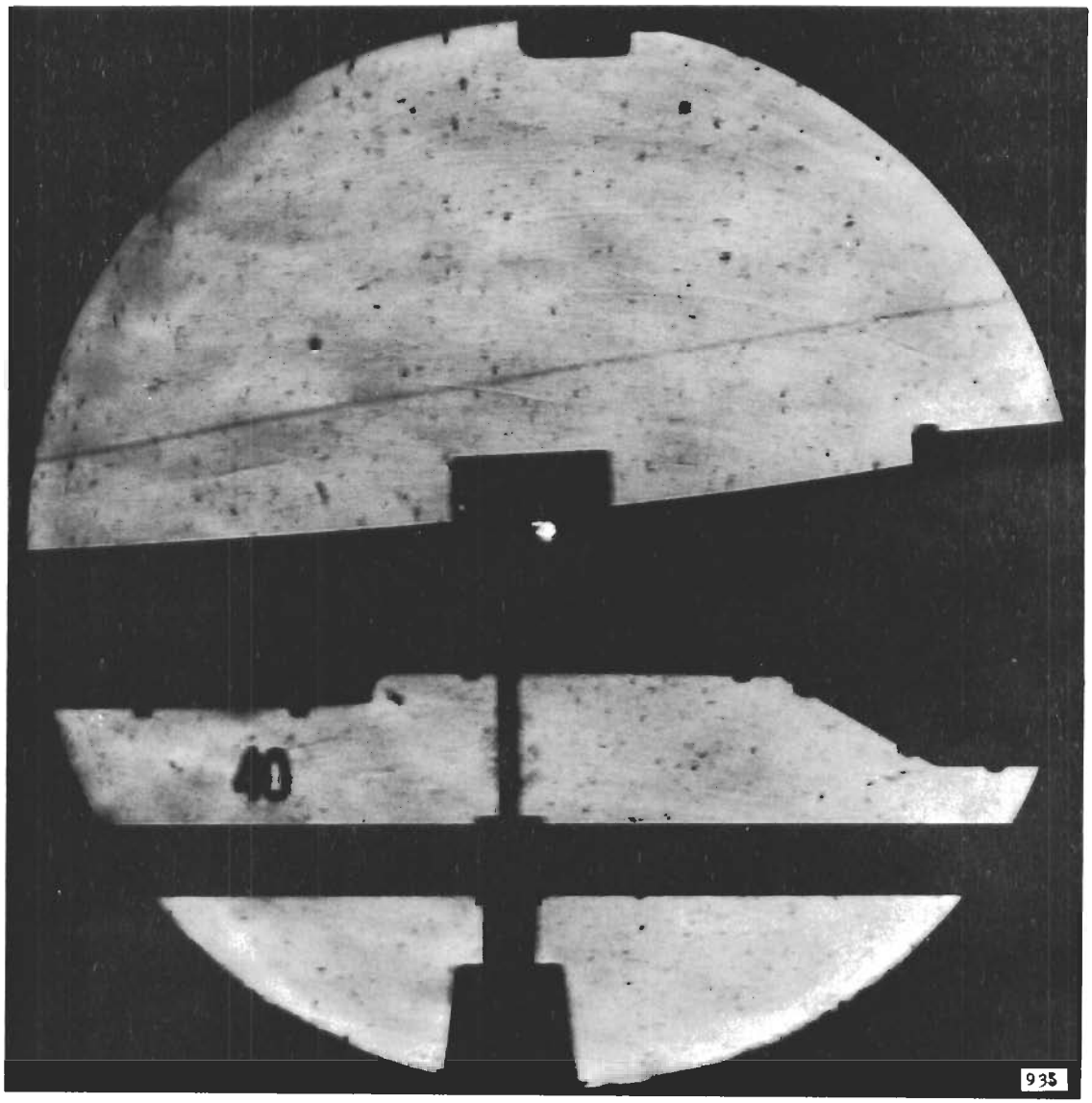


Figure 21 (Cont'd.) (g) MODEL 2D2, RUN 40

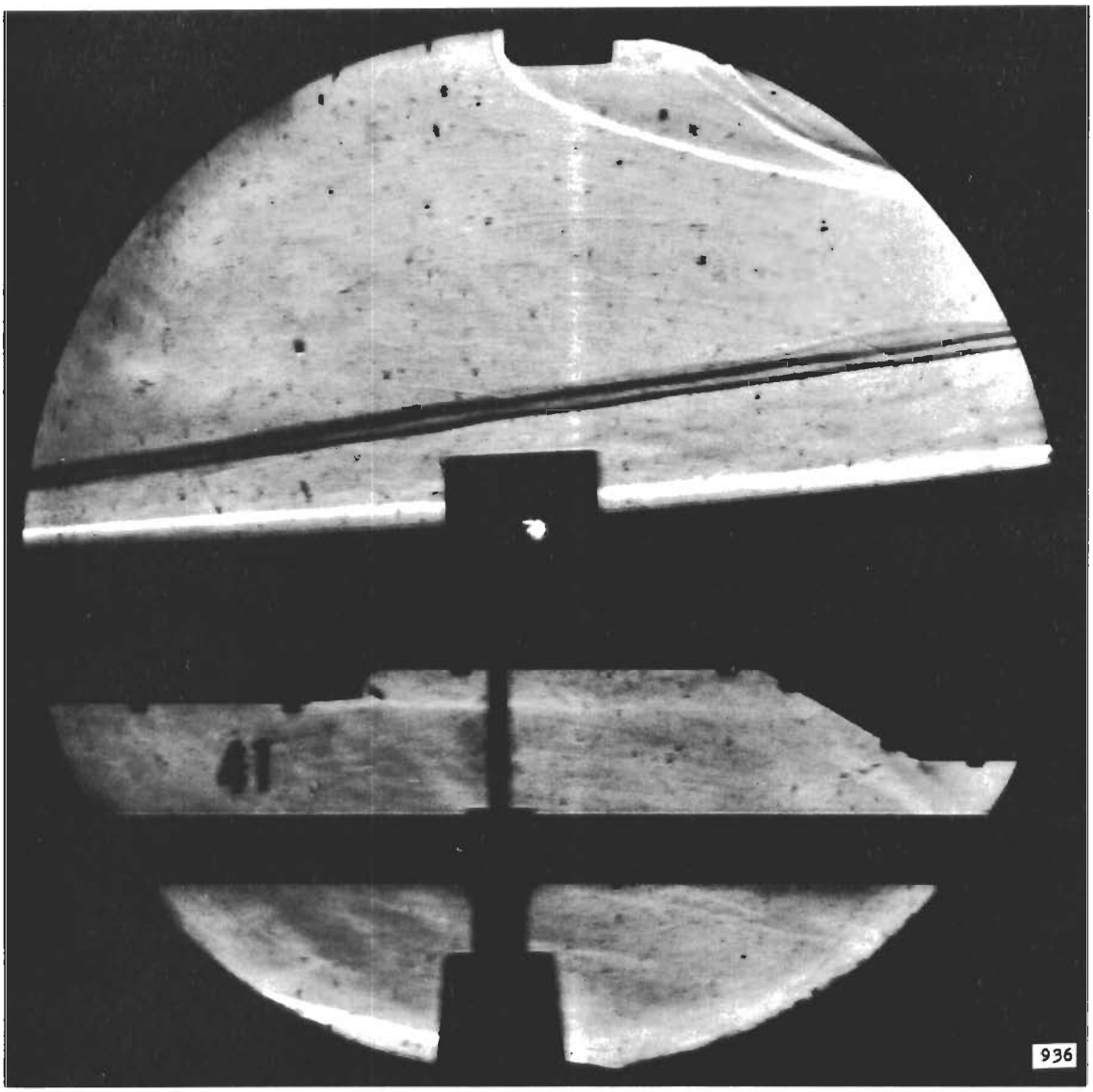


Figure 21 (Cont'd.) (h) MODEL 2D1, RUN 41

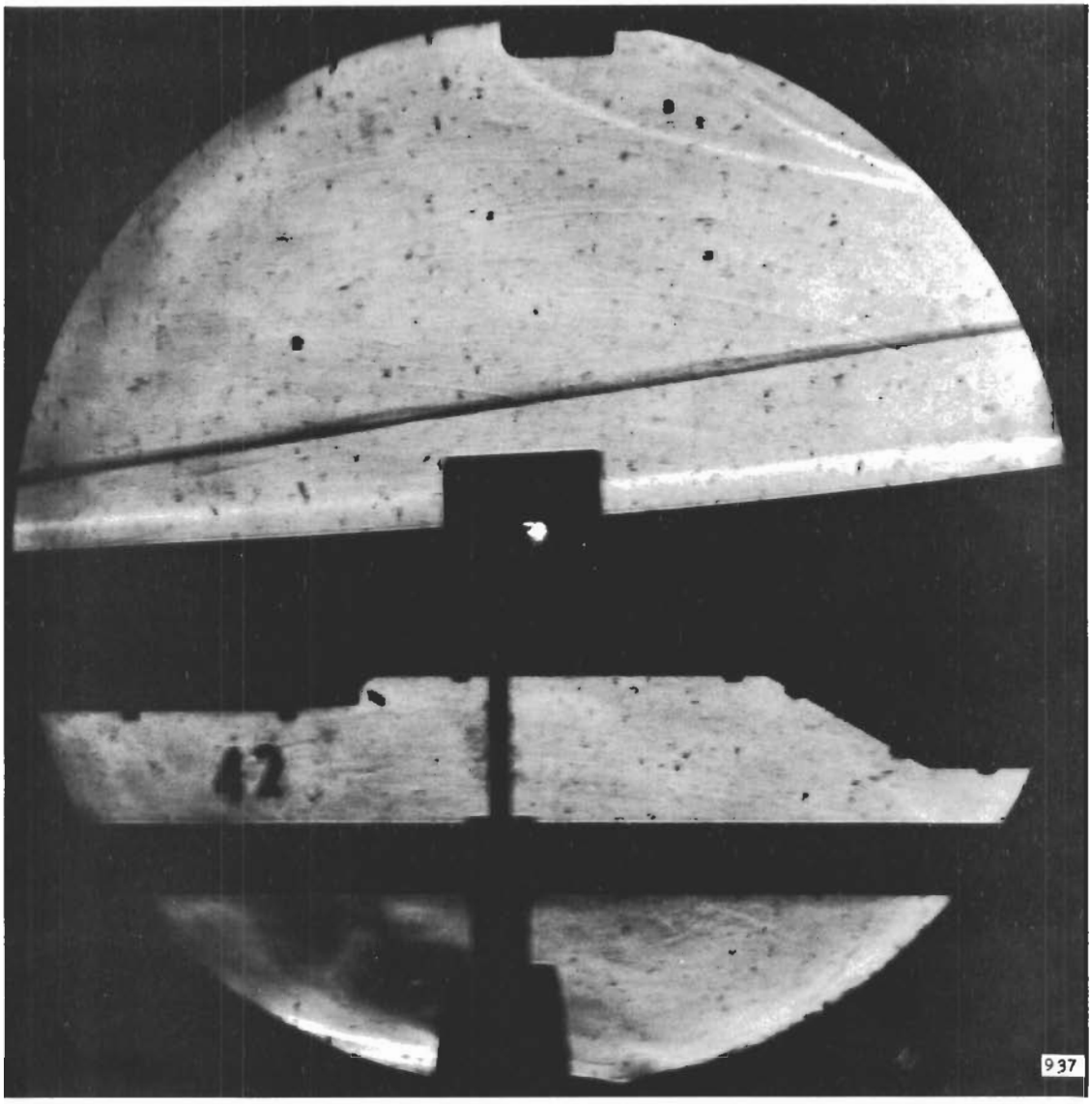


Figure 21 (Cont'd.) (i) MODEL 2D1, RUN 42

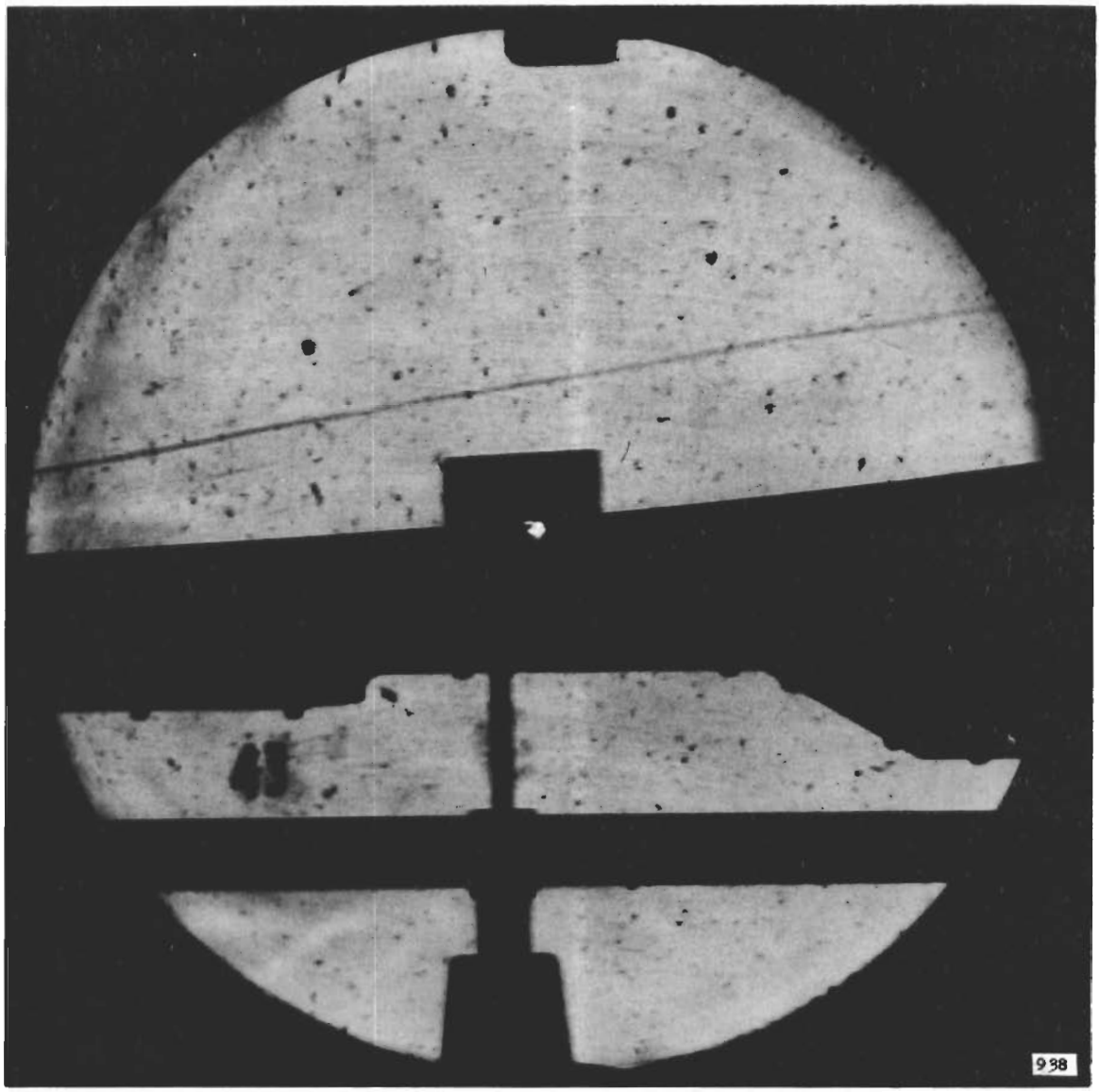


Figure 21 (Cont'd.) (j) MODEL 2D1, RUN 43

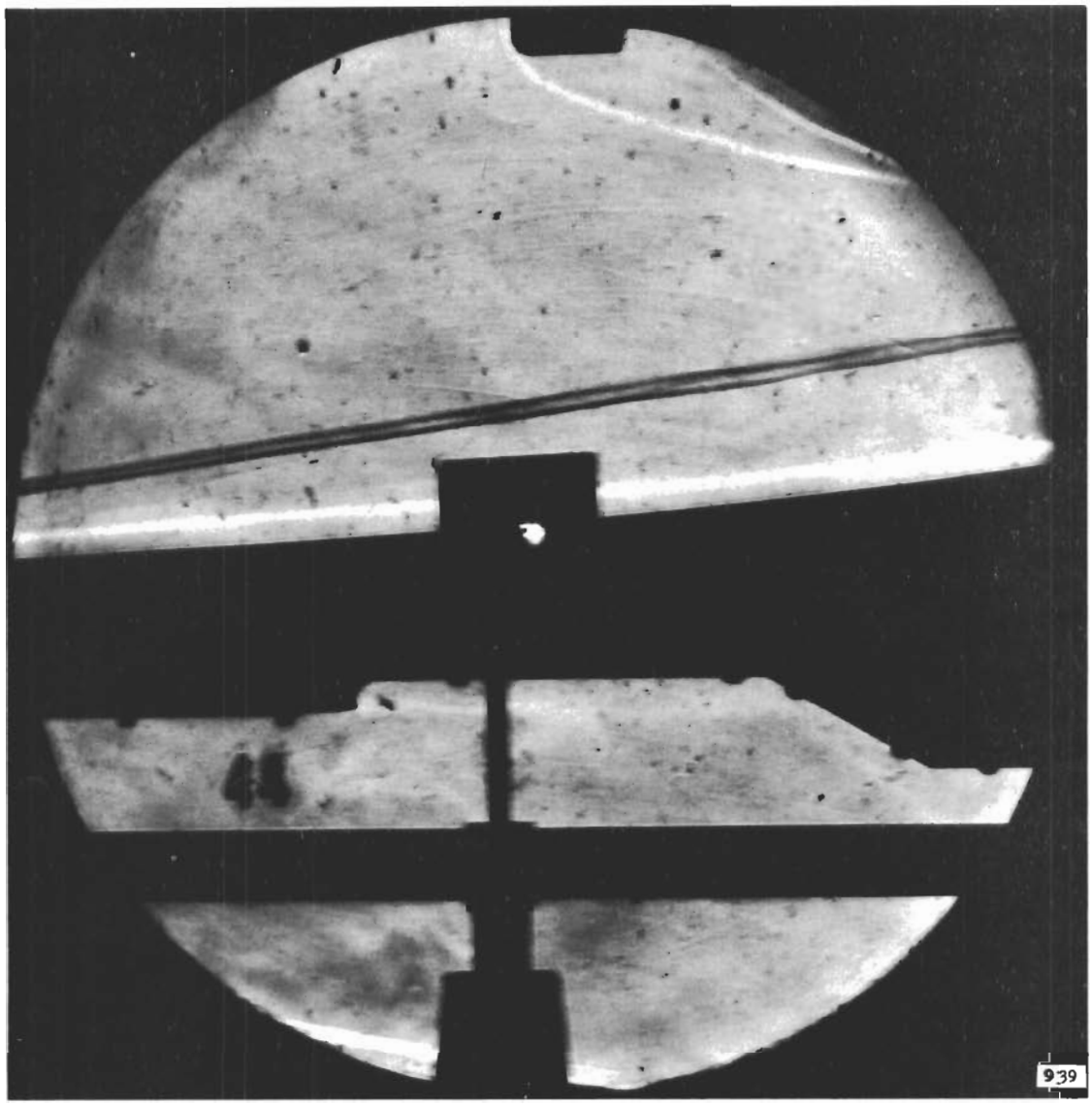


Figure 21 (Cont'd.) (k) MODEL 2D1, RUN 44

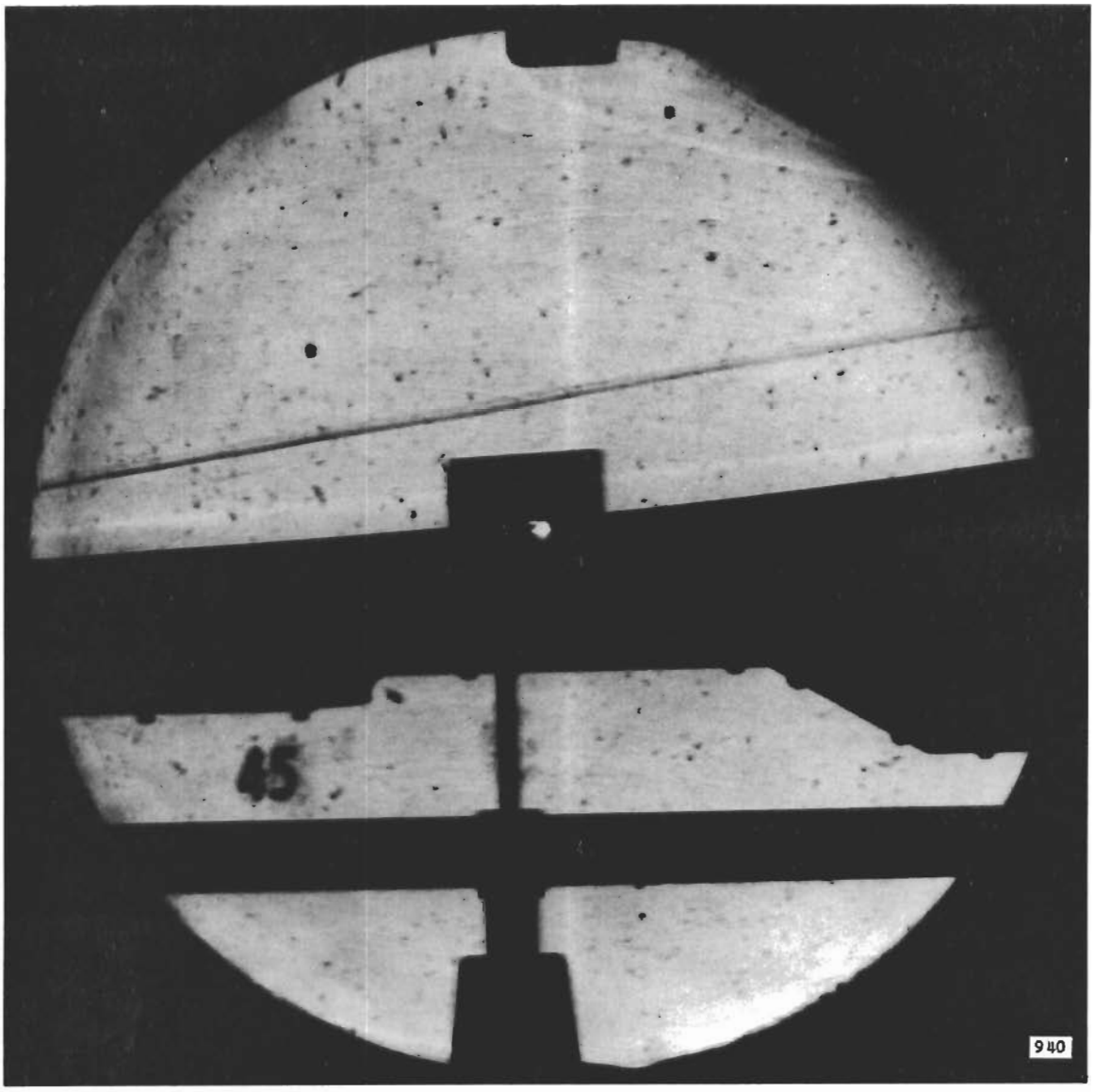


Figure 21 (Cont'd.) (1) MODEL 2D1, RUN 45

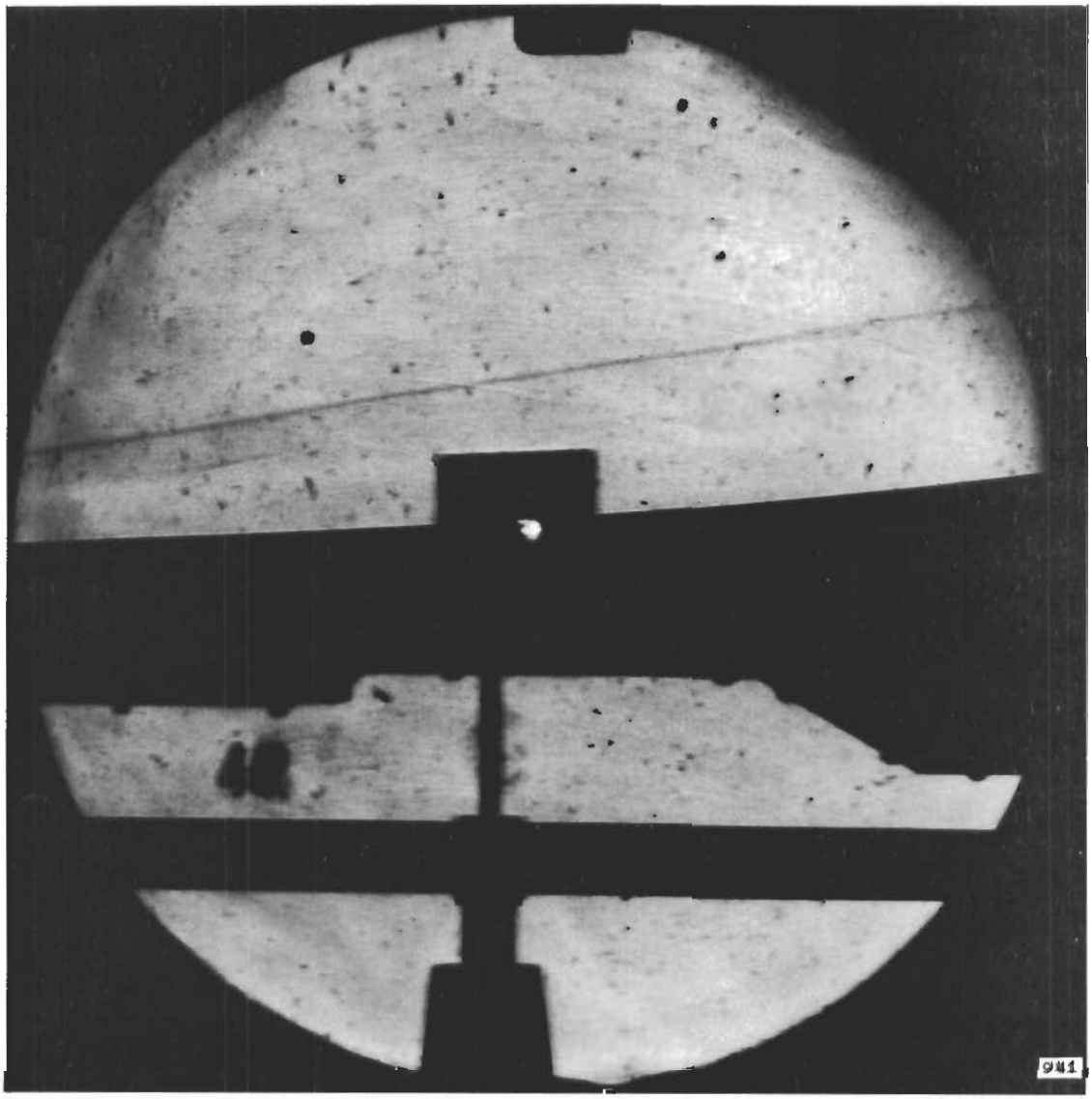

Figure 21 (Cont'd.) (m) MODEL 2D1, RUN 46

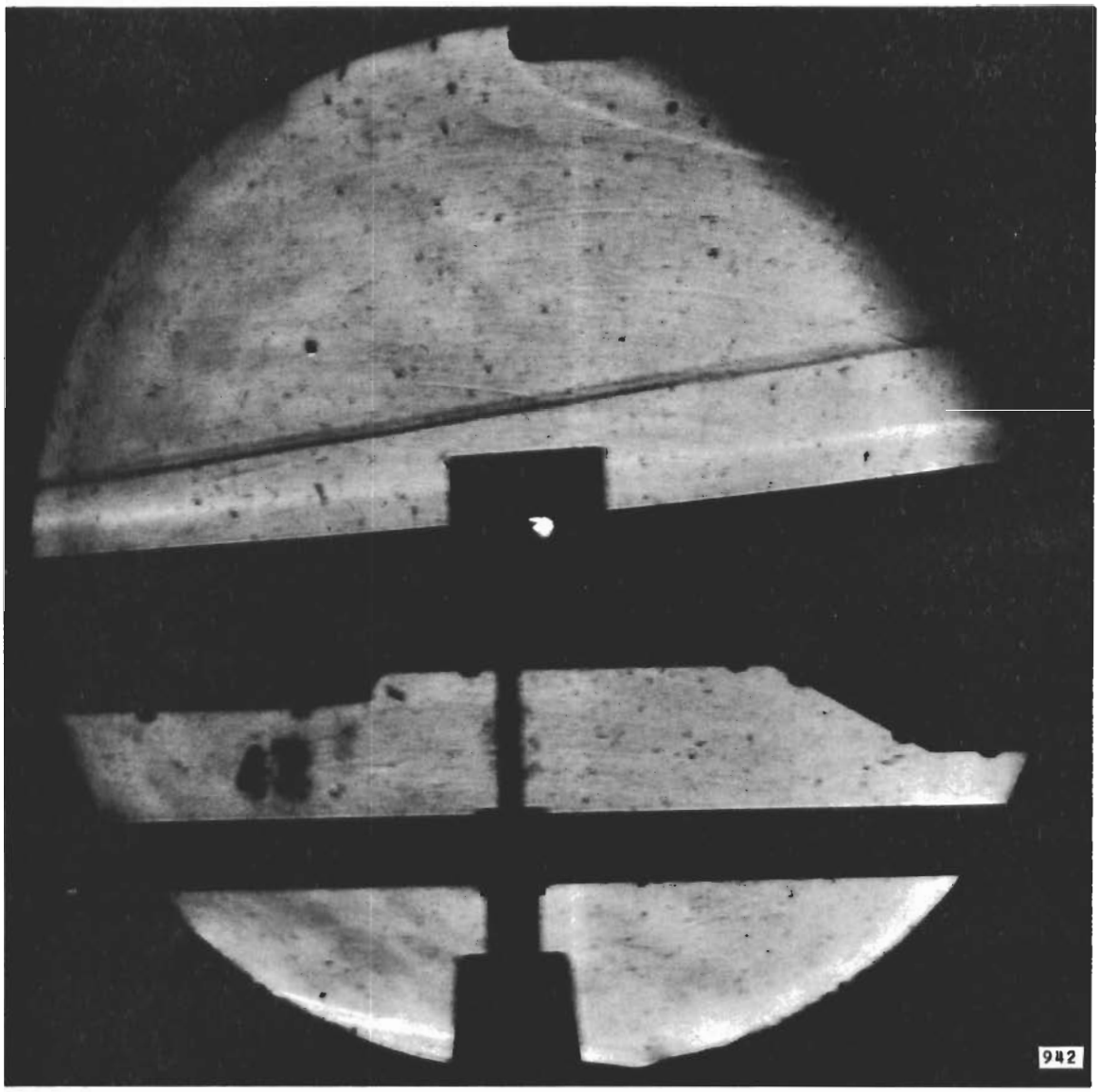


Figure 21 (Cont'd.) (n) MODEL 2D1, RUN 47

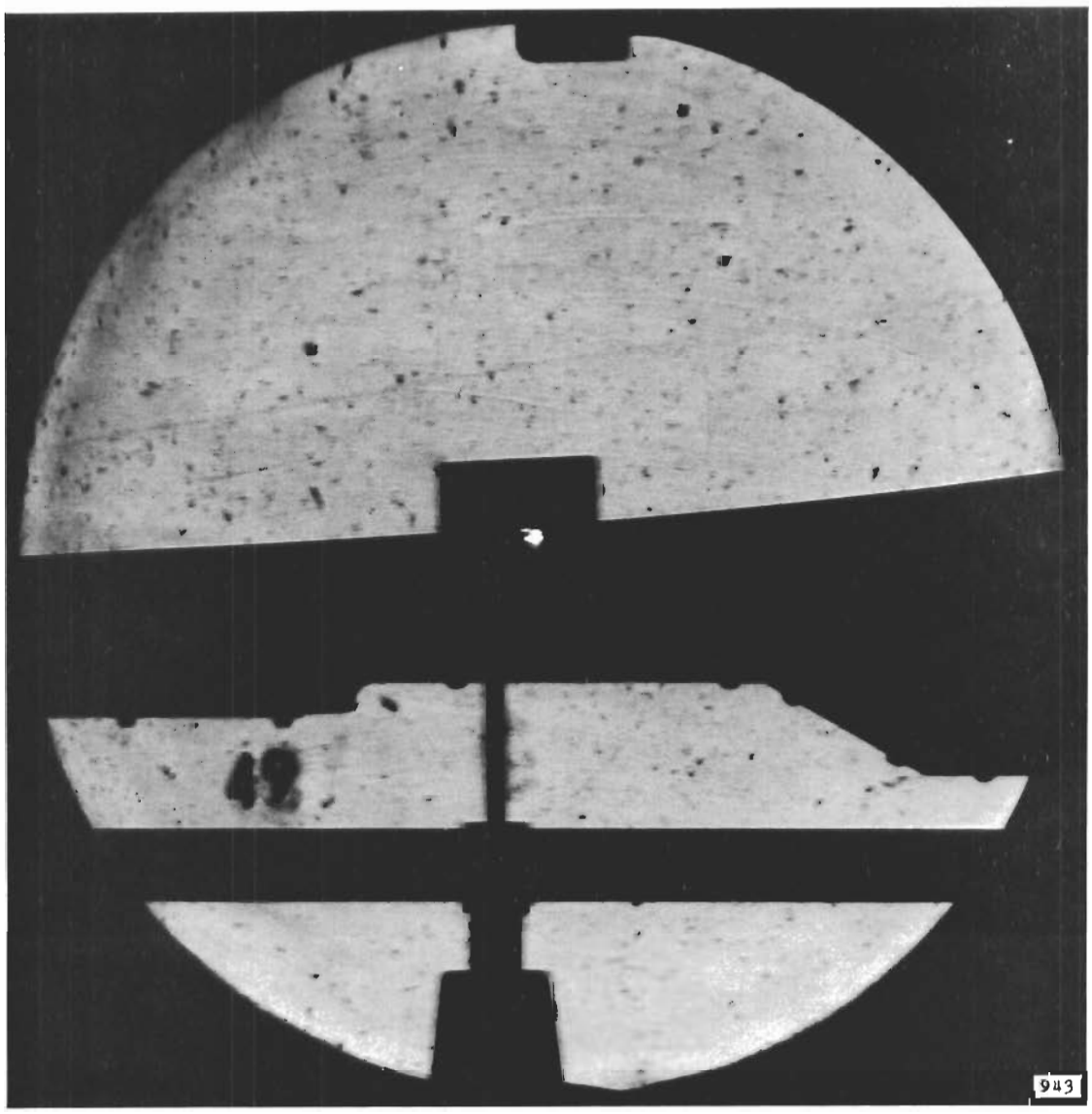


Figure 21 (Concluded) (o) MODEL 2D1, RUN 49

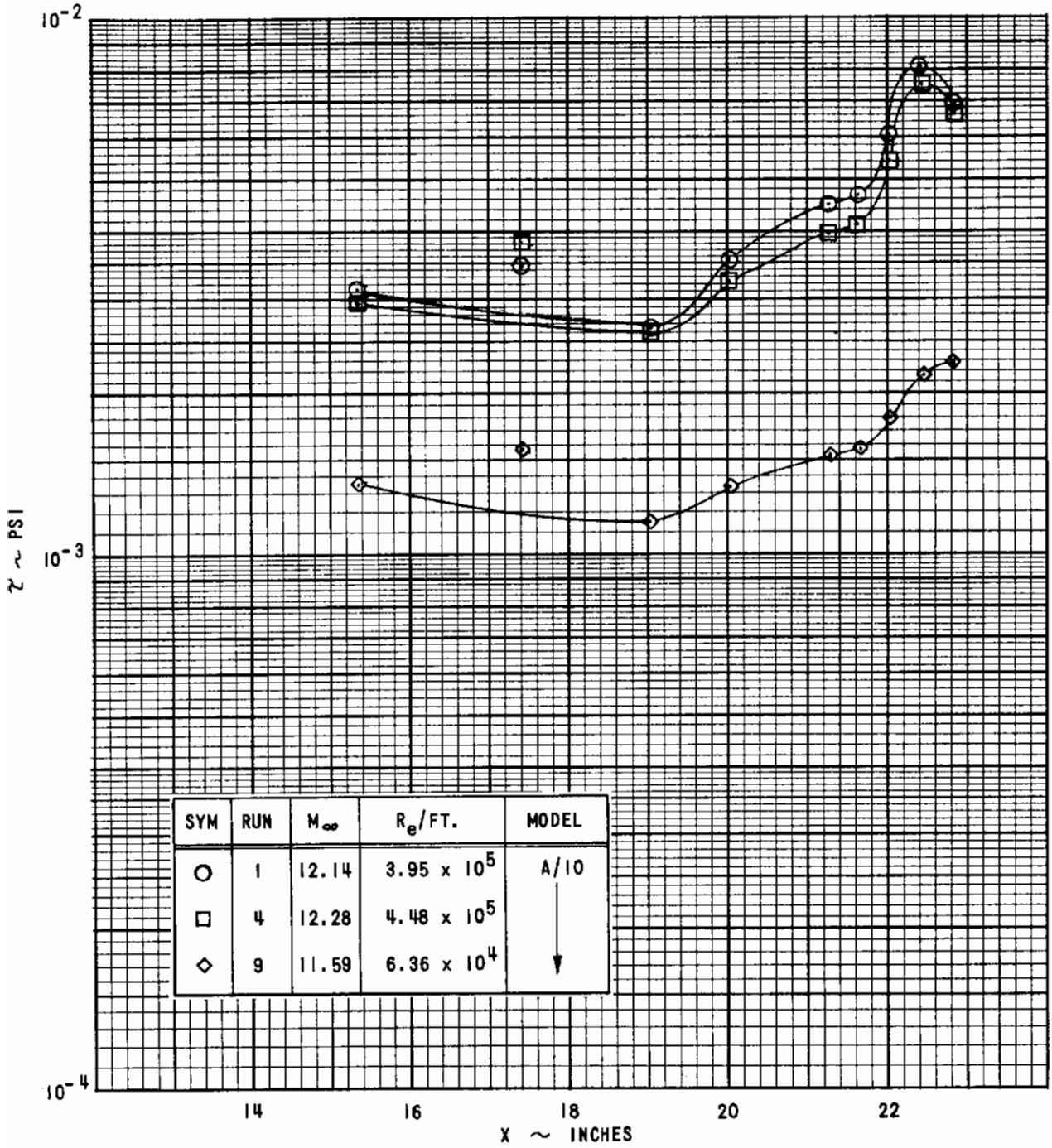


Figure 22 SKIN FRICTION DISTRIBUTIONS ON THE AXISYMMETRIC MODELS
(a) MODEL A/10, MACH NUMBER 12

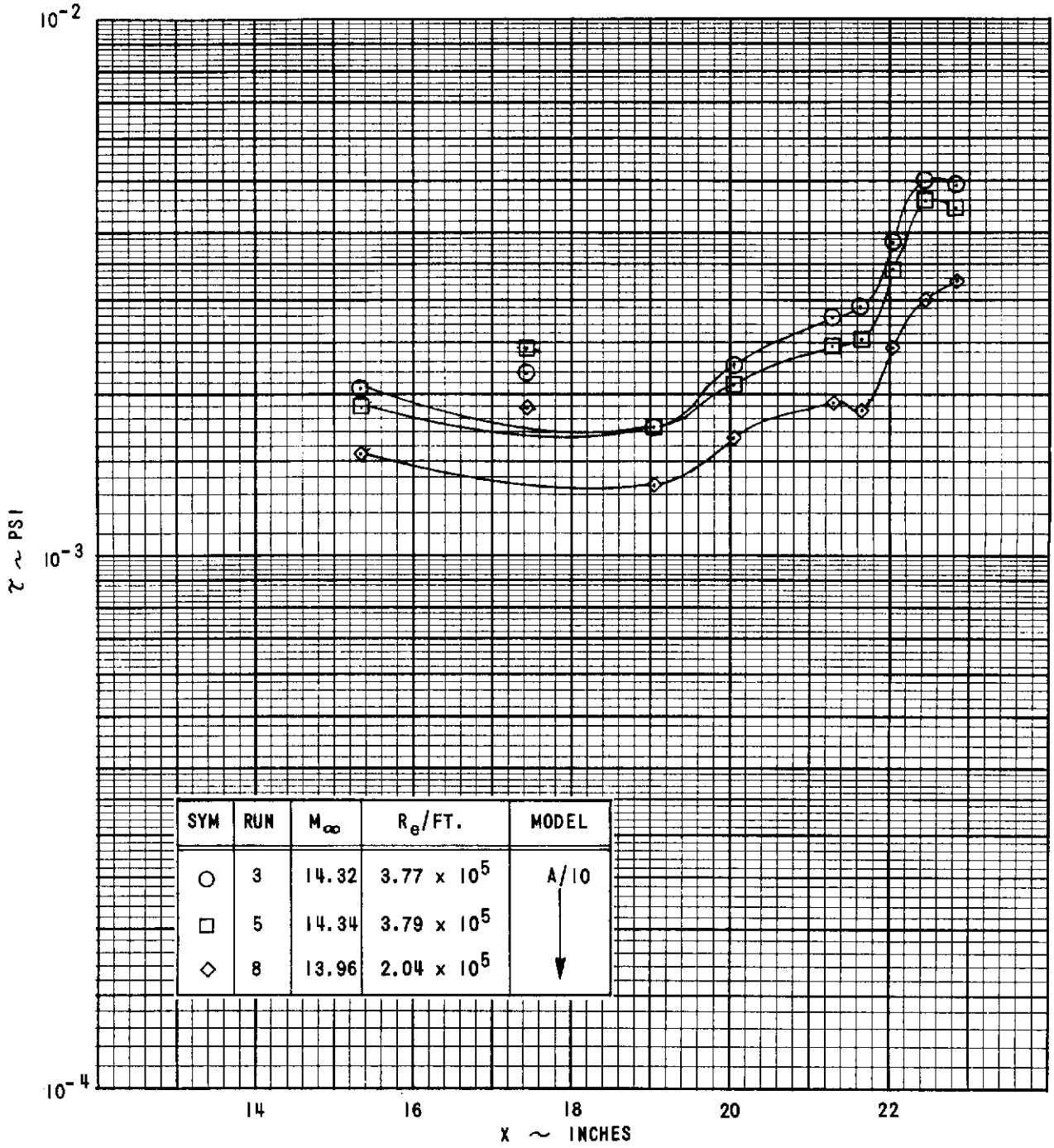


Figure 22 (Cont'd.) (b) MODEL A/10, MACH NUMBER 14

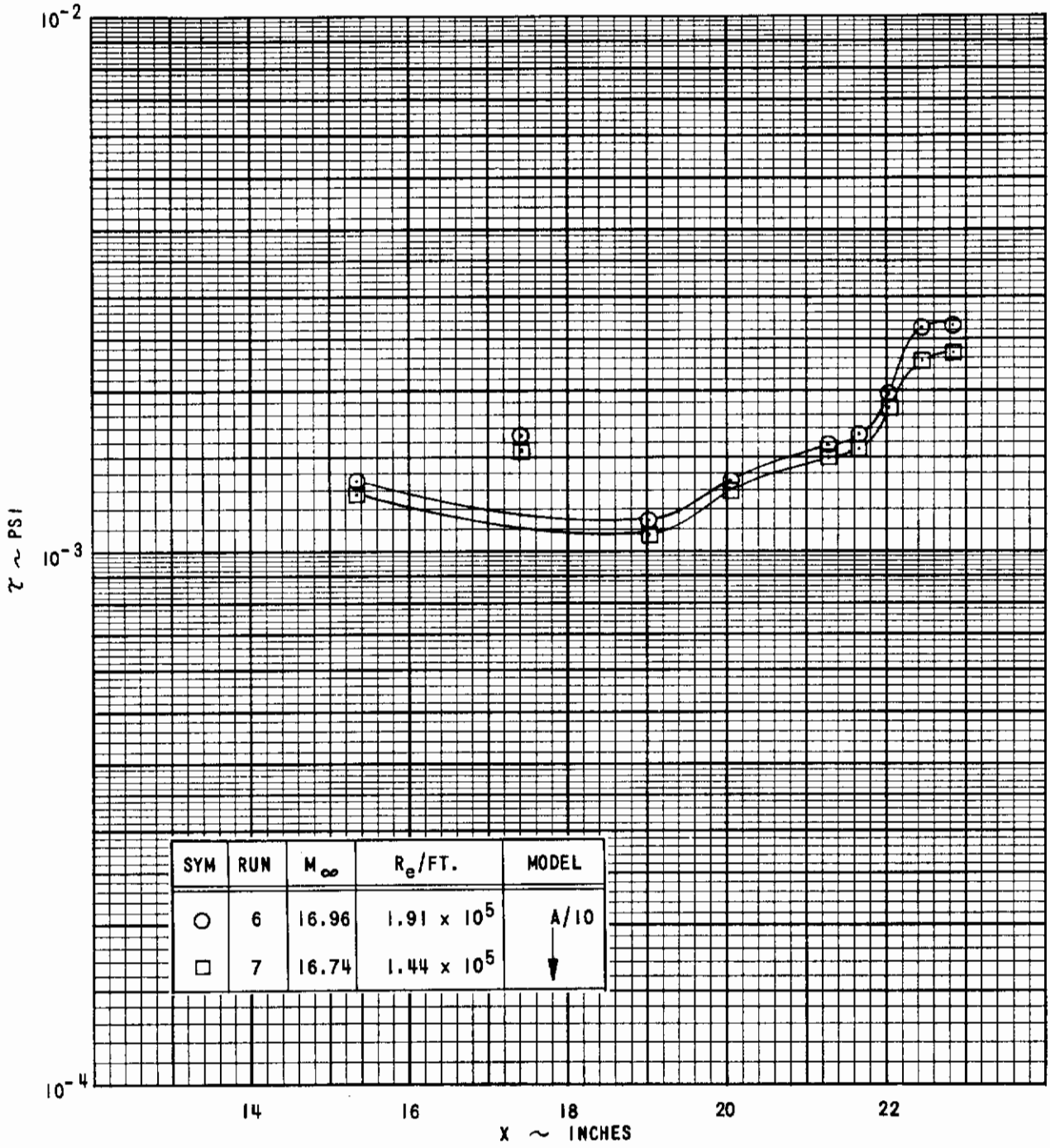


Figure 22 (Cont'd.) (c) MODEL A/10, MACH NUMBER 16

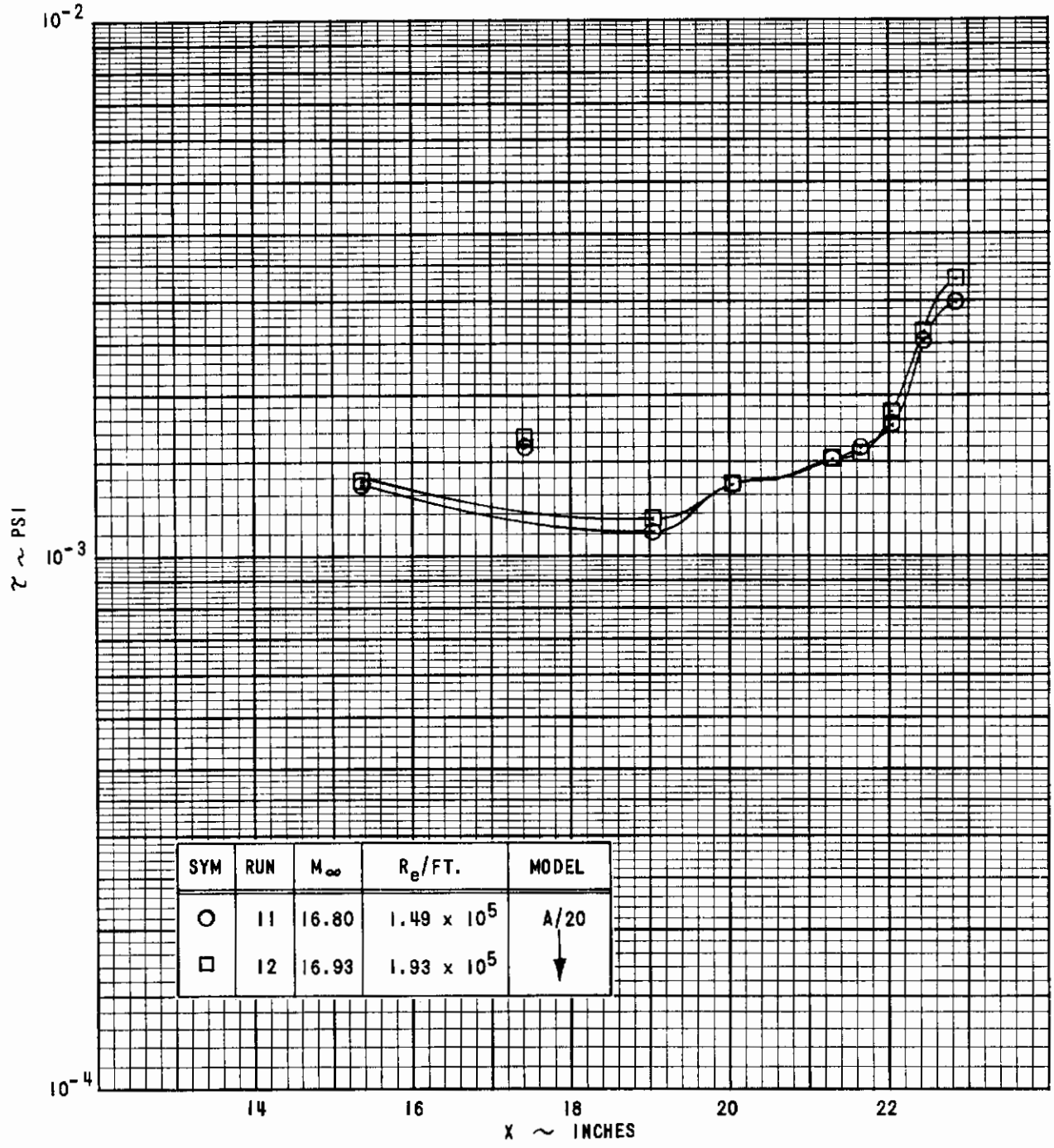


Figure 22 (Cont'd.) (d) MODEL A/20, MACH NUMBER 16

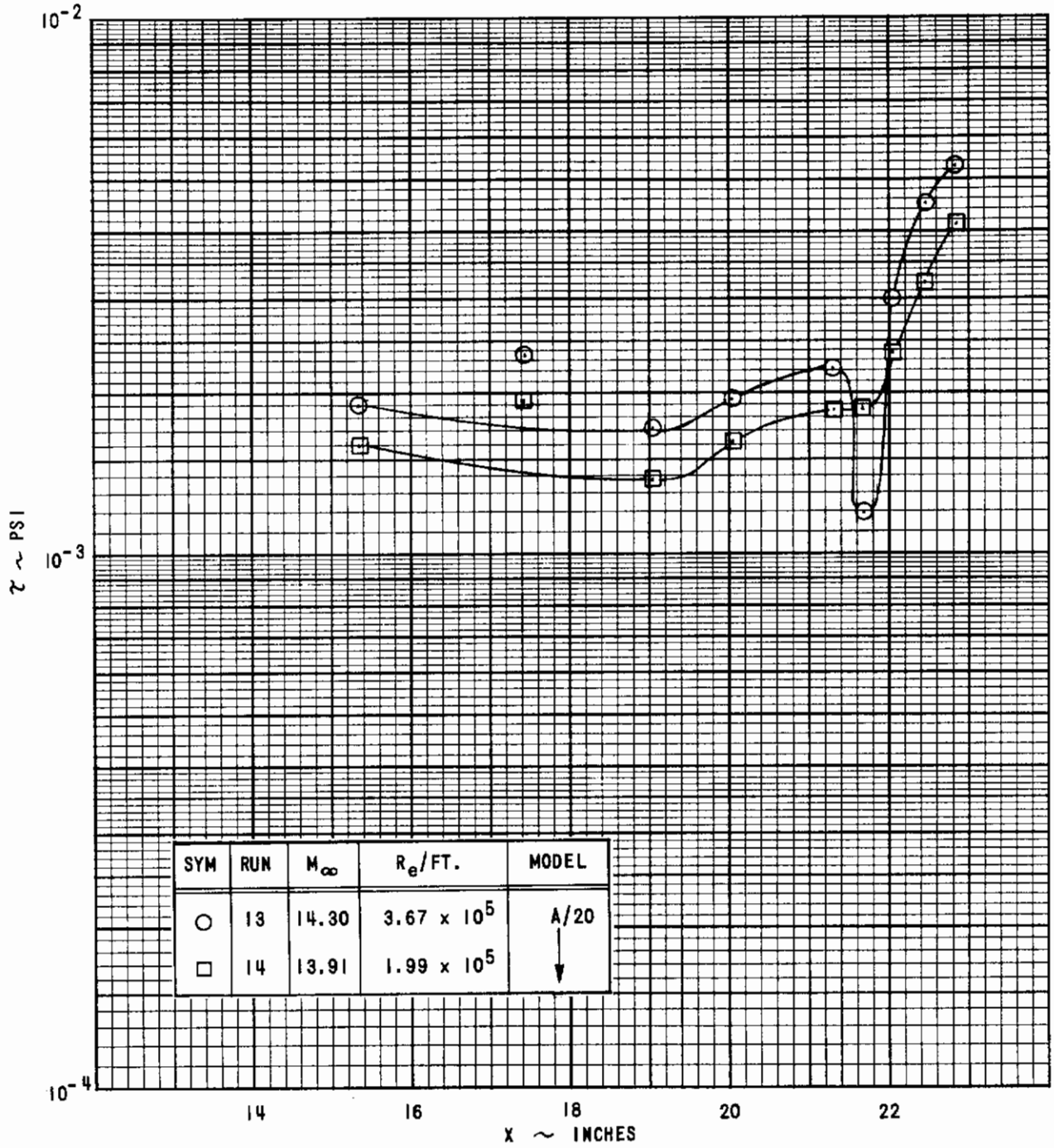


Figure 22 (Cont'd.) (e) MODEL A/20, MACH NUMBER 14

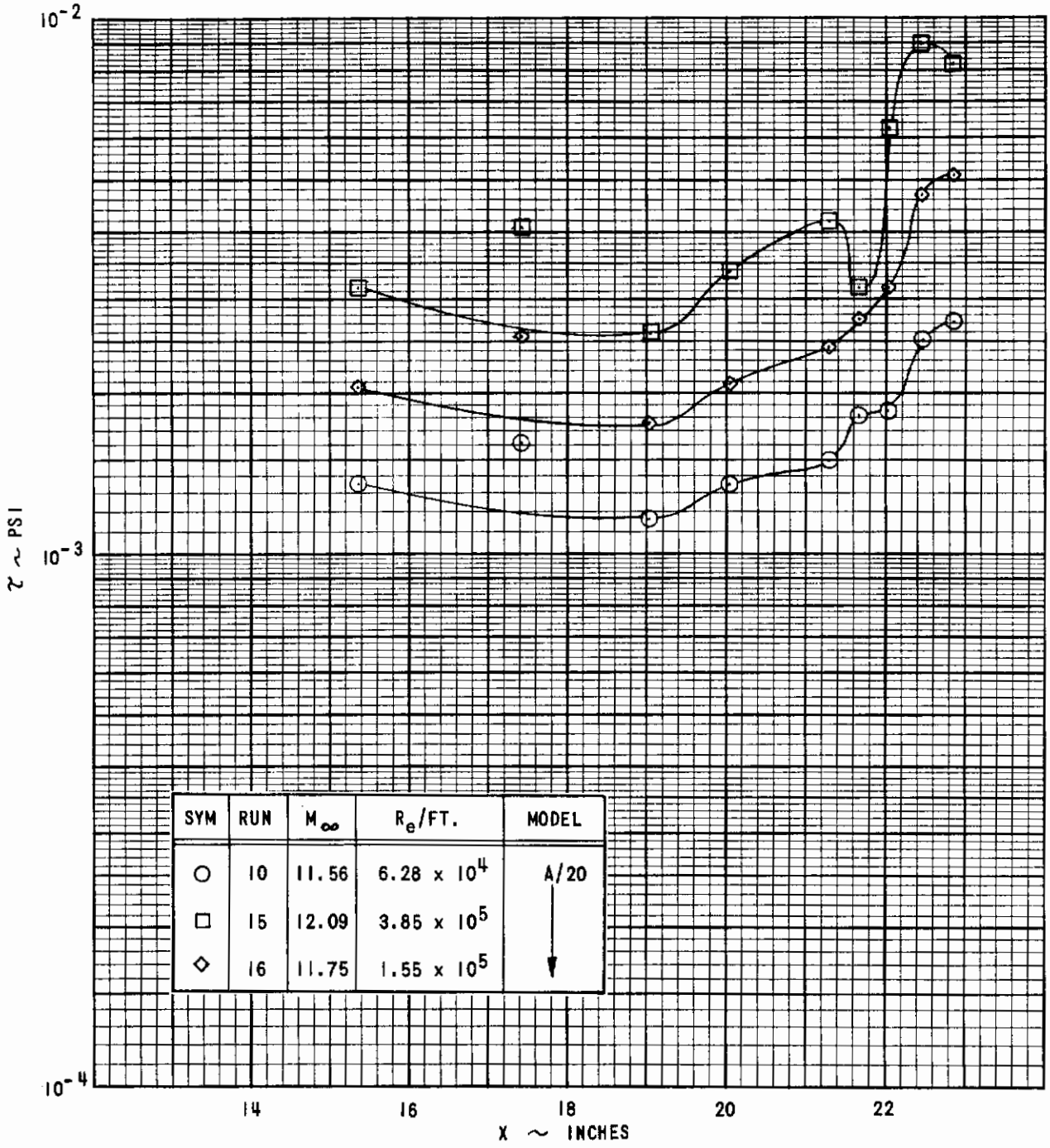


Figure 22 (Cont'd.) (f) MODEL A/20, MACH NUMBER 12

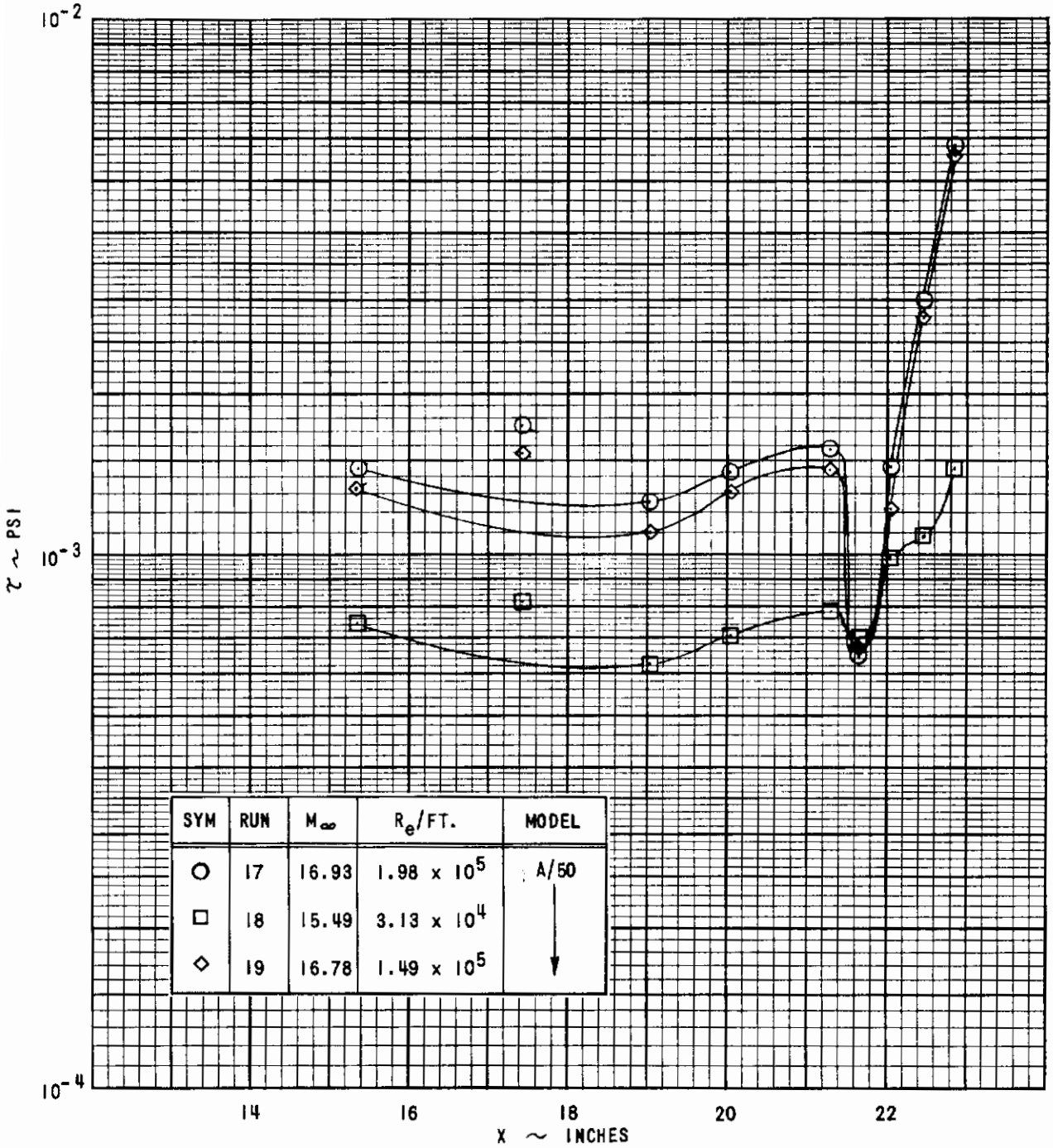


Figure 22 (Cont'd.) (g) MODEL A/50, MACH NUMBER 16

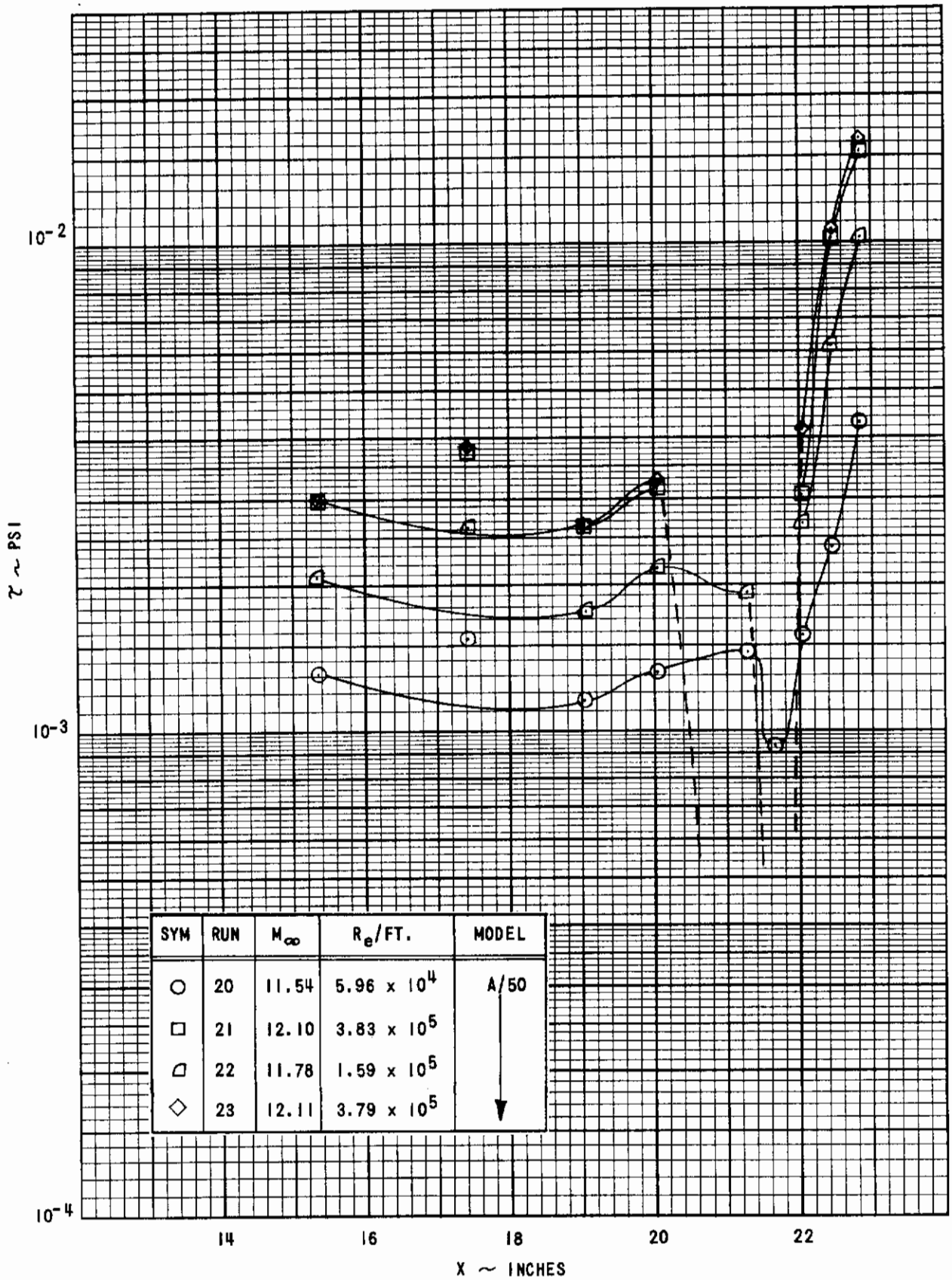


Figure 22 (Cont'd.) (h) MODEL A/50, MACH NUMBER 12

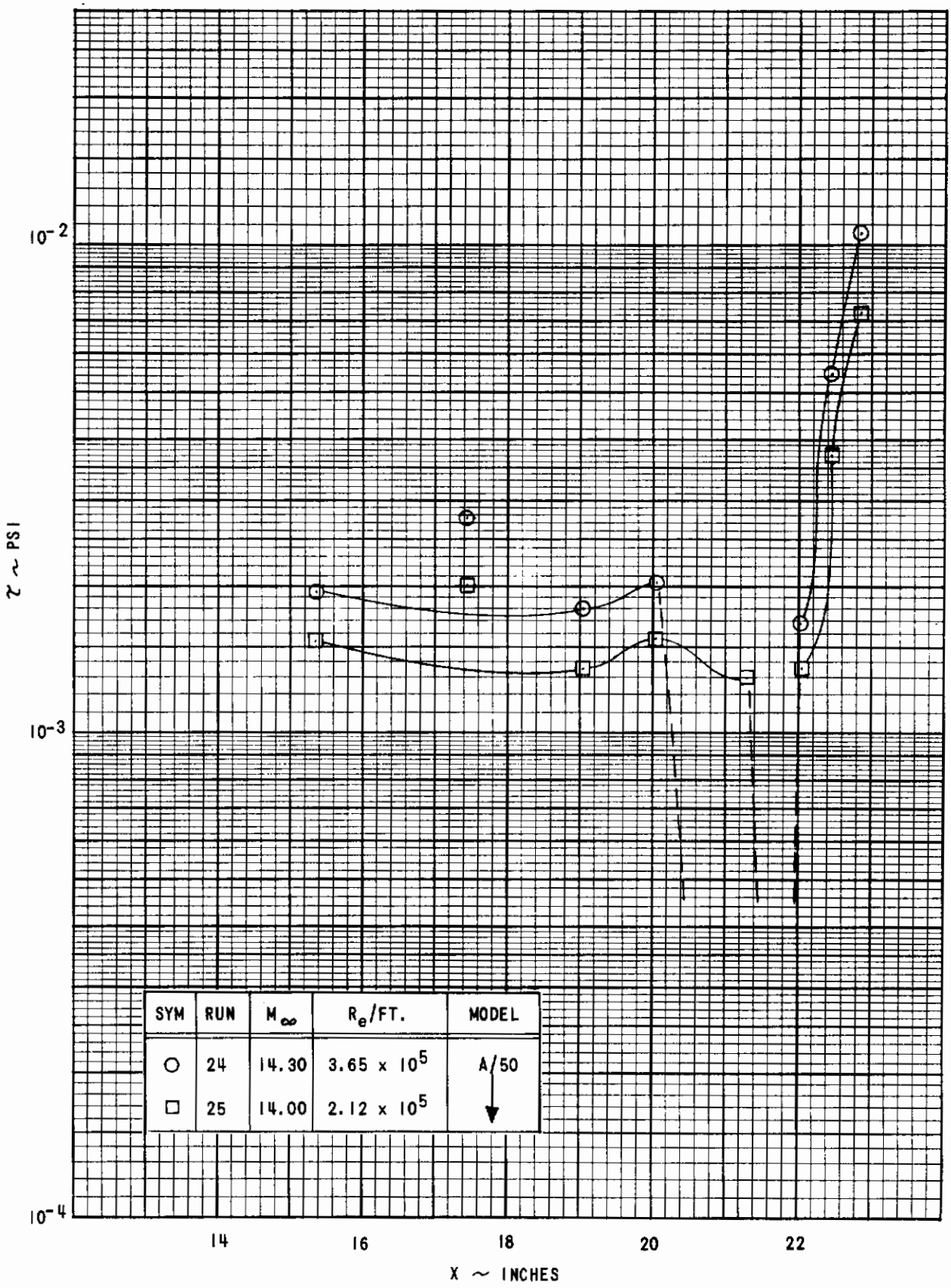


Figure 22 (Cont'd.) (i) MODEL A/50, MACH NUMBER 14

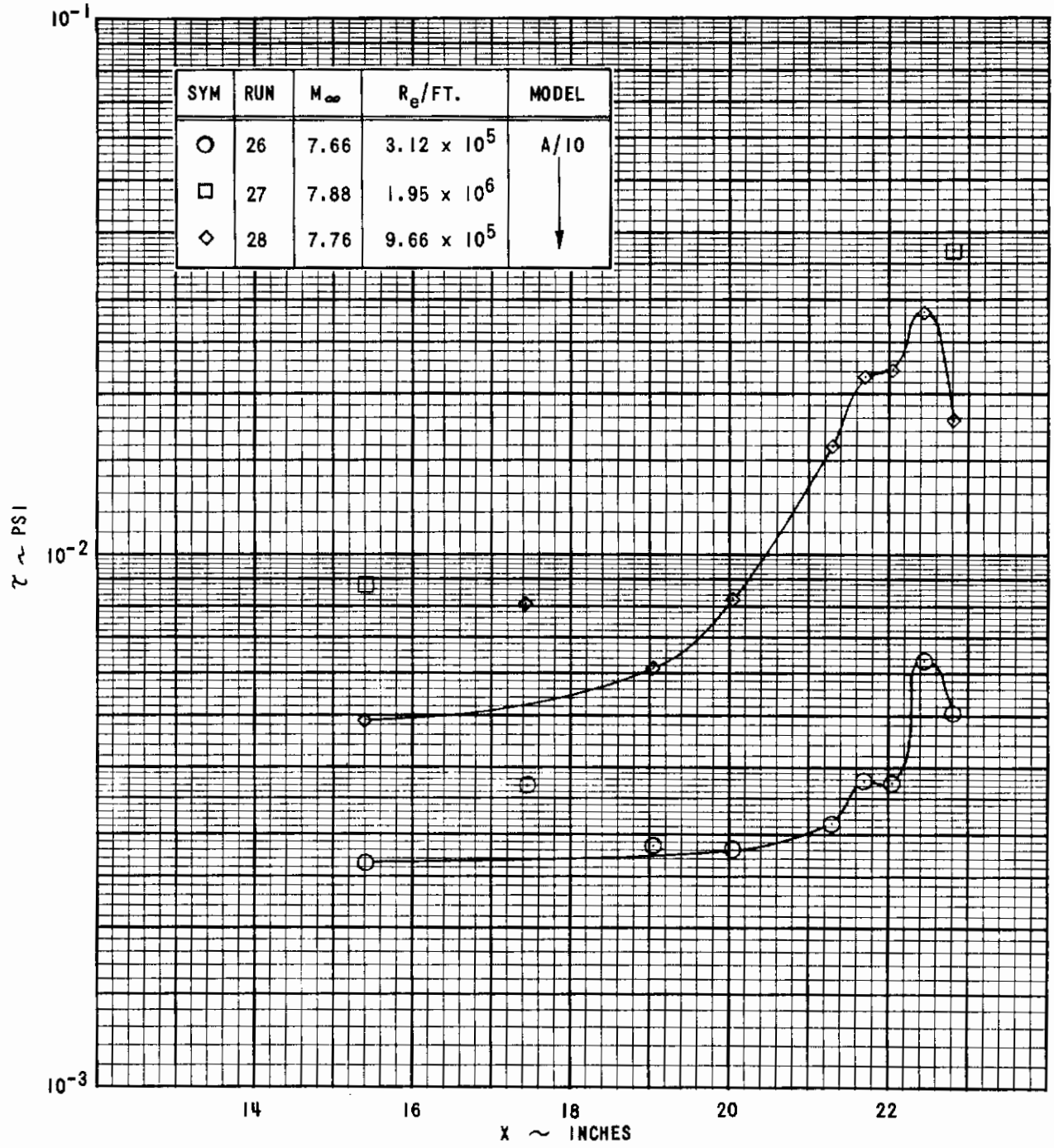


Figure 22 (Cont'd.) (j) MODEL A/10, MACH NUMBER 7.5

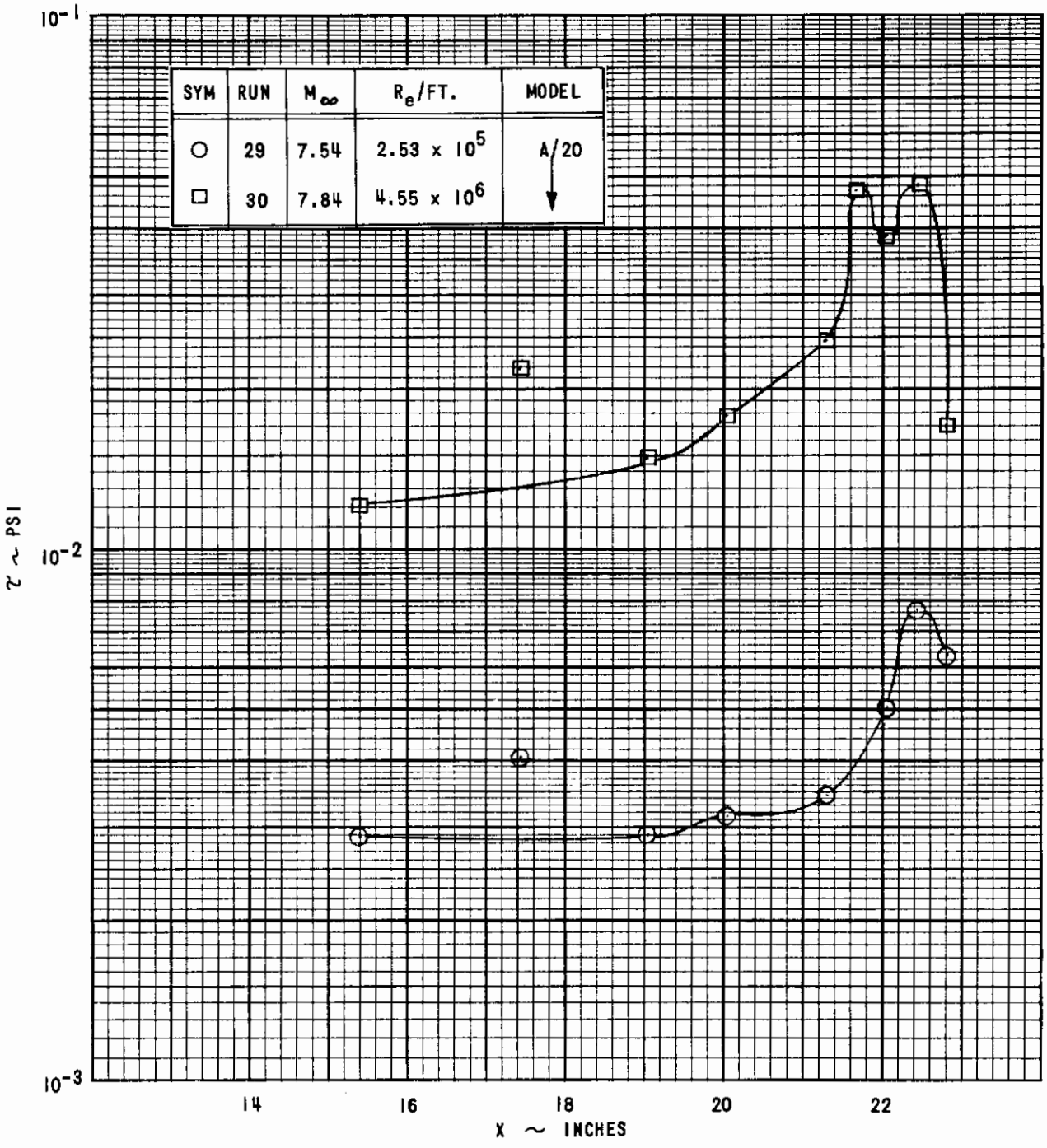


Figure 22 (Cont'd.) (k) MODEL A/20, MACH NUMBER 7.5

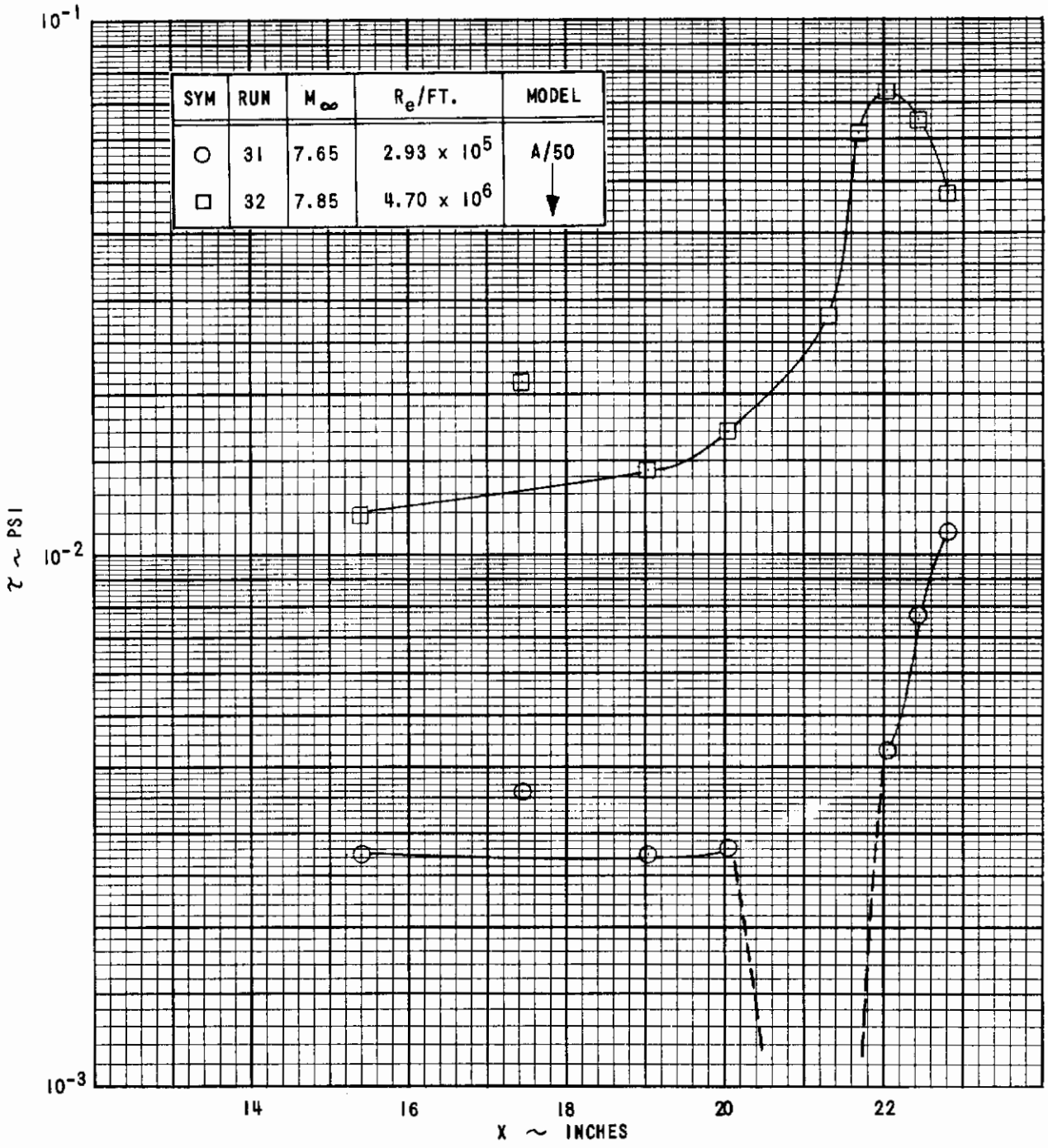


Figure 22 (Concluded) (1) MODEL A/50, MACH NUMBER 7.5

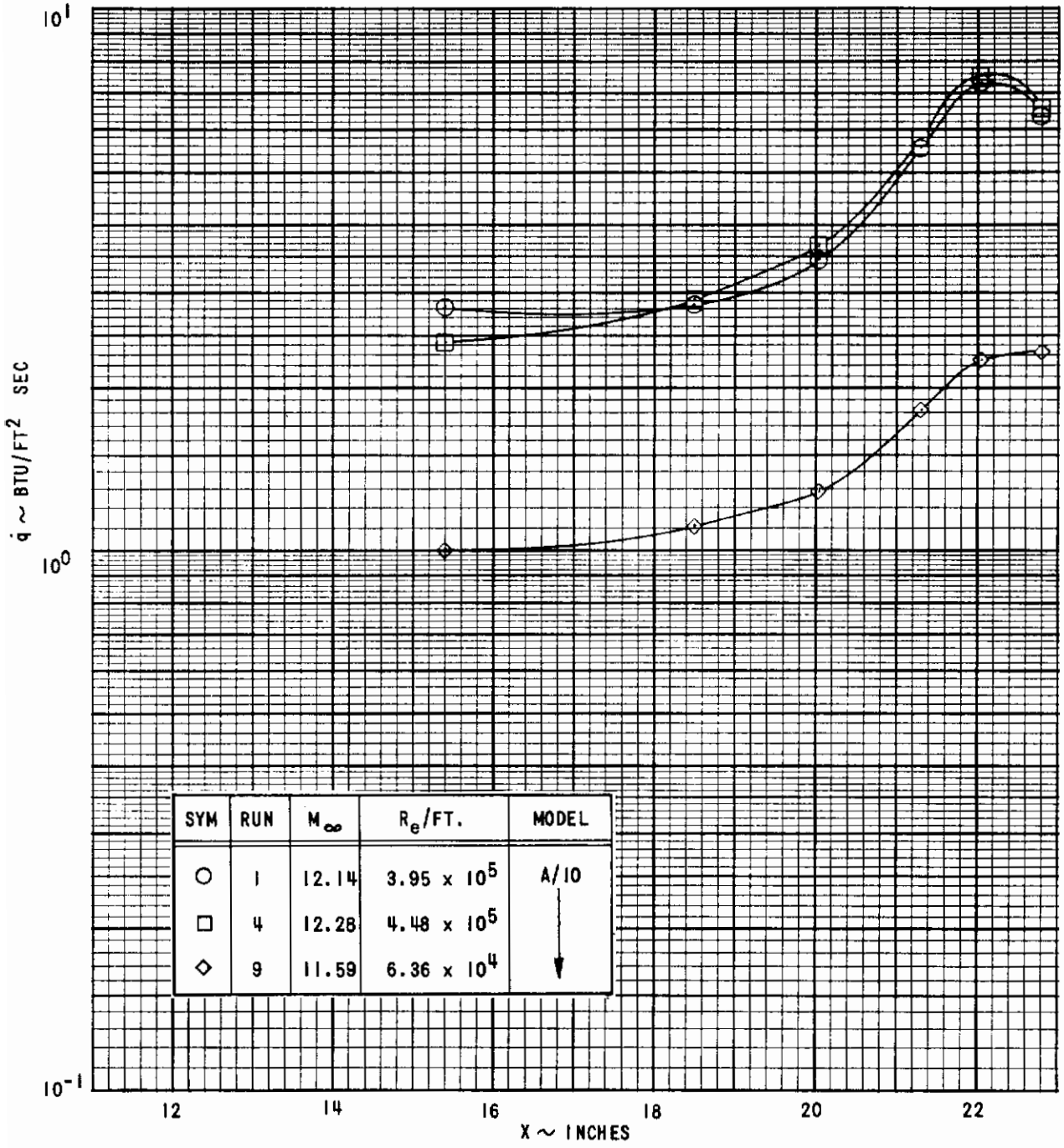


Figure 23 HEAT TRANSFER DISTRIBUTIONS ON THE AXISYMMETRIC MODELS
(a) MODEL A/10, MACH NUMBER 12

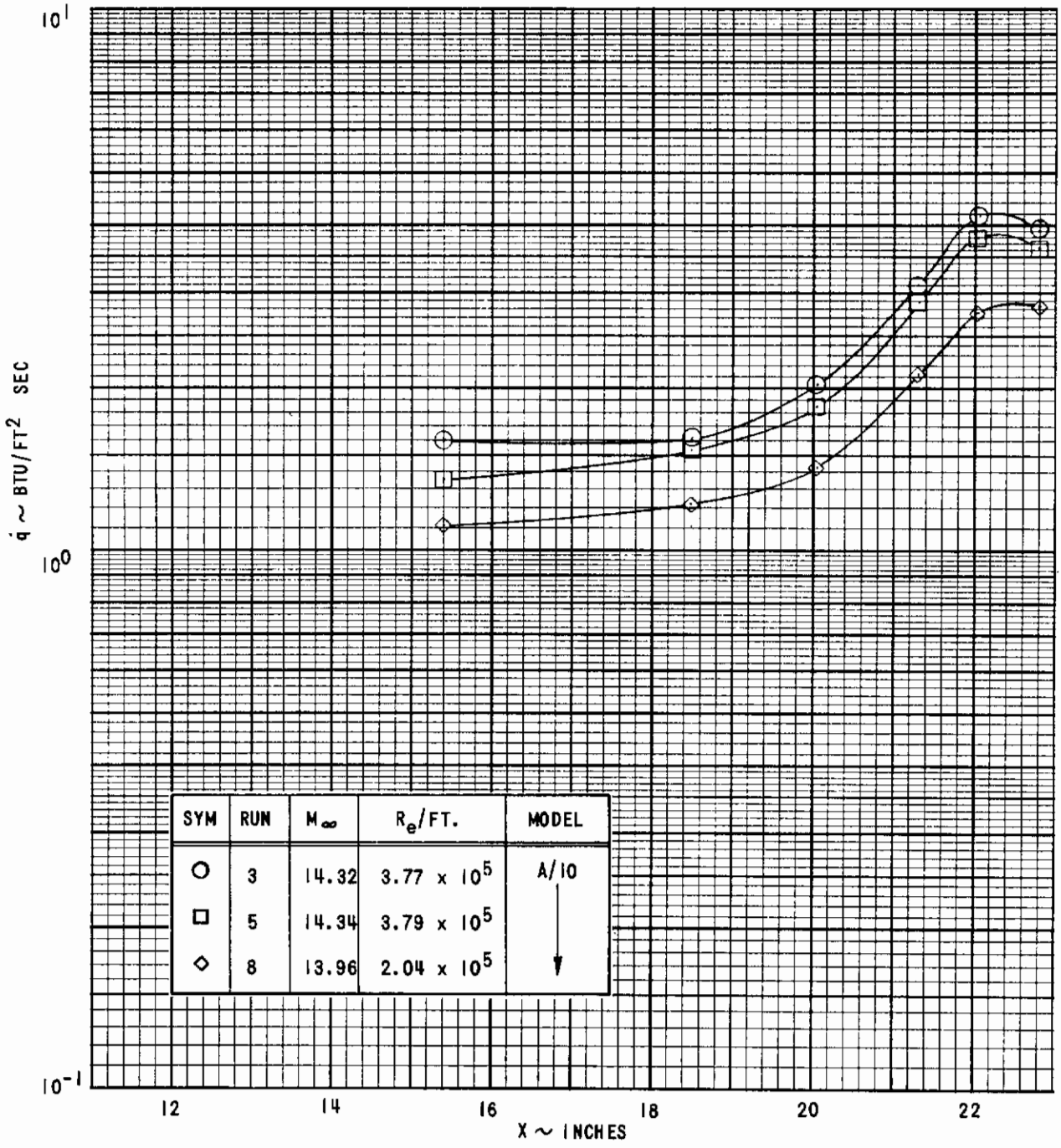


Figure 23 (Cont'd.) (b) MODEL A/10, MACH NUMBER 14

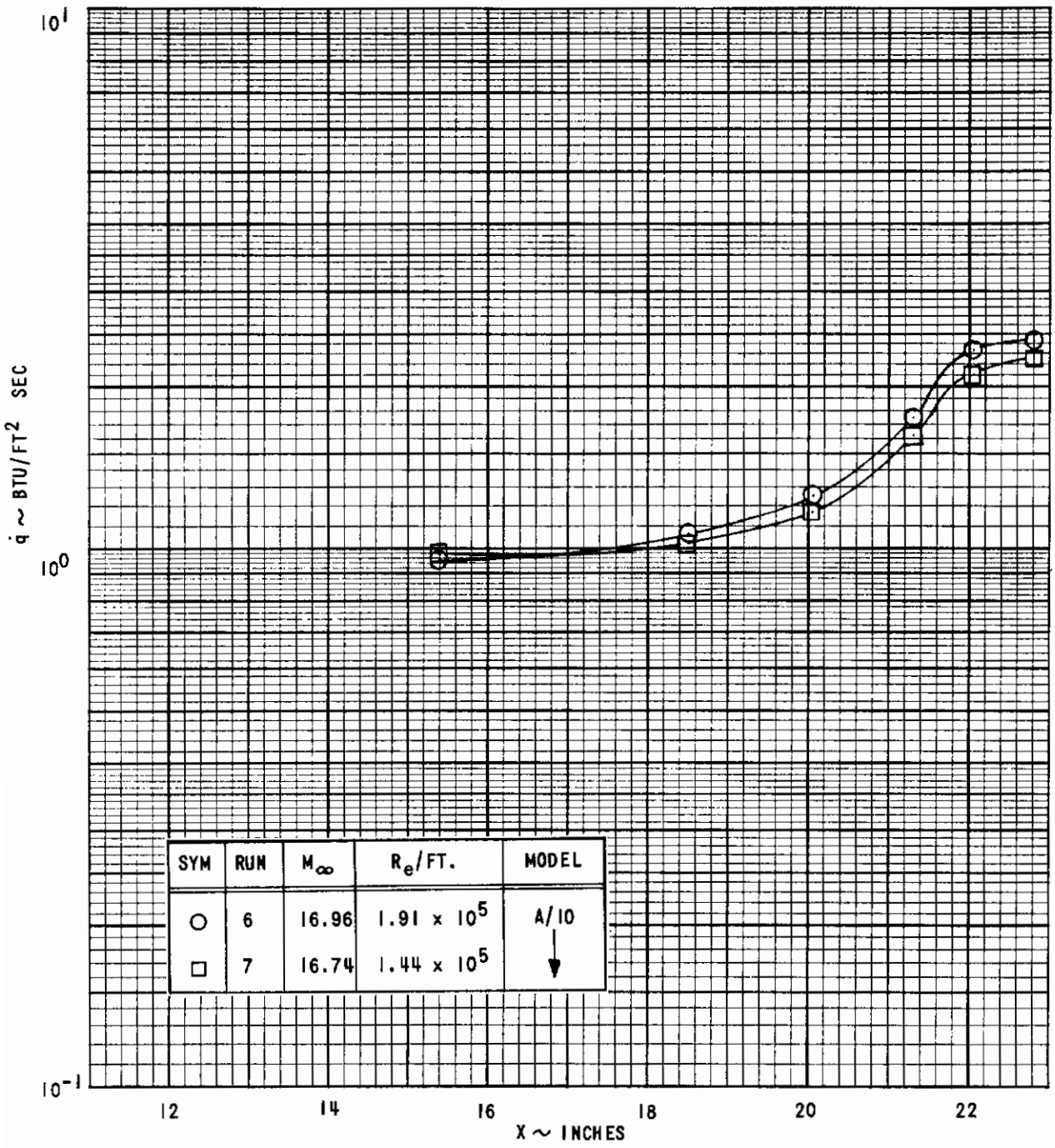


Figure 23 (Cont'd.) (c) MODEL A/10, MACH NUMBER 16

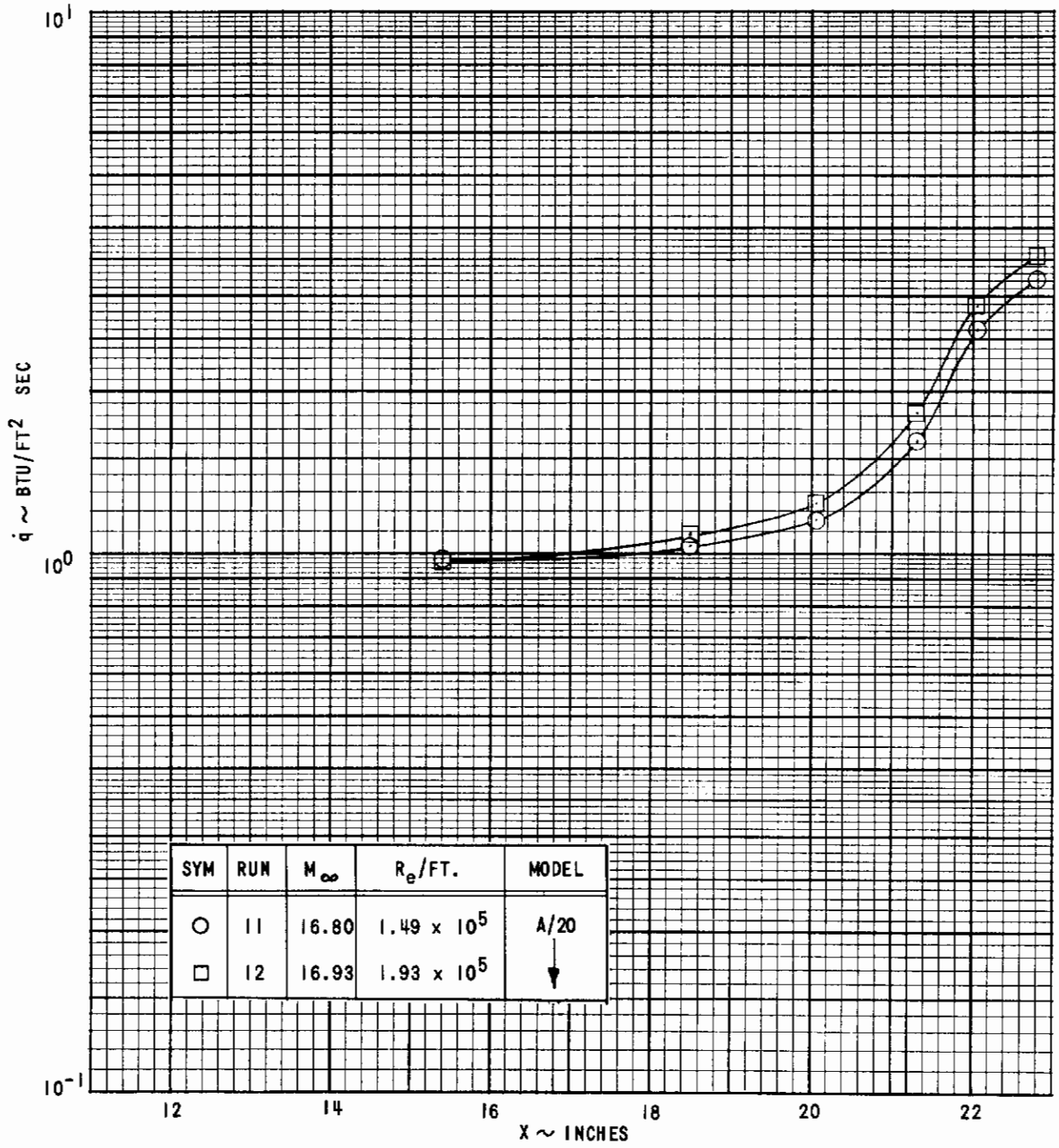


Figure 23 (Cont'd.) (d) MODEL A/20, MACH NUMBER 16

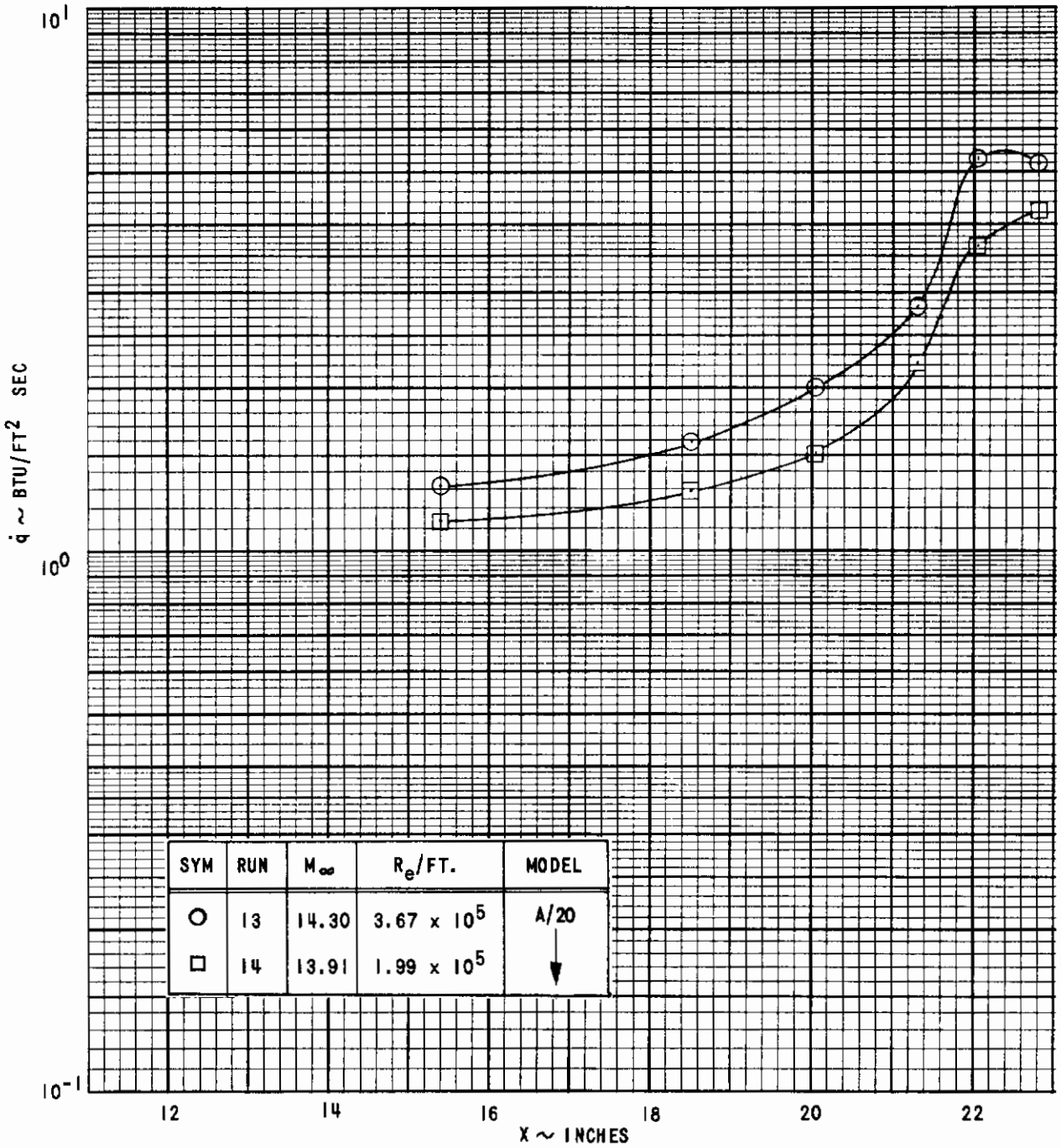


Figure 23 (Cont'd.) (e) MODEL A/20, MACH NUMBER 14

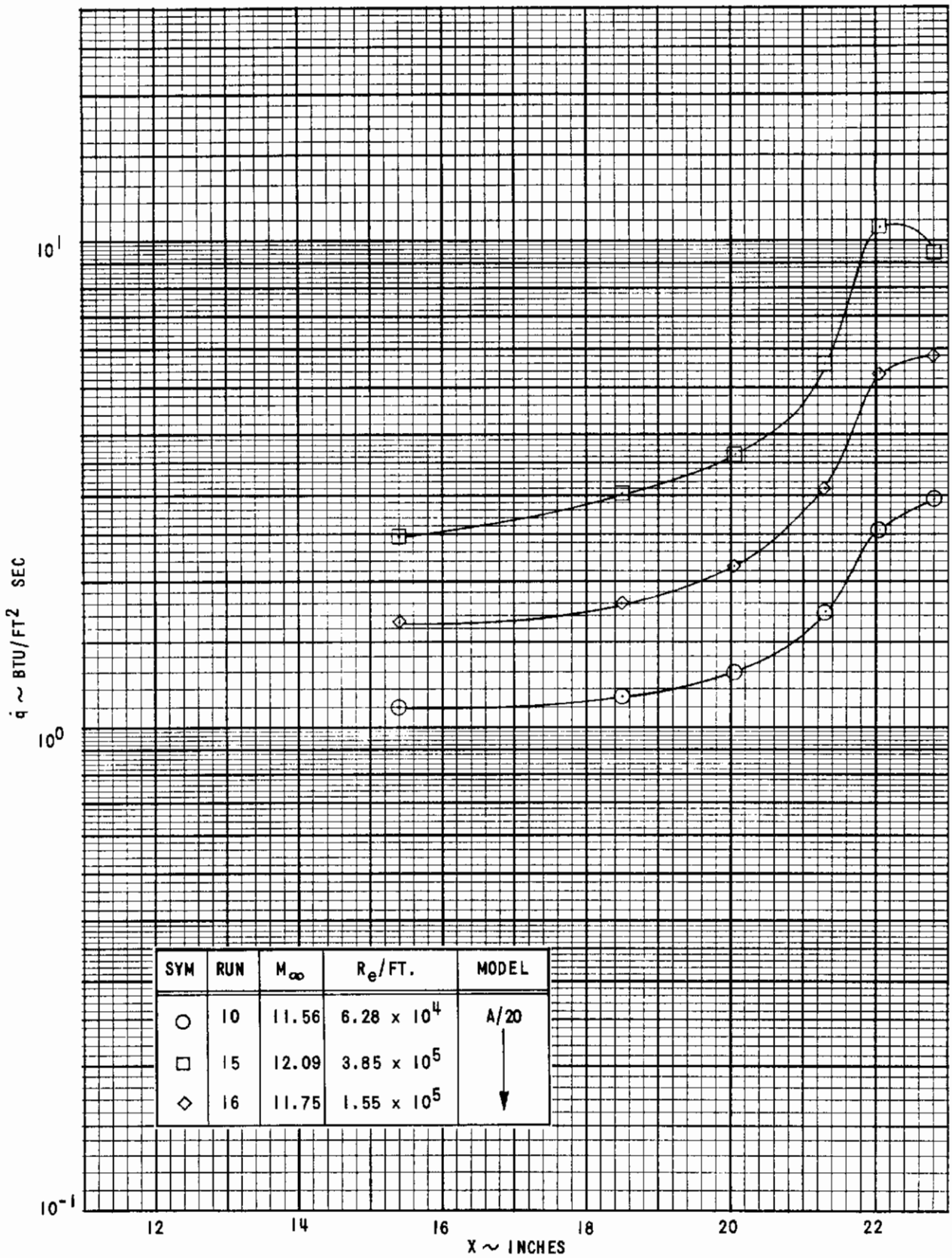


Figure 23 (Cont'd.) (f) MODEL A/20, MACH NUMBER 12

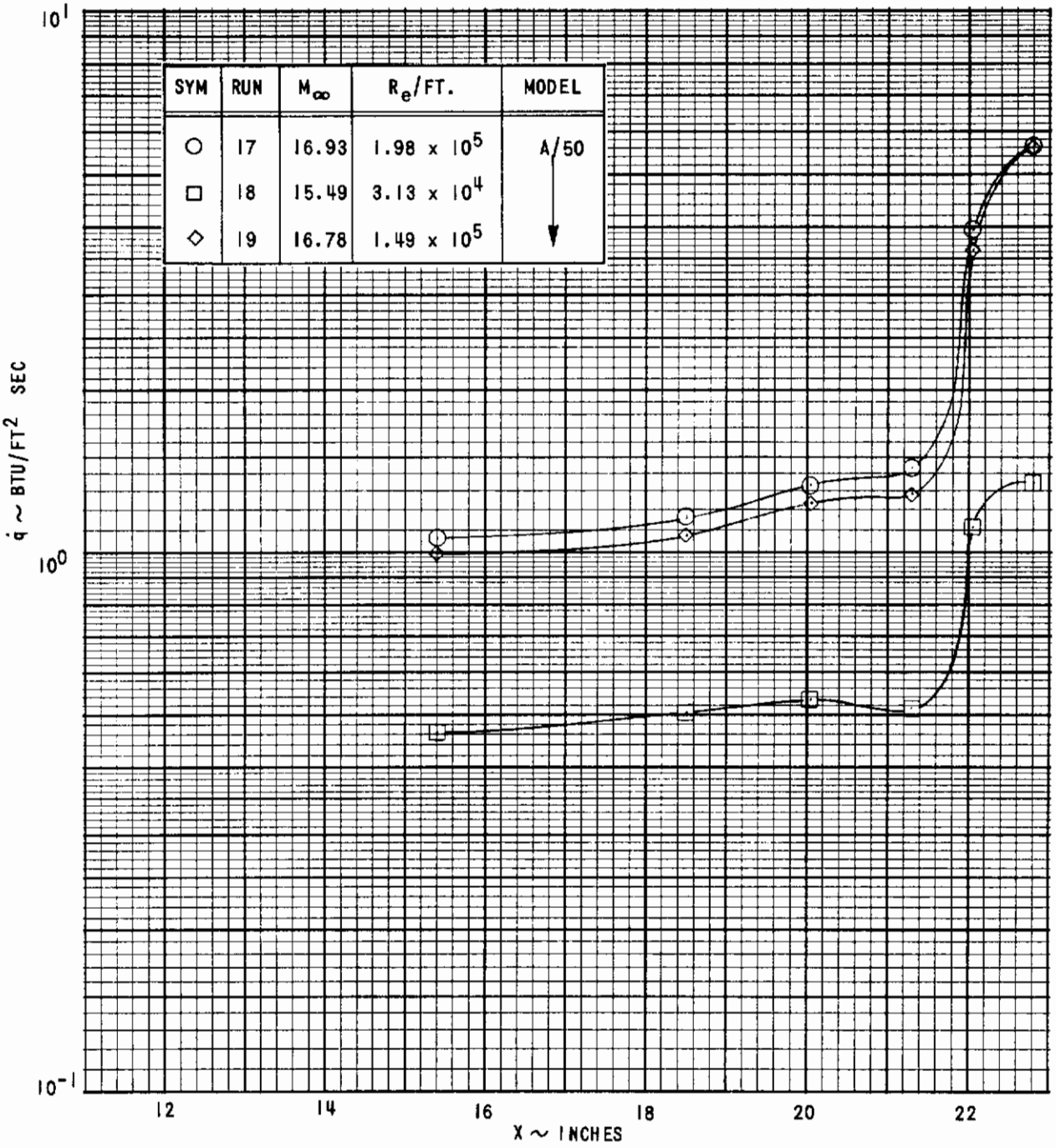


Figure 23 (Cont'd.) (g) MODEL A/50, MACH NUMBER 16

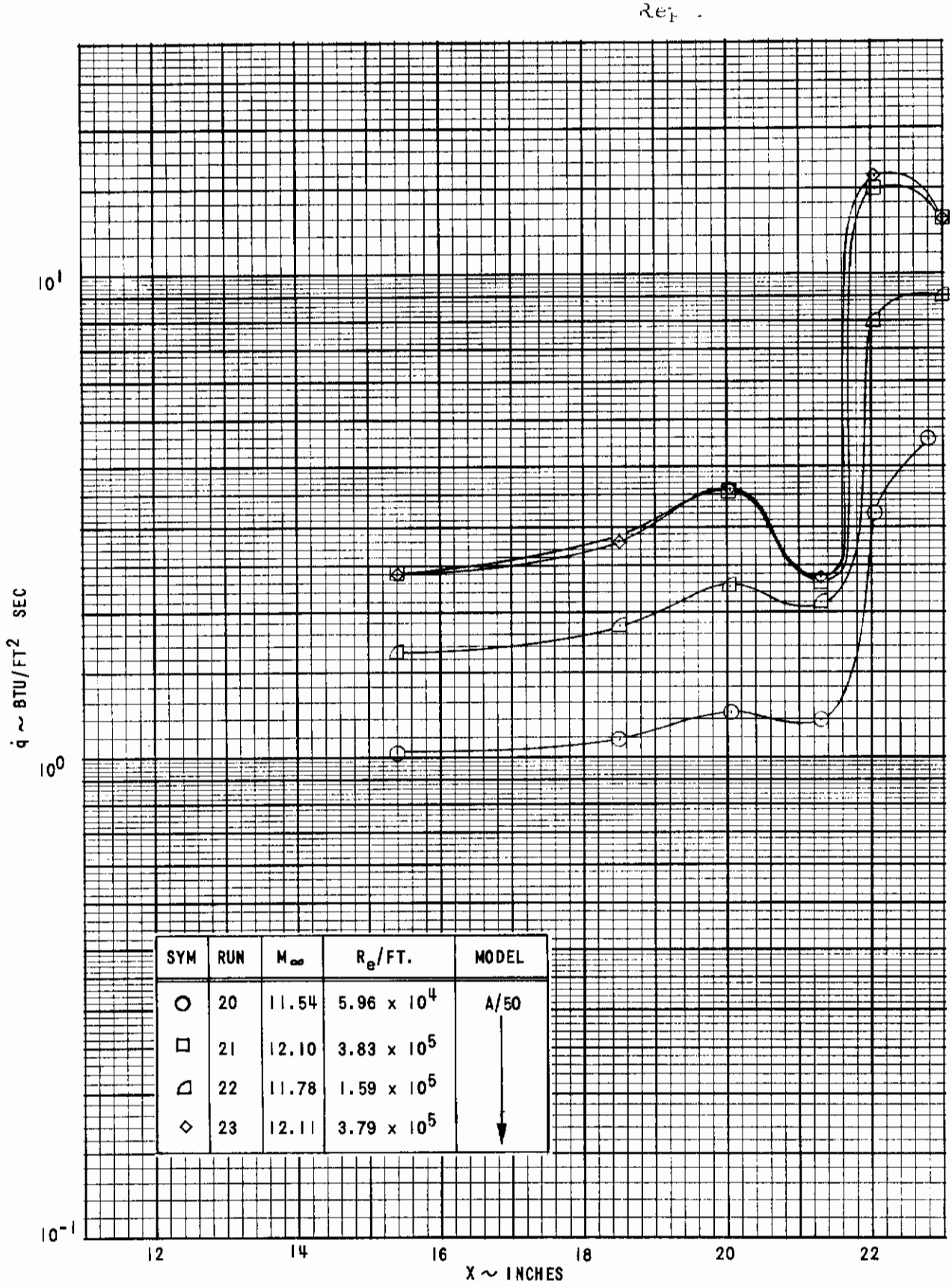


Figure 23 (Cont'd.) (h) MODEL A/50, MACH NUMBER 12

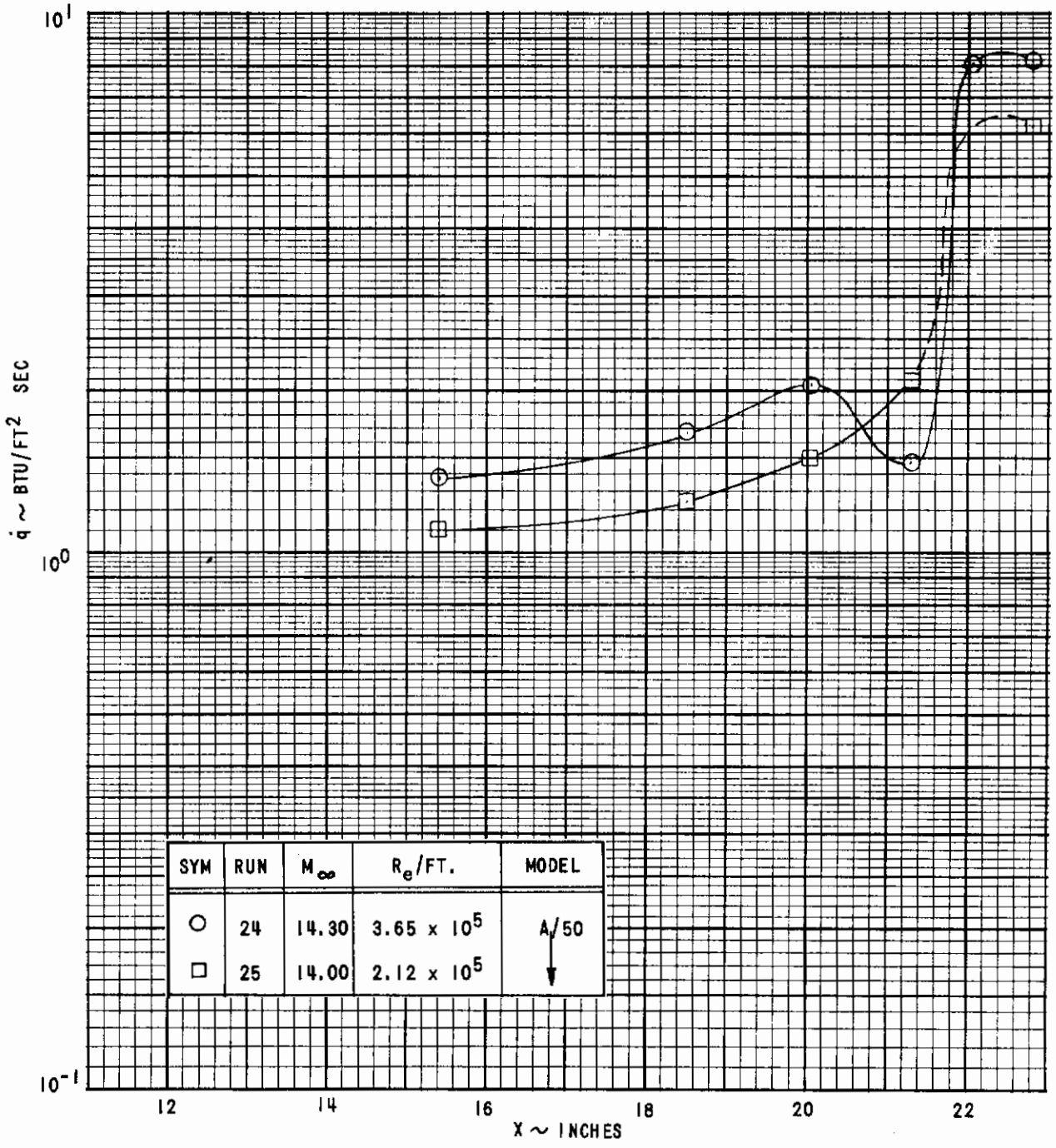


Figure 23 (Cont'd.) (i) MODEL A/50, MACH NUMBER 14

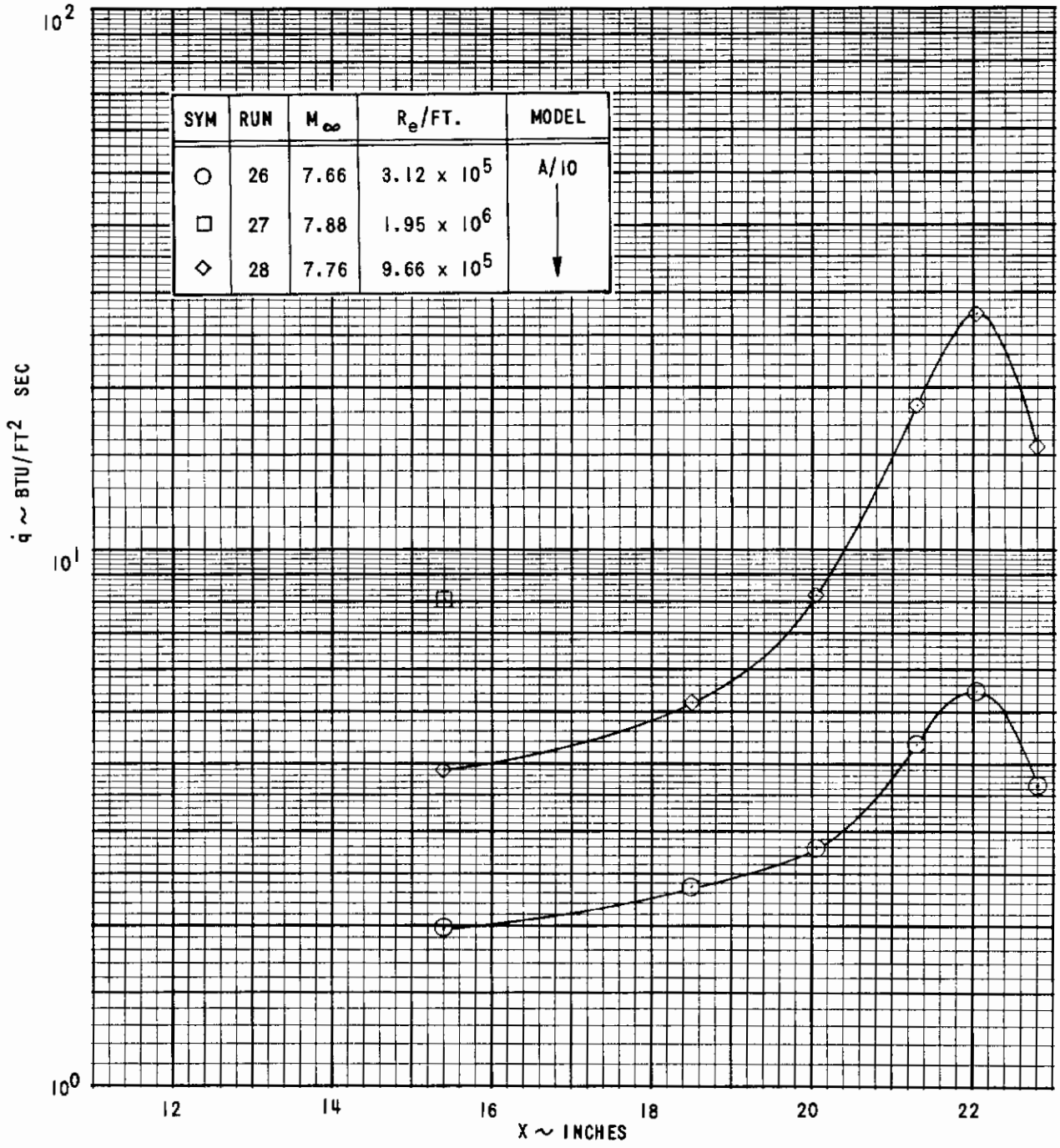


Figure 23 (Cont'd.) (j) MODEL A/10, MACH NUMBER 7.5

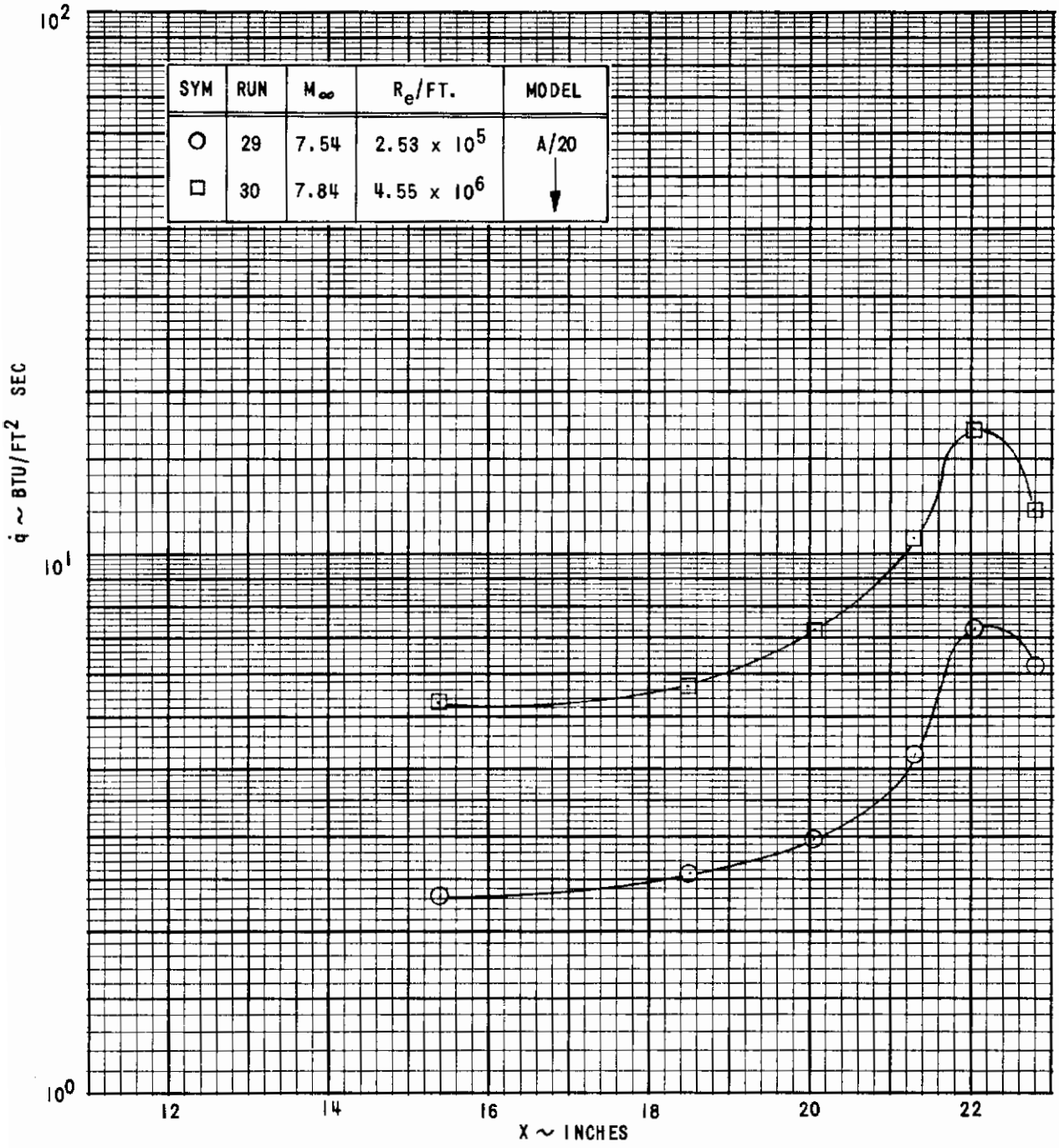


Figure 23 (Cont'd.) (k) MODEL A/20, MACH NUMBER 7.5

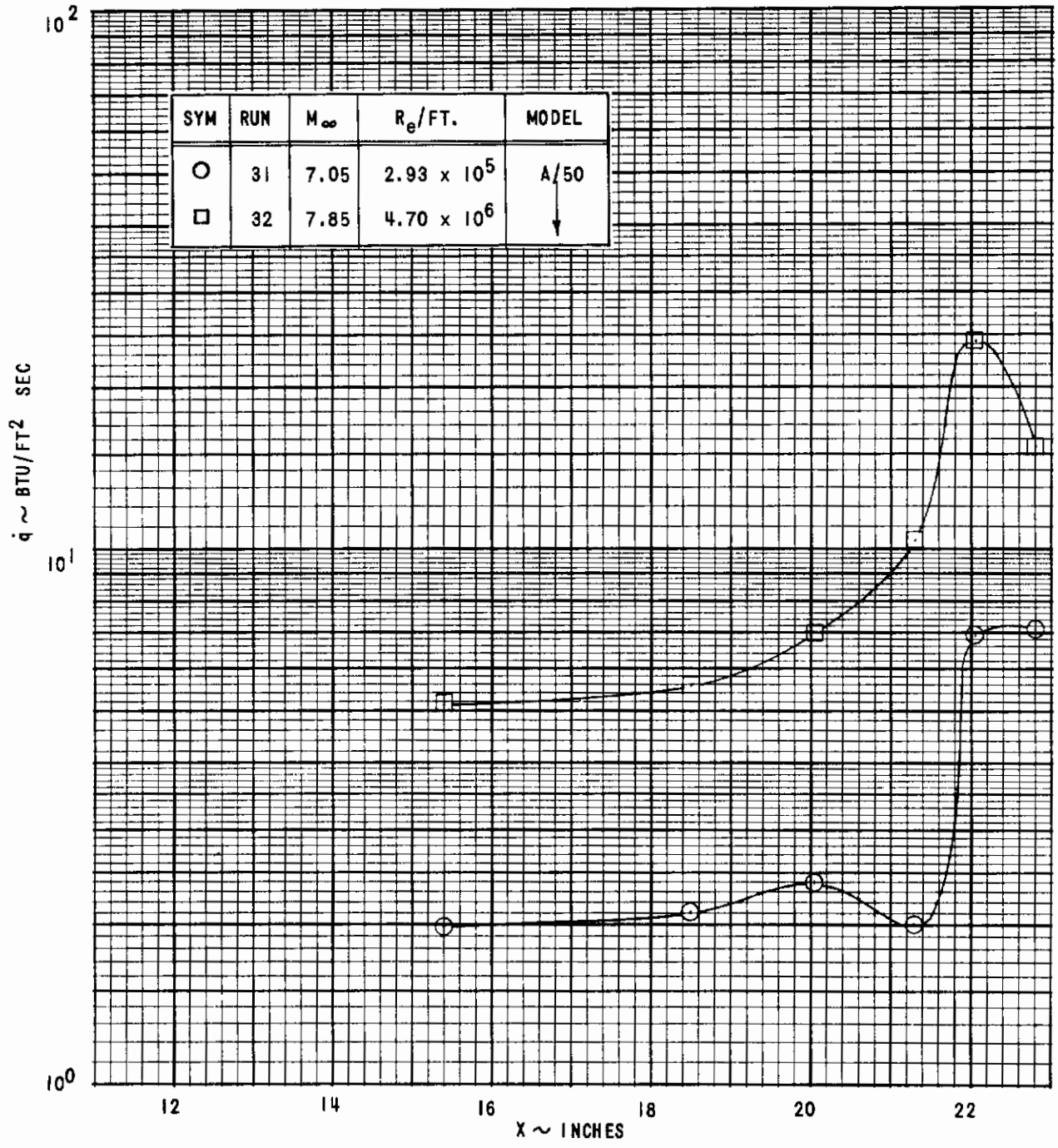


Figure 23 (Concluded) (1) MODEL A/50, MACH NUMBER 7.5

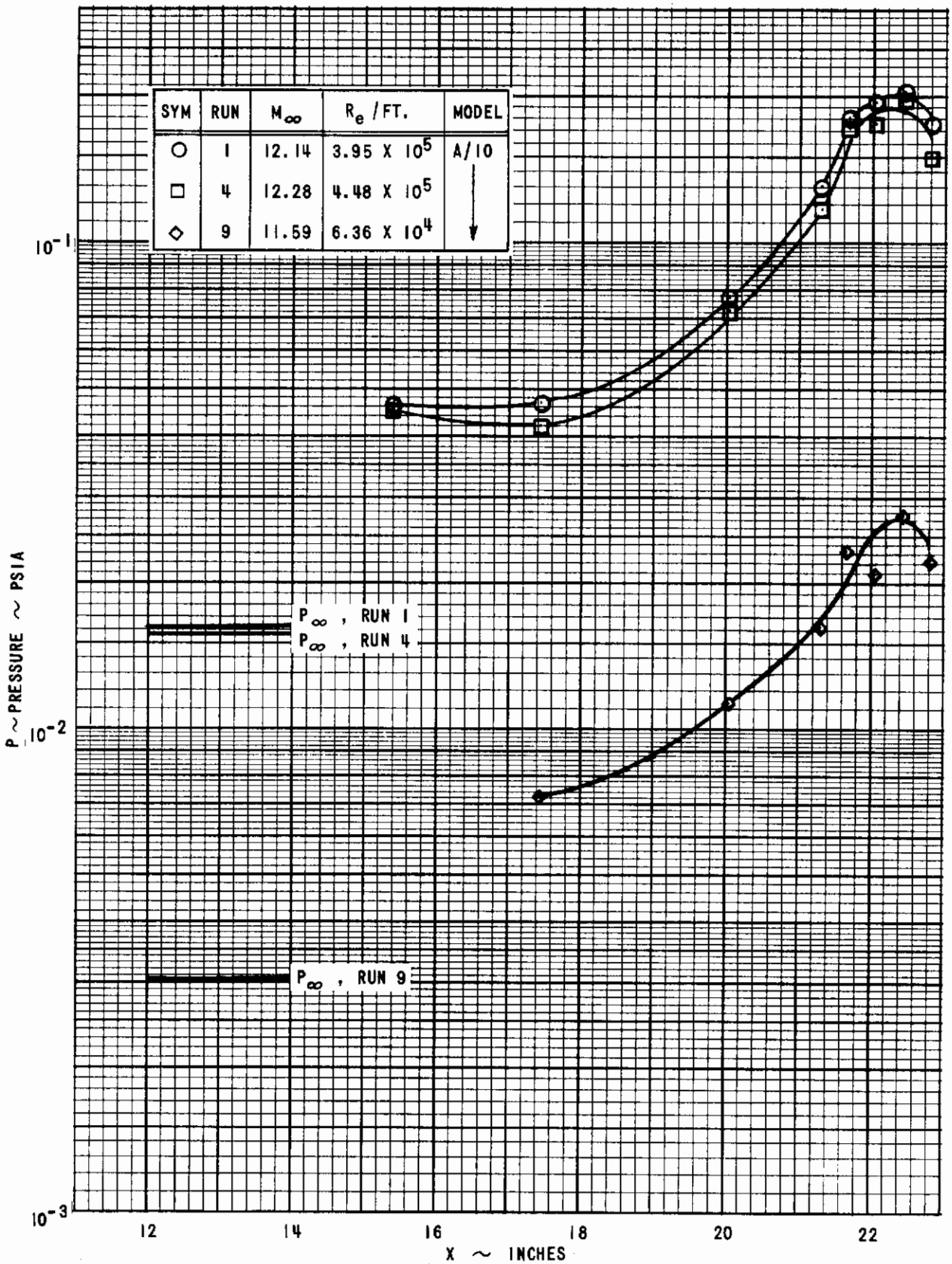


Figure 24 PRESSURE DISTRIBUTIONS ON THE AXISYMMETRIC MODEL
(a) MODEL A/10, MACH NUMBER 12

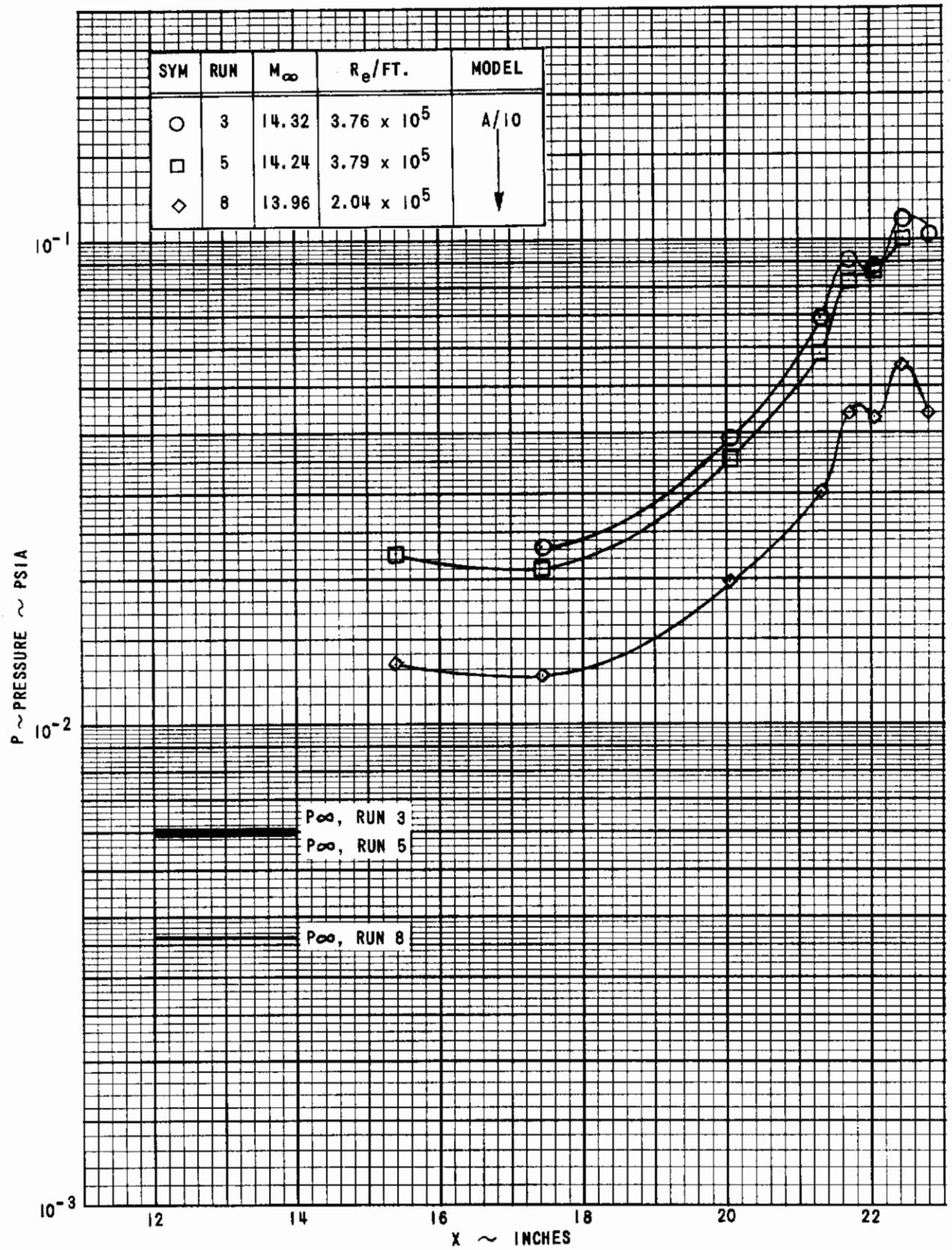


Figure 24 (Cont'd.) (b) MODEL A/10, MACH NUMBER 14

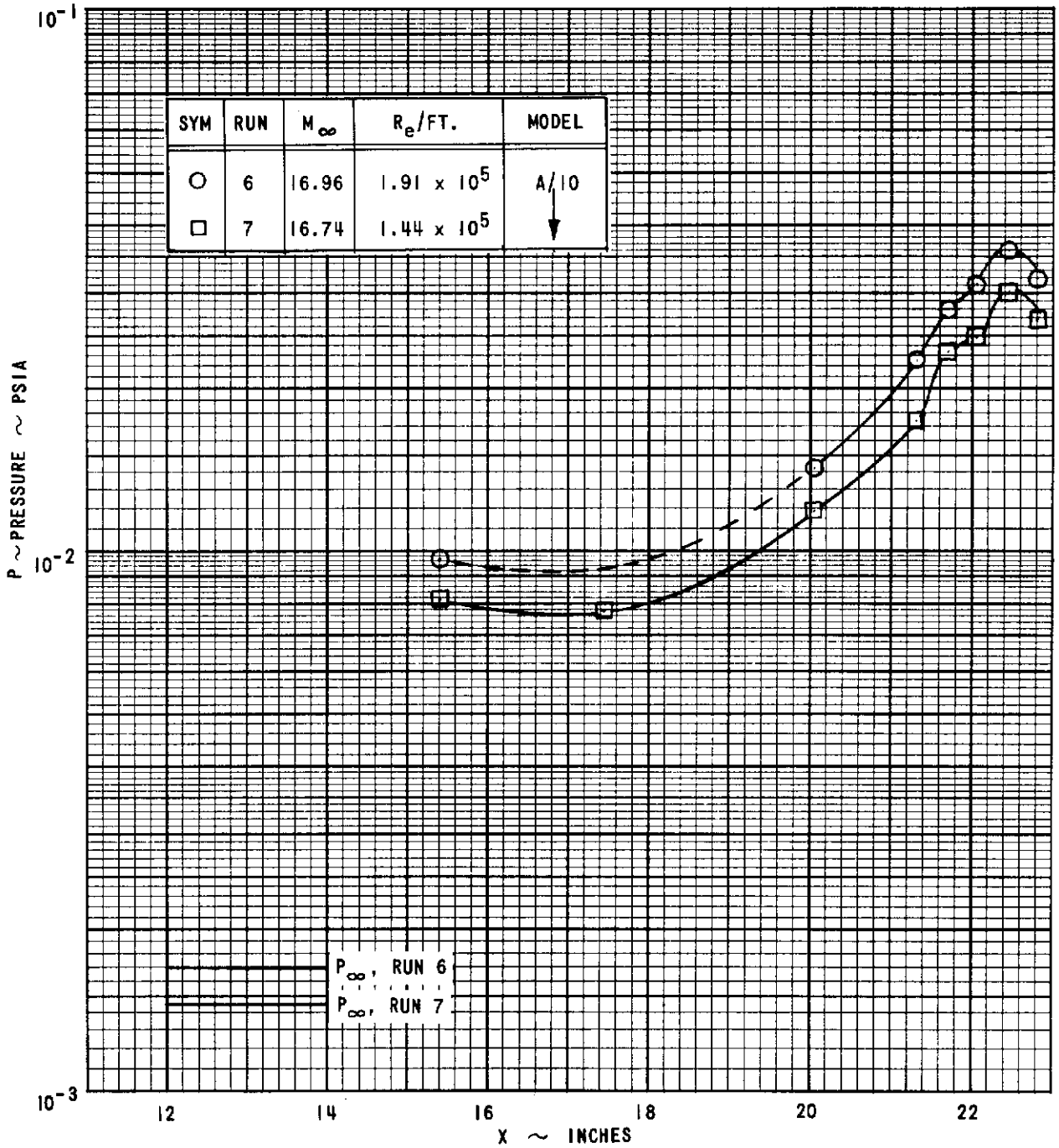


Figure 24 (Cont'd.) (c) MODEL A/10, MACH NUMBER 16

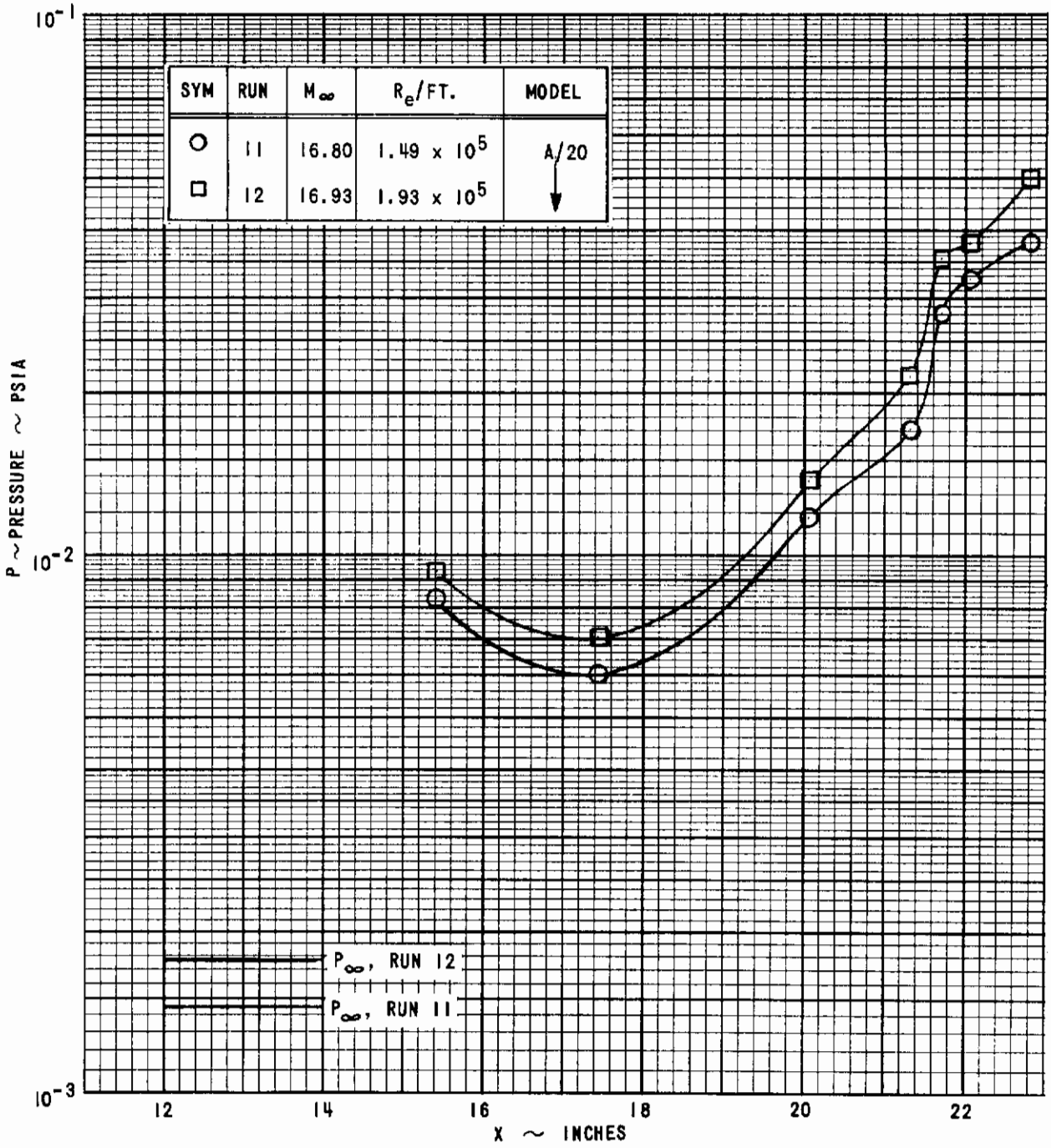


Figure 24 (Cont'd.) (d) MODEL A/20, MACH NUMBER 16

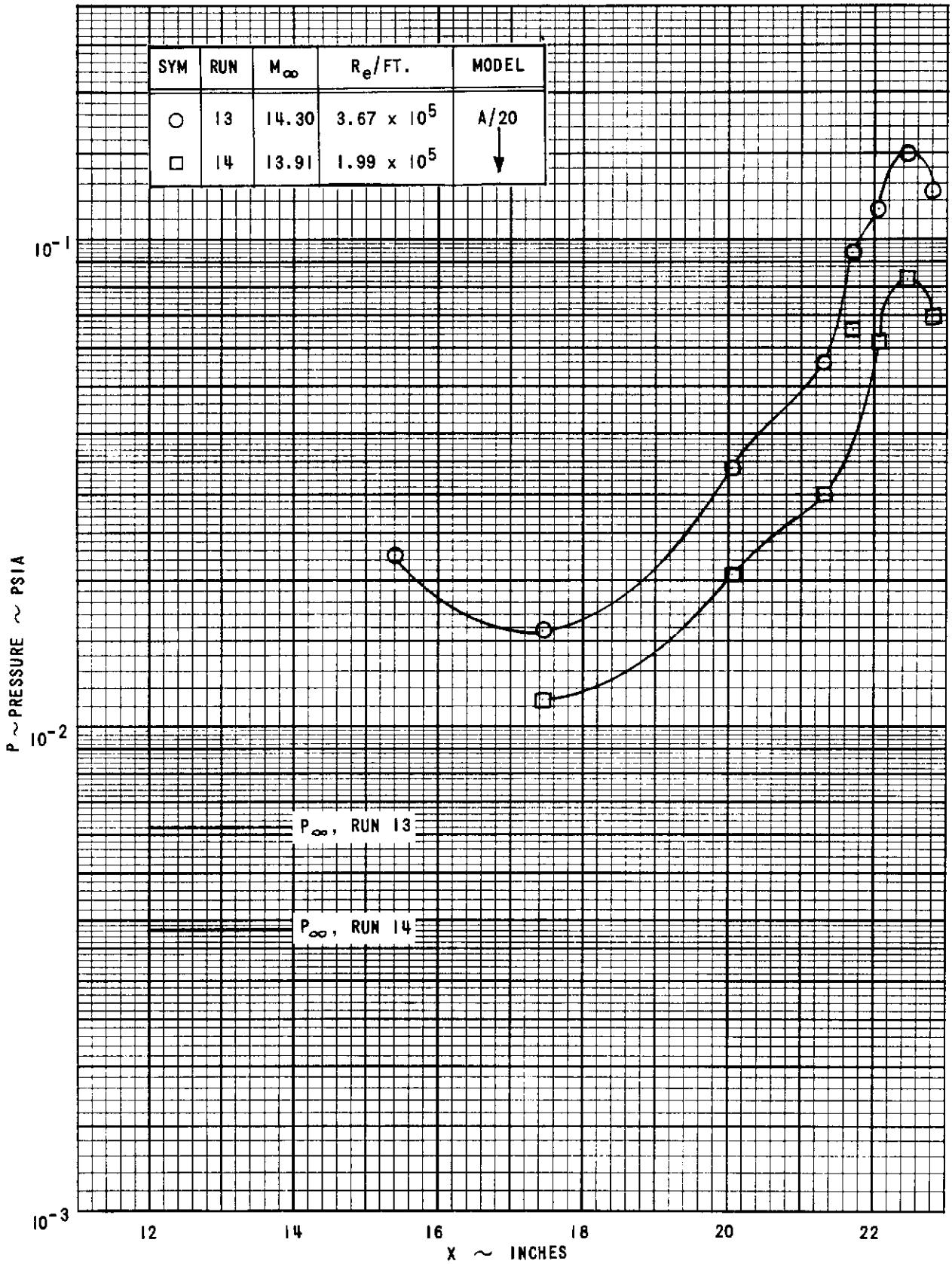


Figure 24 (Cont'd.) (e) MODEL A/20, MACH NUMBER 14

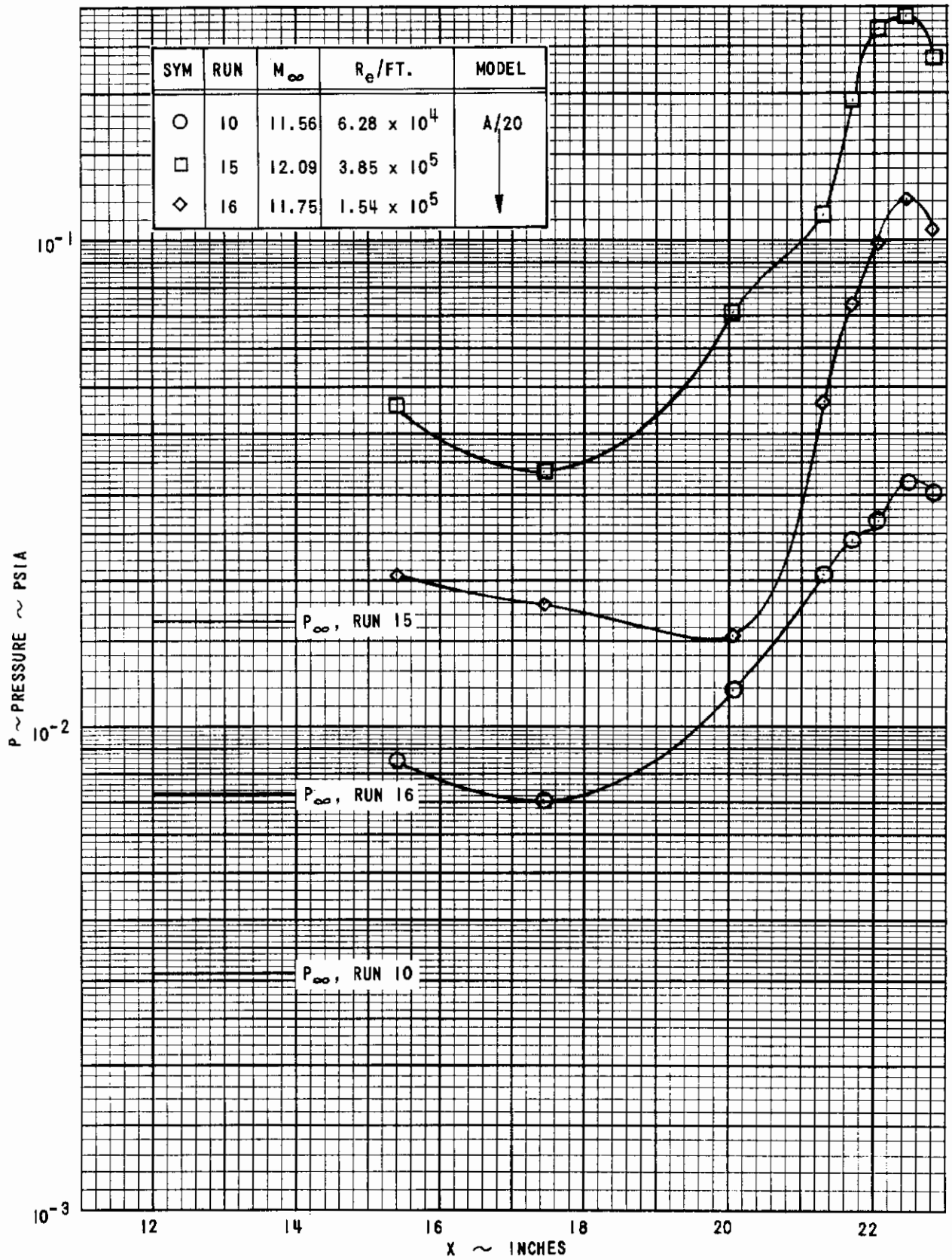


Figure 24 (Cont'd.) (f) MODEL A/20, MACH NUMBER 12

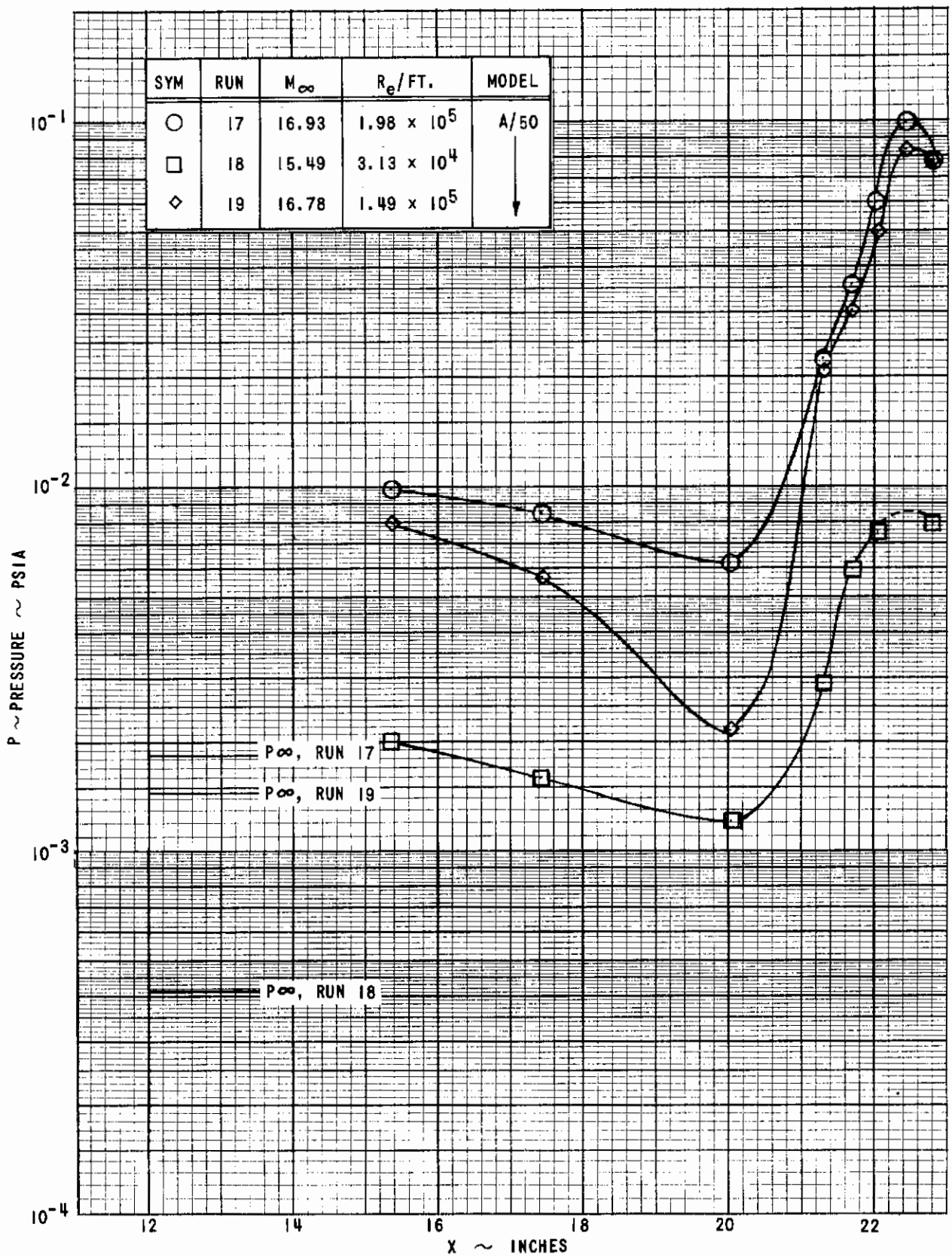


Figure 24 (Cont'd.) (g) MODEL A/50, MACH NUMBER 16

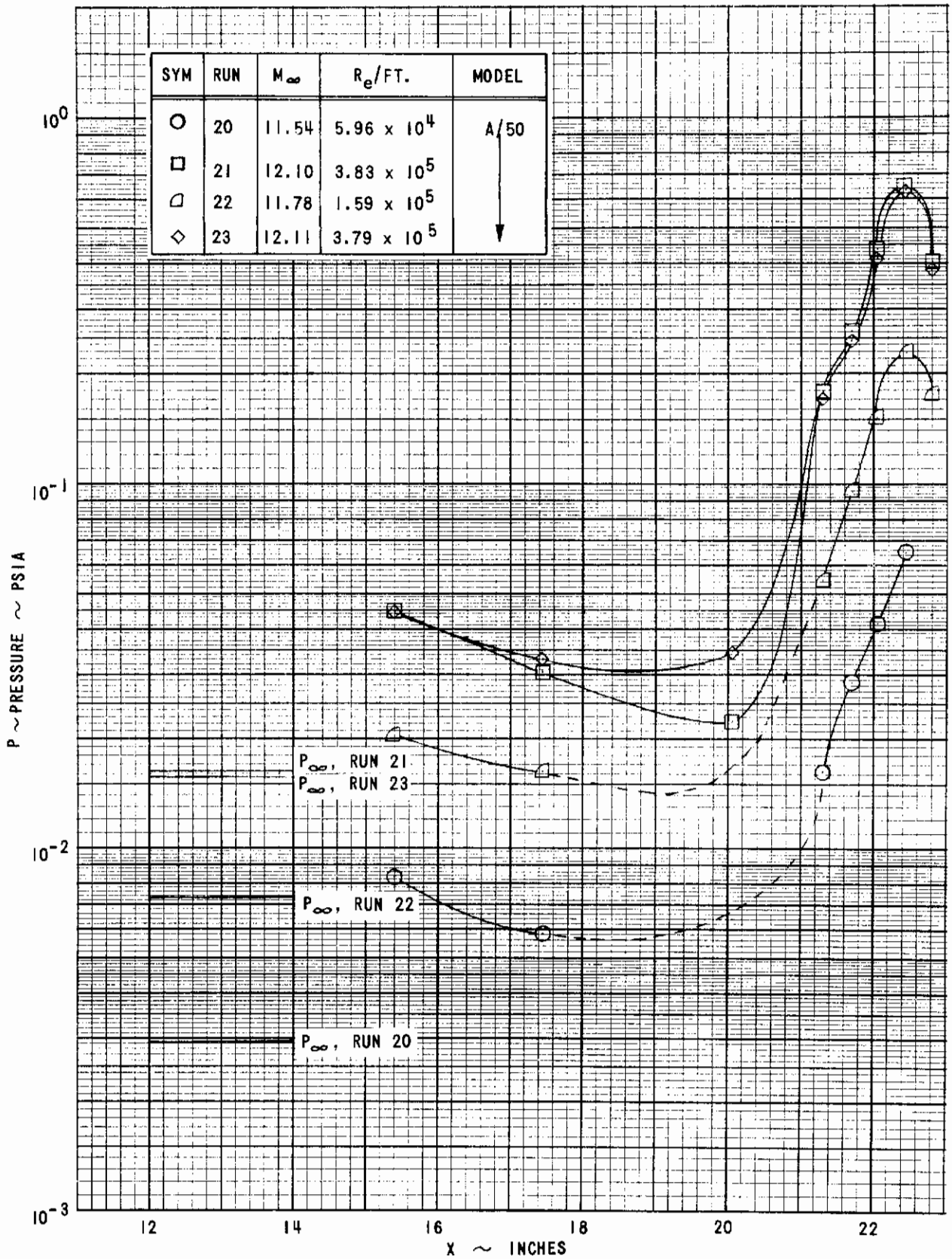


Figure 24 (Cont'd.) (h) MODEL A/50, MACH NUMBER 12

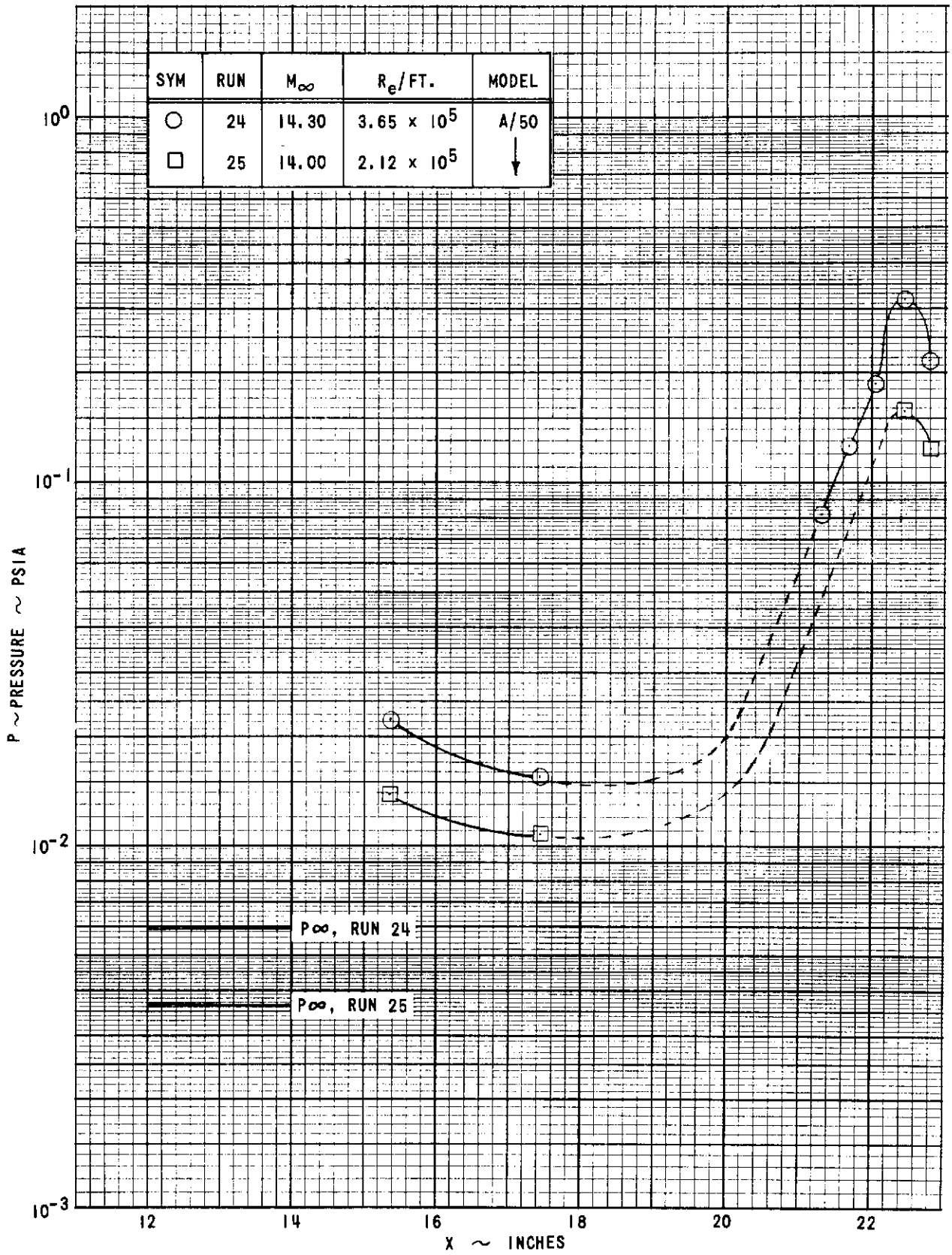


Figure 24 (Cont'd.) (i) MODEL A/50, MACH NUMBER 14

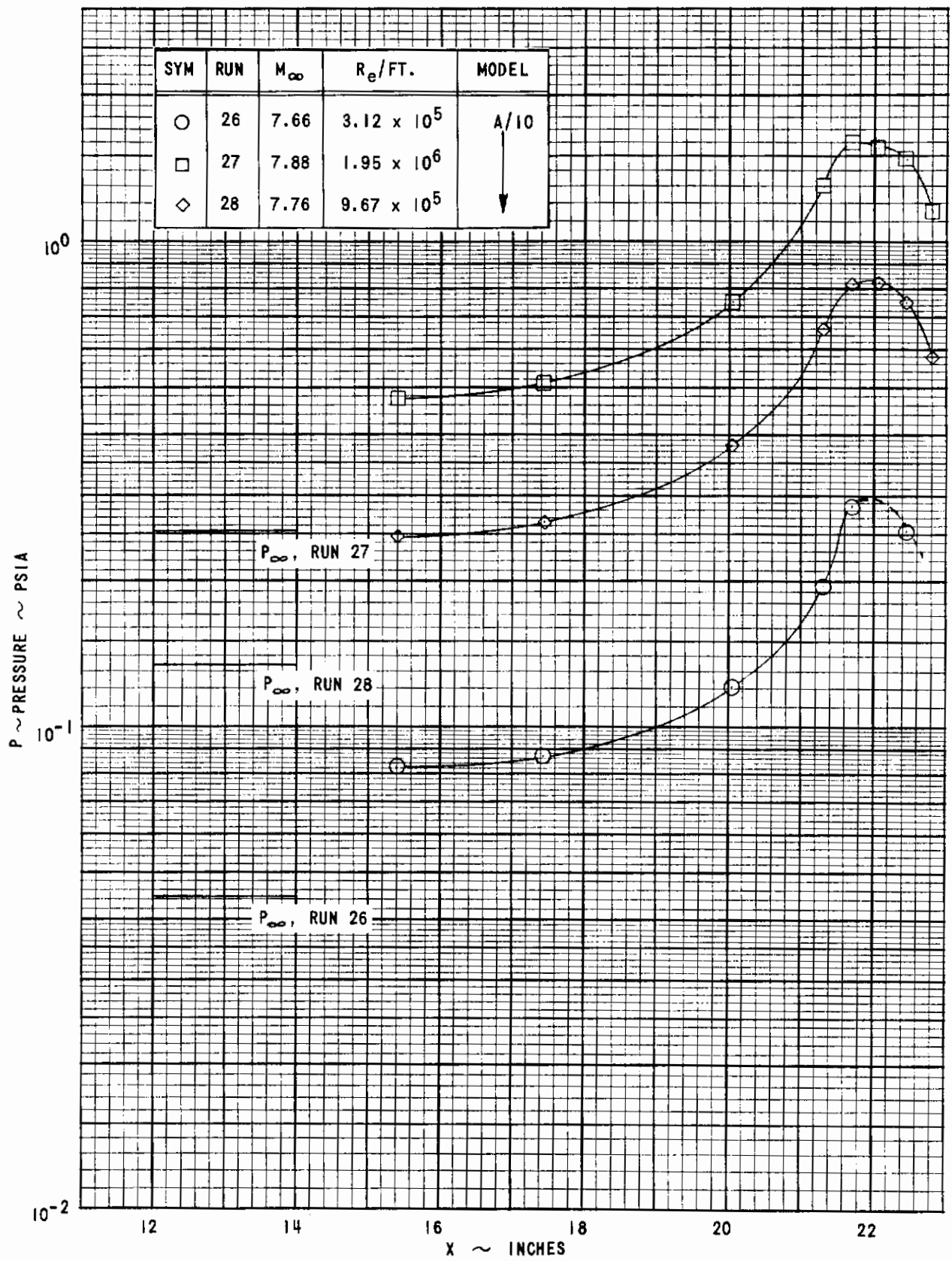


Figure 24 (Cont'd.) (j) MODEL A/10, MACH NUMBER 7.5

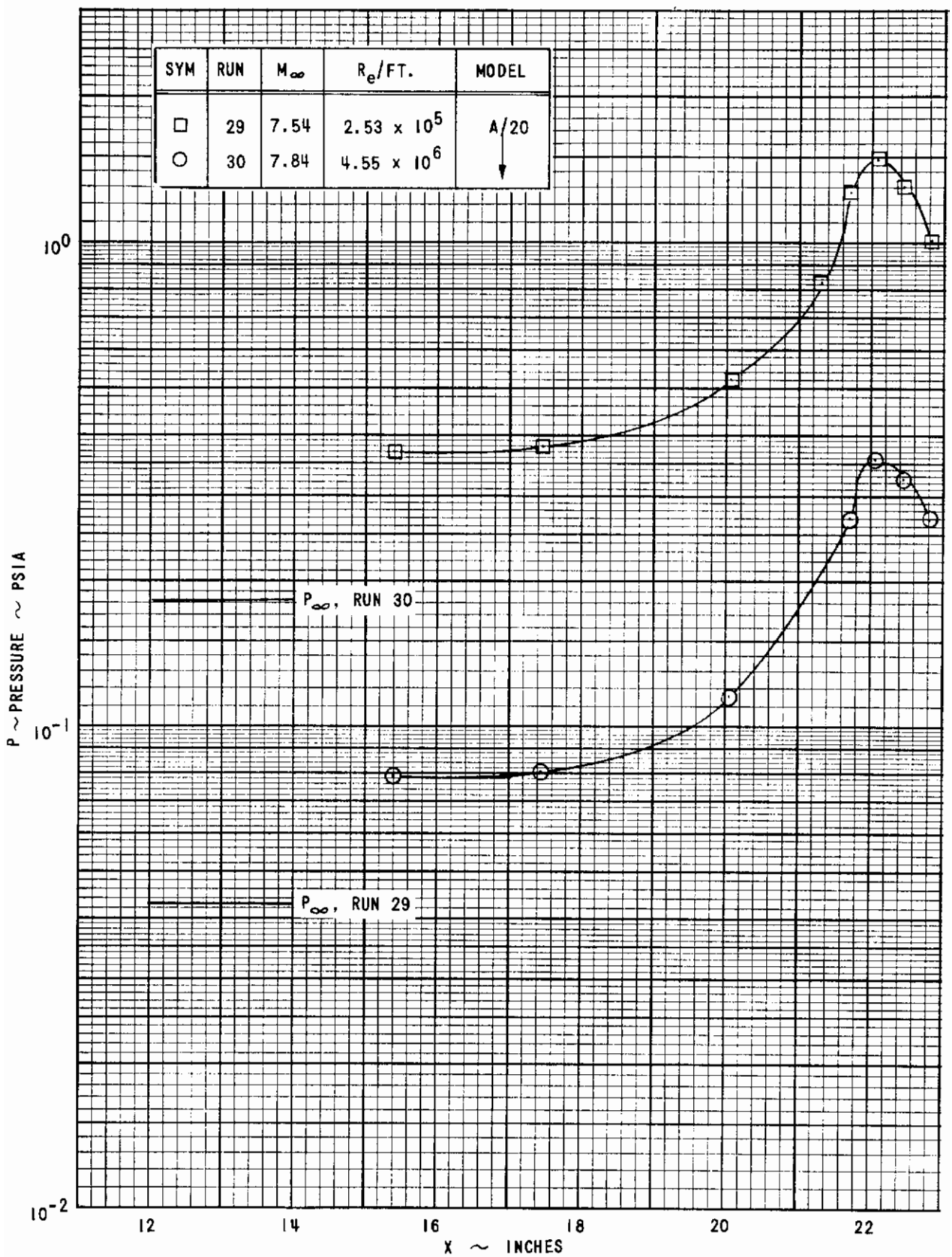


Figure 24 (Cont'd.) (k) MODEL A/20, MACH NUMBER 7.5

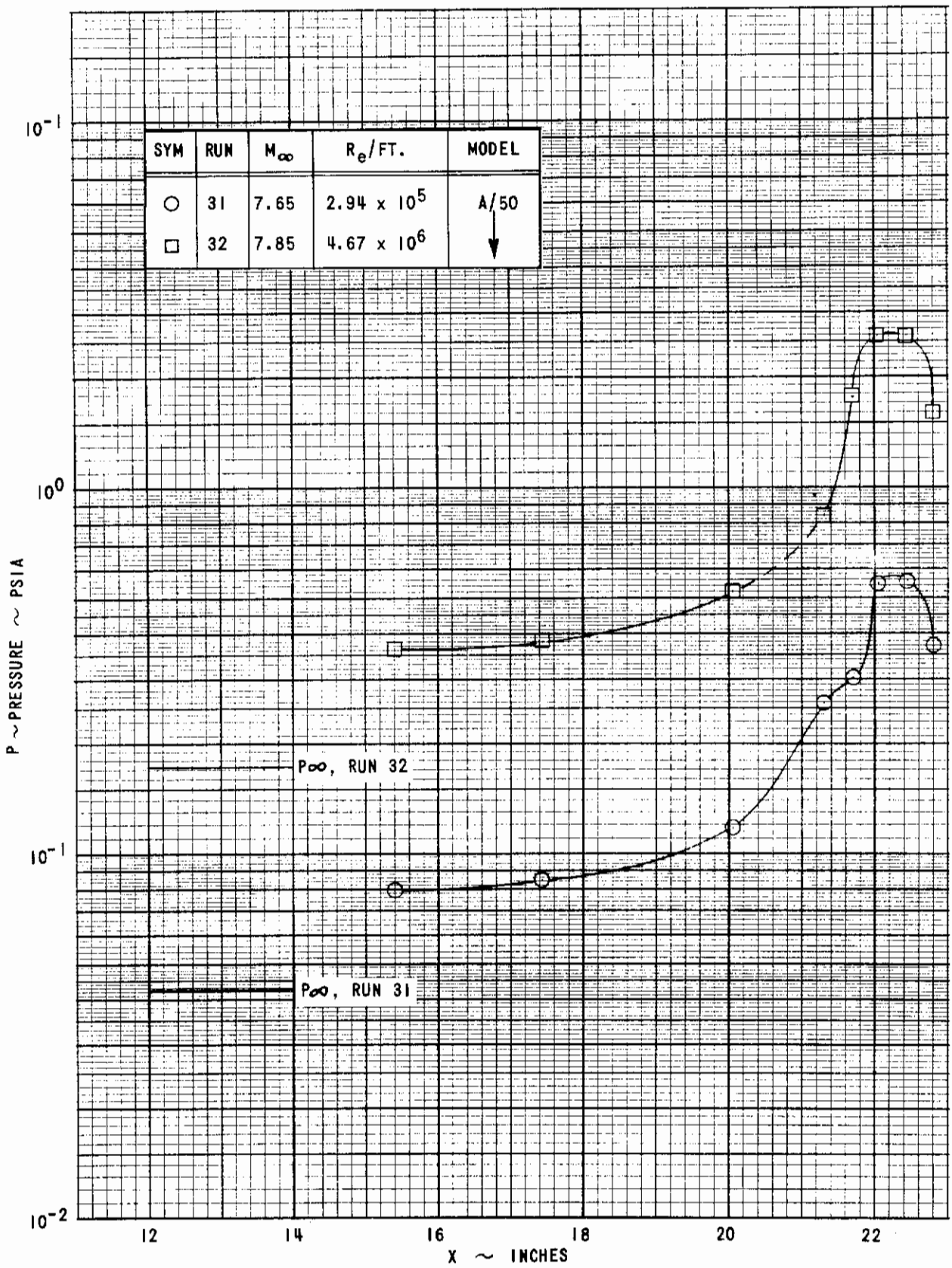


Figure 24 (Concluded) (1) MODEL A/50, MACH NUMBER 7.5

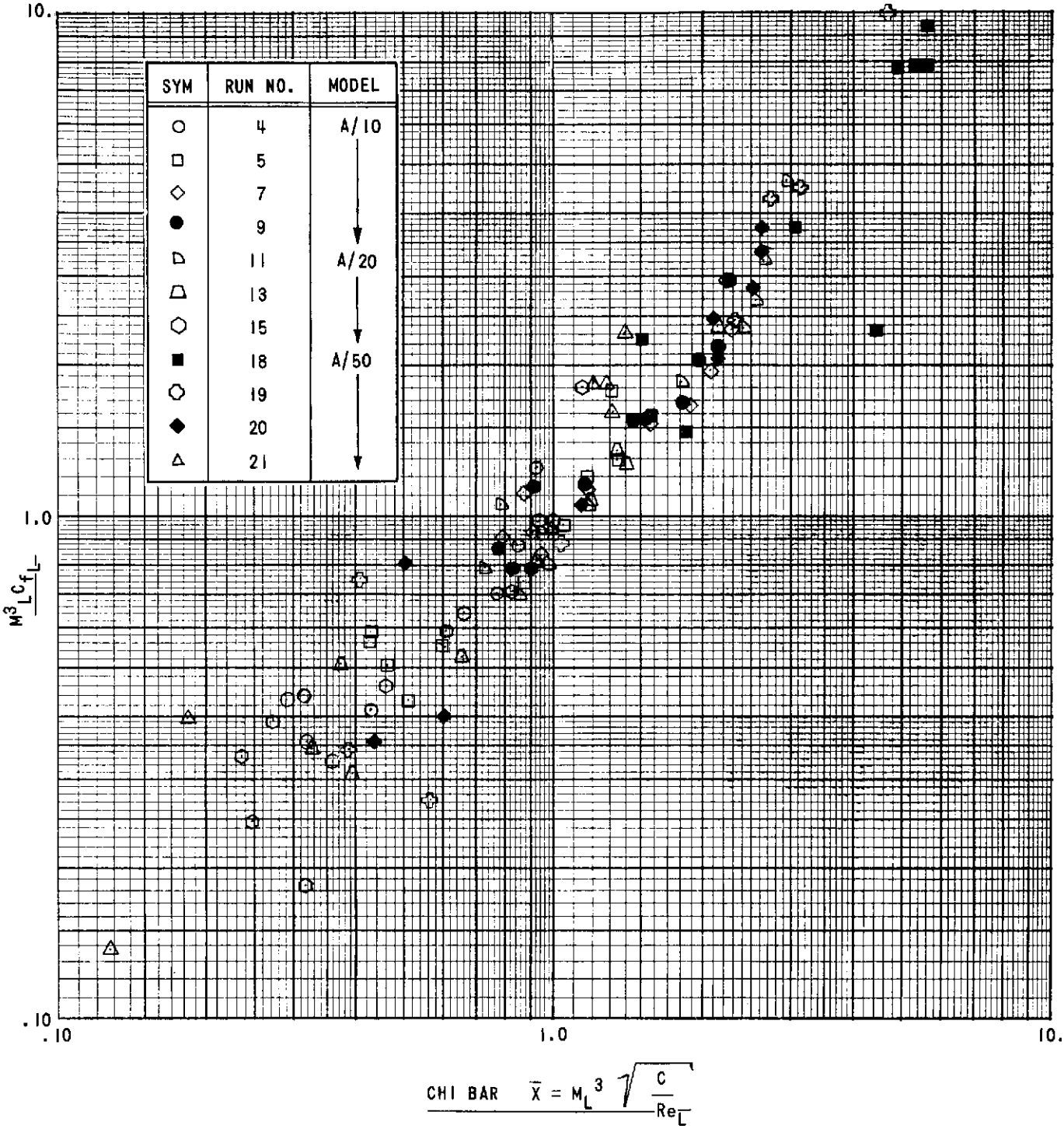


Figure 25 CORRELATED SKIN FRICTION DATA FROM THE AXISYMMETRIC MODEL TESTS

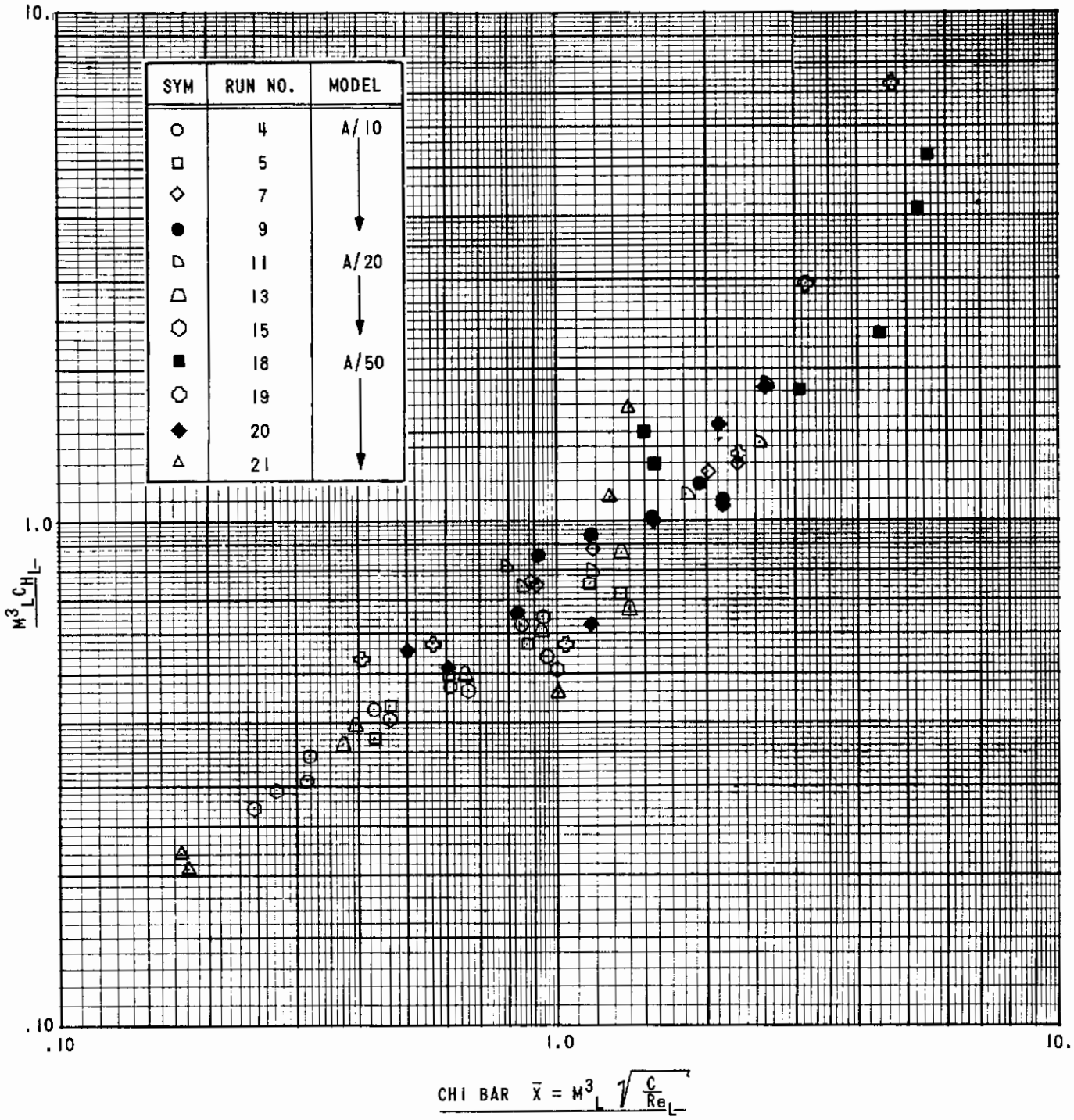


Figure 26 CORRELATED HEAT TRANSFER DATA FROM THE AXISYMMETRIC MODEL TESTS

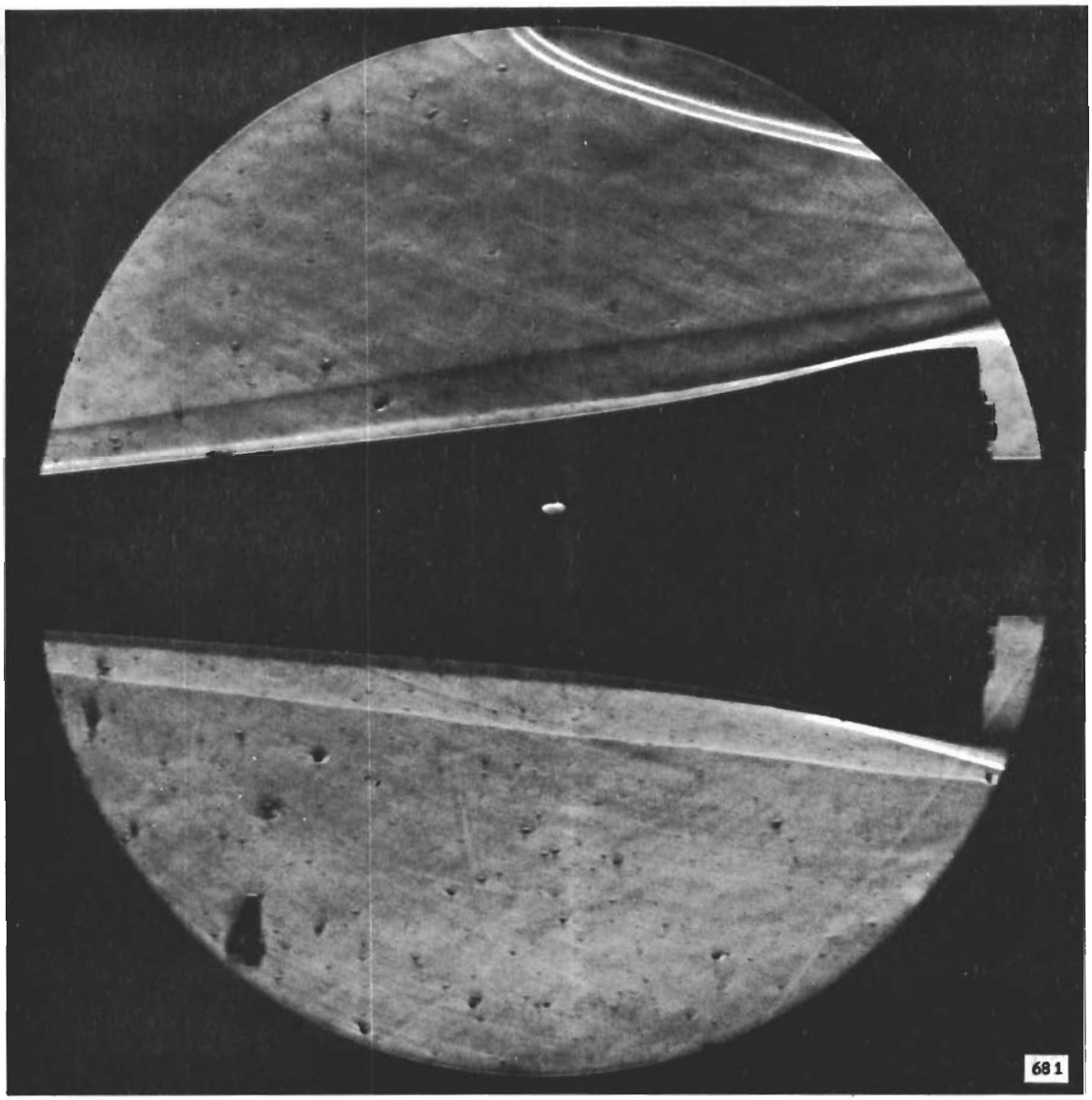


Figure 27 AXISYMMETRIC MODEL SCHLIEREN PHOTOGRAPHS
(a) MODEL A/10, RUN 4


Figure 27 (Cont'd.) (b) MODEL A/10, RUN 5

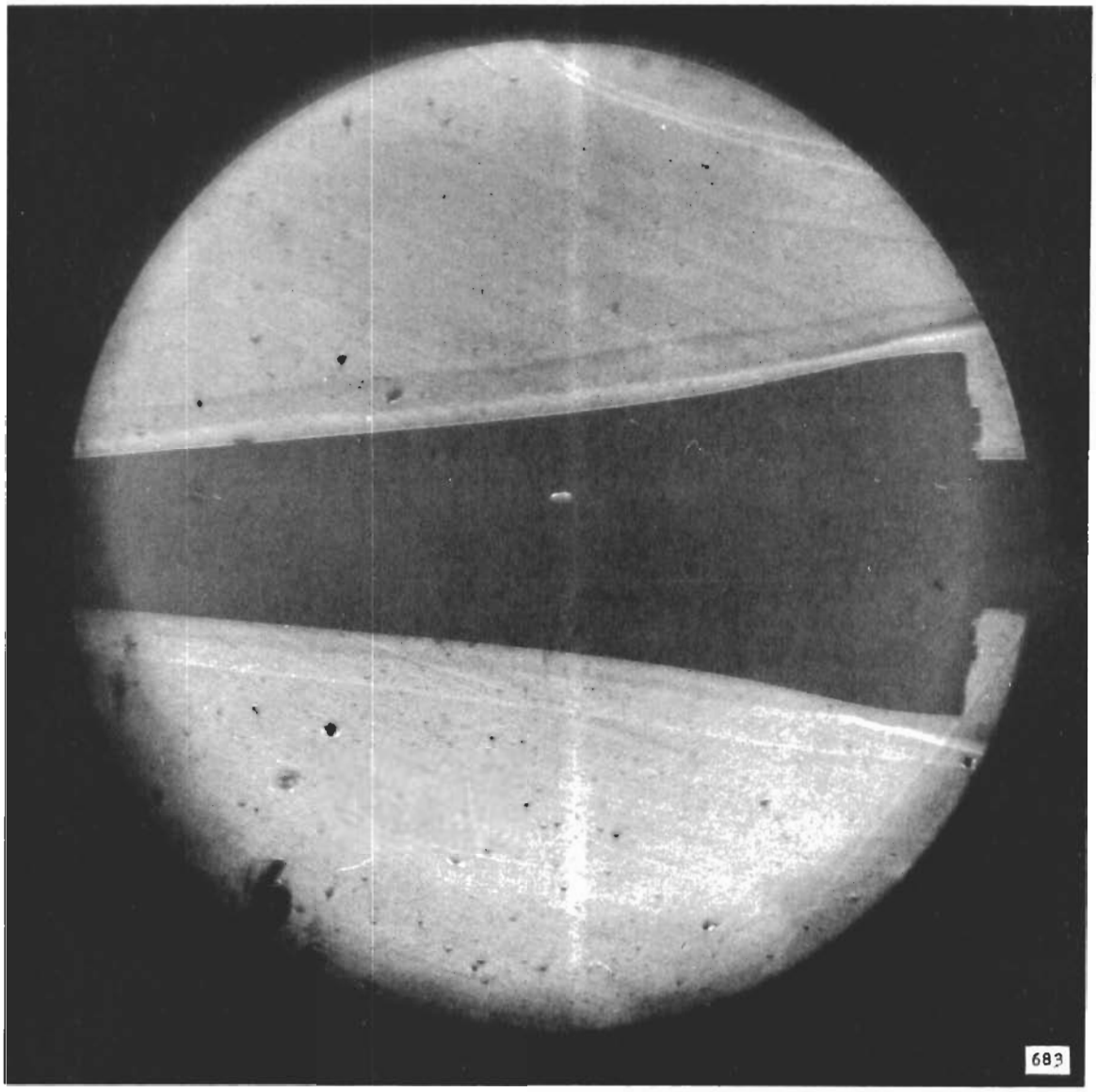


Figure 27 (Cont'd.) (c) MODEL A/10, RUN 6

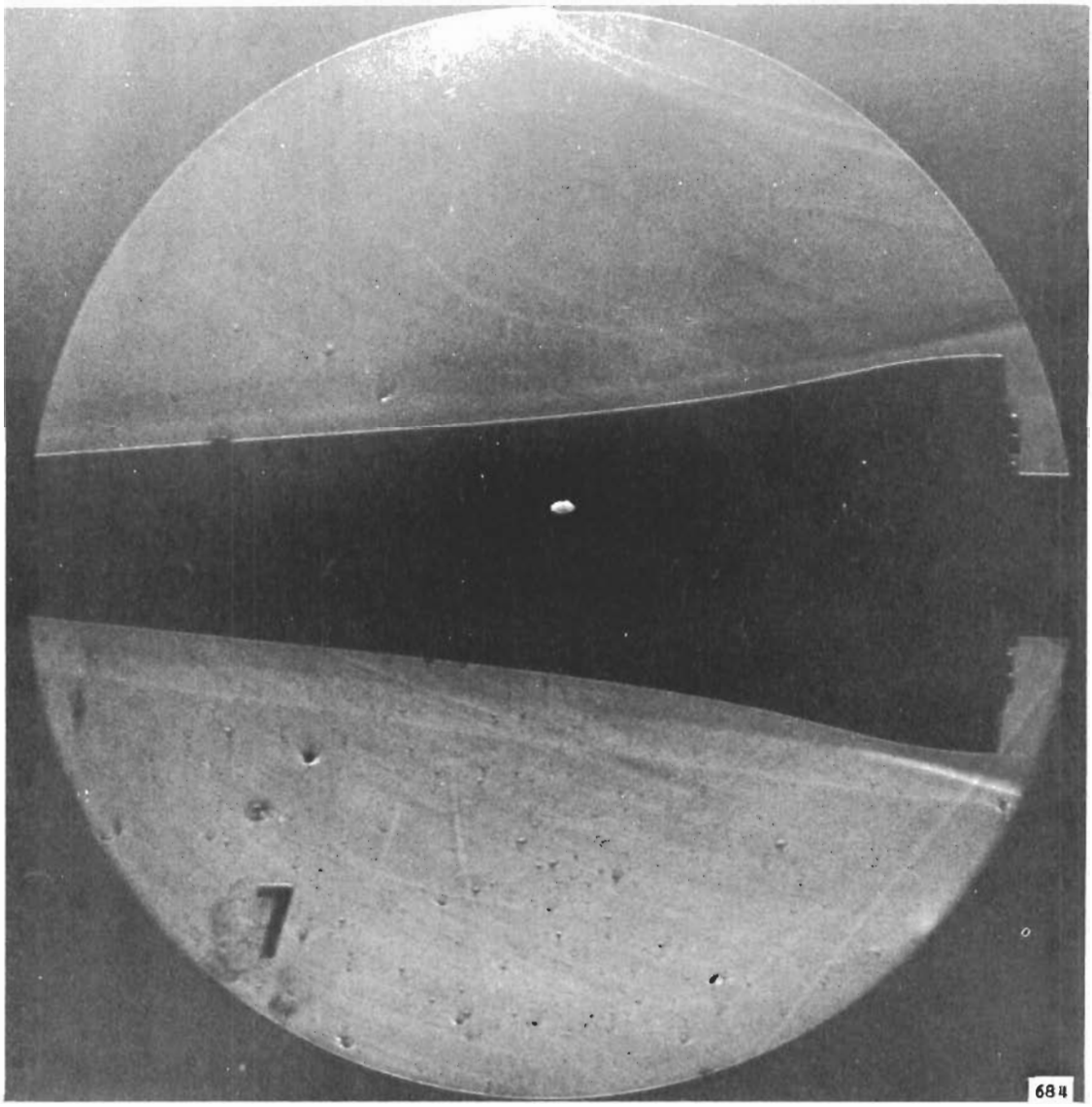


Figure 27 (Cont'd.) (d) MODEL A/10, RUN 7

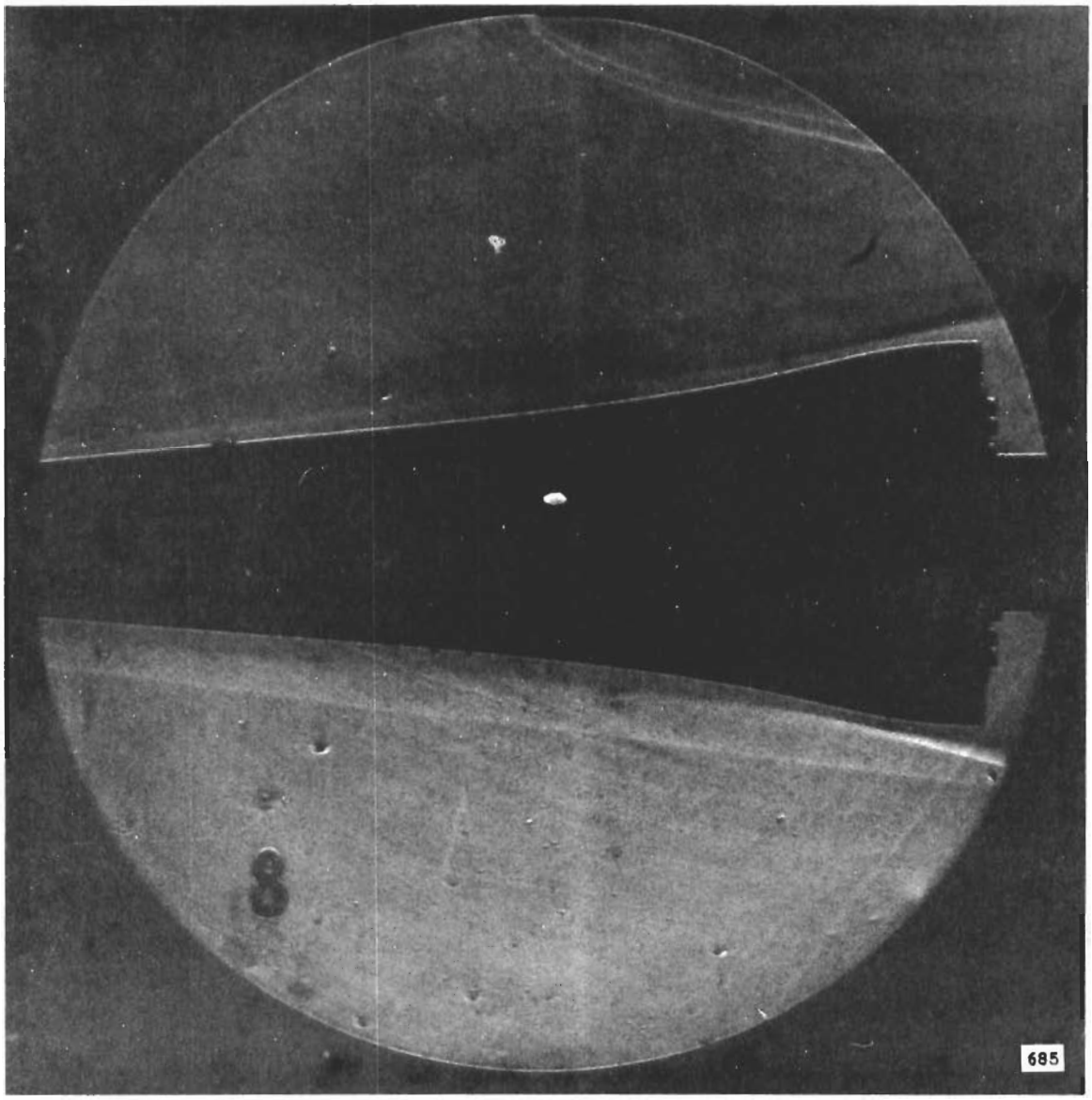


Figure 27 (Cont'd.) (e) MODEL A/10, RUN 8

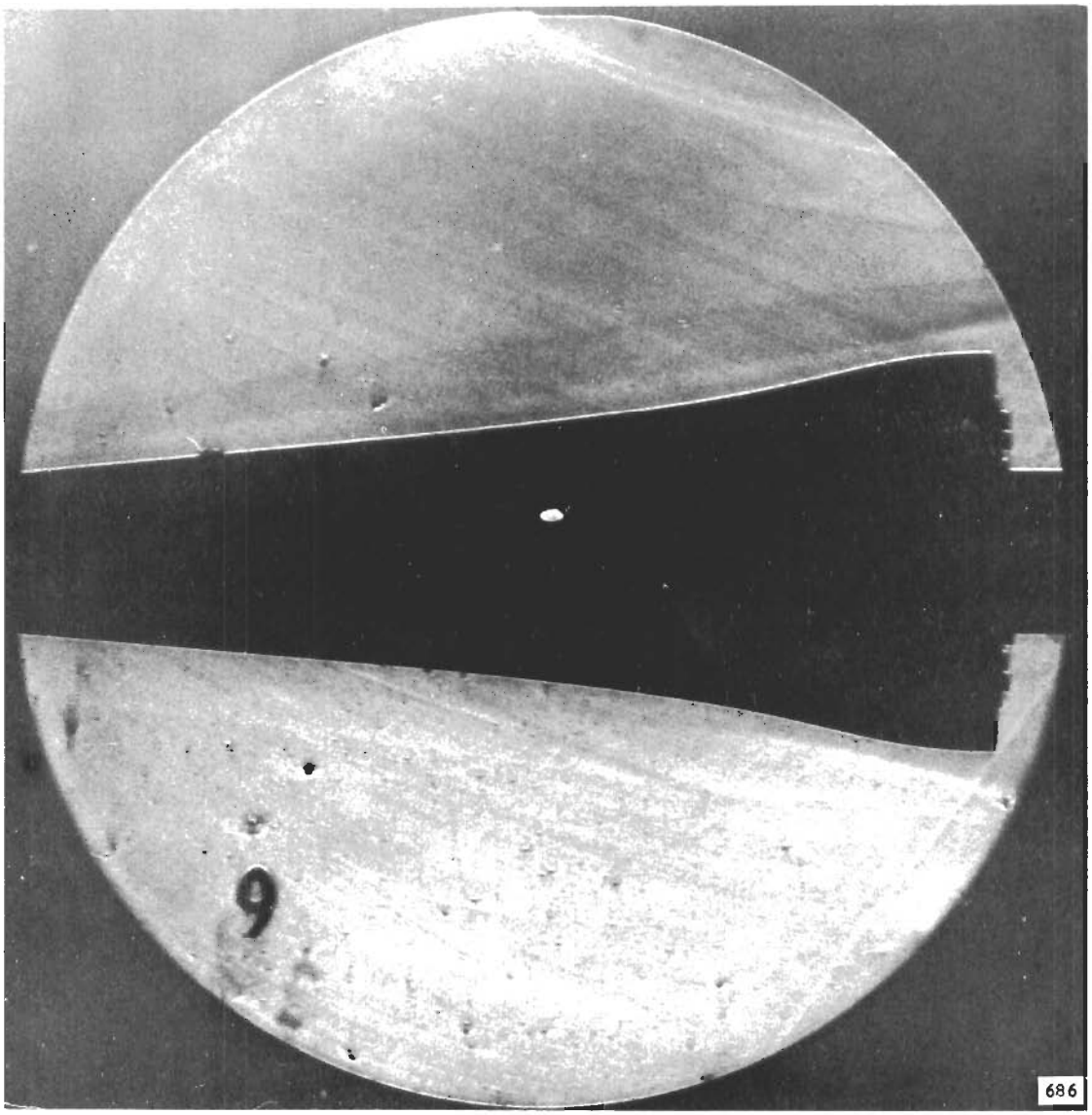


Figure 27 (Cont'd.) (f) MODEL A/10, RUN 9

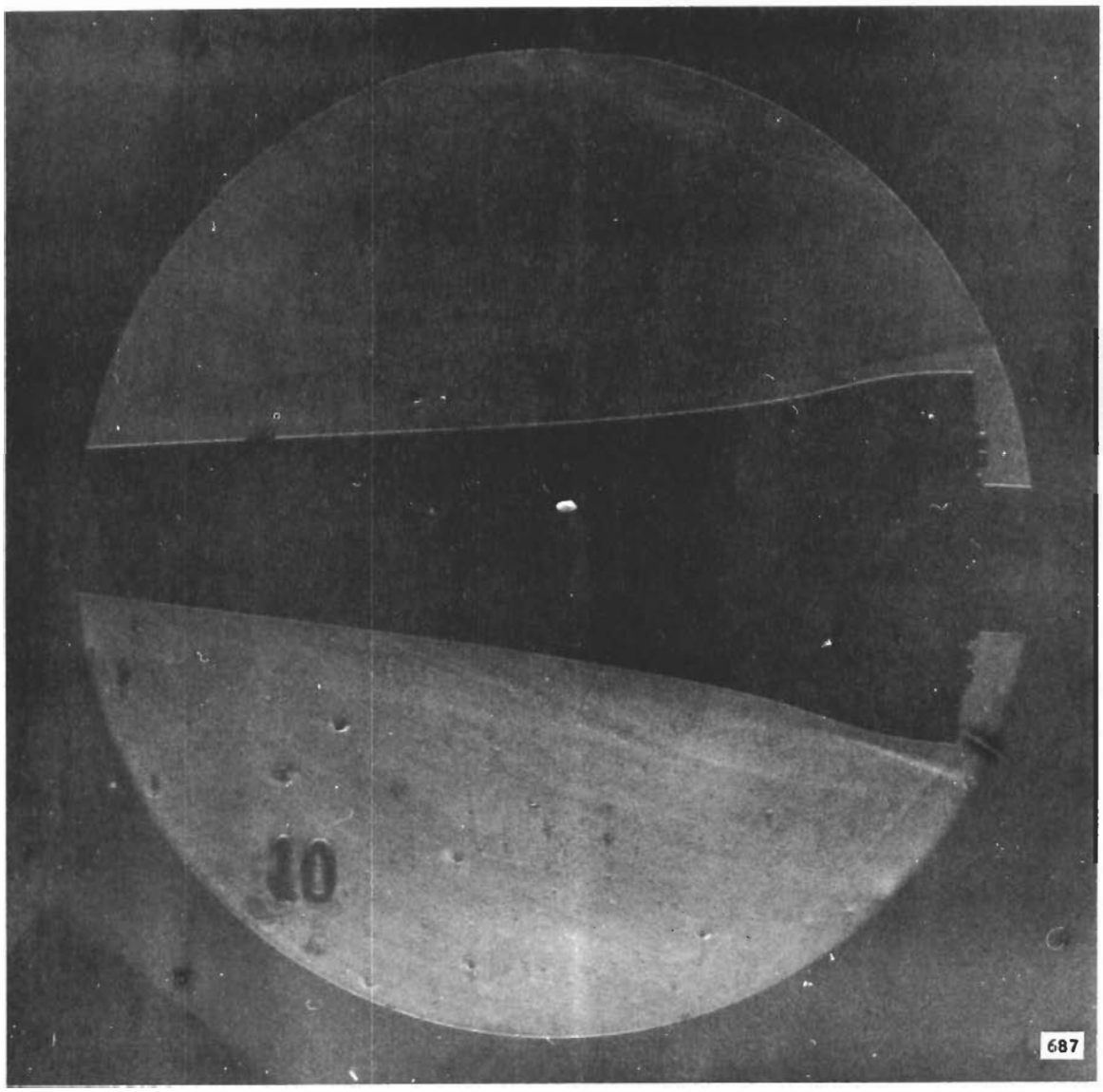


Figure 27 (Cont'd.) (g) MODEL A/20, RUN 10

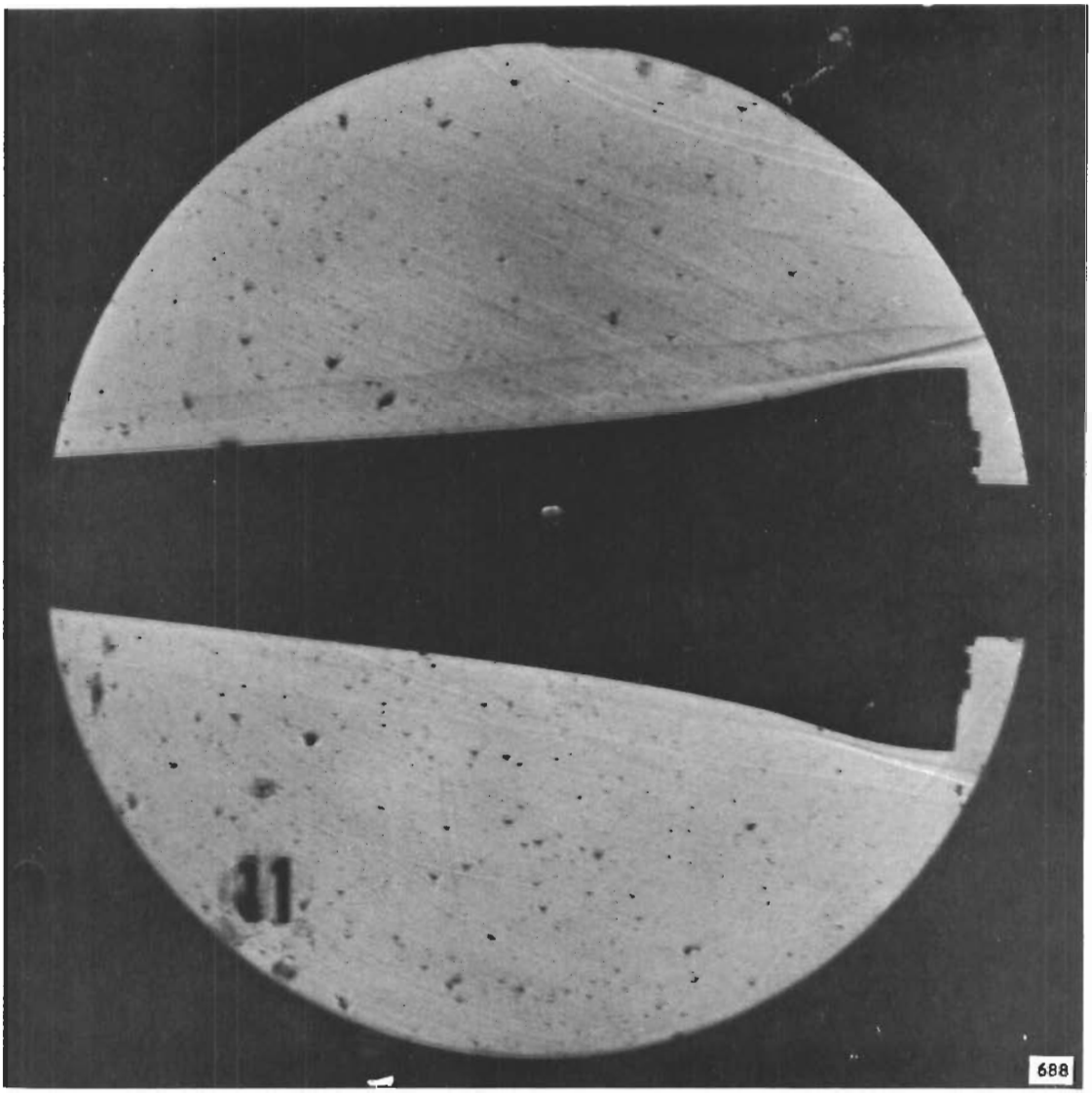


Figure 27 (Cont'd.) (h) MODEL A/20, RUN 11

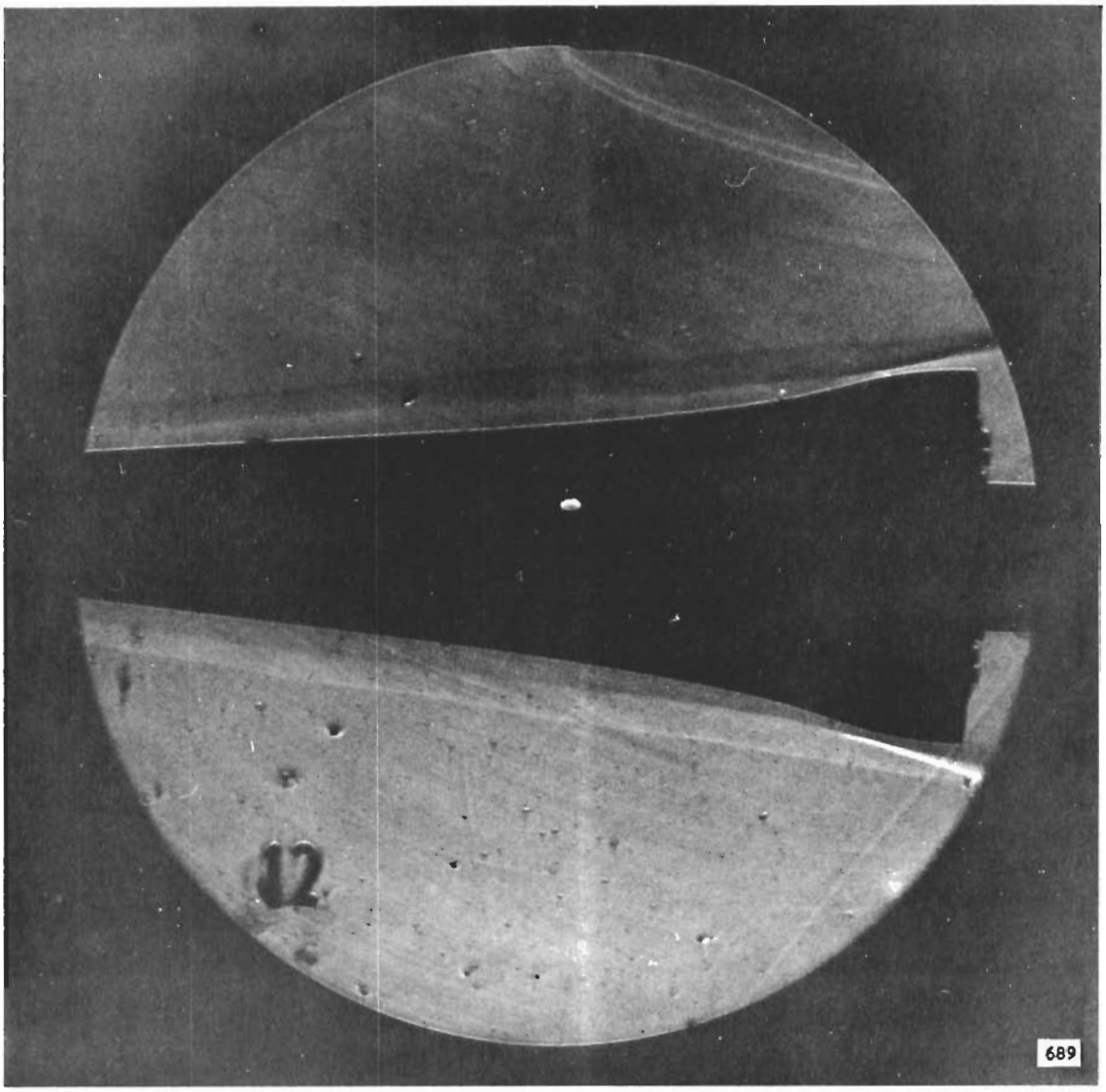


Figure 27 (Cont'd.) (i) MODEL A/20, RUN 12

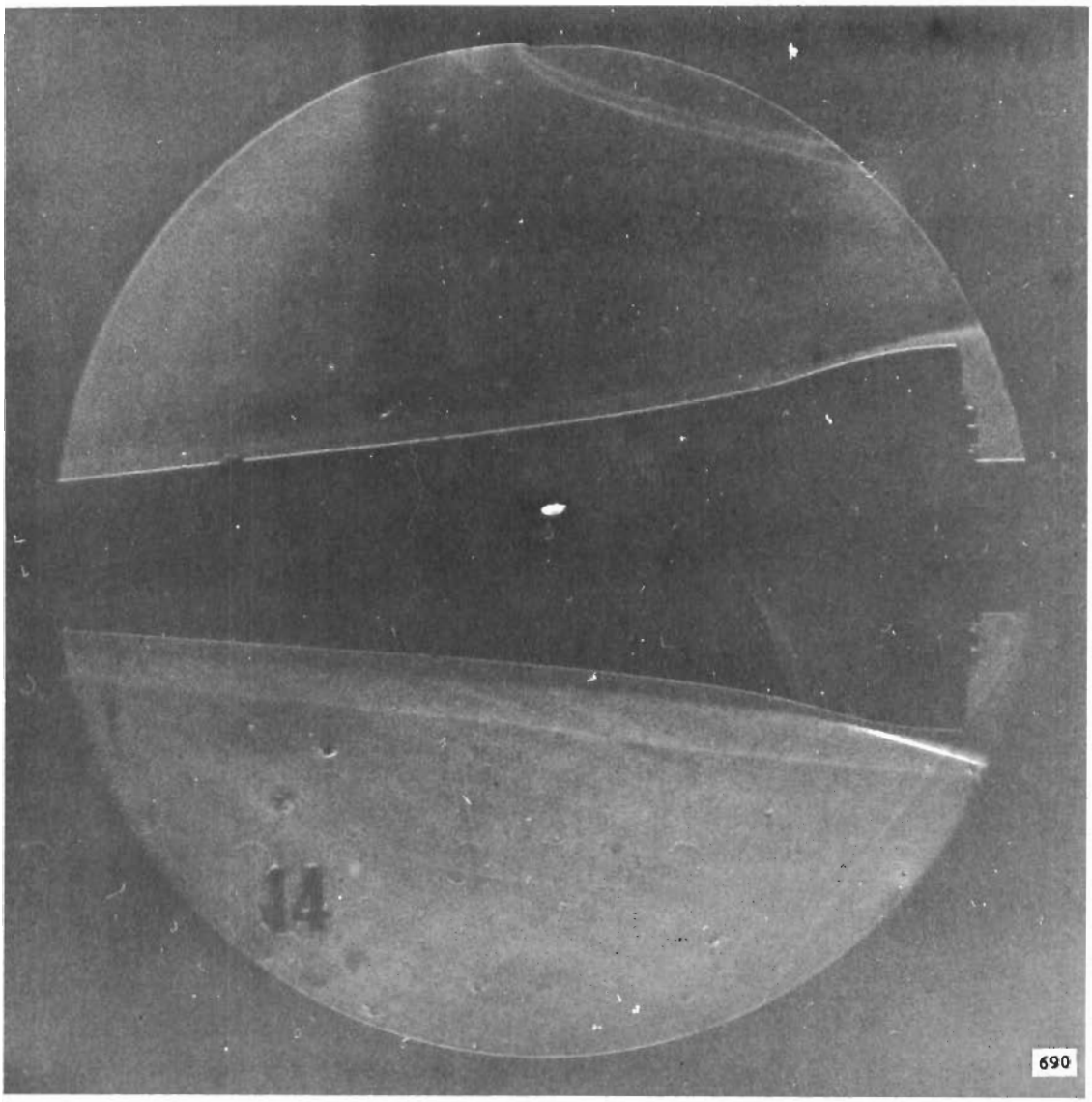


Figure 27 (Cont'd.) (j) MODEL A/20, RUN 14

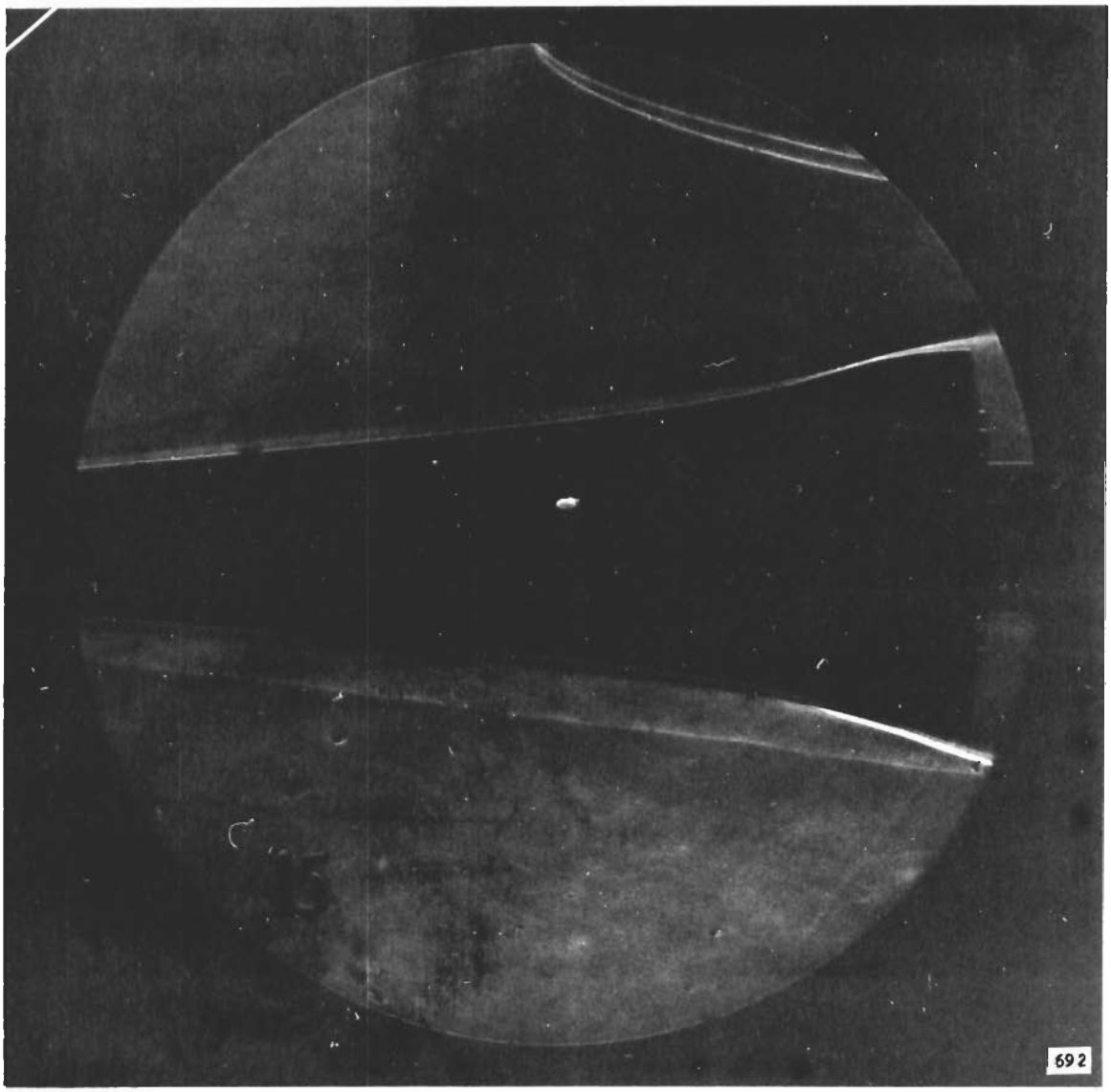


Figure 27 (Cont'd.) (k) MODEL A/20, RUN 15

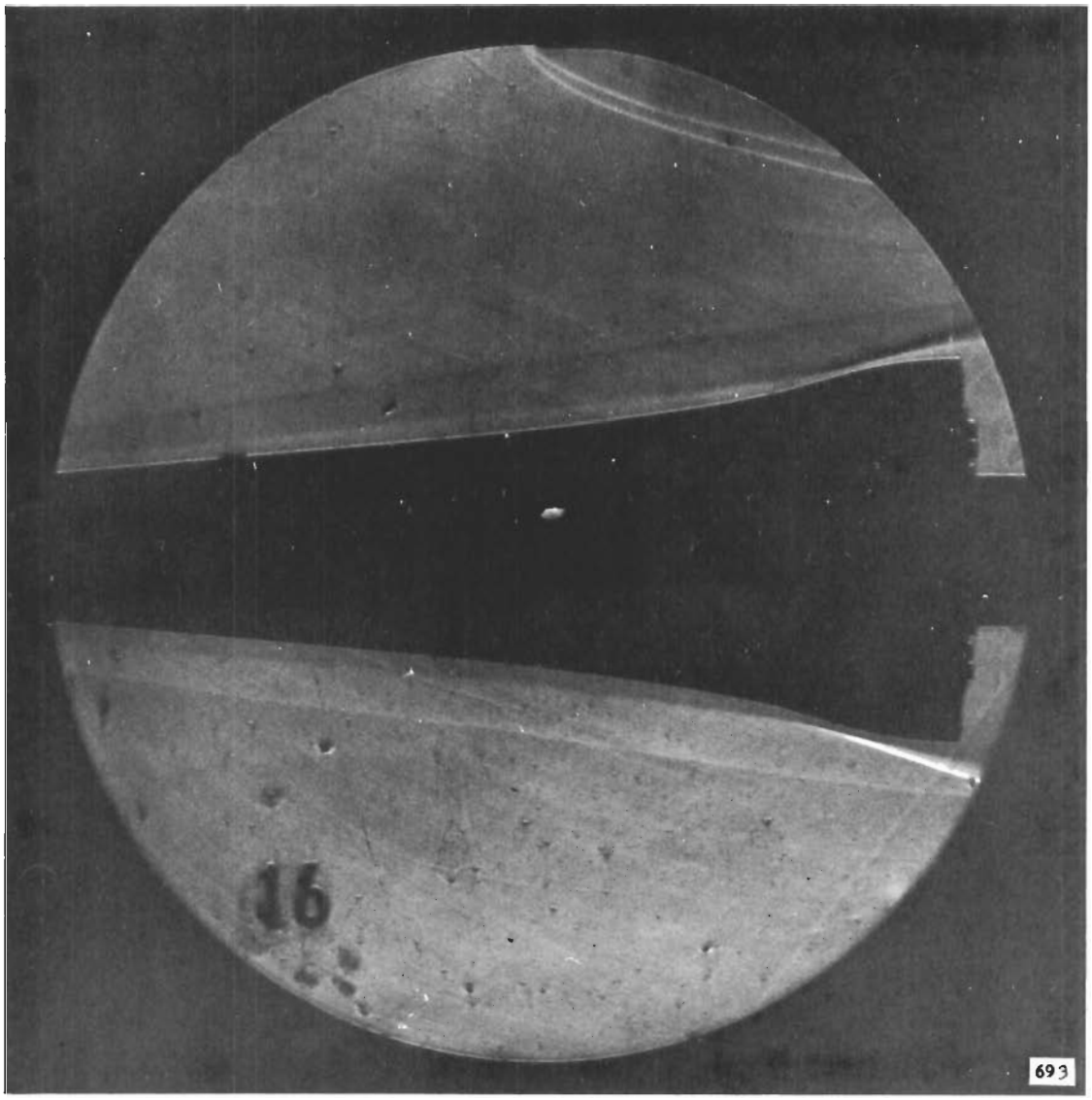


Figure 27 (Cont'd.) (1) MODEL A/20, RUN 16

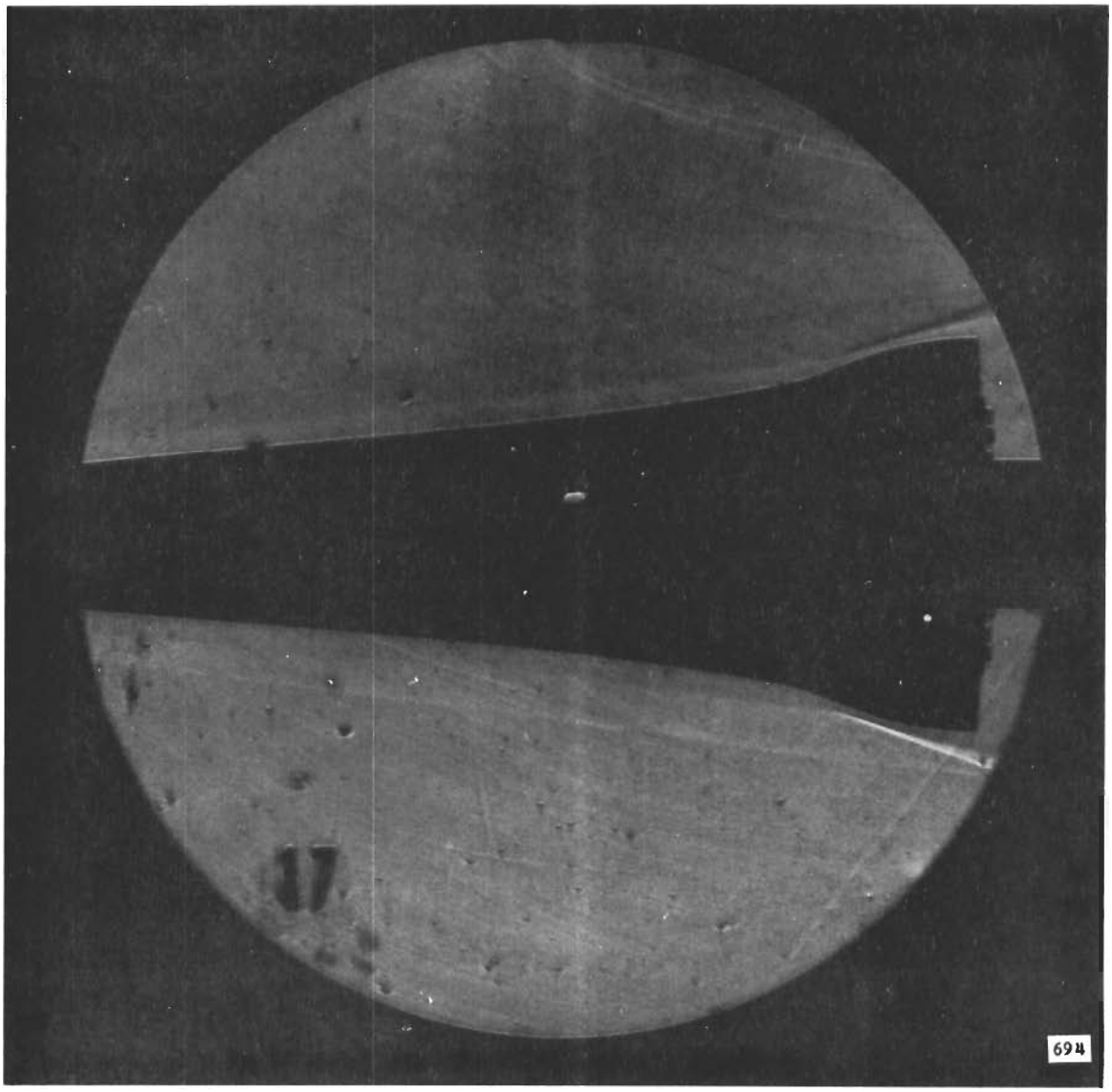


Figure 27 (Cont'd.) (m) MODEL A/50, RUN 17

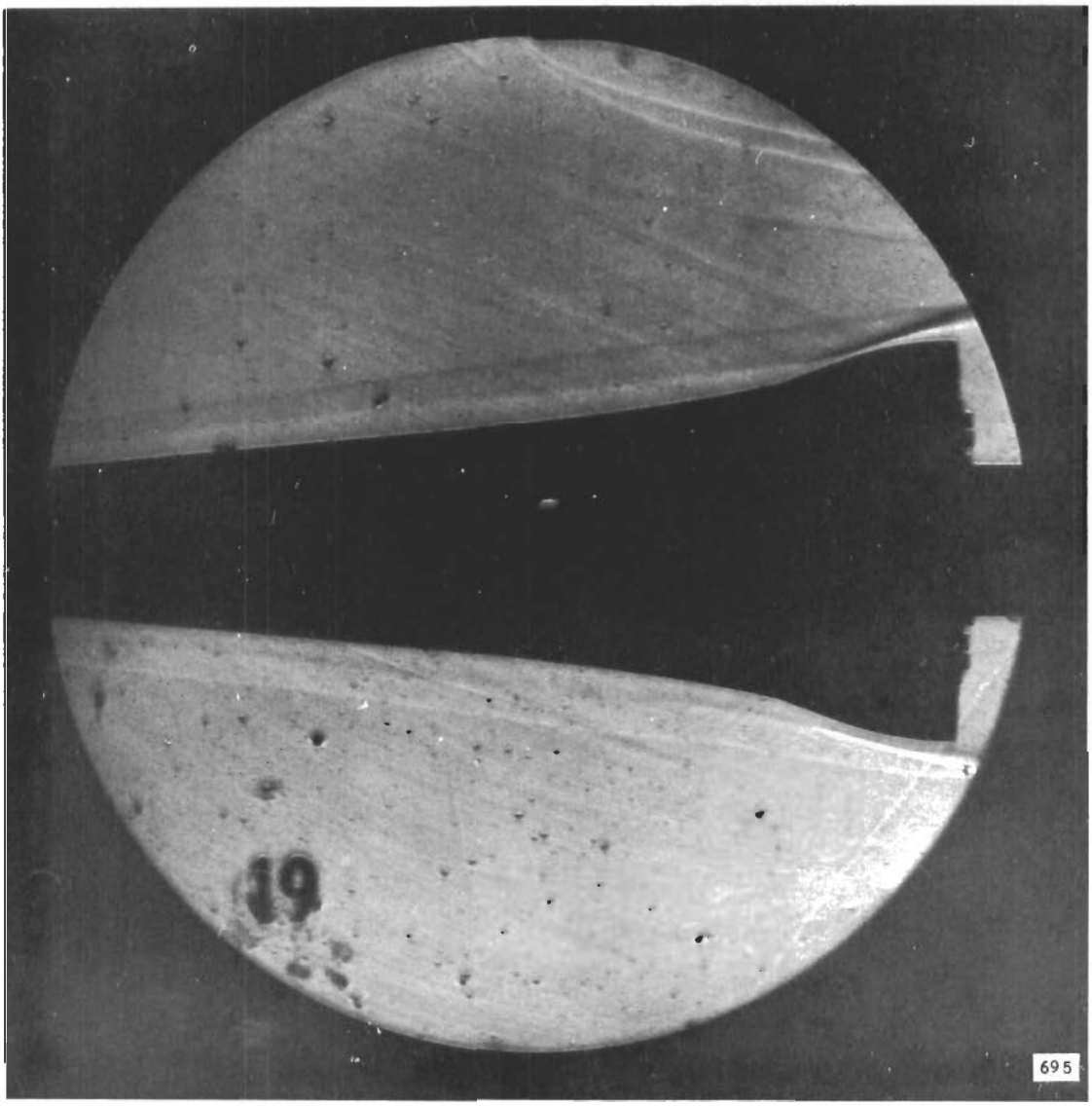


Figure 27 (Cont'd.) (n) MODEL A/50, RUN 19

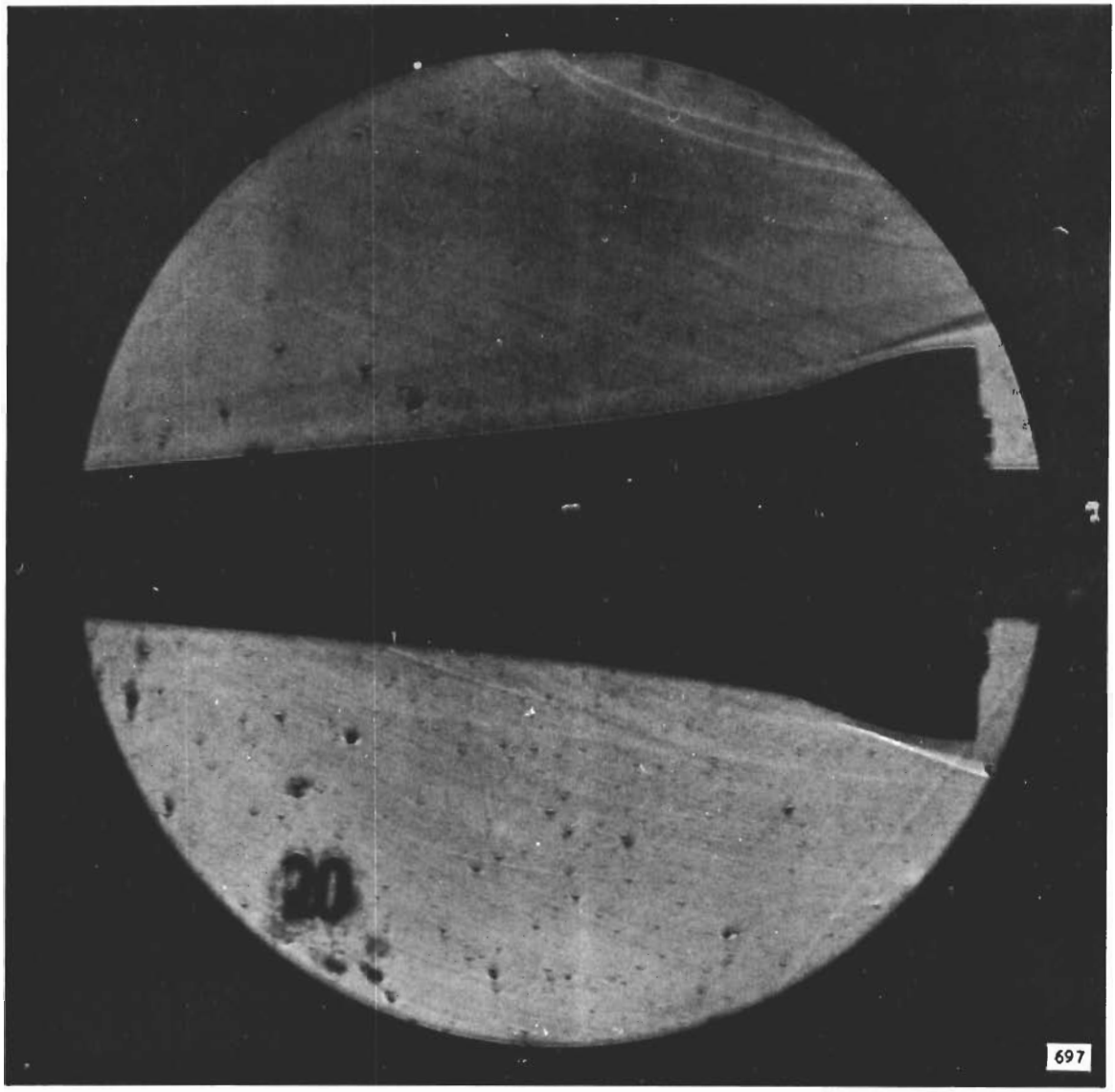


Figure 27 (Cont'd.) (o) MODEL A/50, RUN 20

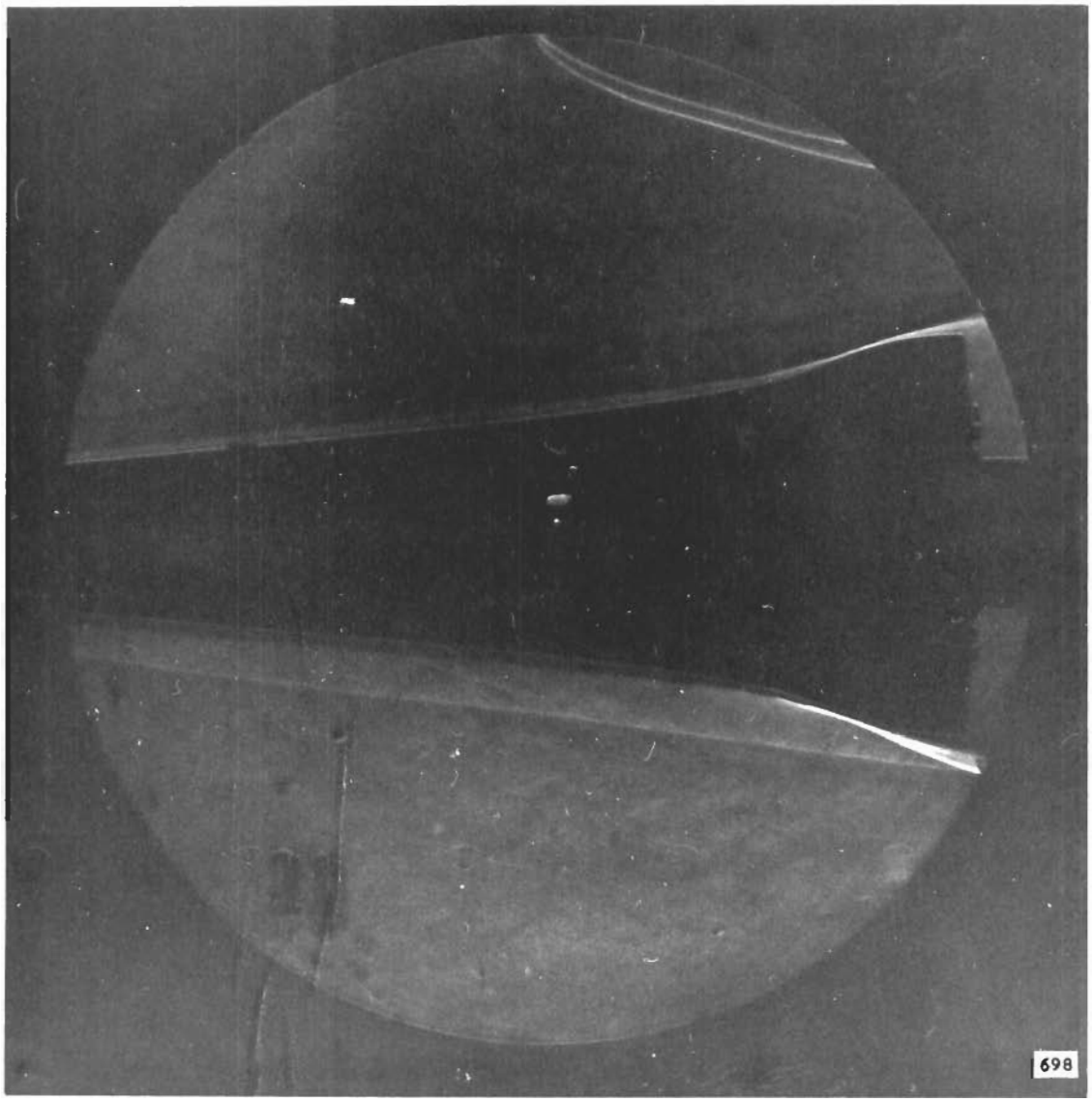


Figure 27 (Cont'd.) (p) MODEL A/50, RUN 21

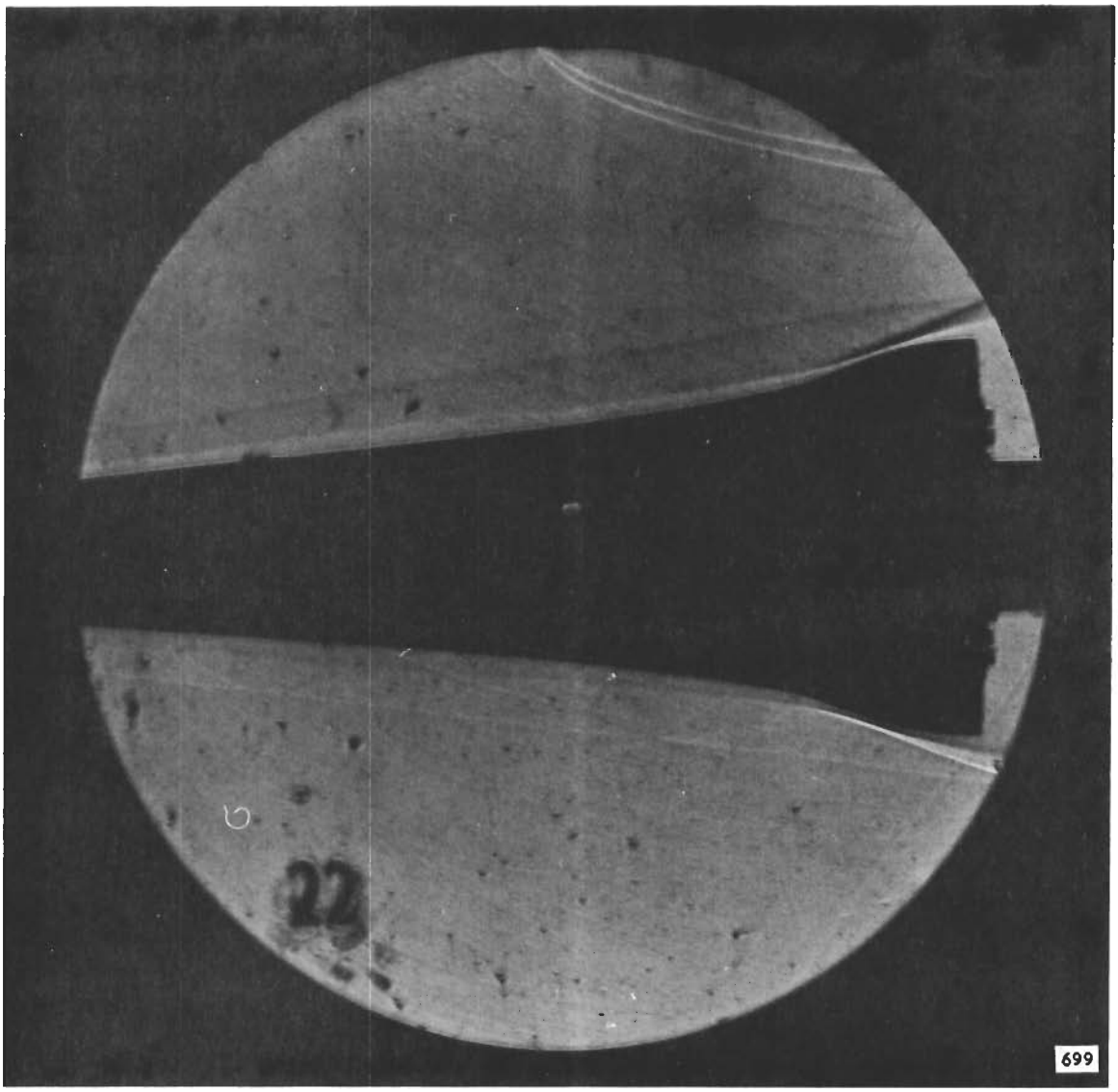


Figure 27 (Cont'd.) (q) MODEL A/50, RUN 22

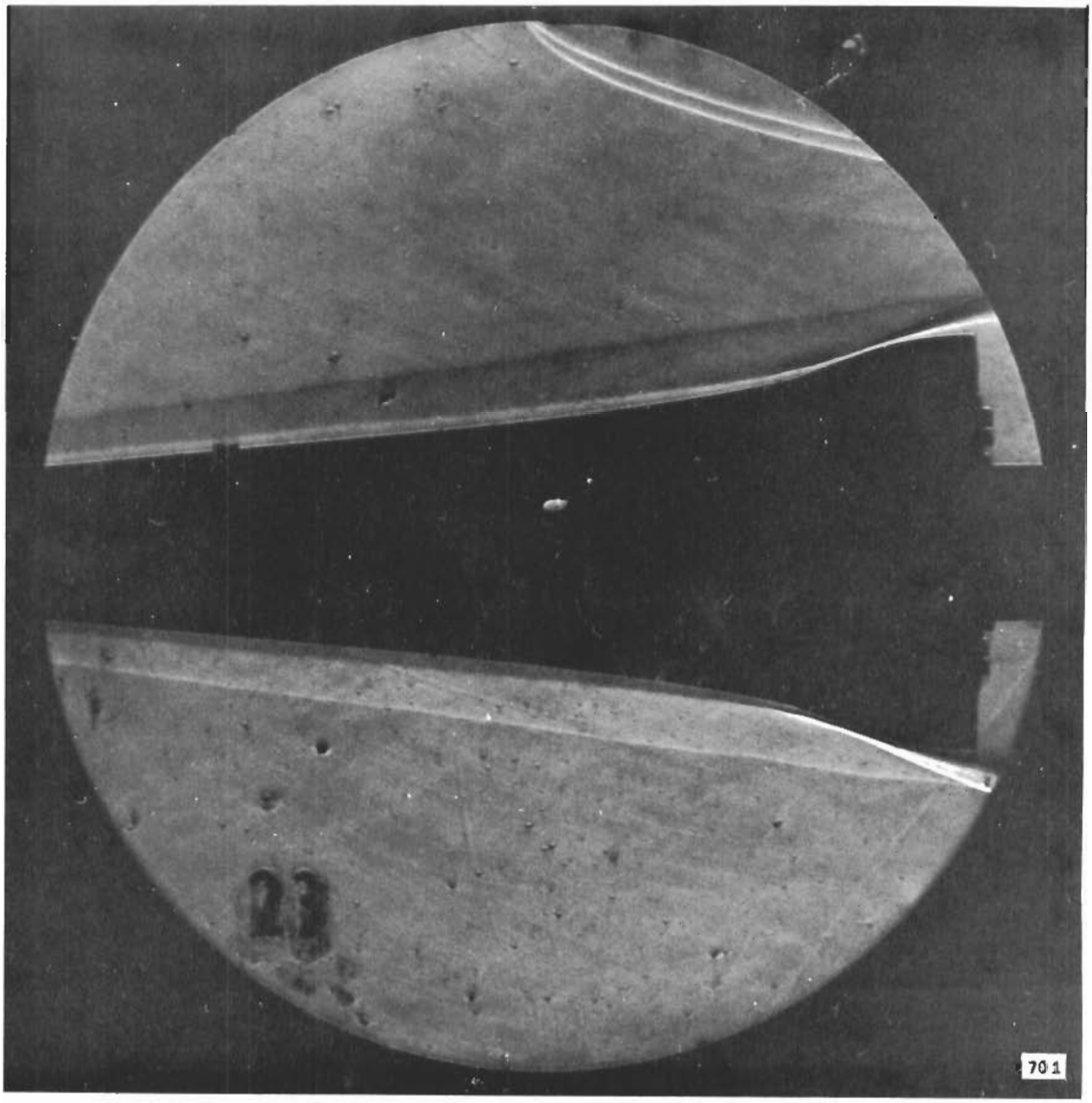


Figure 27 (Cont'd.) (r) MODEL A/50, RUN 23

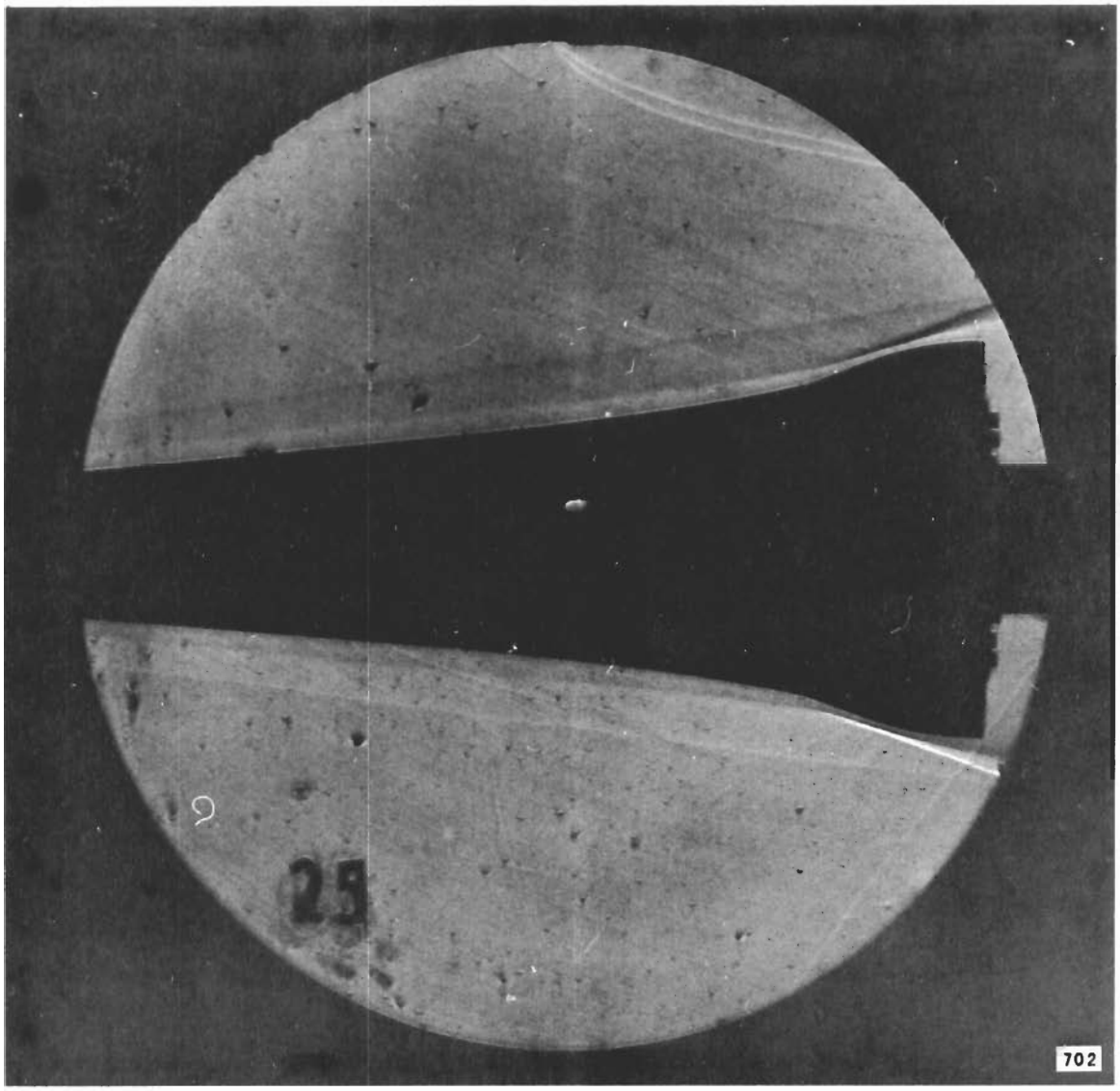


Figure 27 (Cont'd.) (s) MODEL A/50, RUN 25

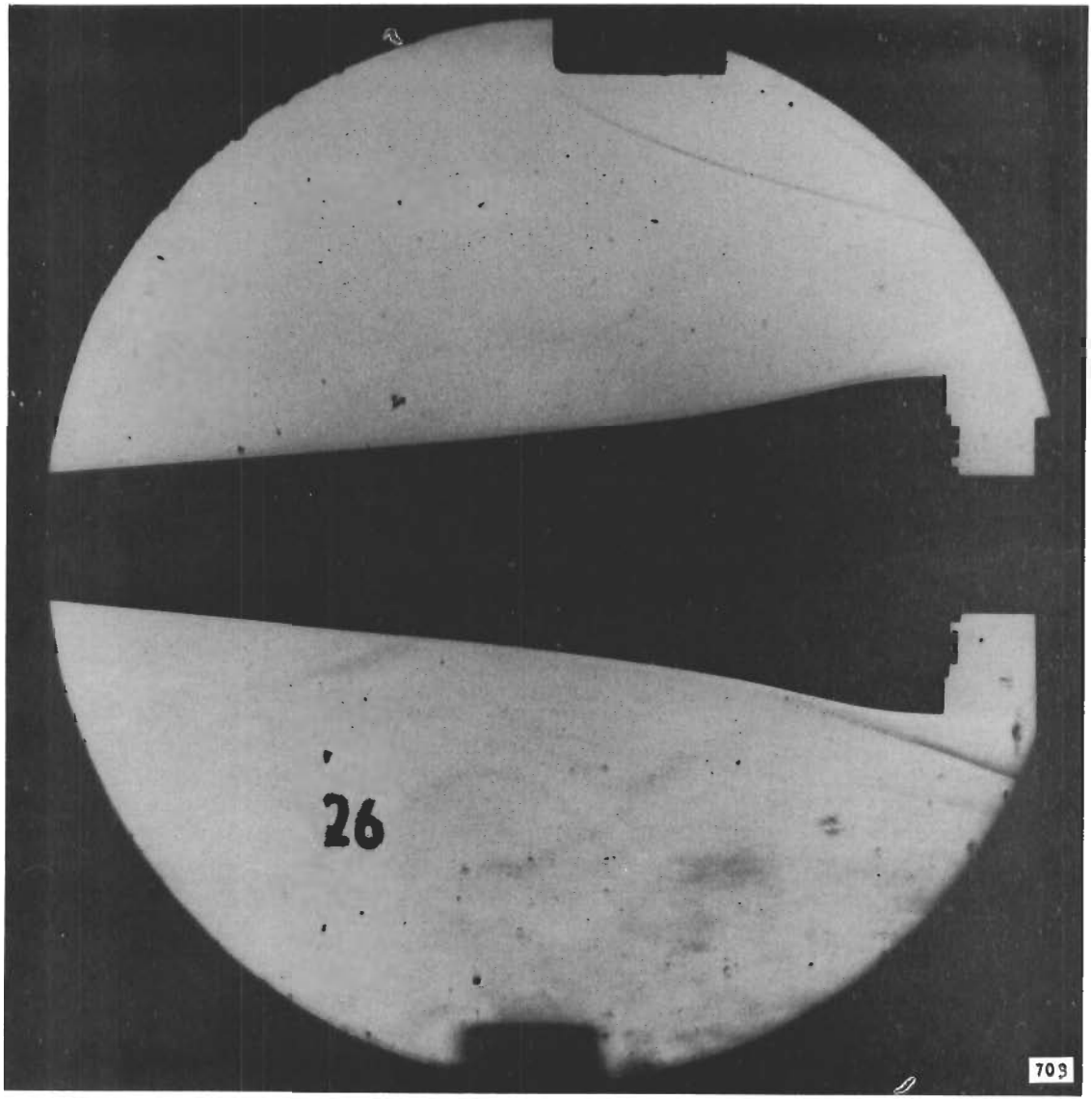


Figure 27 (Cont'd.) (t) MODEL A/10, RUN 26

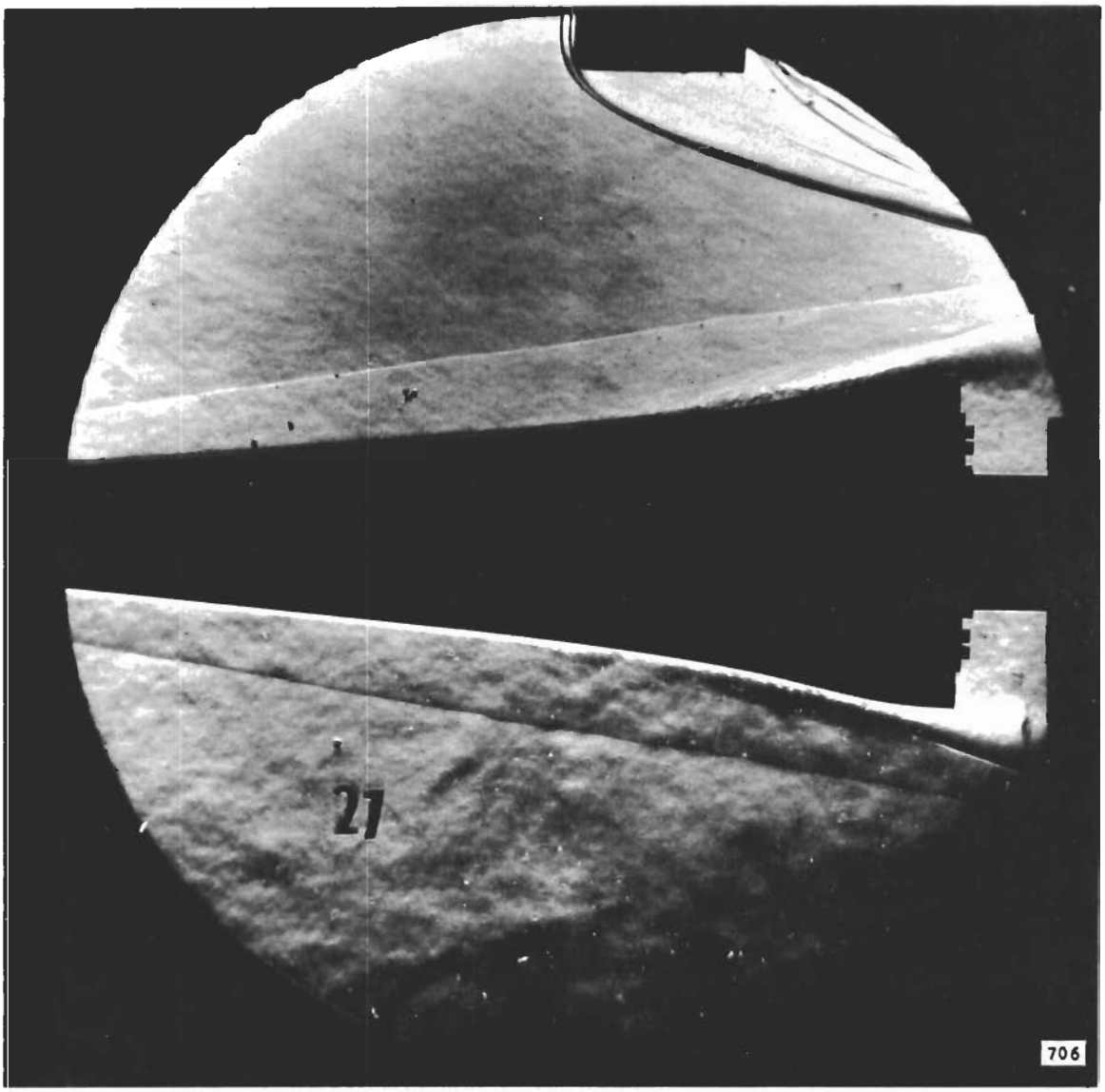


Figure 27 (Cont'd.) (u) MODEL A/10, RUN 27

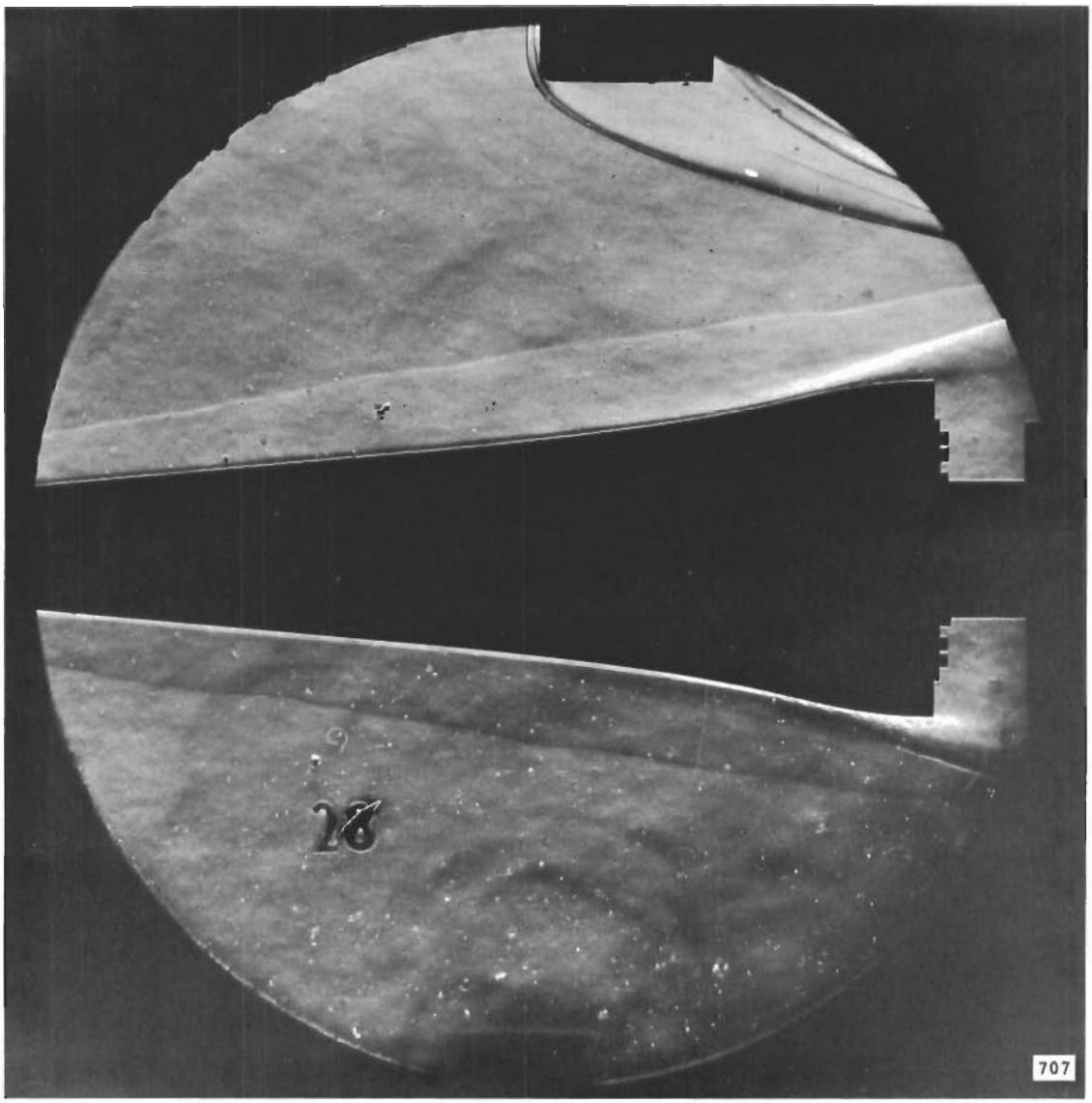


Figure 27 (Cont'd.) (v) MODEL A/10, RUN 28

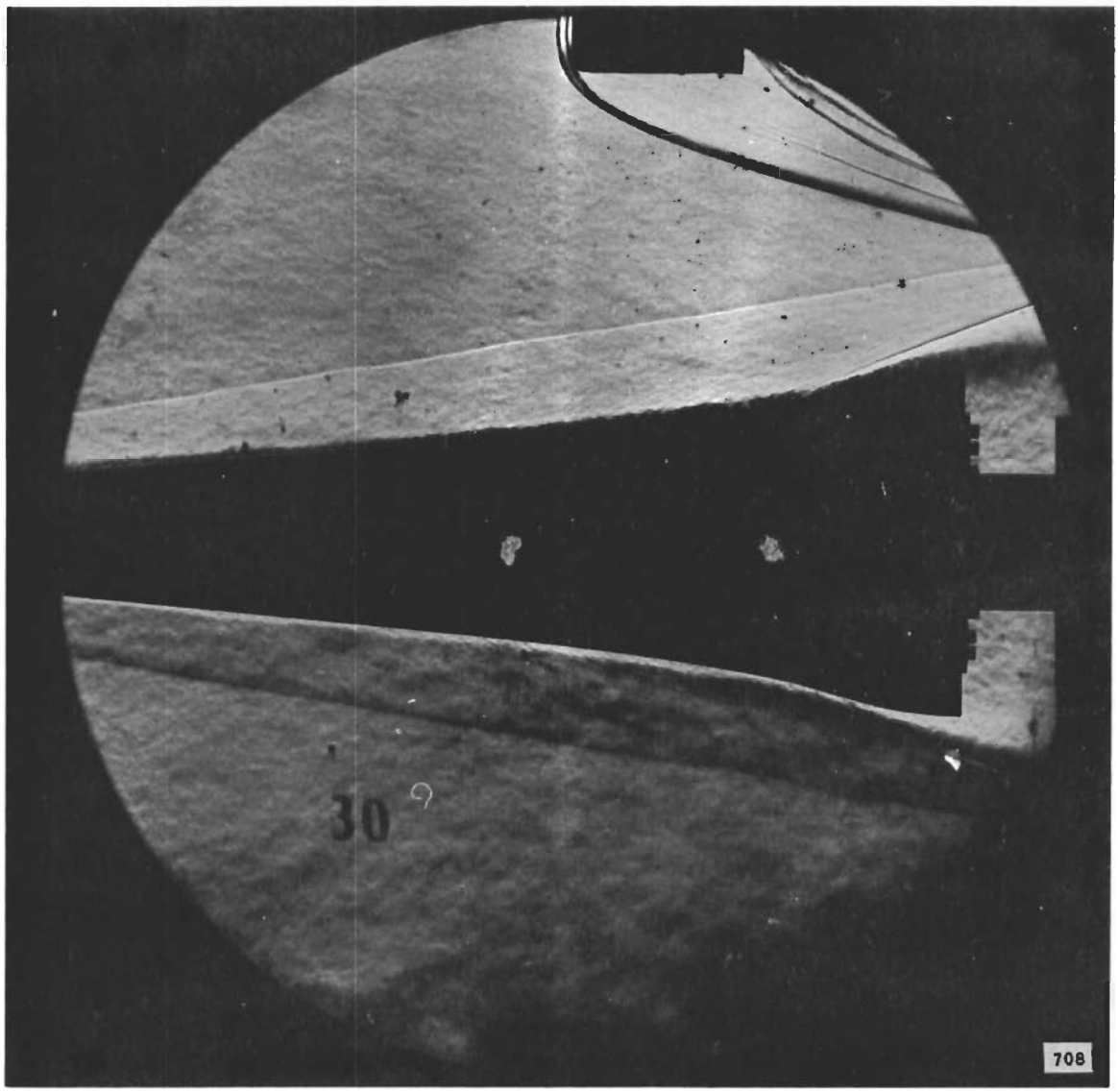


Figure 27 (Cont'd.) (w) MODEL A/20, RUN 30

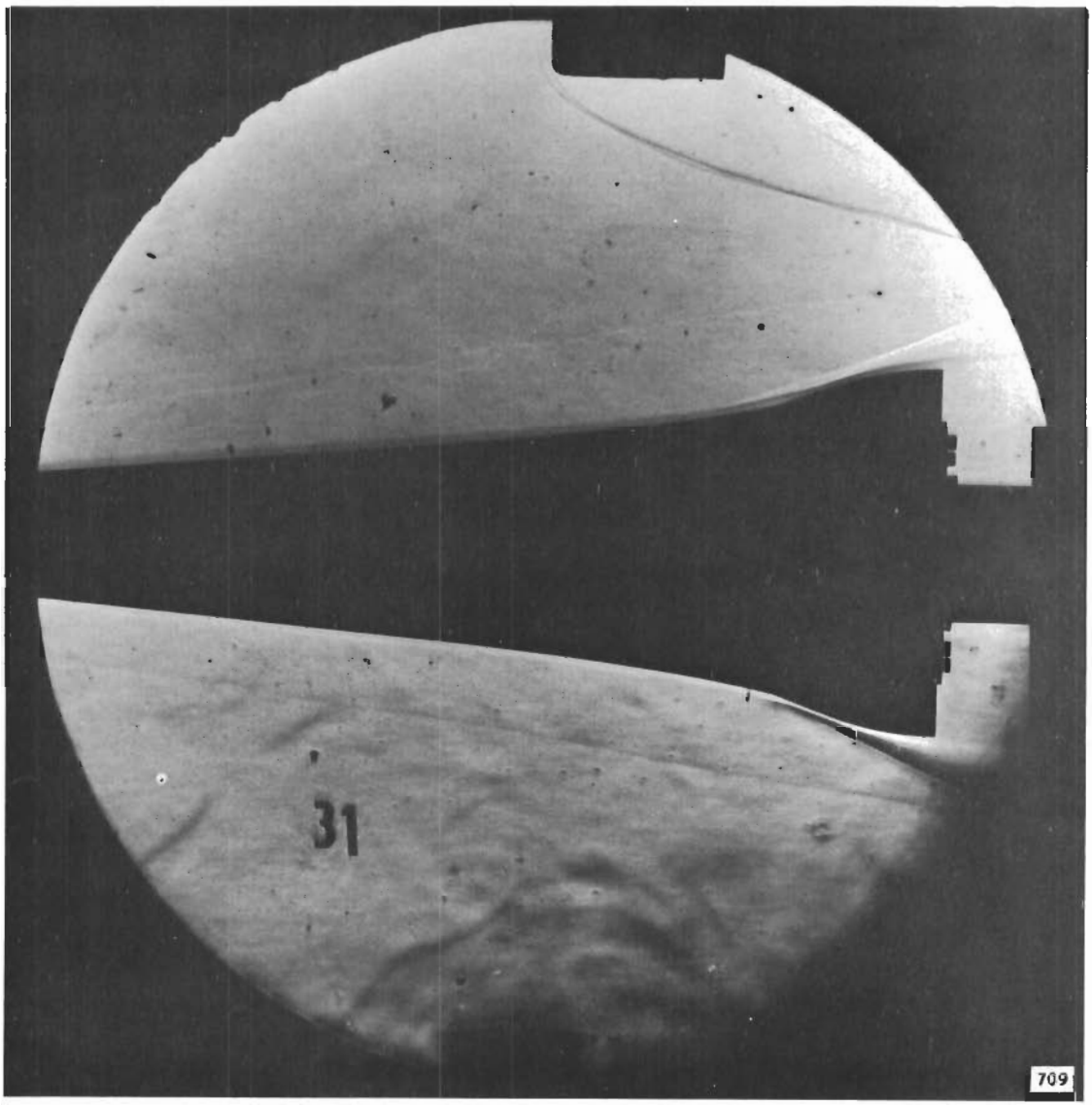


Figure 27 (Cont'd.) (x) MODEL A/50, RUN 31

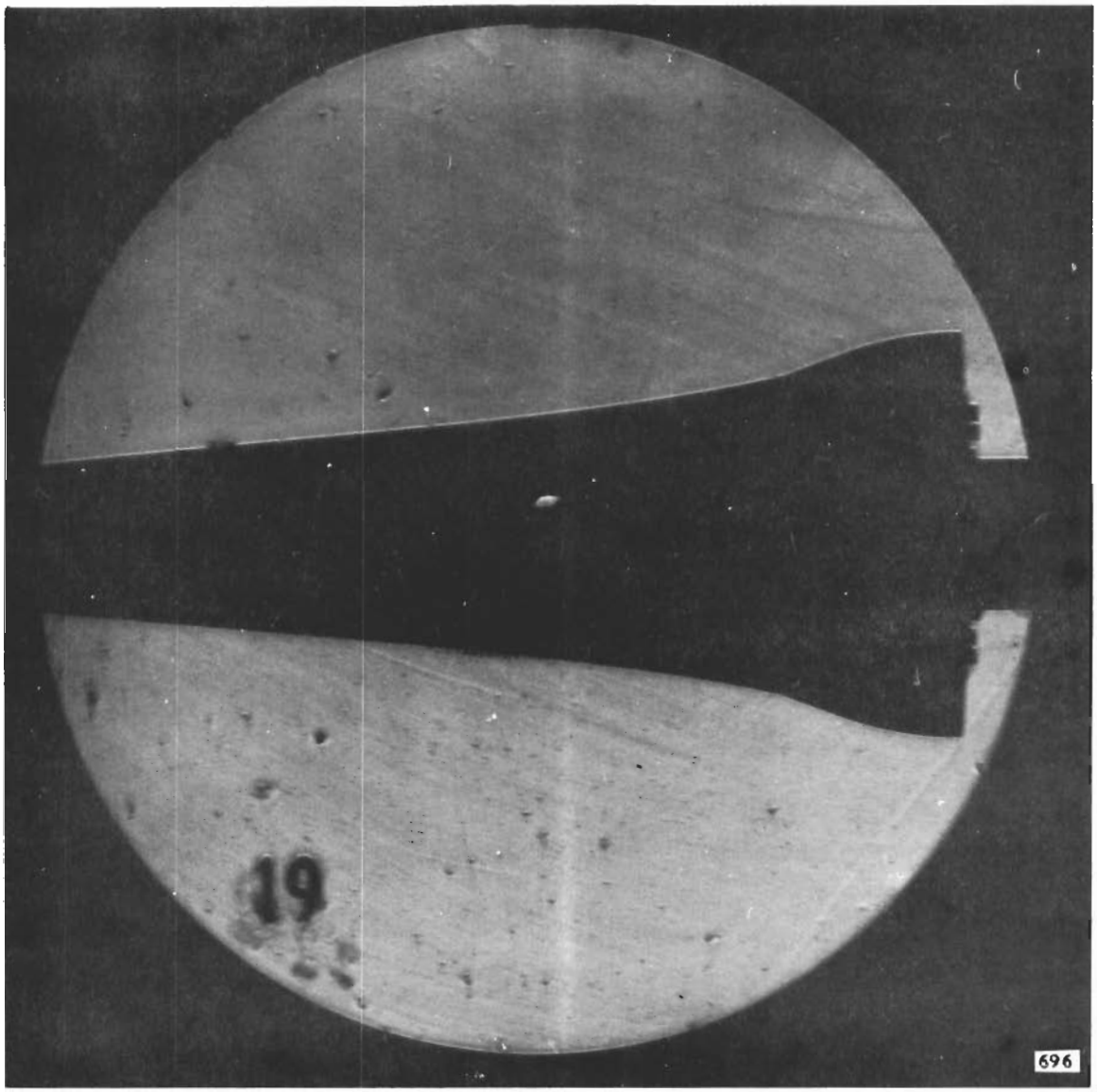


Figure 27 (Concluded) (y) NO-FLOW SCHLIEREN PHOTOGRAPH

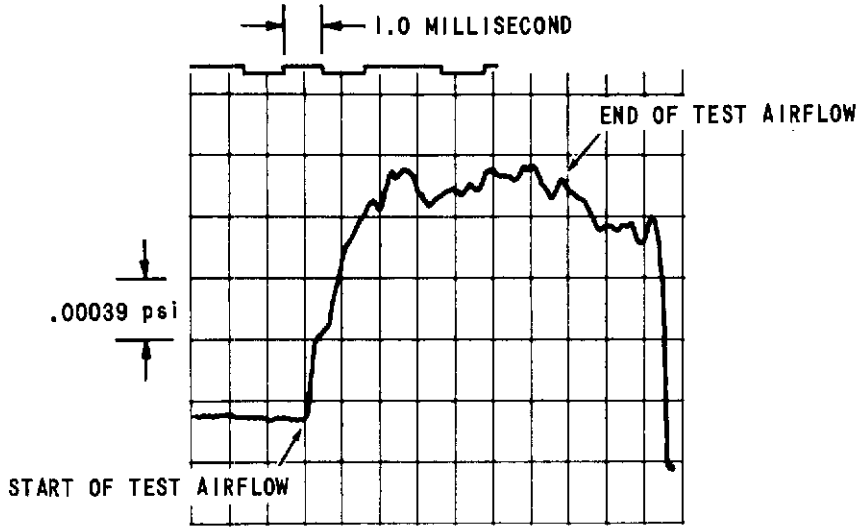


SKIN FRICTION POSITION 6

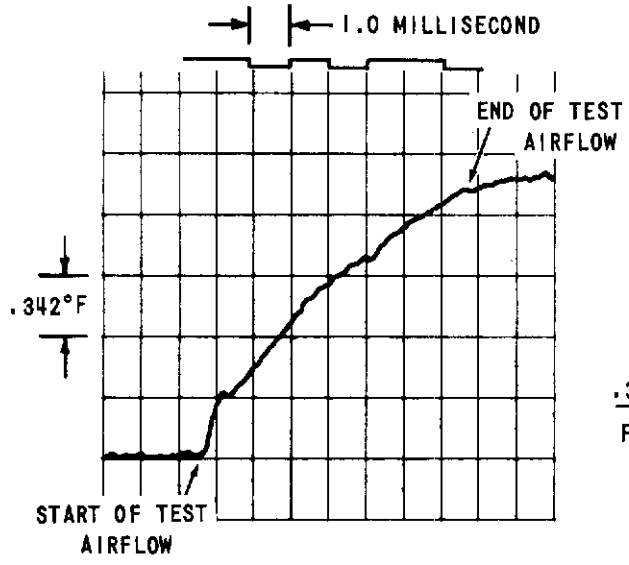


TEMPERATURE HISTORY FOR POSITION 4

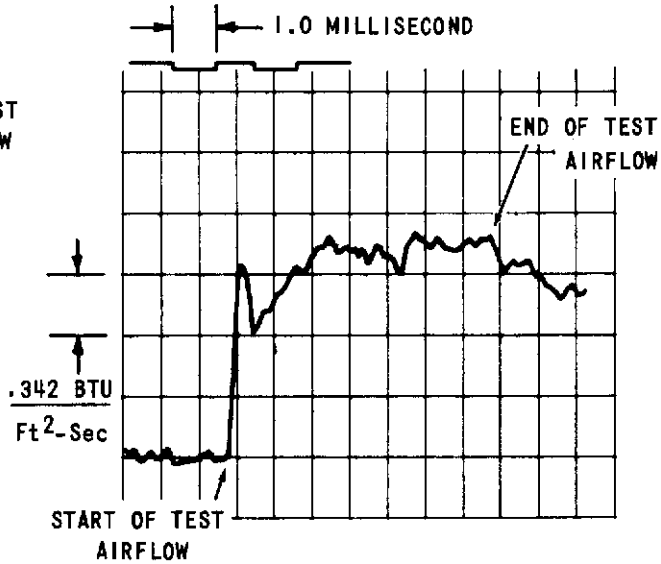


ANALOG CIRCUIT OUTPUT USING TEMPERATURE TRACE ON LEFT AS INPUT

Figure 28 TYPICAL SKIN FRICTION AND HEAT TRANSFER GAGE RESPONSES
(a) IN ATTACHED BOUNDARY LAYER FLOW - RUN 20

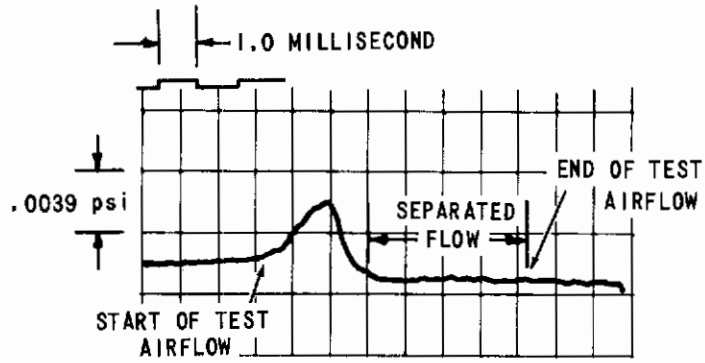


SKIN FRICTION POSITION 6

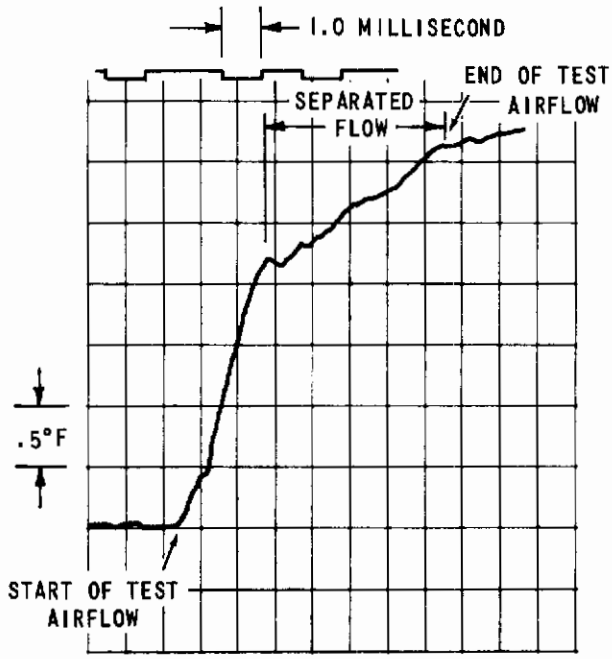


TEMPERATURE HISTORY FOR POSITION 4

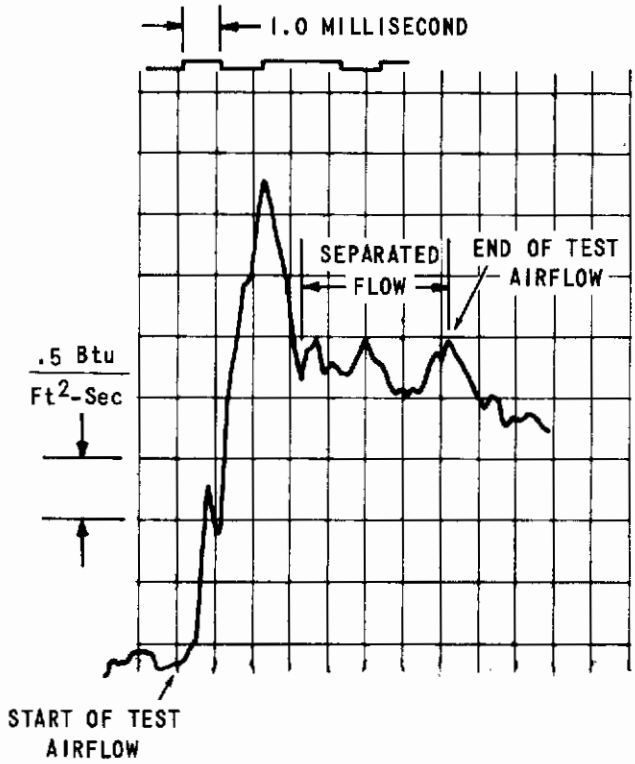


ANALOG CIRCUIT OUTPUT USING TEMPERATURE TRACE ON LEFT AS INPUT

Figure 28 (Concluded) (b) IN SEPARATED BOUNDARY LAYER FLOW - RUN 23

**DOCUMENT CONTROL DATA - R&D**

*(Security classification of title, body of abstract and indexing annotation must be entered when the overall report is classified)*

1. ORIGINATING ACTIVITY *(Corporate author)*
Cornell Aeronautical Laboratory, Inc.
Buffalo, New York

2a. REPORT SECURITY CLASSIFICATION
Unclassified

2b. GROUP
None

3. REPORT TITLE
SKIN FRICTION, HEAT TRANSFER AND PRESSURE MEASUREMENTS ON HYPERSONIC INLET COMPRESSION SURFACES IN THE MACH NUMBER RANGE 7.5 to 16

4. DESCRIPTIVE NOTES *(Type of report and inclusive dates)*
Final Report, May 1964 - December 1965

5. AUTHOR(S) *(Last name, first name, initial)*
Ryder, Melvin O. Jr.

| 6. REPORT DATE | 7a. TOTAL NO. OF PAGES | 7b. NO. OF REFS |
|---|---|---|
| December 1965 | | 18 |

| 8a. CONTRACT OR GRANT NO. | 9a. ORIGINATOR'S REPORT NUMBER(S) |
|---|---|
| AF 33(615)-1845 | AA-1948-Y-3 |
| b. PROJECT NO. 1366 | |
| c. Task No. 136605 | 9b. OTHER REPORT NO(S) *(Any other numbers that may be assigned this report)* AFFDL-TR-65-199 |
| d. | |

10. AVAILABILITY/LIMITATION NOTICES
(1) Qualified requesters may obtain copies of this report from DDC.
(2) This report has been released to CFSTI.

| 11. SUPPLEMENTARY NOTES | 12. SPONSORING MILITARY ACTIVITY |
|---|---|
| None | Air Force Flight Dynamics Laboratory Research and Technology Division, AF Systems Command, Wright-Patterson AFB |

13. ABSTRACT

An experimental study of boundary layer flow, under the influence of adverse pressure gradients typical of hypersonic inlets, was conducted in the Cornell Aeronautical Laboratory 48-inch Hypersonic Shock Tunnel on two two-dimensional and three axisymmetric compression surface models instrumented with skin friction, heat transfer and pressure gages. Tests were conducted over a Mach and Reynolds number range of 7.5 to 16 and $3.2 \times 10^4$ per ft. to $4.7 \times 10^6$ per ft., respectively. The boundary layers on the two-dimensional models were laminar and attached for all conditions tested. Local laminar separation occurred for some conditions of the axisymmetric tests. Boundary layer transition occurred for the high Reynolds number runs at a Mach number of 8 on the axisymmetric models but the adverse pressure gradients were not large enough to cause the turbulent boundary layers to separate.

A data correlation based on local flow conditions at the edge of the boundary layer and zero pressure gradient is presented which correlates the heat transfer data quite well. The skin friction data are shown to correlate in a similar manner when the adverse pressure gradient is small but the correlation fails at large pressure gradients and for separated flow.

An important conclusion resulting from this program was that the skin friction gages gave a more accurate indication of localized boundary layer separation than either the heat transfer or static pressure distributions on the models tested.

DD FORM 1 JAN 64 1473

| 14. KEY WORDS | LINK A | | LINK B | | LINK C | |
|---|---|---|---|---|---|---|
| | ROLE | WT | ROLE | WT | ROLE | WT |
| Boundary Layer Separation<br>Adverse Pressure Gradients<br>Skin Friction<br>Hypersonic Inlet<br>Heat Transfer | | | | | | |

## INSTRUCTIONS

1. ORIGINATING ACTIVITY: Enter the name and address of the contractor, subcontractor, grantee, Department of Defense activity or other organization *(corporate author)* issuing the report.

2a. REPORT SECURITY CLASSIFICATION: Enter the overall security classification of the report. Indicate whether "Restricted Data" is included. Marking is to be in accordance with appropriate security regulations.

2b. GROUP: Automatic downgrading is specified in DoD Directive 5200.10 and Armed Forces Industrial Manual. Enter the group number. Also, when applicable, show that optional markings have been used for Group 3 and Group 4 as authorized.

3. REPORT TITLE: Enter the complete report title in all capital letters. Titles in all cases should be unclassified. If a meaningful title cannot be selected without classification, show title classification in all capitals in parenthesis immediately following the title.

4. DESCRIPTIVE NOTES: If appropriate, enter the type of report, e.g., interim, progress, summary, annual, or final. Give the inclusive dates when a specific reporting period is covered.

5. AUTHOR(S): Enter the name(s) of author(s) as shown on or in the report. Enter last name, first name, middle initial. If military, show rank and branch of service. The name of the principal author is an absolute minimum requirement.

6. REPORT DATE: Enter the date of the report as day, month, year; or month, year. If more than one date appears on the report, use date of publication.

7a. TOTAL NUMBER OF PAGES: The total page count should follow normal pagination procedures, i.e., enter the number of pages containing information.

7b. NUMBER OF REFERENCES: Enter the total number of references cited in the report.

8a. CONTRACT OR GRANT NUMBER: If appropriate, enter the applicable number of the contract or grant under which the report was written.

8b, 8c, & 8d. PROJECT NUMBER: Enter the appropriate military department identification, such as project number, subproject number, system numbers, task number, etc.

9a. ORIGINATOR'S REPORT NUMBER(S): Enter the official report number by which the document will be identified and controlled by the originating activity. This number must be unique to this report.

9b. OTHER REPORT NUMBER(S): If the report has been assigned any other report numbers *(either by the originator or by the sponsor)*, also enter this number(s).

10. AVAILABILITY/LIMITATION NOTICES: Enter any limitations on further dissemination of the report, other than those imposed by security classification, using standard statements such as:

(1) "Qualified requesters may obtain copies of this report from DDC."

(2) "Foreign announcement and dissemination of this report by DDC is not authorized."

(3) "U. S. Government agencies may obtain copies of this report directly from DDC. Other qualified DDC users shall request through _____."

(4) "U. S. military agencies may obtain copies of this report directly from DDC. Other qualified users shall request through _____."

(5) "All distribution of this report is controlled. Qualified DDC users shall request through _____."

If the report has been furnished to the Office of Technical Services, Department of Commerce, for sale to the public, indicate this fact and enter the price, if known.

11. SUPPLEMENTARY NOTES: Use for additional explanatory notes.

12. SPONSORING MILITARY ACTIVITY: Enter the name of the departmental project office or laboratory sponsoring *(paying for)* the research and development. Include address.

13. ABSTRACT: Enter an abstract giving a brief and factual summary of the document indicative of the report, even though it may also appear elsewhere in the body of the technical report. If additional space is required, a continuation sheet shall be attached.

It is highly desirable that the abstract of classified reports be unclassified. Each paragraph of the abstract shall end with an indication of the military security classification of the information in the paragraph, represented as *(TS), (S), (C), or (U)*.

There is no limitation on the length of the abstract. However, the suggested length is from 150 to 225 words.

14. KEY WORDS: Key words are technically meaningful terms or short phrases that characterize a report and may be used as index entries for cataloging the report. Key words must be selected so that no security classification is required. Identifiers, such as equipment model designation, trade name, military project code name, geographic location, may be used as key words but will be followed by an indication of technical context. The assignment of links, roles, and weights is optional.